AN INVESTIGATION OF

THE EFFECTS OF SHEARFREE DEFORMATION AND

THE ROLE OF MISCIBILITY ON THE STRUCTURE AND

PROPERTIES OF IN SITU THERMOPLASTIC COMPOSITES

by

Jose Paulino de Souza

Dissertation submitted to the Faculty of the

Virginia Polytechnic Institute and State University

in partial fulfillment of the requirements for the degree of

DOCTOR OF PHILOSOPHY

in

Chemical Engineering

APPROVED:

Donald G. Baird

Dr. Donald G. Baird, Chairman

William L. Conger

Dr. William L. Conger

Richey M. Davis

Dr. Richey M. Davis

Alfred C. Loos

Dr. Alfred C. Loos

Garth L. Wilkes

Dr. Garth L. Wilkes

January 27, 1994

Blacksburg, Virginia

to Rosecler, Paulo Felipe and Julia Christina

...all of my love to you.

AN INVESTIGATION OF

THE EFFECTS OF SHEARFREE DEFORMATION AND

THE ROLE OF MISCIBILITY ON THE STRUCTURE AND

PROPERTIES OF IN SITU THERMOPLASTIC COMPOSITES

by

Jose Paulino de Souza

Dr. Donald G. Baird, Chairman

Chemical Engineering

(ABSTRACT)

Injection Molding

The effects of partial miscibility on the mechanical properties and morphology of thermotropic liquid crystalline polymer blends were investigated in this part of the work. Blends of an immiscible (Vectra A900) and partially miscible (HX1000) thermotropic liquid crystalline polymer (TLCP) with a polyetherimide (PEI) were used in the investigations. The blends were injection molded into mini-tensile bars and rectangular plaques, and their mechanical properties were evaluated. Interfacial, rheological, and morphological properties along with molecular orientation analysis were carried out in order to explain the mechanical properties of the blends. Mechanical tests showed that both the tensile and flexural modulus deviate positively from the law of mixtures. However, for the PEI/HX1000 system the deviation from the law of mixtures appeared at lower TLCP concentrations compared to the PEI/Vectra A900 system. It was found that the tensile modulus correlated well with the structure developed during injection molding. Morphological tests show that finer higher aspect ratio TLCP fibers developed in the PEI/HX1000 system relative to the PEI/Vectra A system. In addition, both blends showed a maximum in the tensile modulus at 90 wt% TLCP. Rheological tests indicated that for TLCP-rich compositions, a higher viscosity was observed for the blends in comparison to the neat TLCPs. Therefore, due to a greater viscosity, higher magnitudes of

stresses, consequently inducing a higher degree of molecular orientation, were experienced by the blends relative to the neat TLCPs. Although partial miscibility seemed to affect more strongly the stiffness of the in situ composite, the ultimate properties of the TLCP strongly dominated the ultimate properties of the PEI/TLCP composite. Mechanical tests showed that the ultimate properties of Vectra A were at least twice those of HX1000. Consequently, for TLCP-rich compositions, higher values of toughness, elongation at break and tensile strength were observed for PEI/Vectra A blends compared to PEI/HX1000 blends. The study presented here seems to suggest that the selection of a TLCP to reinforce a polymeric matrix is not only dependent upon whether partial miscibility or compatibility between the TLCP and matrix polymer exist, but also on the mechanical properties of the TLCP.

Shearfree Elongational Deformation

The effects of uniaxial, planar and biaxial deformations on the morphology and mechanical properties of bends of a polyetherimide with thermotropic liquid crystalline polymers were investigated in this part of the work. Extruded sheets and molded plaques of PEI/Vectra A and PEI/HX1000 blends were used in the studies. In the case of injection molded plaques, in which the initial morphology was that of fibers and droplets, the direction of the applied deformation relative to the initial direction of the TLCP fibrils was an important factor in affecting the resultant morphology and corresponding mechanical properties of the blends. If the direction of the applied uniaxial deformation was parallel to the initial fiber direction, the deformation tended to increase the average aspect ratio of the TLCP fibers and mechanical properties were enhanced along the direction of deformation. However, if the deformation was applied transverse to the initial fiber direction, the fibers tended to follow the deformation and a 90° rotation was observed. In terms of mechanical properties, an increase in the transverse direction properties accompanied by a reduction in the flow direction properties followed the

realignment of the fibers. In addition, equal flow and transverse mechanical properties appeared at 0.5 units of transverse uniaxial strain. Planar deformation led to the spreading of the fibers in the plane of deformation and a ribbon-like morphological structure developed. However, at comparative magnitudes of planar strains, transverse planar compression tends to promote a greater spreading of the fibers relative to planar compression applied parallel to the initial direction of the fibers. In addition, planar stretching applied in a direction perpendicular to the initial direction of the TLCP fibers was effective in reducing the mechanical anisotropy of the molded plaques. Samples showing equal flow and transverse properties were obtained when planar strains greater than 0.5 units were applied in a direction perpendicular to the initial direction of the fibers. In the case of extruded sheets, in which the initial morphology was that of drops, it appeared that partial miscibility was an important factor in affecting the final morphology of the sheet. For the immiscible PEI/Vectra A system, longer and more stable TLCP fibrils were found compared to PEI/HX1000 system. It is believed that, due to lower interfacial tension, stress induced fiber breakup occurred during stretching of the PEI/HX1000 blend.

Thermoforming of In Situ Composites

The use of in situ thermoplastic composites based on blends of a polyetherimide with an amorphous and a semicrystalline liquid crystalline polymer in the thermoforming process was explored in this part of the work. Injection molded and extruded samples, in which the initial morphology of the dispersed TLCP phase was either in the form of fibers or droplets, were subjected to thermoforming. It was found that in the case where the initial morphology of the dispersed TLCP phase was that of droplets, the elongational stresses generated during forming were capable of deforming the TLCP phase into fibers, and the aspect ratio of the fibers was increased with depth of draw. However, when the initial morphology of the the TLCP

phase was in the form of fibers, then the relative alignment of the fibers with respect to the forming direction was an important factor in affecting the final structure of the TLCP phase in the formed tray. When the fibers were aligned parallel to the forming direction, the elongational strains generated during forming tended to further increase the aspect ratio of the fibers. In the case where the initial TLCP fibers were aligned transversely to the forming direction, the fibers tended to spread into a ribbon-like structure after forming. Pre-stretching of the samples prior to thermoforming tended to contribute to an increase in the aspect ratio of the TLCP fibers. As a result, an enhancement in the deflection resistance of the pre-stretched/formed samples was observed. In situ thermoplastic composites seemed to be advantageous compared to glass reinforced thermoplastics in thermoforming applications. The elongational stresses generated during forming tended to deform the TLCP phase into a specific morphology. Depending on the relative direction of the deformation, either fibers or a ribbon-like structure may be developed. This is in contrast to glass reinforced PEI, in where breakage of the glass fibers occurred upon forming, which may contribute to a reduction in the mechanical performance of glass reinforced materials.

Acknowledgements

The author wishes to express his sincere appreciation to his advisor, Professor Donald Baird, for his support, guidance and criticism along the course of this work. It is very doubtful whether this work could be accomplished without his support. The author wishes to extend his appreciation to Professor Wilkes, for his interest and suggestions which were very important to the completion of this work. He also extends appreciation to Professors Conger, Davis and Loos for serving in his advisory committee. The use of Professor Wilkes' laboratory for much of the morphological investigations is greatly appreciated.

The author wishes to express his most sincere appreciation and gratitude to his wife Rosecler de Souza who gave up her career to follow him in the pursuit of his dreams. The author would never made it this far without her constant support and love. It was always comforting to come home to the same arms that have embraced and loved him for over ten years now.

The author would like to express his sincere gratitude to his parents, Jose Joao and Noemia de Souza, for always standing behind him for all this years. The author is very thankful for all the encouragement and love they have provided him along the years. Right words spoken at the most crucial moments made all the difference in his life.

The author would like to extend his appreciation to Dr. John Ballweg, president of the Partners of the Americas Program, who made possible, through the Atlantic Richfield Foundation Scholarship, his attendance at Virginia Tech. The author extends his appreciation to Ms. Nell Doss for all the love and affection given to his family. The author and his family feel very fortunate to have such wonderful friends.

The author thanks the following people whom in their own special way have contributed to the accomplishment of his goals:

- Dimitris Collias and Tina Handlos for their many hours of SEM's and also for making sure that all those hours were logged in correctly.
- To all members of Professor Baird's research group, past and present without any exception, for providing entertainment, motivation and also for riding along our very own special rollercoaster.
- Don Brandom for his contagious enthusiasm and also for being such a swell working partner (not to mention the amounts of underground DSC work).
- Billy Williams for turning into steel most of the author's sketchy ideas and, more importantly, for being such a passionate racing fan (God bless the Fords).
- Wendall Brown for always providing a good helping hand.
- Diane C., Sandy, Carol and Diane P. for their help and occasional encouragement.
- Dr. Kenn Gardner at DuPont's experimental station for helping with the X-ray work.
- The Center for Innovative Technology of Virginia for providing financial support.
- Anybody else who the author might have inadvertently forgotten to mention.

Original Contributions

The author regards the following as his original contributions:

1. The development of a thermoforming process, referred to as *Stretch-Thermoforming Process*, in which controlled uniaxial strains are applied to the blank to generate reinforcing fibers of a liquid crystalline polymer in situ just prior to the forming step of the process. The advantage of this method is that it not only enables the pre-stretching of the sample prior to forming, which may lead to an increase in the aspect ratio of the TLCP fibers, but also the relative direction of the deformations (pre-stretching and forming) may be combined leading to a large range of morphological and mechanical properties variations that can be accomplished with the method.
2. Applying shearfree elongational kinematics to obtain controlled morphologies and mechanical properties of liquid crystalline/thermoplastic polymer blends. For a TLCP/polymer blend showing an initial morphology of the TLCP phase in the form of droplets, the droplets would deform into reinforcing fibers upon uniaxial elongation, spread into a ribbon-like structure upon planar deformation and deform into a disc-like structure upon biaxial elongation. When the initial morphology of the TLCP phase in the blend is that of fibers then the direction of the applied deformation relative to the initial

direction of the fibers becomes an important variable in affecting the final morphology of the sample.

Table of Contents

List of Illustrations

List of Tables

1.0. Introduction

The growing industrial sector creates a continual demand for improved materials that satisfy stringent requirements such as high tensile strength, modulus, thermal conductivity, heat distortion temperature, and lower thermal expansion. These requirements, which often involve a combination of properties not easily satisfied by a single material, can often be satisfied by a composite material, whose constituents act synergistically to fill the needs of an application. For example, fiber-reinforced polymer composites are frequently used today in the aircraft, automobile, and marine industries (1).

Compounding of reinforcing materials such as graphite, carbon, glass or polyaramide fibers with thermoplastic or thermosetting matrices leads to high mechanical strength and stiffness, good environmental resistance, and high dimensional stability properties (2). However, the presence of solid phase reinforcement during processing operations results in a substantial increase in viscosity, and raising the processing temperature to reduce viscosity might cause thermal degradation of the polymeric matrix. Moreover, the high energy requirement increases the costs of the final article. Other problems that can arise from the inclusion of solid phase fibers are the difficulties of achieving a uniform dispersion of the reinforcing material, wearing of the surfaces in relative motion of the processing machinery, and breakage of fibers during the processing operations. In addition, the forming of long fiber

reinforced composites is difficult, and fiber breakage and/or buckling are likely to occur during the forming process, especially around the corners of a mold. For these and other reasons, it would be highly desirable to find an approach in which the reinforcing material would not be present before the processing of the resin, but come into existence during the processing. This could conceivably eliminate the compounding step and reduce overall manufacturing costs.

1.1. In Situ Composites

The addition of short reinforcing fibers to a polymer is a common and important technology for improving mechanical properties. However, the addition of fibers (most commonly chopped glass) to a polymer melt results in many problems. Possibly the most significant are wear on the processing equipment due to abrasion, increase in the viscosity of the molten polymer, and difficulties in compounding (3). Since the glass fibers remain solid during the processing operation and are extremely hard, surfaces in relative motion, such as screw flights and barrels, will wear and need replacement. Even before the machine is sufficiently damaged, product quality may suffer because of drift in the process settings, contamination by metal from the wearing surfaces, and changes in critical dimensions in molds and dies (4). The increased viscosity may also lead to problems by exceeding the operating limits of the equipment, resulting in flash or short shots and freezing off of thin-walled sections in the molded part. Raising the processing temperature to reduce viscosity may lead to problems with thermal degradation of the polymer matrix. In any case, even if the part can be made satisfactorily, the expenditure of energy will be greater. In addition, the compounding step itself presents an extra expense because of the cost of machinery, the time required to perform it, and the cost of maintenance and inventory of various grades with different filler levels.

One possible way to circumvent the processing problems of fiber reinforced polymers is to develop compositions that can be processed as homogeneous melts from which a rigid reinforcing phase develops during processing (3). The in situ formation of the reinforcing species has led to the term *in situ composites* to describe these materials.

An early approach to the formation of in situ composites was the concept of in situ crystallization (5-9). In this approach an additive is introduced into the polymer, melted at the processing temperature, and crystallized into elongated crystals as the polymer cools. However, this approach failed to offer any significant advantage relative to fiber reinforced systems. The weak van der Walls forces that bond the crystals together prevent the use of organic crystals as reinforcing additives to high performance composites.

An extension of in situ crystallization is the concept of in situ polymerization (10-15). Here the idea is to form needle-like crystals of a monomeric species during processing, and then to polymerize the monomer to a highly oriented fibrous polymer. A composite using this approach was patented on the basis of control of the thermal expansion coefficient made possible by this technique (16). However, in situ polymerization offers little, by way of versatility, to property enhancement relative to fiber reinforced systems.

A more recent and promising approach in the development of in situ composites is to use fiber forms of thermotropic liquid crystalline polymer (TLCP) to reinforce thermoplastics (3,17-22). The genesis of the idea of self-reinforcing a polymer by the addition of a TLCP lies in the ability to melt process these blends in such a way that the TLCP forms a fibrillar reinforcing phase during processing (23). These systems are unique in that the reinforcing LCP fibers are generated during processing rather than added in a separate step as in the case of both short and continuous fiber reinforced thermoplastics.

In situ thermoplastic composites may exhibit mechanical properties as high as those of short fiber reinforced thermoplastics (4). For example, injection molded tensile bars (ASTM D638) of polyetherimide (PEI) reinforced with 30 wt% glass fibers show a tensile modulus of the order of 10 GPa (82). PEI/TLCP in situ composites may show values of tensile modulus as high as 12 GPa at 30 wt% TLCP concentration when injection molded into mini tensile bars

(ASTM D638 type 5) (61). This represents a fourfould increase relative to the modulus of the neat PEI (3 GPa) (82).

Before any further comments are made about this novel technique, some general introductory remarks about liquid crystalline polymers are necessary.

1.2. Liquid Crystalline Polymers

In the last section the need for the development of in situ polymeric composites was presented. The addition of a solid phase reinforcement into a polymeric material results in improvement of the polymer's mechanical properties. However, as was shown previously, the presence of a solid phase reinforcement makes the processing of such systems very difficult and energy intensive. Some of the early approaches to the development of in situ composites were also presented. This section will present some introductory remarks about liquid crystalline polymers, which have shown outstanding mechanical properties upon processing and great potential in the development of self-reinforcing in situ composites.

The liquid crystalline phase can be observed in certain organic compounds that possess rigid molecular segments. This is a phase which is intermediate to the solid crystalline and the isotropic liquid phases. A liquid crystal can flow like an ordinary liquid, but other properties, such as birefringence for example, are reminiscent of the crystalline phase (24). This combination explains the name liquid crystal. Other names in use to describe a liquid crystalline phase are *mesophase* and *mesomorphic phase.*

In this mesophase, the molecules are aligned in a preferred direction, defined by the director. Different types of mesophases can be distinguished. The most familiar are (25,26): nematic (molecules that possess only orientational order), smectic (molecules that possess orientational and positional order) and cholesteric (local scale ordering similar to nematic, but

on a larger scale the structure appears to be formed by twisting a series of parallel nematic layers, resulting in a periodic helical structure).

LCPs can be divided into two main categories: lyotropic (LLCP), in which a mesophase is formed in solution at a certain concentration level, and thermotropic (TLCP), in which a mesophase is formed above the crystalline melting point. LLCPs are usually wholly aromatic polymers and consequently very rigid. The intermolecular interactions in the solid state are so strong that these polymers do not melt before degradation occurs, so that they can only be processed from solutions (83).

The practical application of LLCPs came with the development of high strength and stiffness fibers, 2.8 GPa and 124 GPa respectively, of poly(phenylene terephthalamide) PPTA, which is spun from concentrated sulfuric acid solutions in the lyotropic state (84). The development of these fibers probably provided most of the early incentives on the research of thermotropic LCPs such as aromatic polyesters which could be processed in the melt state, unlike LLCPs..

One of the first TLCPs synthesized was a copolymer of ethylene terephthalate and p-hydroxybenzoic acid (28). It was followed by the development of many other classes of TLCPs (29-31). To lower the melting point below the degradation temperature, chain stiffness and/or molecular interactions are reduced by the introduction of a flexible spacer, such as ethylene terephthalate.

The mechanical properties of TLCPs are inherently lower than those of LLCPs because of reduced chain interactions. However, most of these materials can be spun into high strength/high stiffness fibers (32-39) with typical tensile modli values in the range of 40-100 GPa and tensile strengths of up to 1 GPa. They can be injection molded into stiff parts (40-42) with tensile moduli of over 20 GPa and can even be blow molded (43). Table 1.1 presents a comparison of fiber strength and moduli of some typical high performance fibers (44). Included in this Table are data for the Spectra 900 fibers which are based on polyethylene (PE) manufactured by Allied-Signal, using a specialized gel spinning process. The SNIA fibers are also PE fibers made by Celanese using a specialized drawing process. It is clear that fibers made

from flexible chain polymers have properties comparable to those of LCP fibers. However, the LCP fibers can be processed by normal melt spinning process rather than the elaborate and complex methods used for PE.

Interest in thermotropic LCPs has grown in recent years due not only to their inherently high stiffness and strength, but to the large range of properties that these materials can offer, such as high use temperatures, excellent chemical resistance, low melt viscosity, low coefficient of thermal expansion, good dielectric properties and heat stability (45). However, despite extensive research and development and several recent commercializations, LCPs currently find relatively few established commercial markets. The material tends to be expensive, due primarily to high monomer costs. LCPs have enjoyed great success not in applications requiring high modulus and stiffness, but rather in the production of intricate moldings in which the ability to fill the mold and the dimensional stability of the molded part are the crucial specifications. Moreover, due to their excellent dielectric properties, LCPs have also found applications in the electronic industry in products such as connectors and circuit boards (46).

1.3. TLCP polymer blends

In the previous section some of the features associated with thermotropic liquid crystalline polymers were discussed. As was shown, these materials can be processed in conventional polymer processing operations into parts with excellent stiffness and strength. For example, fibers with high stiffness, in the range of 40 to 100 GPa, can be obtained by the conventional spinning process of TLCPs. It was also mentioned that despite their inherently high mechanical properties, the cost of such specialized polymers inhibits a more widespread application of LCPs.

Table 1.1. Comparison of fiber strengths and moduli of some typical high performance fibers (44).

	SPECTRA 900	SNIA‡	ARAMID	LPC‡‡
Tenacity (G/D)	30	13	22	22
Tensile Strength (10 × 3 psi)	375	163	400	358
Tensile Strength (GPa)	2.6	1.2	2.8	2.5

‡ Special drawing of PE.
‡‡ Vectran liquid crystal fiber.

	SPECTRA 900	SNIA	ARAMID	LPC
Tensile Modulus (G/D)	1400	700	1000	600
Tensile Modulus (10 × 6 psi)	17	8.5	19	9.0
Tensile Modulus (GPa)	117	58	124	60

SPECTRA 900 fibers are manufactured from gel spinning of PE.
SNIA fibers are manufactured utilizing special drawing of PE.
ARAMIDE fibers are manufactured from solution spinning of PPTA.
LPC fibers are the Vectran liquid crystal fibers.

Blending TLCPs with other thermoplastics offers the opportunity to exploit many of the LCP's desirable characteristics, such as high stiffness and strength. Furthermore, using LCPs as blends with other thermoplastics might also help to reduce material costs. The use of TLCPs in blends with flexible chain polymers is discussed in this section. As will be shown, the addition of a liquid crystalline phase to a flexible chain polymer may enhance the mechanical properties of the hosting resin at levels comparable to short glass fiber reinforcement. Furthermore, TLCP/polymer blends represent a novel and promising technique in the development of in situ thermoplastic composites.

In reinforcing thermoplastics by the addition of a TLCP phase, the thermotropic LCP is dispersed in a thermoplastic matrix in a conventional mixing step and in a subsequent processing step involving strong shear or preferably extensional flow, the TLCP domains are elongated into fibrils that reinforce the matrix in a fashion analogous to inorganic fibers (47). Thus, the reinforcing TLCP fibrils are formed in situ during processing. In this manuscript the term in situ composites wil be used solely in the case of TLCP/thermoplastic polymer blends.

To better illustrate what is meant by an in situ composite, Figure 1.1 shows a scanning electron micrograph (SEM) of a blend containing polyethyleneterephthalate (PET) and hydroxybenzoic acid/hydroxynaphthoic acid (HBA/HNA) based thermotropic copolyester (commercially available as Vectra A 900) at a composition ratio of 70/30 w/w (48). This blend was extruded, using a dual extruder mixing process (48), through an 18-element static mixer. The extruded strand was then etched in n-propylamine for 40 hs to remove excess PET phase. A rather dramatic aspect of the remaining Vectra A 900 phase is the formation of continuous fibrils, infinite in aspect ratio. This very striking characteristic of a thermotropic liquid crystalline polymer, fibrillation upon certain processing conditions, has given TLCPs great potential as reinforcing species for thermoplastic polymers. As a quick illustration of such a capacity, the strands of the blend mentioned above (PET/Vectra A 900 70/30) revealed a tensile modulus of 5.45 GPa compared to the modulus of the neat PET of 1.87 GPa, or, an improvement relative to the pure PET of about 300%. The draw ratio of such strands was about 2.5 (48).

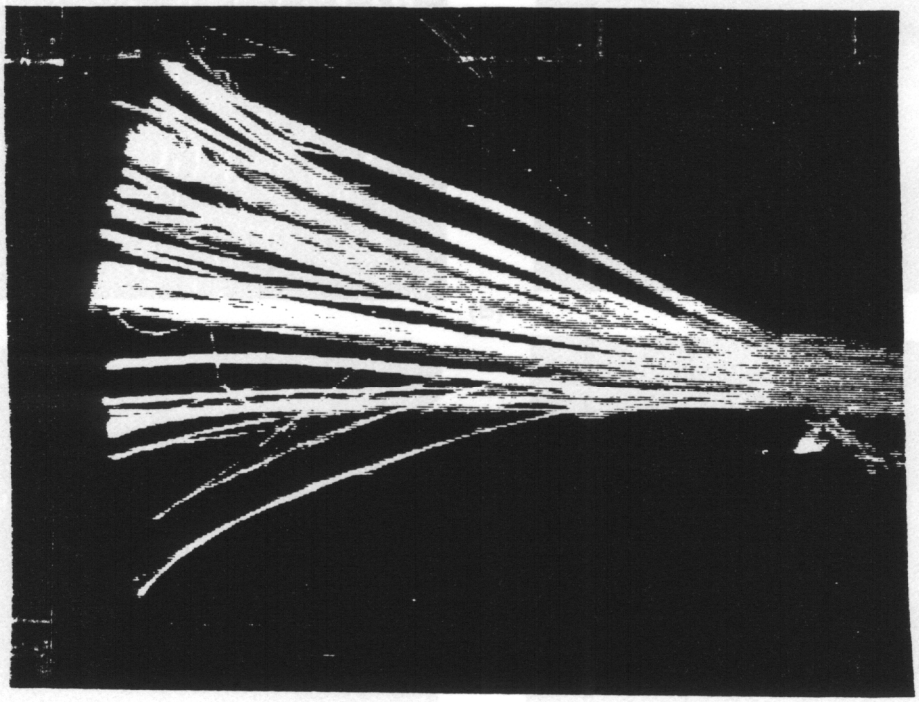

Figure 1.1. Photograph of the residue of a PET/Vectra A 900 70/30 w/w strand extruded utilizing a especiallized dual mixing process (48) etched in n-propylamine for 40 hours. Length of the sample is about 5 cm.

In general, as will be shown in the following section, drawing or stretching of the blend extrudates results in the formation of LCP microfibrils that are highly oriented in the direction of stretch (49-51). Increased orientation of the dispersed LCP microfibrils formed by drawing can result in greatly improved mechanical properties (50-53). For instance, strands of PET/Vevtra A900 blends at a 70/30 wt% composition ratio revealed an almost fourfold increase in the tensile modulus (from 5.45 to 18.99 GPa) on increasing the draw ratio from 2.5 to 50 (48).

In summary, thermotropic liquid crystalline polymers can form reinforcing fibrils under certain processing conditions in blends with flexible chain polymers. Extruded strands of a PET/LCP blend at 70/30 w/w concentration ratio showed a 300% increase in the tensile modulus relative to the neat PET, and LCP fibrils, infinite in aspect ratio, are observed after extrusion through an 18-element static mixer. The ability of TLCPs to form reinforcing fibrils can be strongly improved by the application of an external elongational flow field, such as post extrusion drawing.

1.4. Mechanical Properties of In Situ Composites

One of the primary objectives of blending thermotropic LCPs with thermoplastic polymers has been to use the LCP as reinforcement for the flexible chain polymers. Mechanical properties of TLCP/polymer blends have been reported in a number of studies (17-22,47-54). However, although fibrillation of the LCP domains is necessary for the LCP phase to act as a reinforcement, especially attained by post extrusion drawing, molecular orientation within the LCP phase is required before significant improvement in physical properties can be achieved (23). In a recent publication Weiss et al. (55) reported results for blends of polycarbonate (PC) with a thermotropic copolyester based on 52 mol% HBA, 28 mol% HNA, and 10 mole% terephthalic acid (TA). An improvement of the modulus on the order of six times (7.0 GPa versus about 1.2 GPa) was obtained with as little as 20 wt% LCP,

but the draw ratio was about 1000. The properties of the filaments obeyed the rule of mixtures for long fiber composites, while the properties of compression molded samples obeyed the rule of mixtures for particulate composites. The modulus of the blend at 60 wt% LCP was 15 GPa or about half of that obtainable with the neat LCP.

Further support for the importance of drawing to the enhancement of the mechanical properties of a TLCP base in situ composite was given by several workers (18,50,56). Baird and co-workers (50,56) generated films based on blends of several engineering thermoplastics, including polyetheretherketone (PEEK), polyphenylenesulfide (PPS), and polyetherimide (PEI), with a variety of LCPs. In general, concentrations of LCP were in the range of 20 to 30 wt% and draw ratios as high as 50 led to films with moduli in the range of 14 GPa. However, the properties of the drawn films were highly anisotropic with transverse properties about those of the matrix polymers.

Injection molding of TLCP-based in situ composites has also received considerable attention in the literature (57-60). Several studies reported significant improvements in mechanical properties of injection molded samples based on blends of LCPs with engineering thermoplastics. Isayev and co-workers studied the injection molding of blends of several engineering thermoplastics with a thermotropic LCP. They used PEEK (57), PEI (58), PPS (59), and polycarbonate (PC) (60) as the matrix materials, and HBA/HNA as the reinforcing LCP. Some studies revealed a very interesting synergism in mechanical properties (57,58,60). Particularly, elastic moduli were above those predicted by the rule of mixtures at a LCP concentration as low as 5% (60). In the case of PEEK/LCP (57) a positive deviation of the modulus from the simple rule of mixtures was observed with the modulus passing through a maxima at about 75 wt% LCP (the maximum value was about 15 GPa). Impact and tensile strengths also passed through a maxima at 75 wt% LCP. However, by means of differential scanning calorimetry (DSC), the polymers were found to be immiscible over the entire composition range. Isayev and Swaminathan have compounded, in one example, PEI/LCP, at a 10 wt% increasing LCP concentration up to 70 wt% LCP, and again, both modulus and strength showed a maximum at 70 wt% LCP concentration (58). Both systems (57,58) were com-

pounded prior to injection molding by either extrusion through a Koch six elements static mixer adapted at the exit of a single screw extruder (57,58) or by using a twin screw extruder (58). They also found that the degree of anisotropy in the dynamic storage modulus, G′, machine versus transverse direction properties, incresed with LCP concentration (57).

It has also been reported that the mechanical properties of in situ reinforced composites approach that of conventional short-fiber reinforced composites (46). Recently, Baird and co-workers (61) have compared the mechanical properties of in situ and short glass fiber reinforced PEI. A summary of their findings is presented in Table 1.2 for a selected reinforcing concentration of 30% w/w of either LCP or glass fibers. The properties for the in situ composites were obtained from injection molded tensile bars (ASTM D638 type 5), and the data for the glass fiber reinforced PEI were obtained from the supplier literature. They used several thermotropic LCPs, encompassing a wide span of chemical structures and processing temperatures to obtain the in situ composites (refer to Table 1.3). Some of the TLCPs used are proprietary and the chemical composition was not disclosed by the authors. As Table 1.2 shows, the LCP reinforcement was able to raise the tensile modulus of PEI as much as glass reinforcement. Furthermore, in one case, PEI reinforced with HX 4000, the tensile modulus of the in situ composite, was superior to that of PEI reinforced with glass fibers. However, not all LCP/polymer blends shown in Table 1.2 exhibited a significant gain in the properties relative to pure PEI. This suggests that the improvement in the mechanical properties of a LCP/polymer blend relative to the properties of the neat matrix polymer is dependent upon the inherent properties of the LCP used in the composite.

In summary, TLCPs can lead to a significant improvement in the modulus of films and fibers, but high draw ratios are required. However, the transverse properties of these films are significantly lower than those along the machine or draw direction. In the case of injection molding, there are situations in which the properties of the blend show a positive deviation from the rule of mixtures and even pass through a maximum as a function of composition. In general 20 to 30 wt% LCP is needed to provide a modulus comparable to that of glass filled systems, depending on the LCP used.

Table 1.2. Mechanical Properties of PEI based composites with 30% w/w reinforcing load of either LCP or glass (61).

	Tensile Modulus (GPa)	Tensile Strength (MPa)	Elong. Break (%)
PEI	3.0	100	60
PEI/glass	8.9 - 11.0	172 - 196	2 - 5
PEI/Vectra A900	5.2 - 6.5	128 - 140	3.2 - 5.3
PEI/HX 1000	8.1 - 9.3	125 - 134	1.6 - 1.2
PEI/HX 4000	10.8 - 11.6	142 - 170	1.7 - 2.1
PEI/Granlar	8.5 - 9.5	123 - 135	2.0 - 2.2

Table 1.3. Thermotropic Liquid Crystalline Polymers (61).

COMPOSITION	TRADE NAME	SUPPLIER	Tg (°C)	Tm (°C)
HBA/HNA 73/27	Vectra A 900	Hoechst-Celanese	105	285
PROPRIETARY	HX 1000	DuPont	187	
HQ/PHQ/TPA	HX 4000	DuPont	179	311
PHQ/PEHQ/TPA 1/1/2	Granlar	Himont	155	311

HBA = p-hydroxybenzoic acid
HNA = 2-hydroxy-6-naphthoic acid
HQ = hydroquinone
PHQ = phenyl hydroquinone
TPA = terephthalic acid
PEHQ = phenyl ethyl hydroquinone

1.5. Advantages of In Situ Composites

In the previous section it was shown that LCPs have the ability to reinforce thermoplastics at least to the degree found for fiber reinforcement (61). With this in mind one wonders whether there are any advantages to using LCPs as reinforcement for thermoplastic materials. In this section, a number of advantages in using LCPs as a means to reinforce thermoplastics are discussed.

In the last section it was shown that the addition of 20 to 30 wt% LCP is needed to provide a tensile modulus for the in situ composite comparable to those of fiber reinforced systems. However, in the case of glass reinforcement, one is limited to a maximum load of the solid phase reinforcement of up to 40 wt% (61). This is because processing of higher loading glass reinforcement would be extremely difficult and costly. On the contrary, in the case of LCP reinforcement these limitations no longer exist. An in situ composite could be processed at any loading of TLCP with no processing difficulties.

Another advantage of in situ composites relative to fiber reinforced materials concerns the surface appearance of an injection molded part (61). The surface of a part molded of glass reinforced materials appears very rough and dull. The flow lines and fiber splay are quite visible. On the other hand, with in situ composites such as PEI/Vectra A900 blends a very homogeneous surface with no flow marks nor segregation of phases results. The surface appears very smooth and glossy compared to fiber reinforced materials.

Fiber reiforced thermoplastics are difficult to form because they lack melt strength and pliability. Furthermore, fiber breakage and/or buckling are likely to occur during the forming process, especially around the corners of a mold. An opposite behavior is observed in the case of in situ composite. In situ composites, such as PEI/Vectra A 900 blends possess enough melt strength and pliability to withstand the drawing process (62), and further drawing of the in situ composite enhances molecular orientation within the LCP phase (50), which may result in parts with improved mechanical properties. Therefore, in situ composites have two

advantages over glass reinforced systems undergoing thermoforming. They have higher melt strength and pliability to withstand the drawing force, and they may orient even further after drawing (50), which may improve the mechanical properties of the formed part.

TLCPs can display apparent viscosities a decade or two lower than conventional engineering thermoplastics. The data in Figure 1.2, which is quite typical, shows that the addition of TLCP can reduce melt viscosities (at a shear rate 150/sec) of TLCP/PC blends by nearly two decades over the entire composition range (63). The addition of only 5 to 10% TLCP lowers the viscosity by 54 and 75%, respectively. Thus, TLCPs can serve as effective flow aides, even at rather low concentrations. Such a behavior is in contrast to glass reinforcement, where the viscosity increases.

Another advantage is that in situ composites can be more readily recycled than glass fiber reinforced systems (46). The LCP fibers can be remelted and the reinforcing LCP phase regenerated on processing. In the case of glass reinforced materials there is a continuous reduction of the glass fibers aspect ratio due to fiber breakage during grinding which consequently reduces reinforcing effectiveness.

In summary, in situ composites offer great potential to surpass short glass fiber reinforced systems not only in applications where mechanical properties are at stake, but also offer improved surface appearance. In situ composites may be suitable in equipment where glass fibers are not, such as thermoforming, compression molding, and film and blow molding (46). Such an advantage is quite remarkable when compared to fiber reinforced materials that have limited processing applications, such as injection molding and sheet extrusion.

1.6. Limitations and Shortcomings

The first and most serious problem encountered in using LCPs as reinforcements for thermoplastic polymers is that the LCP domains, due to the rod-like nature of their chains,

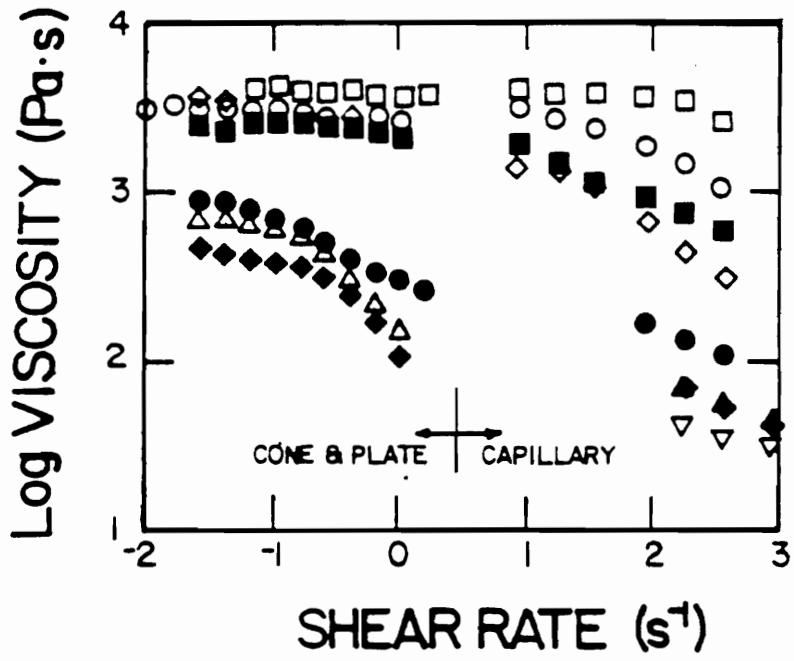

Figure 1.2. **Viscosity versus shear rate data for LCP/PC blends at 270°C. (□) 0%, (○) 5%, (▪) 10%, (◇) 20%, (•) 40%, (△) 60%, (▲) 80%, (▽) 100% LCP (63).**

become highly oriented in the flow direction, producing materials with high mechanical anisotropy (64). The rod-like nature of their chains gives LCPs the ability to form highly oriented domains in the presence of an external strain field. This preferred flow orientation results in a rather high degree of mechanical anisotropy in LCPs and LCP/polymer blends.

An illustration of such mechanical anisotropy is presented in Figure 1.3 (81). Blends of PEI/HX 4000 and PEI/HX 1000 were injection molded into rectangular plaques from which rectangular strips were cut along and perpendicular to the injection molding flow direction. Subsequently, flexural moduli were measured according to ASTM D 790 in both directions. The flexural moduli for PEI/HX 4000 and PEI/HX 1000 blends in the transverse direction are much lower than those in the machine direction. They all lie in the range of 2 to 3 GPa regardless of blend composition. The transverse moduli of the blends are almost the same as that of the unreinforced PEI. Such a difference in the flexeral moduli can be attributed to the strong flow orientation attained by the LCP domains during the injection molding process (65).

The mechanical anisotropy developed during the processing of TLCP/polymer blends is a consequence of the strong flow direction orientation attained by the LCP domains present in the blend (65). The mechanical anisotropy of injection molded parts made from neat LCPs is shown in Figure 1.4 (64). The liquid crystalline polymer used in this study was a thermotropic copolyester containing 60 mole% PHB and 40 mole% PET. As one further notices, mechanical anisotropy, evaluated as flow and across directions of flexural moduli, can be strongly reduced, eventually become biaxial, by increasing the thickness of an injection molded part. Such behavior can be explained on the grounds of morphological structuring attained by the part during the injection molding process (65). A more detailed explanation of the morphology development during the injection molding process is deferred to the literature review section.

In addition to mechanical anisotropy, another shortcoming is associated with the use of TLCPs as reinforcement for thermoplastic materials. Fibrillation of the LCP domains in a blend can only be attained under favorable processing conditions, such as viscosity ratio and applied stress field (23). The viscosity ratio of the reinforcing LCP phase to the hosting matrix

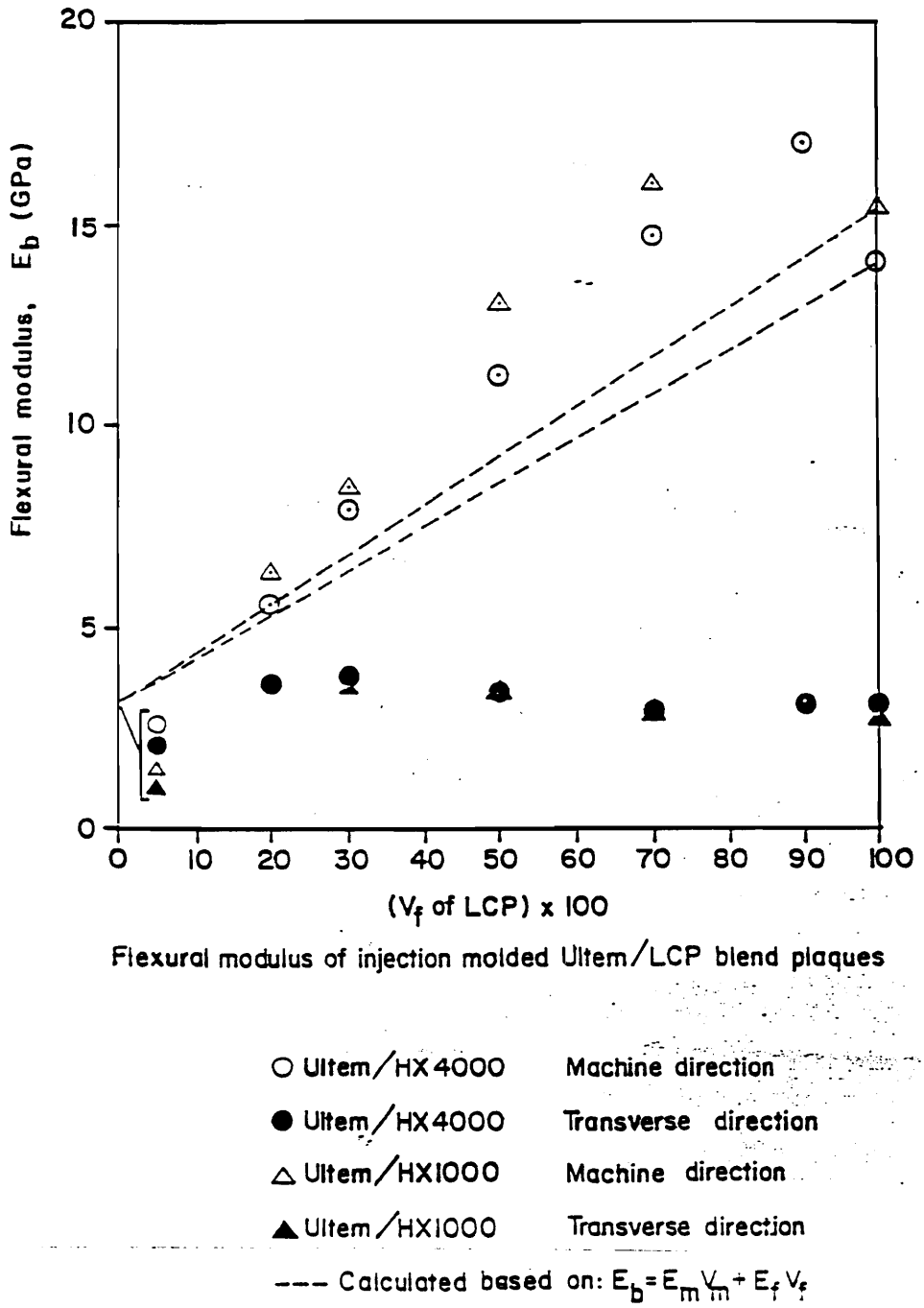

Figure 1.3. Flow and transverse directions flexural moduli of injection molded PEI/LCP blends as a function of LCP concentration (81).

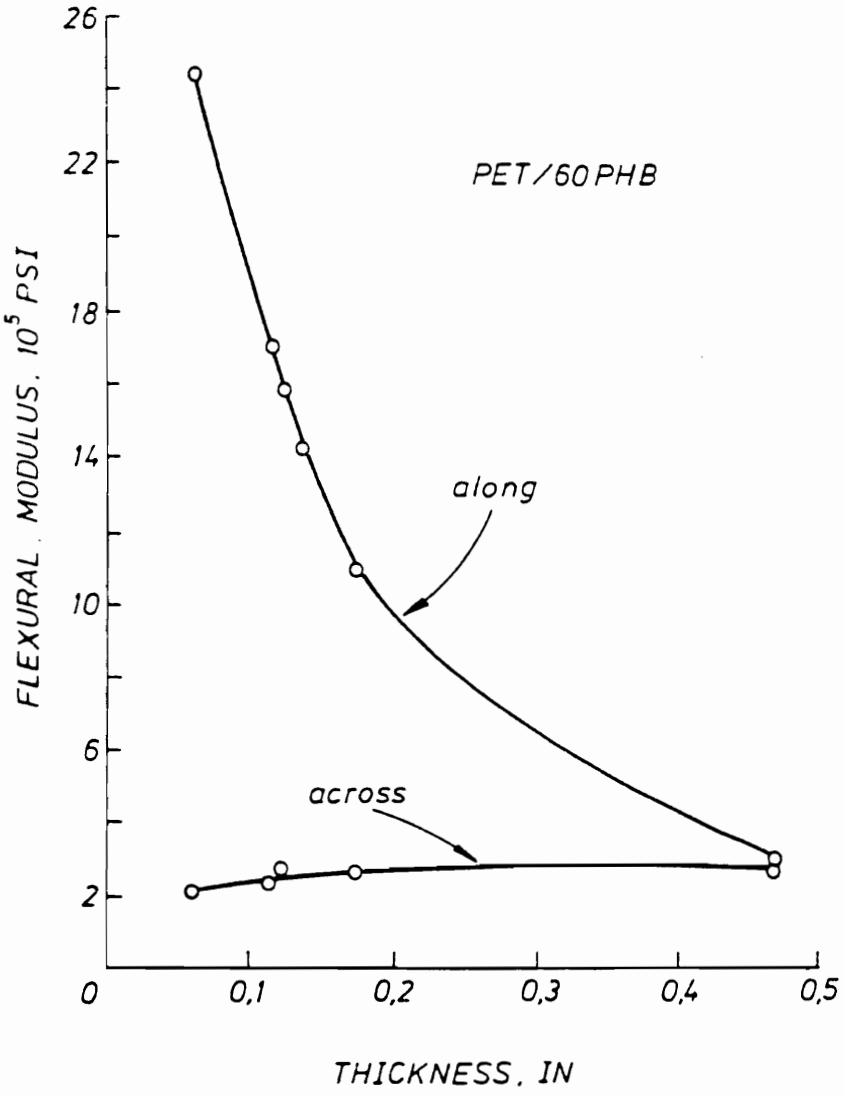

Figure 1.4. Effects of thickness on along- and across-the-flow flexural modulus of PHB/PET thermotropic copolyester (64).

polymers must fall as closely as possible to unity (23). This problem has been investigated by several researchers (66-70). Nobile et al. (67) have addressed the effects of the viscosity ratio on fibrillation in PC/LCP60 blends containing 10 wt% of LCP60 (LCP60 is the 60 mole% PHB and 40 mole% PET thermotropic copolyester). Fibers were melt spun in a Rheoscope 1000 provided with a capillary die (L/D = 10) and melt spinning unit. The blends were melt spun at 220°C and 260°C. Both optical as well as scanning electronic microscopies showed that the LCP fibrils developed only at the lower drawing temperature (220°C), whereas at 260°C the LCP phase remained as spherical droplets. A lower viscosity of the PC at higher temperature was thought to be incapable of deforming the LCP domains which consequently remained as droplets. The authors concluded that the viscosity ratio between the LCP60 and PC was the determining factor for the fibrilltion of the LCP domains to occur.

Another limitation associated with thermotropic LCPs is that they have high melting temperatures. This results in rather high processing temperatures, which are often near or above the thermal degradation of most thermoplastics (especially commodities resins). Also, the presence of an LCP dispersed phase frequently results in low viscosity of the blend at the processing temperature. On one hand, this reduction in viscosity is welcomed in terms of energy savings but, on the other hand, it leads to low melt strengths, making processing such as extrusion and blow molding difficult, and any post-extrusion drawing nearly impossible for some LCP/polymer blends.

1.7. Research Objectives

Extensive work has been done to formulate an in situ composite. Workers have thus far been successful in detailing certain features of these systems. Reduction of the system viscosity upon addition of the LCP (63,71-77), and enhancement of mechanical properties in

the machine direction (17-22,47-54) are apparently the most common findings of the investigations.

However, most work in this area has been repetitive without adding any substantially new information. Consequently, many problems and unanswered questions remain regarding the development of these complex systems. For instance, the effects of miscibility and interfacial surface tension on the morphology and consequently the properties of the in situ composite have not received adequate consideration in the literature. Studies of droplet deformation have thus far considered only the deformation of a single droplet in a sea of a molten polymer, mostly of the times considering only the deformation of a single Newtonian droplet in a Newtonian fluid (78-80). The effects of the discrete phase concentration on droplet deformation are most often completely ignored. The effects of LCP concentration in a blend on the fibrillation of the LCP domains, and consequently the final morphology of the composite, have still not received proper attention in the literature.

It has been recognized that extensional flow fields are more effective in imparting fibrillation to the LCP domains relative to shear deformations. The extensional flow fields studied thus far reflected only uniaxial deformation imposed on the system after melt extrusion of the composite. Several investigations (18,50,56) can be found which deal with post-extrusion drawing of in situ composites as a means of introducing orientation to the LCP domains. What still remains unclear is the effect of shearfree flow fields on the final morphology of the in situ composite. For instance, what would be the effect of planar and biaxial deformations on the final morphology and properties? Moreover, what processing operations would give us the same morphology as those achieved by extensional deformations, and, furthermore, can we predict the final performance of the composite by knowing only the morphology attained after processing? These questions need to be thoroughly understood in order to increase the application of in situ thermoplastic composites.

As was shown previously, the most serious problem encountered in using TLCPs as reinforcements for thermoplastic polymers is that the TLCP domains become highly oriented in the flow or draw directions, consequently producing materials with high mechanical

anisotropy. The flow direction properties of a polymer can be greatly enhanced by the addition of an LCP phase, and even, depending on the LCP used, superior to those of glass reinforced polymers. However, the transverse properties of an in situ composite remain almost unchanged with values similar to those of the unreinforced matrix (64). With further increase in LCP concentration, which enhances flow direction properties (64), the mechanical anisotropy of the in situ composite becomes even more pronounced, consequently reducing commercial applicability of such systems.

The main objectives of this research are briefly outlined as follows. A complete discussion of the research objectives is postponed until after the literature review. In essence there are three thrusts to this research. The first goal is to enhance the transverse mechanical properties of the in situ composite, which could reduce the mechanical anisotropy of the system. The second goal is to determine the effects of miscibility between the LCP and the hosting matrix polymer on the morphology and mechanical properties of the in situ composite. Finally, the last goal is to determine the suitability of in situ composites to other processing alternatives, such as thermoforming and compression molding.

The materials used in this research consist of two thermotropic liquid crystalline polymers and an engineering thermoplastic. The TLCPs are Vectra A 900 from Hoechst-Celanese and HX 1000 from DuPont (refer to Table 1.3 for chemical structures). The engineering thermoplastic is an polyetherimide (PEI) from General Electric Plastics. Injection molded plaques and extruded sheets of blends of the above materials are produced.

A brief introduction to the subject of in situ composites was presented in this chapter. Some of the findings of the literature were briefly outlined and the main objectives of this research were given. In the following chapter, the literature review pertained to this research will be presented. At the end of Chapter 2, a detailed presentation of the research objectives will be given.

2.0 Literature Review

Polymer-polymer blending is one the most exciting and promising routes in polymer science to generate novel materials with improved performances from many different polymers. The almost infinite possibility of polymer combinations have created a great flurry in research activities. As a result of the active research pursued in this field, the literature available in such an area is quite abundant from both the theoretical and the experimental view points. Most recently, the topic that has been most widely investigated is the development of self reinforcing blends in which a fibrillar morphology of a dispersed liquid crystalline phase is sought. In this Chapter, a survey of the published literature concerned with the development of thermoplastic in situ composites will be presented.

The aspects of fibrillation of a thermotropic LCP phase in a polymer matrix (self reinforcement of the matrix polymer by the LCP phase) are directly related to the phenomena of the deformation of a fluid droplet (into a cylindrical or thread-like form) suspended in a fluid matrix. Thus, most of the topics reviewed later are directly related to this phenomena. Section 2.1 gives a brief review of the general area of polymer blends along with some of the terminology currently employed. In section 2.2 a thorough review of the fundamental aspects of droplet deformation and break up is presented. Both theoretical and experimental works are presented to establish the current research status of the phenomena. This section will cover

the droplet deformation and breakup phenomena in simple shear and extensional flows and the many possible combinations involving Newtonian and viscoelastic fluids in which both or either represent the matrix and/or the suspended droplet. A brief discussion on the stability of the elongated domains formed by the deformation of droplets is presented in section 2.3. In Section 2.4 some features of Liquid Crystalline Polymers and their use as in situ reinforcement of polymers are presented. Following this, a complete survey of the current status on the research of in situ composites is presented in Section 2.5. Special attention is given to composites that show synergism in the mechanical properties.

The fundamental objective of this research is to develop an in situ composite with a better balance of mechanical properties which will lead eventually to development of a commercially viable product. Thus, in Section 2.6 the literature pertaining to this subject will be critically reviewed. Finally, in Section 2.7 the objectives of this research are presented.

2.1 Polymer Blends: General Concepts

2.1.1 Polymer-Polymer Miscibility

A polymer blend may be defined as any combination of two or more polymers resulting from common processing steps (85). Polymer blends may be qualitatively considered miscible, partially miscible or immiscible, depending on the level of molecular interaction. The parameters that can be used to differentiate between single-phase mixtures and multiphase mixtures are numerous: rheologic, optical, scattering behavior, and mechanical behavior. Most commonly accepted is the glass transition temperature. When a mixture exhibits two glass transition temperatures, it is accepted as a two phase system. When only one glass transition is detected, the mixture is defined as miscible. Partial miscibility may also exist. In this case, a shift in the glass transition temperature of the blend components from their original values will be observed. The mechanical properties of miscible blends (modulus, toughness, strength, etc.) usually vary monotonically with composition (85-87), and are bounded by the properties of its constituents.

A class of polymer-polymer blends which is of more interest to this research is the one involving immiscible systems. In immiscible systems interactions take place at the interface of the blend constituents, and the mechanical properties of such systems are strongly dependent on the structure attained upon processing (88,89). However, the phase structure or morphology is a function of the processing history and the dispersed phase concentration (88-91). Consequently, careful attention should be paid to the selection of the processing parameter and a thorough knowledge of the rheology of the components is necessary to produce a blend with desired properties. Later discussions of the development of in situ composites will bring more clarity to this point.

Very often the term *compatibility* is used synonymously with miscibillity. Compatibility has been used by many investigators of polymer blend behavior to describe systems that are homogeneous and have enhanced physical properties (85). Included in this definition of compatible systems are also those systems exhibiting good interfacial adhesion between the blend components. Thus, by the above definitions, an immiscible but compatible system will provide the most advantage in terms of improved mechanical properties.

A good example of controlled morphology and resultant properties upon processing is the work of Subramanian and Mehra (92). These authors were able to improve the permeability barrier properties of a polyethylene (PE) film by blending it with a polyamide (PA). By controlling the processing conditions, they were able to obtain a film with a laminar stratified morphology of the PA phase at a PA concentration of 20 wt%. Variations during process would change this morphology to a dispersion of PA droplets in the PE matrix which would not show as good barrier properties as the stratified morphology.

The purpose of this section has been to introduce some of the terminology and aspects of polymer-polymer blends. As has been shown, the properties of a immiscible polymer blend can be strongly affect by compatibility between the blend constituents. Further, it has been shown that the morphology attained by the system upon processing plays a major role in determining the system's properties. A discussion of the thermodynamic aspects that govern polymer miscibility will be briefly addressed in the next section.

2.1.2 Thermodynamic Considerations in Polymer Blends

In the thermodynamic sense, two phases can mix only when the free energy of mixing is negative: $\Delta G^m < 0$ (86). This inequality is required but not sufficient, since partial phase separated states can exhibit lower free energies than single phase states. An additional demand is required for a system to be defined as miscible in the thermodynamical sense. When $\frac{\partial^2 G}{\partial \phi^2} > 0$, then the system forms a single phase, otherwise the mixture will phase separate.

Calculation of the free energy of mixing for a polymer-polymer mixture from the combined entropy and enthalpy yields the famous Flory-Huggins equation (93):

$$\Delta G^m = \left(\frac{RTV}{V_r}\right)\left(\frac{\phi_1}{x_1} \ln \phi_1 + \frac{\phi_2}{x_2} \ln \phi_2 + \chi_{12}\phi_1\phi_2\right) \quad (2.1)$$

where: V_r is the reference volume which is taken as close to the molar volume of the smallest repeat unit as possible, ϕ_i is the volume fraction and x_i is the degree of polymerization of component i (i=1,2), with respect to the reference volume V_r, and χ_{12} is the Flory-Huggins interaction parameter. The poor miscibility of macromolecules is clearly depicted by the above equation. Since the molecular sizes are large, the entropy contribution is low, and the macromolecules should be strongly interacting (negative χ) to yield a negative free energy of mixing. Misciblity among polymers must generally be induced through specific interchain interactions resulting in sufficient heat of association, such that the free energy of the polymer pair decreases upon mixing (86).

One of the early attempts to quantify the interaction parameter, χ, for blends involving flexible chain polymers was by the use of the Hilderbrand solubility parameter δ (94,95). When the solubility parameter of a polymer is not readily available, estimations can be performed based upon methods of group contributions. Several authors have devised approaches for performing such calculations (96-99). The estimated value of the solubility parameter can then be used to calculate the interaction parameter, χ. Several authors have used the method of melt point depression more successfully for the determination of χ in crystallizable miscible systems (100).

However, when dealing with blends of rigid rod and flexible chain polymers the situation is more complex. First, liquid crystalline polymers show limited solubility in common solvents, therefore posing an impossibility to the use of the solubility parameter method to the calculation of the interaction parameter χ. Further, the chemical structure of liquid crystalline polymers, when available, is very complex and therefore calculating χ through group contribution techniques can be challenging.

Flory and co-workers (113-118) have used the lattice model theory (119) to derive an expression which would account for the rodlike character of LCPs in a ternary blend involving a rodlike polymer, a flexible chain polymer and a solvent (117). Based upon numerical calculations, they have concluded that due to the low entropy of mixing and high orientability of the rigid component, miscibility between the blend components was thermodynamically unfavorable and phase segregation existed. Further, phase separation increased with increasing the aspect ratio of the rod-like molecule, even at low concentrations of the rigid rod component.

Some thermodynamic considerations regarding the miscibility of flexible chain polymer blends have been briefly reviewed in this section. It has been shown that the determination of the interaction parameter for blends involving liquid crystalline polymer is not so straight forward. A complicating factor is the fact that TLCPs are not soluble in regular solvents which makes impossible the use of solubility parameter to determine interaction. In the next section a discussion regarding interfacial tension in polymer blends will be presented.

2.1.3. Interfacial Tension in Polymer Blends

Since most polymer blends are not miscible because of the thermodynamic reasons discussed above, the interfacial tension of molten polymer systems is a vital parameter in determining the morphology of a blend. Interfacial energy affects the morphology, dispersion, and interphase adhesion of a blend, and ultimately its mechanical properties. Thus, the prediction of the interfacial tension between the blend components is useful in determining whether compatibility will exist. In this section, the method of the harmonic mean theory (101) for the calculation of interfacial tension is presented. Following this, a review of experimental works performed to determine the interfacial tension of TLCP/polymer blends is discussed.

The surface or interfacial tension is, in essence, the energy density of a surface or interface. The theories of Folkes (102), Good (103), and Wu and co-workers [101] describe the

connection of adsorption and wetting with respect to adhesion by the study of interfacial layers using equilibrium thermodynamics (104-110). One example of the application of their theories is given by a liquid droplet on a plane surface. The three phases of the system (liquid (L), solid (S) and vapor (V)) consist of each of one component leading to the equilibrium condition. The sum of the forces acting on the system will be equal to zero at equilibrium conditions. From a vector representation of the acting forces on the three-phase system, the basic Young's equation (101) of the surface tension of the solid phase, γ_{SV}, can be derived:

$$\gamma_{SV} = \gamma_{SL} + \gamma_{LV} \cos \Theta \tag{2.2}$$

Considering two solid phases being in mutual contact, the work of adhesion may be calculated as follows (101):

$$W_A = \gamma_1 + \gamma_2 - \gamma_{12} \tag{2.3}$$

where the indices 1 and 2 correspond to the surface tension of the respective phase, and index 12 characterizes the interfacial tension between the two phases. In the case of the identity of the two phases ($\gamma_1 = \gamma_2$, $\gamma_{12} = 0$), the reversible work of cohesion of phase i can be determined.

Folkes assumed that the surface tension is additively composed of the contributions of the various interactions potential (102). In the case of polymers the surface tension can be divided into a dispersive and a polar part:

$$\gamma = \gamma^d + \gamma^p \tag{2.4}$$

According the Equation 2.4 the work of adhesion (Eq. 2.3) can be split into two parts, the first depending on dispersive interactions and the second caused by dipole-dipole forces (101):

$$\gamma_{12} = \gamma_1 + \gamma_2 - W_A{}^d - W_A{}^p \tag{2.5}$$

According to Wu (101,110) the two terms W_A^d and W_A^p can be expressed in terms of the surface energies of the two phases:

$$W_A^d = \frac{4\gamma_1^d \gamma_2^d}{\gamma_1^d + \gamma_2^d} \quad and \quad W_A^p = \frac{4\gamma_1^p \gamma_2^p}{\gamma_1^p + \gamma_2^p} \tag{2.6}$$

Combining Equations 2.5 and 2.6, the harmonic mean of the surface tension can be transformed into (101):

$$\gamma_{12} = \gamma_1 + \gamma_2 - \frac{4\gamma_1^d \gamma_2^d}{\gamma_1^d + \gamma_2^d} - \frac{4\gamma_1^p \gamma_2^p}{\gamma_1^p + \gamma_2^p} \tag{7}$$

The measurement of the surface tension of the polymer could then be performed using two test fluids with well known values of γ_L^d and γ_L^p. By introducing the equation of harmonic mean (Eq. 2.7) into the Young's equation (Eq. 2.2) the result is:

$$(1 - \cos\Theta)\gamma_L = \frac{4\gamma_S^d \gamma_L^d}{\gamma_S^d + \gamma_L^d} + \frac{4\gamma_S^p \gamma_L^p}{\gamma_S^p + \gamma_L^p} \tag{2.8}$$

where the indices L and S characterize the liquid and the solid phase respectively. By measuring the contact angle of the two test fluids, two simultaneous quadratic equations with γ_S^d and γ_S^p as unknown quantities can be solved.

An experimental application of the method of the harmonic mean theory of the interfacial tension (101) to the calculation of the interfacial tension between the components of LCP/thermoplatic blends has recently been used by Meretz and co-workers (111). The authors measured the contact angle (Θ) of two different liquids on a polished surface of a solidified polymer material. The liquids were selected on the basis of the dispersive and polar components of the surface tension. A high polar (distilled water) and a high dispersive (methylene iodide) liquid were used. The objectives of their experiments were to the select the best combination of a TLCP and a flexible chain polymer from a set of 49 different combinations, that would have the lowest value of interfacial tension. After the selection of the TLCP

and the flexible polymer, blends of these two materials would be performed by means of a bidirectional piston mixer containing a steel wire mesh as a static mixer. This procedure would generate a blend containing very fine dispersed TLCP particles in the matrix material. Their experimental work revealed that the most compatible system was LCP60 and PET.

Recently, Crevecoeur (112) has utilized two methods to determine the interfacial tension of TLCP/polymer composites. First, he measured the contact angle by immersing fibers from the materials into ethylene glycol. The fibers were attached to a microbalance that could measure the wetting force of the fiber and the liquid. With this method he could calculate the surface tension of the fiber. Second, he utilized the sessile drop method to calculate the interfacial tension of the blend components in the melt state. This method consists of placing a drop of polymer melt 1 with the lowest density on a substrate of polymer melt 2, and the interfacial tension is calculated from the curvature of the equilibrium interface between the two liquids.

Some considerations regarding calculations and predictions of the interfacial tension between the components of polymer-polymer blends have been discussed in this section. The methods available as well as the procedure to determine interfacial tension of TLCP/polymer blends have also been discussed. The work of Meretz and co-workers (111) have shown a systematic procedure to estimate the interfacial tension between the components of TLCP/polymer blends by the use contact angle determinations.

In the next section, a thorough review regarding the phenomenon of droplet deformation and breakup is presented. The two types of flow used to analyze the deformation of a drop suspended in a matrix polymer are shear and shearfree flows. The relative motion of the material particles in these two types of flow is very different. In simple shear flows, the velocity gradient is perpendicular to the flow direction and the fluid element rotates under deformation. While, in shearfree flows, the velocity gradient is parallel to the flow. The fluid elements are under tension upon flow. Consequently, shearfree or elongational flows are specially potent in inducing high molecular orientation due to its non rotational nature. By

contrast, simple shear flows due to its rotational component, should not be expected to induce high orientation to the polymer molecule (156).

2.2. Droplet Deformation and Breakup

When two polymers are compounded, such as in a single screw extruder or in the barrel of an injection molder, the initial stages of the mixing process are governed by the amount of interface created, which is proportional to the total strain applied to the material. In this early stage of the mixing process, called distributive mixing, the deformation of the dispersed particles is initially affine with the macroscopic flow (120). However, as the mixing process proceeds, the elongated particles continuously decrease in diameter, and consequently the capillary pressure σ/a (with σ the interfacial tension and a the radius of the droplet) increases, and finally will be of the same order of the shear stress applied. This process, called dispersive mixing, starts with the growth of distortions of the deformed particles, surface tension driven Rayleigh disturbances, and eventually leads to the breakup into a series of droplets. This process continues until the shear stress is counterbalanced by the interfacial tension, and the droplets have attained their equilibrium size (120). This process is of fundamental importance to the processing of multi-phase polymer blends and will be discussed thoroughly in this section.

Basic research on the deformation and breakup of a liquid drop of viscosity, μ_d, due to the motion of an immiscible, viscous suspending liquid of viscosity, μ_m, dates back to the pioneering work of G.I. Taylor (78,121,122). Taylor was the first to investigate the deformation of a viscous liquid droplet in uniform shearing and plane hyperbolic flow fields (refer to Figure 2.1). Subsequently, a number of researchers carried out theoretical (123-127) and experimental [128-133] studies on this subject. The majority, however, have dealt with the defor-

mation of a Newtonian droplet suspended in another Newtonian fluid, subjected to either shearing flow or uniaxial elongational flow.

The basic principle of droplet deformation and breakup is that as soon as the disruptive stresses due to viscous drag of the suspending fluid overcome the cohesive effect of the surface tension, the droplet bursts, i.e., elongates to a cylindrical (thread-like) form. The droplet continues to elongate and will eventually break up into small aligned droplets when the shearing and/or elongational stresses exceed the interfacial forces resisting to this deformation (128).

From the theoretical point of view, the drop deformation problem is extremely difficult. The equations of motion must be solved for the flow both inside and outside the drop, with boundary conditions applied to its surface. However, the shape of the drop is not known *a priori* and must be determined as part of the solution. Taylor (121), extending Einsten's theory for the viscosity of fluid containing rigid spheres in suspension (134), used the general solution of Stoke's equation for creeping flow to determine the velocity and pressure fields inside and outside the fluid drop.

In a subsequent study, Taylor (78) formulated a first order theory for the drop deformation in steady, uniform and small shear deformations and showed that the droplet deforms into a spheroidal form. Moreover, the shape of the droplet depends on the viscosity ratio of the droplet phase, μ_d, to the medium, μ_m, ($\lambda = \frac{\mu_d}{\mu_m}$) and the ratio of the product of the local shear stress and the droplet radius to the interfacial tension, often called Weber or Capillary number. This is defined as $We = \frac{\mu_m \dot{\gamma} a}{\sigma}$, where $\dot{\gamma}$ is the shear rate, a is the initial droplet radius, and σ is the interfacial tension.

It should be pointed out, however, that Taylor's theory is limited to the case where either the interfacial surface tension is dominant over the viscous effects, or the viscous effect is dominant over the interfacial surface tension effects. In the case when interfacial tension effect dominates the viscous effect (i.e. $\lambda = O(1)$, $We << 1$), the deformation D and the orientation angle α of the droplet are expressed as:

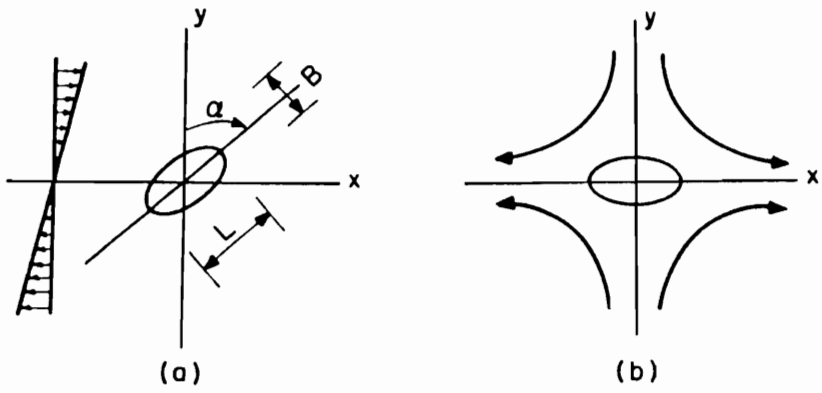

Figure 2.1. Schematic of droplet deformation: (a) in uniform shear flow field; (b) in plane hyperbolic flow field (120).

$$D = We\frac{(19\lambda + 16)}{(16\lambda + 16)}, \qquad \alpha = \frac{\pi}{4} \tag{2.9}$$

In the case where the viscous effects are dominant over the surface tension effects (We = O(1) and $\lambda >> 1$), Eq. 2.9 reduces to:

$$D = \frac{5}{4}\lambda, \qquad \alpha = 0. \tag{2.10}$$

where D is the deformation parameter defined as:

$$D = \frac{(L - B)}{(L + B)} \tag{2.11}$$

in which L and B are the length and breadth of the deformed droplet, respectively.

By equating the maximum pressure difference in the matrix fluid at the interface of a spherical droplet, with initial radius *a*, to the Laplace equation for capillary pressure, $\frac{2\sigma}{a}$, Taylor derived an expression to predict the conditions where droplet burst would occur. The critical shear rate, or critical Weber number necessary for bursting, were defined by Taylor as:

$$\dot{\gamma}_c = \frac{\sigma}{2\mu_m a}\left(\frac{16\lambda + 16}{19\lambda + 16}\right) \quad or \quad We_c = \frac{1}{2}\left(\frac{16\lambda + 16}{19\lambda + 16}\right) \tag{2.12}$$

where $\dot{\gamma}_c$ is the critical shear rate at burst, and We_c is the critical Weber number.

To experimentally simulate a planar extensional flow, Taylor (78) invented a four-roll mill apparatus, which has subsequently been used in several laboratories for studies on droplet deformation (79). From experimental observations, Taylor concluded that his theory developed for simple shear flows would apply well to the case of droplet deformation in planar extensional flows when $\dot{\gamma}$ was substituted by $\frac{\dot{\varepsilon}}{2}$, where $\dot{\varepsilon}$ is the elongational rate. Several experimental works (78,130,135-138) have shown the applicability of the above equations for viscosity ratios between 0.1 and 1 ($0.1 < \lambda < 1.0$).

The remarkable feature of Taylor's early investigations is that he uncovered most of the qualitative phenomena characteristic of droplet deformation and breakup in steady flows. His findings can be summarized as follows (79):

1. At low flow strengths, droplets of all viscosity ratios deform into prolate spheroids. The longest axis of the drop is initially aligned with the principal axis of strain for both irrotational (extensional) and simple shear flows.

2. When the drop viscosity is low compared with that of the suspending fluid, i.e. $\mu_d \ll \mu_m$, the shear rate required to burst it becomes quite large, and the drops attain highly deformed steady shapes with pointed ends.

3. When the ratio of drop to suspending fluid viscosity is quite large, i.e. $\mu_d \gg \mu_m$, drop behavior is qualitatively different from simple shear and extensional flow fields. In extensional flows, burst occurs at low strain rates. In simple shear flow, on the other hand, viscous drops assume slightly deformed shapes which are unaffected by further increases in shear rate, and drop bursts becomes impossible beyond a certain critical viscosity ratio.

Taylor's theory on droplet deformation and breakup was later improved by the work of Chaffey and Brenner (139). They obtained a second order solution in terms of the deformation parameter E, which was defined as:

$$E = We \frac{(19\lambda + 16)}{(16\lambda + 16)}, \qquad \alpha = \frac{\pi}{4} \tag{2.13}$$

Later, Turner and Chaffey (140), based upon the comparison with experimental results, concluded that the range of accuracy of the second order theory was not significantly beyond that of Taylor's first order theory. This was unexpected, because the predictions were based on a

second order solution. Unrealistic values of the deformation parameter were obtained when $E > 0.24$ in uniform shear flow, and when $E > 0.22$ in plane hyperbolic flow.

A second order theory has been also developed by Cox (123), using the deformation parameter D as the perturbation parameter, to determine the shape of the fluid drop as a function of time in transient (step change in applied shear) and steady shear flow fields. For longer periods of time after the application of the step change in shear, his equation for the apparent deformation (D) and for the orientation angle (α) of the major axis of the drop, reduces to:

$$D = \frac{5(19\lambda + 16)}{4(1+\lambda)\sqrt{\left(\frac{20}{We}\right)^2 + (19\lambda)^2}} \tag{2.14}$$

and

$$\alpha = \frac{\pi}{4} + \tfrac{1}{2}\tan^{-1}\left(\frac{19\lambda We}{20}\right) \tag{2.15}$$

In the case of planar elongational deformations, the generalized theory of Cox (123). yields the time dependent deformation of a droplet on a step in extensional rate for all values of λ:

$$D(t) = 2We\left(\frac{19\lambda + 16}{16\lambda + 16}\right)\left(1 - e^{-\left(\frac{19\lambda t}{20We\dot{\varepsilon}}\right)}\right) \tag{2.16}$$

where $We = \mu_m a \frac{\dot{\varepsilon}}{\sigma}$

The validity of Eq. 2.16 was shown by various authors (78,138). One important observation from Cox's treatment is the great difference between shear and extensional flows. Since hyperbolic flow does not permit the droplet to rotate, even highly viscous droplets can be deformed in extensional flows. Given time, they may reach even higher deformations than low viscosity droplets.

To extend Cox's theory (123) to higher deformations, Barthes-Biesel and Acrivos (124) carried out a second order perturbation analyses, using We as the perturbation parameter, on droplet deformation in a time dependent shearing flow to determine the onset of bursting. However, their theory, due to its mathematical complexity, often predicted smaller values of $\dot{\gamma}_c$ and We_c than corresponding observed experimental values.

It should be pointed out that the analyses mentioned thus far consider only the behavior of isolated droplets in a flowing matrix. This assumption no longer holds in the case of practical blending operations, because a finite dispersed phase concentration is usually present (120). The influence of dispersed phase concentration on the droplet break up was consider by Choi and Showalter (141) in their study of the rheology of concentrated suspensions. Starting from Cox's theory (123), they developed an expression for droplet break up for moderately concentrated emulsions in shear flow as a function of the dispersed phase concentration (C). Their expression reduces to Cox's (64) when C → 0.

$$D = We\left(\frac{19\lambda + 16}{16\lambda + 16}\right)\left[1 + \frac{5(5\lambda + 2)}{4(\lambda + 1)}C\right] \tag{2.17}$$

when We $<<$ 1, λ = O(1),

$$D = \frac{5(19\lambda + 16)}{4(1 + \lambda)\sqrt{\left(\frac{20}{We}\right)^2 + (19\lambda)^2}}\left[1 + \frac{5(5\lambda + 2)}{4(\lambda + 1)}C\right] \tag{2.18}$$

when We $<<$ 1, $\lambda >>$ 1, and

$$D = \frac{5}{4\lambda}\left(1 + \frac{25}{4}C\right) \tag{2.19}$$

when We = O(1), $\lambda >>$ 1.

Perturbation solutions for the droplet deformation problem have proven to be very limited in predicting the final shape attained by the droplet after deformation (127). The mathematical complexities involved in their solutions discouraged the use of higher order

solutions to increase the accuracies of the predications. It has been observed in many experimental studies of droplet deformation and breakup (138) that the droplets assumed a long and slender shape upon deformation at high strain rates, specifically when the viscosity ratio was small. Taylor (153) proposed, then, the use of the technique of slender-body theory in order to solve such a problem analytically. In subsequent studies, Buckmaster (142,143) presented a mathematically systematic and detailed treatment of this general problem. He showed that for large values of strain rates the shape of the drop is given by:

$$r = \xi R(z) = \frac{\xi(1 - |z|^{\nu})}{2\nu} \tag{2.20}$$

where r and z are, respectively, the radial and axial coordinates. ξ is defined as $\frac{\sigma}{\dot{\varepsilon}\mu_m \ell}$, ℓ as the half length of the droplet, $\dot{\varepsilon}$ as the extensional rate, and $\nu = \frac{1}{2}\Delta P - 1$, where ΔP is the difference in pressures inside and outside the droplet. The procedure introduced by Buckmaster (143) has later been followed by Acrivos and Lo (144) to the solution of the slender body deformation where the parameter ν could be readily determined at all cases, except for one.

A fundamental assumption in all these analyses, however, is the continuity of the tangential stresses at the droplet interface. This boundary condition physically means that the interface must be free of surfactants. The effects of surfactants on the droplet deformation phenomena have recently, been studied by Stone and Leal (154), both experimentally and numerically. Their results indicated that at $We << 1$, the presence of surfactants causes larger deformations than would be expected for a droplet with a constant interfacial tension. They claimed that the increased deformations were caused by the surfactant being swept to the end of the droplet and, consequently, locally reducing the interfacial tension, requiring an increase in the deformation to satisfy the normal stress balance. At higher We, however, the authors observed that the above convective effect competed with the dilution of the surfactant due to the interfacial area increase.

From a series of studies on particle motion in sheared suspensions, Rumscheidt and Mason (138) differentiated several breakup models for the deformation of droplets in simple shear and planar elongational flows, over a wide range of interfacial tensions and viscosity ratios. A summary of their observations is presented in Figure 2.2. It can be observed from their experiments that droplet breakup in shear flows was only possible at $0.1 < \lambda < 1.0$. At $\lambda < 0.1$ the droplet attained a sigmoidal shape and small droplets were shed from the tops. A phenomenon that would be later called as tip streaming. For viscosity ratio greater than 4, droplet break up did not occur at all. The tip streaming phenomenon was also observed in elongational flows at $\lambda < 0.1$. Contrary to shear flows, however, droplet deformation was possible for $\lambda > 1.0$ in elongational flows. Another noteworthy observation from the experiments is the importance of the interfacial tension to the droplet deformation process. At comparable values of λ, the droplet deformed into a much more stable thread-like form in the system where the value of σ was the highest.

The observations of Rumscheidt and Mason (138) are of particular importance to the development of in situ thermoplastic composites where the reinforcing fibrils will be developed from the deformation of a molten thermotropic liquid crystalline dispersed phase undergoing either shear or elongational flow. The success of generating LCP fibrils in a TLCP/polymer blends will depend on the ability to control the processing conditions, consequently λ and We, in such a way that a deformed fibrillar structure of the dispersed TLCP phase would be obtained upon application of shear or elongational flows.

Experimental data on the relation between the critical Weber number (We_c) and viscosity ratio (λ) on the droplet deformation and breakup phenomena have been reported by several authors (135-138). One of the most comprehensive studies in this subject was done by Grace (135), who studied droplet deformation and breakup over a record breaking range of viscosity ratio from 10^{-6} to 10^{3}, in both simple shear and planar elongational flows. A summary of his finding is depicted in Figure 2.3, which shows the We_c required for droplet breakup in simple shear (rotational) and planar elongational (irrotational) flows. The We_c required for breakup in plane hyperbolic irrotational flow is comparable to that of rotational

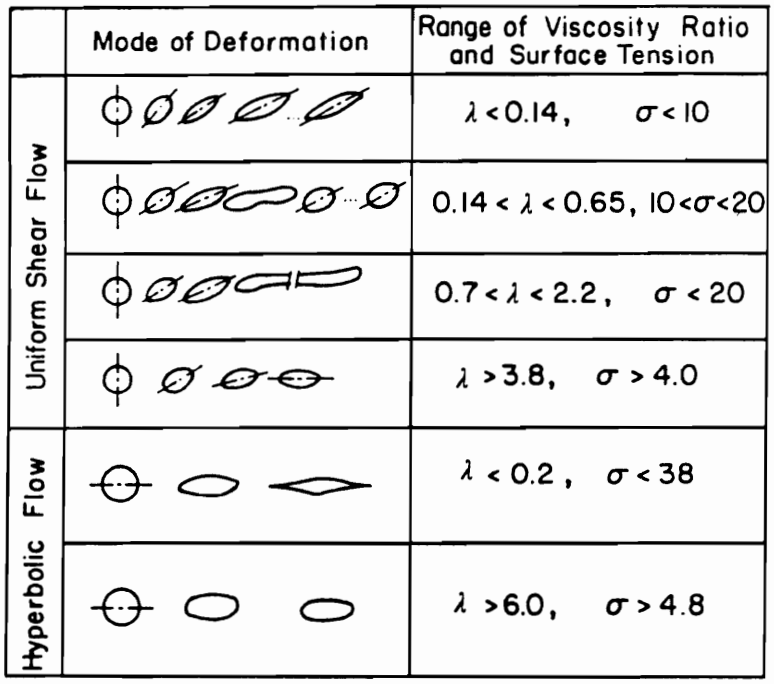

Figure 2.2. Schematic showing the mode of droplet deformation in different flow fields (138).

shear becomes even smaller as the viscosity ratio moves away from 1.0 in either direction. For equal shear rates, planar elongation appears to be more effective in the deformation of a droplet than simple shear flows, even at low viscosity ratios. In the case of simple shear (couette) the breakup seems to occur more readily at $0.1 < \lambda < 1.0$. Similar results for the case of simple shear flows have also been observed by Karam and Bellinger (130).

The dramatic qualitative difference in drop burst between pure-straining flow and simple shear flow have motivated Bentley and Leal (79) to investigate drop deformation and burst process in flows with intermediate vorticity. They built a similar four-roll mill invented by Taylor (39), with the exception that in their case they have used a computer controlled drive system to control the speed of the rolls individually. This procedure enabled them to reproduce any intermediate flow regime between the two limiting cases studied by Taylor and others, simple shear and plane hyperbolic flows. The streamlines of such intermediate flows, including the two limiting cases, are presented in Figure 2.4. In the figure, the parameter α specifies the relative strength of the strain rate and vorticity in the flow ($\alpha = 0$ for simple shear flow, and $\alpha = +1$ for pure straining flow). Some of their results are as follows. For viscosity ratio less than unit ($\lambda < 1$), the Weber number required for burst and the deformation at the point of burst both decreased with increasing viscosity ratio for all strong flows (i.e. flows in which the magnitude of the strain rate exceeds that of the vorticity). In the case of extensional flows (irrotational), the critical value of the Weber number reached a constant value with further increase in the viscosity ratio. Finally, for the case of simple shear flow, it was observed that the critical Weber number goes through a minimum at a viscosity ratio of about 1.0 and there exists an upper limit in the viscosity ratio beyond which no burst is possible.

The experimental and theoretical results on droplet behavior reviewed thus far have included only the cases where Newtonian systems were involved. Consequently, the above relations have limited applicability to polymer blending because molten polymers, in general, exhibit shear-rate dependent viscosity and normal stresses. Several investigators (144,145) have proposed the use of viscosity functions and fluid elasticity on the theoretical treatment

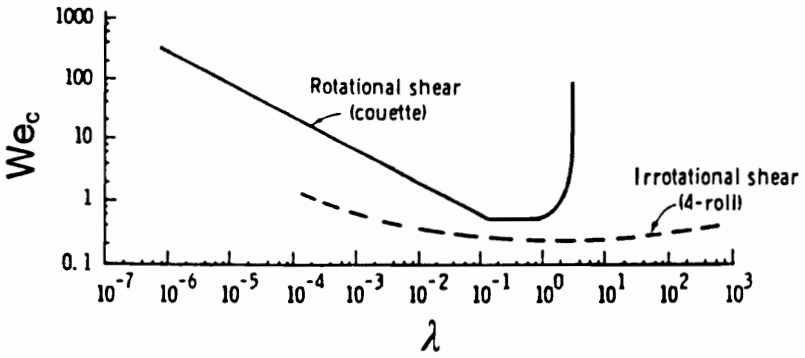

Figure 2.3. Comparison of the effect of viscosity ratio on the critical Weber number in simple shear (rotational) and planar elongational (irrotational) flow fields (135).

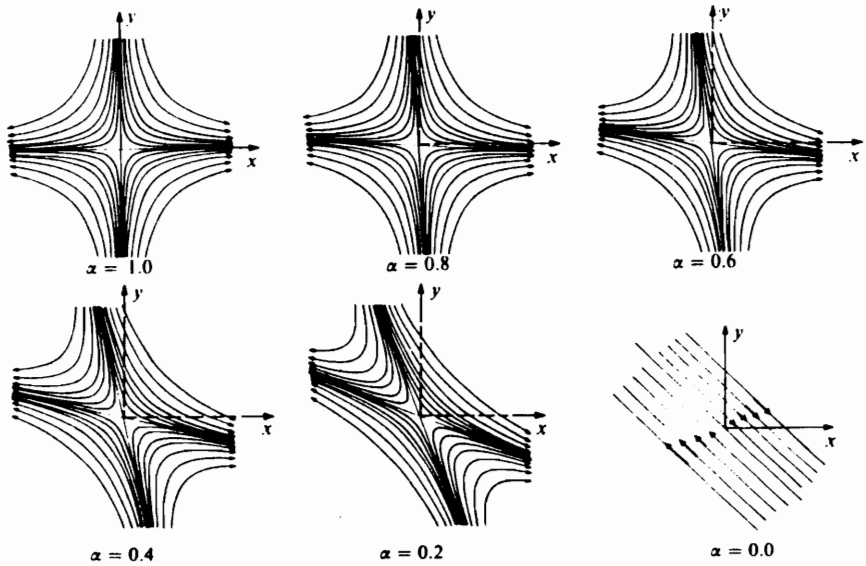

Figure 2.4. Streamlines of flow fields between simple shear ($\alpha = 0$) and extensional ($\alpha = 1.0$) flows (79).

for the phenomena of droplet deformation in the case of viscoelastic systems. A relation which accounts for the effects of elasticity on droplet deformation in viscoelastic systems has been derived by Van Oene (146). He suggested that the interfacial tension between the fluid matrix and the droplet phase should be corrected to account for the difference in the first normal stress differences of the dispersed and matrix phases, by the relation:

$$\sigma_{dm} = \sigma + \frac{a}{6}\left[(\tau_{11} - \tau_{22})_d - (\tau_{11} - \tau_{22})_m\right] \tag{2.21}$$

where the indices m and d refer to the matrix and dispersed phases, respectively. The Van Oene relation suggests that in cases where the the dispersed phase elasticity is greater than the matrix elasticity, $\sigma_{dm} > \sigma$, the droplet will attain a more stable form compared to Newtonian systems at similar values of $\dot{\gamma}$. The opposite is observed when matrix elasticity dominates. Van Oene has successfully predicted droplet deformation in viscoelastic system using the proposed corrections for fluid viscosity and elasticity into Cox's relations (123).

The influence of fluid elasticity on the droplet deformation behavior has also been reported by Elmmnedorp and Maalcke (147). By dissolving varying concentrations of polyacrylamides with varying molecular weights these authors we able to obtain a set of solutions with equal shear-dependent viscosities, but different elasticities. From their studies on viscoelastic droplets suspended in Newtonian matrices, they conclude that droplets having higher normal stresses appeared more stable. However, for Newtonian droplets suspended in viscoelastic matrices, normal stresses exhibited by the matrix tended to increase the deformation of the droplet. Their results were in qualitative agreement with Van Oene's (146) relations.

Quite recently, Milliken and Leal (148) studied the deformation of viscoelastic droplets suspended in Newtonian matrices in planar extensional flow. They have used Boger fluids ($\eta = \eta_0$ and $N_1 > 0$), purely viscous fluids ($\eta = \eta(\dot{\gamma})$ and $N_1 = 0$), and fully viscoelastic fluids ($\eta = \eta(\dot{\gamma})$ and $N_1 > 0$) in their experiments. From experimental observations, they concluded that a critical viscosity ratio of the order of 1.0 determined the mode of droplet breakup for

both Newtonian and polymeric droplets. Droplets of viscosity ratio of 1.0 and higher, exhibited a steady shape regardless of fluid characteristics. Droplets of viscosity ration lower than 1.0 manifested markedly differences in the mode of deformation. Particularly, lower viscosity polymeric droplets did not display the the highly deformed steady shape characteristic of Newtonian droplets. Instead, low viscosity ratio polymeric droplets formed cusped ends followed by fragmentation by tip streaming. This observation was not seen in Newtonian droplets. They further concluded that the mechanisms of droplet breakup, regardless of fluid used, were more dependent upon the magnitude of the Deborah number (De), defined as the ratio of the relaxation time scale of the fluid relative to the inverse of the strain rate of the undisturbed flow, than on the nature of the fluid used.

The influence of matrix shear-thinning behavior on the deformation and breakup of Newtonian droplets in steady and unsteady shear fields was studied by Flumerfelt (131). His results indicated that for all the systems studied, there was a minimum droplet size, a_{min}, below which breakup could not be achieved. The elasticity of the continuous phase was seen to increase both a_{min} and $\dot{\gamma}_c$ required for breakup when $a > a_{min}$. Both $\dot{\gamma}_c$ and a_{min} decreased significantly under unsteady shear as compared to steady shear conditions. The viscosity of the matrix was seen to have an opposite effect. With the increase in shear rate the matrix viscosity decreases, making λ increase with shear rate. When $\lambda > 3.0$, droplet breakup was no longer possible. On the other hand, the studies of Torza and co-workers have indicated that the mechanism of droplet breakup was more dependent on the rate of increase in shear ($\partial\dot{\gamma}/\partial t$) than on the viscosity ratio. They have found from their experimental studies in uniform shear flow, that the product of $\dot{\gamma}_c$ and the droplet radius a remained nearly constant for a given viscosity ratio.

Droplet deformation and breakup in the case of viscoelastic systems are rarely studied. One of such rare studies is the work of Chin and Han (127,149). They considered the deformation of a viscoelastic droplet suspended in another viscoelastic fluid subjected to a steady axisymmetric elongational flow. They obtained a first order perturbation solution, using a Coleman-Noll second order fluid constitutive equation, to describe the change of the initial

droplet radius as a function of the deformation. Based on theoretical calculations, the authors concluded that the medium viscosity plays a much more important role in determining the droplet deformation that the medium elasticity. Their theoretical predictions for the deformation attained by the viscoelastic droplet after deformation was very limited. The mathematical complexities involved in the analytical development of the method discouraged them from further improving the predictions by using higher order solutions.

A study on the rheological and interfacial effects on the dispersion process during melt extrusion of polymer/rubber blends in a co-rotating twin screw extruder was carried out recently by Wu (128). He observed that the droplet size of the dispersed phase was directly proportional to the interfacial tension. For all blends studied, the smallest particle size was seen to occur at a viscosity ratio of unity, and when the interfacial tension is lower. He also observed that the formation of the dispersed phase during melt blending could be described by a master curve relating the Weber number and the viscosity ratio. In addition, he observed droplet breakup of viscoelastic droplets at viscosity ratios higher that 4.0, which was attributed to the elastic effects, the presence of an elongational flow field and the complex viscosity-temperature profile along the extruder barrel. In another study regarding the deformation of viscoelastic systems, the authors (150) found that droplet breakup could occur at a viscosity ratio as high as 17. This was attributed again to elastic effects and elongational flow fields during mixing of polypropylene/polycarbonate blends utilizing a Brabender.

The behavior of droplets in *nonuniform* shear flow, for instance in Poiseuille flow, differs from that of in uniform shear flow. The velocity gradient, as consequence of nonuniform shear, varies with radial distance in Poiseuille flow, while it is constant in uniform shear. Thus, in nonuniform shear the extent of droplet deformation varies depending of the location of the droplet in the plane of shear, whereas in uniform shear this is not the case (120). It is worth pointing out that from the point of view of polymer processing operations, droplet deformation in nonuniform shear fields, for instance, injection molding or extrusion through a capillary, is of far greater importance than in uniform shear field. Hence, the nature of the deformation

will have a strong effect on the final morphology attained by the polymer blend after a uniform or nonuniform shear deformation.

It has been shown by Goldsmith and Mason (151) that in Poiseuille flow, depending on the fluids viscosities, Newtonian droplets suspended in a Newtonian medium migrate towards the tube axis. It was also reported by Gauthier and co-workers (152) that for Newtonian droplets suspended in a pseudoplastic liquid subjected to Poiseuille flow, a two way migration was observed. The droplets initially close to the tube axis migrated toward the tube wall and those close to the tube wall migrated toward the tube axis and attained an intermediate equilibrium position between the tube axis and the wall. However, in a viscoelastic medium, the droplets were observed to always migrate toward the tube axis. This fact indicates that the behavior of droplets suspended in another liquid depends on the type of the flow field and the nature of the suspending medium.

In conclusion, it can be said that from the numerous results cited, the type of flow field and the viscosity ratio are critical in determining the mode of droplet deformation and burst. Extensional flows appear to be far more favorable in the deformation of droplets than simple shear flows. The dependence of the critical Weber number at droplet breakup to the viscosity ratio is much less pronounced in elongational flows compared to simple shear flows. Furthermore, it is well known (155) that elongational viscosity is less sensitive to the deformation rate than shear viscosity, ensuring an easier breakup of droplets in shear thinning systems.

In simple shear flows, three separate regimes of viscosity ratio were determined to govern the deformation and breakup. For Newtonian systems, droplet burst was not possible for viscosity ratios greater than 4.0, regardless of We. The droplets show a small but stable deformation and the critical Weber number required for burst approached infinity. In the case of viscoelastic systems, droplet breakup was possible for viscosity ratio as high as 17 (150). The We_c required for burst goes through a minima at $0.1,\lambda < 1.0$ in both shear and elongational flows for small values of σ.In the case of extensional flow, droplet breakup seems to occur over a wide range of viscosity ratios and the Weber number required for burst is much less than that of simple shear at the same viscosity ratio. In the case of viscoelastic systems, the

influence of elasticity on the droplet deformation phenomena may be illustrated as follows: droplets showing higher elasticity than the fluid matrix tend to acquire a much more stable form upon deformation, whereas higher elastic matrices tend to reduce We_c required for burst.

In the above section, the parameters that govern the deformation and breakup of droplets of one liquid suspended in another have been discussed. The importance of both the Weber number and the viscosity ratio in the deformation process was established. It was seen that in the case where the viscosity of the dispersed phase was much lower than that of the matrix the droplets were able to achieve highly deformed and stable forms. The situation for viscosity ratios greater than 3 is different in that although no burst is possible, it also becomes more difficult to deform a droplet, in shear flow, to any appreciable extent. Further, it was also observed that in shear flows there exists both an upper and a lower limit of viscosity ratio beyond which no drop burst is possible. Drop break up in extensional flow fields is possible over a a much wider range of viscosity ratios showing that extensional flow fields are more effective than uniform shearing flow fields in breaking up droplets.

It should be pointed out, however, that most of the theories and experimental work regarding droplet deformation and break up were carried out in well controlled conditions to give a very uniform and steady flow field in both cases of shear and extensional flows. Therefore, such theories must be looked on with some caution in their applicability to polymer blends. Polymer processing operations will not provide the same controlled flow fields as the above experiments.

2.3. Capillary Instabilities

In the previous section, it was shown that the dynamic and viscous forces acting on the surface of a small spherical droplet will tend to distort it, whereas the interfacial tension will tend to resist these forces and keep the droplet spherical. However, as the dynamic and

viscous forces become larger than the interfacial forces, the droplet will deform and eventually break up into small droplets. It has also been shown that it is of fundamental importance to control the processing conditions, named viscosity ratio and stress fields, at which droplet deformation will occur into a desirable thread-like form. The morphology of a polymer blend of incompatible polymers is governed, not only by the deformation and break up of the dispersed phase, but also by capillary instabilities of the thread-like particles and by coalescence of the dispersed phase (156). In this section a discussion dealing with the stability of the fibril entities, which plays an important role in determining the final part morphology will be addressed. The stability of a liquid cylinder surrounded by an immiscible matrix has been the topic of investigation in numerous studies (149,157). However, the concern of this section is to review the literature with direct relation to the problem of polymer blending.

The break up of liquid threads was first mentioned in the scientific literature by Plateau (158), who observed the amplification of distortions leading to a the break up of water jets flowing down from orifices. However, this surface-induced process, neglecting the viscosity of either phase, received a complete theoretical description through the classical work of Lord Rayleigh (159).

An extension of this problem to Newtonian liquid threads embedded in Newtonian matrix was given by Tomotika (160). He considered the stability of a sinusoidally distorted thread, as shown in Figure 2.5:

$$R(z) = \bar{R} + \xi \sin(\frac{2\pi z}{\Lambda}) \tag{2.22}$$

where: $\bar{R}$ is the average thread radius, ξ is the distortion magnitude and z is the coordinate along the thread.

From the conservation of volume, it can be shown that:

$$\bar{R}^2 = R_0^2 - \frac{\xi^2}{2} \ . \tag{2.23}$$

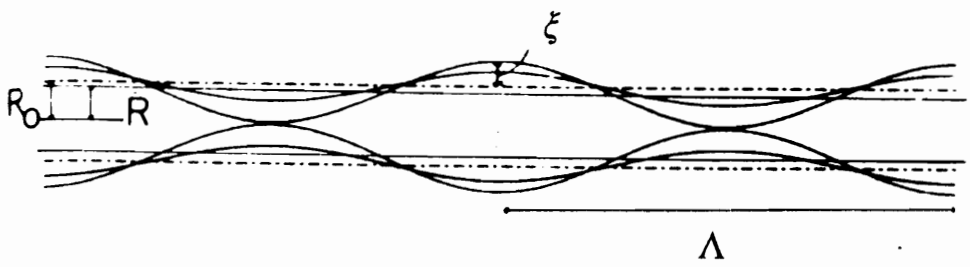

Figure 2.5. Sinusoidally distorted cylinder (160)

From experimental observations (160), it has been detected that when $\Lambda > 2\pi R$, the interfacial area decreases when the distortion amplitude increases. For this reason, a liquid thread will be unstable when the wavelength of the distortions become larger than the circumference of the thread. Tomotika's theory shows that when $\Lambda > 2\pi R$ the distortion amplitude ξ grows exponentially with time, according to the expression:

$$\xi = \xi_0 e^{(qt)} \tag{2.24}$$

where ξ_0 is the distortion at t = 0, and

$$q = \frac{\sigma}{2\eta_m R_0} \Omega(\xi, \lambda) \tag{2.25}$$

where σ is the interfacial tension, η_m is the matrix viscosity, and λ is the viscosity ratio. The most striking feature of the function $\Omega(\xi, \lambda)$, the growth rate of disturbance, is that it was found to exhibit a maximum for a certain value of wavelength, Λ_m, which depends on the viscosity ratio λ (161). Assuming that the thread will contain all wavelengths with initial amplitudes at the time of creation, the distortion at which $\Omega(\xi, \lambda)$ is maximum, Λ_m, is expected to induce thread breakup.

It follows from Equation 2.22 that thread breakup will occur when the amplitude of distortion equals the average radius of the thread, or for $\xi = 0.8\ R_0$. Substituting these values into Equation 2.24, the time necessary to reach this distortion can be calculated as:

$$t_B = \frac{1}{q} \ln\left(\frac{0.8\ R_0}{\xi_0}\right) \tag{2.26}$$

Thus, in the development of in situ thermoplastic composites, where the reinforcing phase will be developed from a deforming LCP phase, if the time for thread breakup exceeds the droplet deformation time, one can expect cylindrical fibrils to be present in the matrix polymer. By controlling the processing conditions, this structure could then be frozen in to yield the reinforcing fibrils into the thermoplastic matrix.

Rumscheidt and Mason (162) have studied this interfacial-driven phenomena of droplet breakup for fluid threads developed during experiments utilizing a four-roller mill apparatus. However, since a four-roller apparatus deforms a spherical element into symmetrical ellipsoids (149), these authors could not obtain perfectly stretched cylinders as the starting point of the experiments.

A different set up to generate the liquid threads was proposed later by Elmendorp (161). This author generated cylindrical threads by rapid concentric flow of two fluids from a pressure barrel into a long tube. This procedure allowed him to develop threads of infinite length. From his experimental investigations, he concluded that Tomotika's (160) relations could predict satisfactorily both the growth rate of disturbances and the dominant wavelength (Λ_m).

Tsebrenko and co-workers (163) and Elmendorp (161) have also experimentally studied this problem of droplet break up. Elmendorp (161) studied both Newtonian and viscoelastic thread break up in a Newtonian medium. This author has studied droplet break up induced mainly by flow instabilities. This was achieved by imposing initial distortions of variable magnitudes and wavelengths of the threads by superimposing a sinusoidally varying flux of the discrete phase flow by means of a plunger pump. A summary of his findings is presented in Figure 2.6. The solid line was calculated from Tomotika's original equations. It can be seen that, despite some experimental scatter, a good agreement was obtained. It is interesting to note that for $\Lambda < 2\pi R$ negative values of q were found, indicating that in these regions distortions are damped rather than amplified. Further, as expected from the theory, the breakup time of the threads decreased with an increase in the magnitude of the relative initial distortions. For different conditions, the breakup time varied from a few seconds to a few hours. However, in the case of viscoelastic threads in a Newtonian medium the data did not fit to the theory too well. Experiments with molten polymers, on the other hand, showed good agreement with Tomotika's theory. The author suggested that the agreement with the theory was due to the low shear rate conditions of the test, causing the fluid viscosities to fall into their zero shear viscosities region.

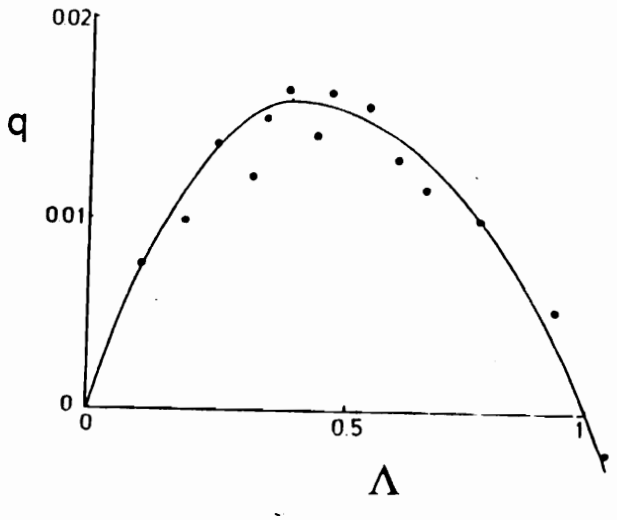

Figure 2.6. Distortion growth rate, q, versus wavelength, Λ, for a viscosity ratio λ (149).

Despite the satisfactory theoretical description, the application of the preceding to the problem of polymer blending is limited by the basic assumption of Newtonian fluid behavior. The number of experimental and theoretical studies of capillary instabilities in viscoelastic systems is limited to the breakup of jets in air (157,164-166). The general conclusion of these investigators is that the breakup of viscoelastic threads is delayed dramatically in the final stages of the process. This phenomenon may be explained by the strain hardening extensional viscosities effect exhibited, in general, by viscoelastic polymers, which could slow the breakup process of viscoelastic threads. In addition, it has been shown (157) that previous stress histories, that might be encountered in freshly created threads, can increase the breakup time enormously when the relaxation times of the fluid thread compete with its breakup time.

An example of the growth of distortion on a viscoelastic thread embedded in a Newtonian matrix is given in Figure 2.7. The points were experimentally determined and the dashed lines were calculated from Tomotika's Newtonian relation, using zero shear viscosity of the fluid thread. It can be seen from the figure that three regions determining the droplet breakup can be distinguished. The initial part of the thread thinning process was predicted fairly well by Tomotika's equations. However, a second region is observed in which the process is accelerated. This acceleration was thought to be caused by shear thinning effects (157). In the final stage of thread breakup the process was severely decelerated, which reflected the effects of strain hardening effects at high stretching conditions (167). These three distinct regions of thread breakup in the case of viscoelastic threads account for a change in the shape of the breaking thread compared to Newtonian systems. In Newtonian threads sinusoidal distortions are observed, whereas in the case of viscoelastic threads, a distinct bead-string shape has been detected (149). Some authors (166) have proposed the use of deforming viscoelastic threads as a means of measuring the elongational viscosity of viscoelatic materials.

Experiments regarding the breakup of threads in molten polymer systems have also been reported in the literature (161,168). The most important conclusion from their collective

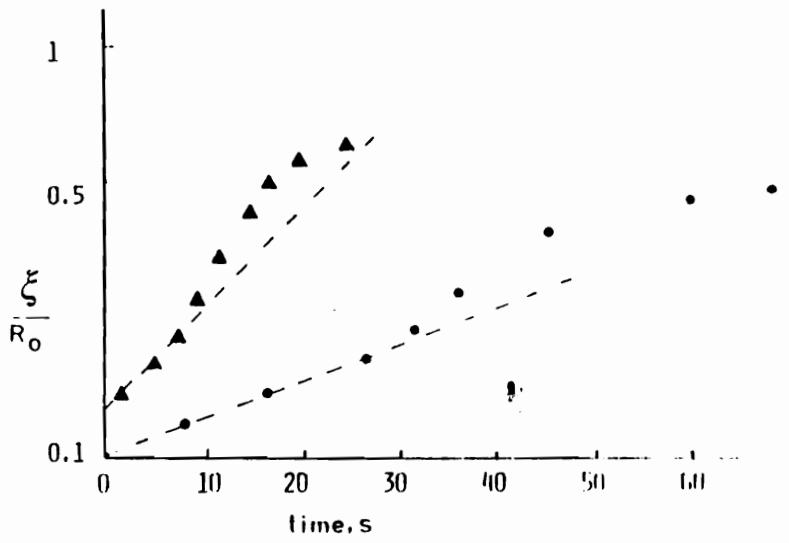

Figure 2.7. Growth of distortions on a viscoelastic thread (1% polyacrylamide solution) embeded in a Newtonian matrix fluid (149).

work is that both the growth and the wavelength of the dominant distortion was predicted satisfactorily by Tomotika's Newtonian results, despite the complex rheologic nature of the materials used. The break up phenomena was more similar to that observed for Newtonian threads than that observed for viscoelastic threads embedded in Newtonian systems, i.e. an absence of the bead-string phenomena. The apparent absence of viscoelastic phenomena during the breakup process was ascribed to the magnitude of the deformation rates used in the experiments, where the polymers used exhibit Newtonian viscosities behavior in the range of the deformation (161).

In summary, Tomotika's Newtonian relations seem to predict droplet breakup from capillary instabilities fairly well, regardless material's properties. One reason may be due to the low magnitude of shear rates used in experiments with polymeric systems, where the viscosities of the polymers used seemed to fall in the range of the Newtonian shear viscosity plateau. At higher deformations, however, the breakup of viscoelastic threads seemed to be delayed by viscosity strain hardening effects. Another distinction between Newtonian and viscoelastic threads regards to the shape attained by the threads preceding burst. In Newtonian threads a sinusoidal shape is observed whereas for viscoelastic threads a distinct bead-string shape is observed. Some authors have suggested such an experiment as a means of determining the elongational viscosity of viscoelastic materials.

2.4 Liquid Crystalline Polymers

In the previous sections, discussions regarding droplet deformation and break up have been presented in some detail. The aspects of fibrillation of a dispersed phase in a matrix material are governed primarily by microrheological characteristics and the type of flow field applied to the system. Moreover, the final morphology attained by the system is strongly de-

pendent upon the conditions at which deformation occurred. Breakup of the deformed fibril may be avoided by controlling processing conditions to minimize Rayleigh disturbances.

A general introduction about liquid crystalline polymers was given in Chapter 1. This section limits to the discussion of the rheological characteristics of thremotropic liquid crystalline polymers. As discussed earlier, fibrillation of a dispersed phase into a matrix polymer is governed essentially by microrheological aspects. Therefore, a complete knowledge of the rheological aspects of thermotropic liquid crystalline polymers is of fundamental importance to the development of in situ thermoplastic composites.

The rheology of thermotropic liquid crystalline polymers is very different from the rheology of flexible chain polymers. For example, TLCPs exhibit no die swell upon extrusion and yet they can show large positive values of primary normal stress difference, which is quite inconsistent. In the case of flexible chain polymers these two aspects are thought to be directly interconnected. Die swell is an indication of elasticity exhibited by the flexible chain polymer. The rheological characteristics of TLCPs is discussed next followed by a discussion on thermal and shear history effects on the rheology of TLCPs.

2.4.1 Rheology of Thermotropic Liquid Crystalline Polymers

Since the rheology of thermotropic liquid crystalline polymers depends on a great extent on their molecular structure, it is adequate to discuss this subject first. Basically there are two structures that can form a liquid crystalline phase. These two structures are: main chain polymers containing mesogenic units and flexible chain polymers containing mesogenic side groups. The term *mesogenic group* means the part of the molecule which is composed of rigid chain segments which are connect together by functional groups in a linear form (169). It is this mesogenic group, usually aromatic, that will determine whether the polymer will exhibit liquid crystallinity or not. Moreover, the temperature range that liquid crystallinity will occur and the type of mesophase is usually determined by the type of mesogenic group. An

essential requirement for the formation of a mesophase is that the mesogen group be very geometrically anisotropic with high aspect ratio (170). Thermotropic LCPs usually are formed by linking the mesogenic groups with either ester, azo or azoxy groups. The majority of the TLCPs available commercially are of the ester linkage type. The chemical structure of some commercial TLCPs are presented in Figure 2.8.

The rheological behavior of thermotropic liquid crystalline polymer, due to the anisotropic nature of their chains, differs tremendously from that of flexible chain polymers in many aspects. For instance, they have an unusually large end correction for capillary flow (171) a phenomenon which is associated with high melt elasticity and/or high extensional viscosity when observed in flexible chain polymers. Further, TLCPs display higher normal stress difference than do flexible chain polymers (172), which is consistent with the capillary correction behavior. Quite inconsistently, however, they show very little die swell (171,172). Another anomaly is the fact that the first normal stress difference,N_1, is about 10 times higher that the dynamic storage modulus, G', compared with the factor of 2 usually observed for isotropic polymer (171).

An example of the viscosity behavior of a TLCp as a function of shear rate and temperature is shown in Figure 2.9 (173). The TLCP used in this experiment was a thermotropic copolyester of 60/40 PHB/PET. As one would notice, at 340°C the flow curve approaches a constant viscosity at low shear rates, with slight shear thinning as the shear rate is increased. At 300°C the flow curve has the *three region* characteristic shape as proposed by Ogoni and Asada (174). In their classification Region I is the low shear rate region of shear thinning behavior. Region II is the plateau or nearly constant viscosity at intermediate shear rates, and its followed by another shear thinning range, which is designated as Region III. However, as the temperature is decreased further, it appears as though Regions I and III are merging, and the flow curve approaches power law behavior. Near 320°C the flow curve is most peculiar, with a range of shear thickening behavior. Such an anomaly in the behavior of LCPs is not yet fully explained.

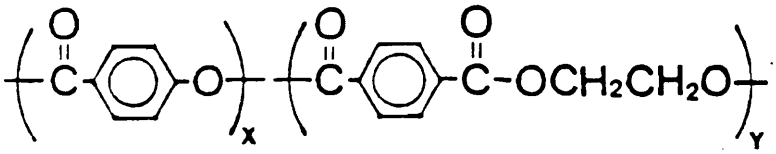

60HBA/PET (LCP60) x = 0.6 y = 0.4

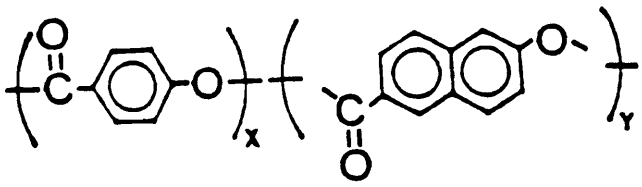

HBA/HNA (Vectra A900) x = 0.73 Y = 0.27

Figure 2.8. Chemical structure of thermotropic liquid crystalline polymers.

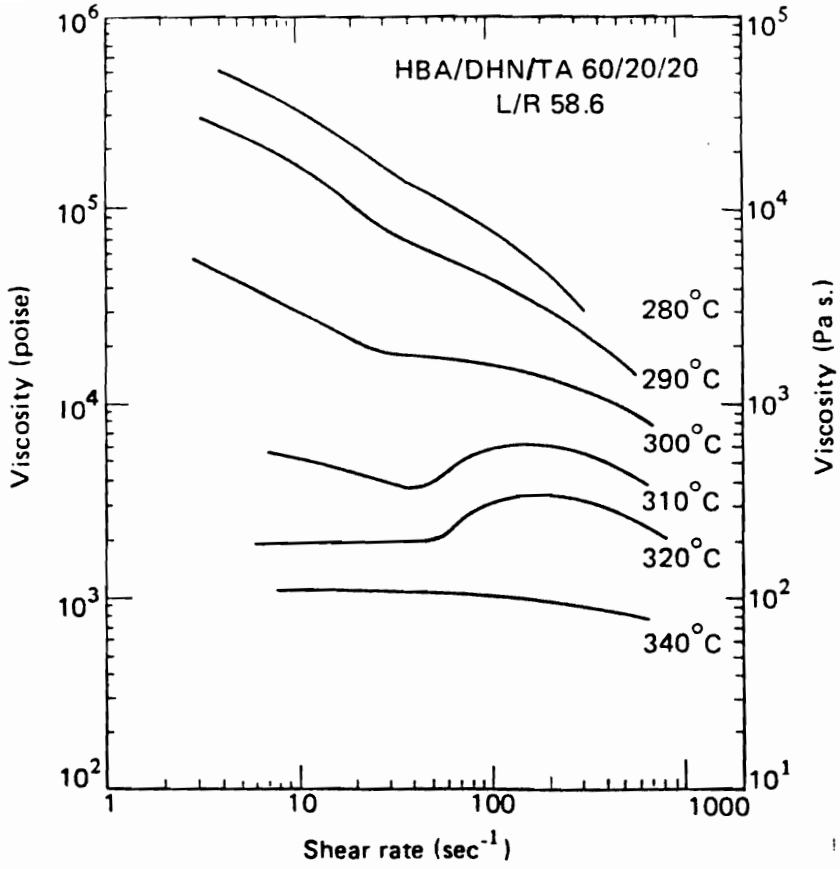

Figure 2.9. Variation of flow curve shape with temperature for a rigid thermotropic polyester (173).

On the basis of rheo-optical measurements, Ogoni and Asada (174) concluded that the low shear rate range of shear thinning behavior (Region I) is one in which flow occurs by relative motions of the polydomains. Polydomains are defined as regions of very different local orientation. In Region II the domains were considered to be transformed by increasing shear stress into a nematic fluid that would act as a suspending medium for the remaining domains. Only in Region III the structure was considered to be of that of a fully oriented nematic liquid (refer to Figure 2.10). A quantitative theory based upon the polydomain concept of Ogoni and Asada has been developed by Marrucci (175) to predict the shear rate dependence of the viscosity of thermotropic LCPs.

Recently, Cocchini and co-workers (176) have investigated the transient and steady rheological behavior of a thermotropic liquid crystal copolymer of 73/27 HBA/HNA, commercially available as Vectra A900 from Hoechst-Celanese. Their experiments were performed utilizing a cone and plate apparatus in steady shear, constant stress and dynamic mode tests. Their results have shown that for the step-up experiments at different shear rates, the stresses scaled with strain, while steady values were obtained at about 200 units of strain. This behavior was attributed to the refinement of the polydomain texture. In the case of steady shear experiments, performed at 300°C, they have noticed that the viscosity behavior of the material followed the three region scheme as discussed earlier. A shear thinning region was observed at low shear rates, a plateau viscosity region at intermediate shear rates, and again shear thinning at higher shear rates. The shear thinning region at low shear rates was also confirmed by the constant stress experiments. This feature is illustrated in Figure 2.11.

In summary, the viscosity of thermotropic liquid crystalline polymers may follow the characteristic "three flow regions" as proposed by Ogoni and Asada (174). Although some arguments in the literature about such a behavior being valid for all LCPs still persists, it was shown that in the case of 60-40 PHB/PET, at 300°C, such a behavior is present. The explanations offered (173) for such viscosity/shear rate behavior of TLCPs are as follows: the first shear thinning region is a consequence of the relative motion of the randomly oriented domain clusters, followed by the transformation of these domains into a partially oriented liquid, giv-

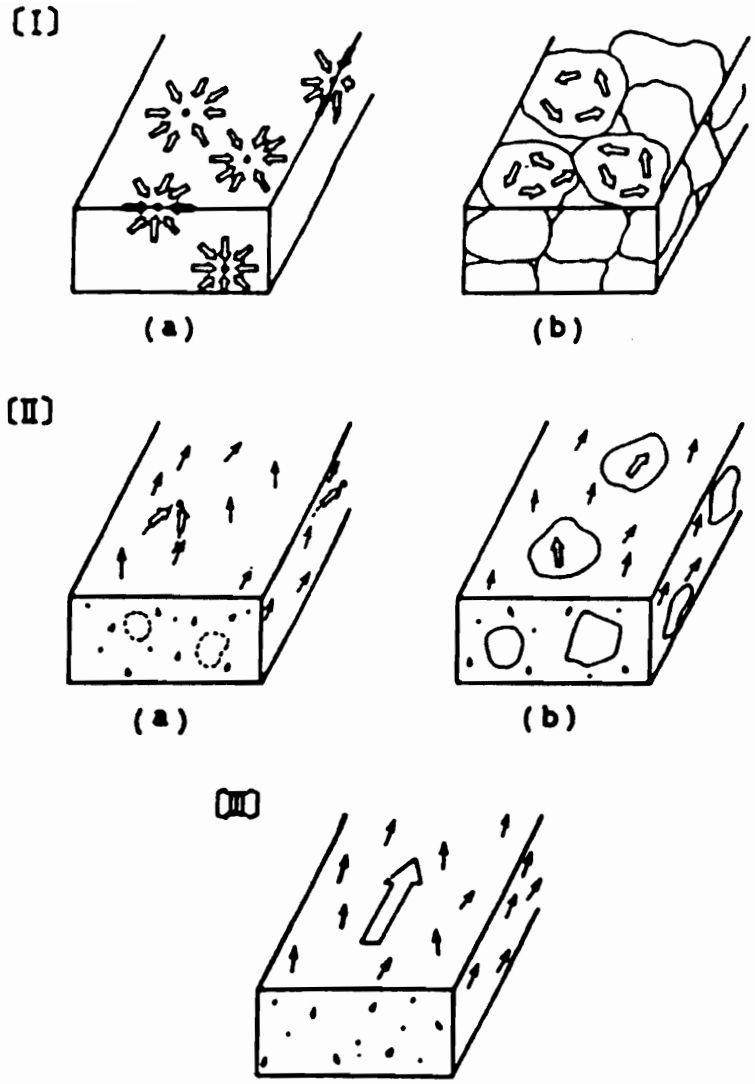

Figure 2.10. Proposed structure corresponding to the three flow regions of a thermotropic LCP as proposed by Ogoni and Asada (174).

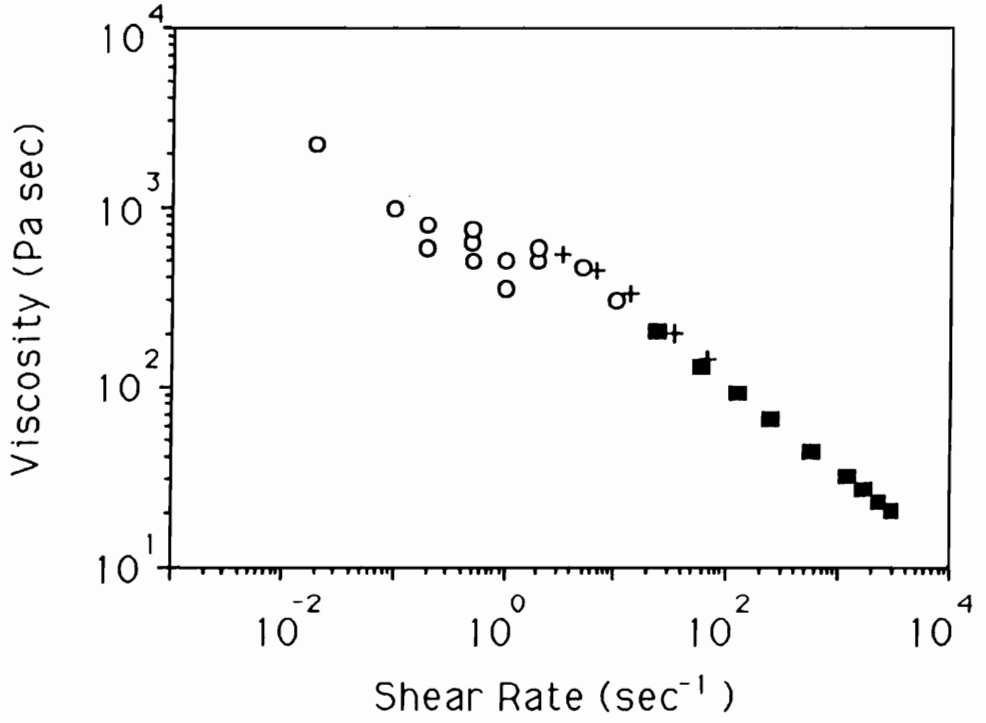

Figure 2.11. Steady viscosity vs. shear rate of Vectra A 900 at 300°C: (○) rotational rheometer; (+) slit die rheometer; (■) capillary rheometer (176).

ing the plateau region. The second shear thinning region comes from the fully nematic orientation of the structure at higher shear rates. Such a behavior is of critical importance to the processing of thermotropic liquid crystralline polymers because variations in shearing conditions are always present in the processing equipment. The rheologic behavior of TLCPs, however, can be strongly affected by previous thermal and shearing histories imposed to the material, and this will be discussed next.

2.4.2 Rheology/Thermal History Dependence

The rheology of thermotropic liquid crystalline polymers is strongly dependent upon thermal histories undergone by the the material prior to the experiments. A striking example of the effect of thermal history on the rheology of TLCPs is illustrated in Figure 2.12 (173). The material used in this study was a thermotropic copolyester of 60/40 PHB/PET. The three flow curves in this figure were all measured at 210°C. The difference among them is that the polymer was loaded into the rheometer at different temperatures, one in the vicinity of (240°C) and one well above (300°C) a DSC endotherm. The melts were then cooled to the the measuring temperature. Preheating to 240°C lowered the viscosity considerably compared to the viscosity measured at 210°C directly without any prior preheating. However, on preheating to 300°C, a qualitative and quantitative change in the flow curve are observed. The shape of the flow curve changes from a solid-like at 210°C to a typical viscoelastic one upon preheating to 300°C. Dilute solution viscosity measurements of the extrudates showed that these striking differences in the shapes of the flow curves did not result from degradation. In addition, DSC and x-ray diffraction analyses supported the hypothesis that the thermal history effect was caused by the melting of PHB crystallites at the preheating temperatures.

Done and Baird (177,178) have studied the effects of thermal history on the rheological properties of three different TLCPs. The materials used in their experiments were two copolyesters of PHB and PET (60-40 PHB/PET and 80-20 PHB/PET) and a copolymer of HBA

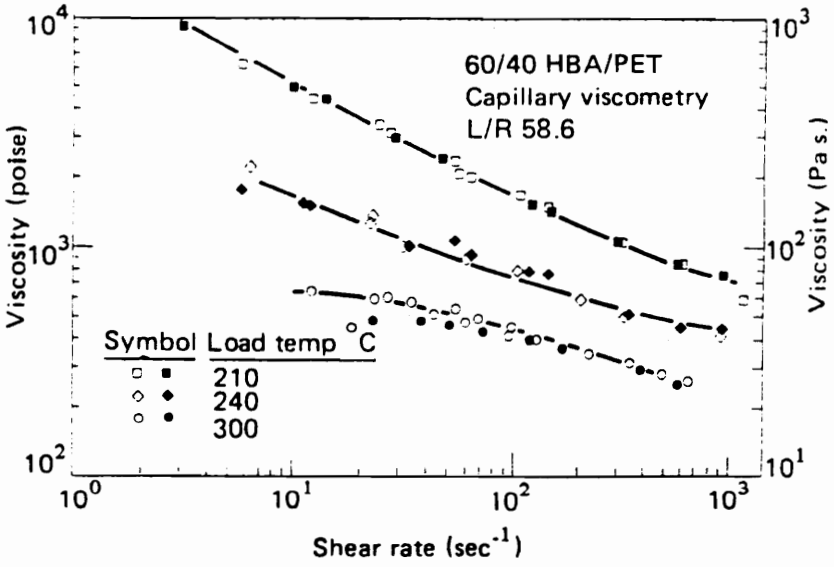

Figure 2.12. Effect of preheating on the viscosity of 60/40 PET/PHB copolyester (173).

and HNA, available as LCP2000 from Hoechst-Celanese. The polymers were preheated above their melting temperatures and then cooled down. During the cooling cycle, the dynamical mechanical properties were monitored. The authors have found that the dynamic shear viscosity, $\eta^{\star}$ and the storage modulus, G′, remained unchanged at temperatures as low as 30°C below the normal melting points of the two copolyesters. For the HBA/HNA copolymer, however, the authors observed a gradual increase in the properties with decreasing temperature. However, a critical temperature was found in where all three systems exhibited a sudden increase in the dynamic properties. This effect is illustrated in Figure 2.13. Subsequent extrusion experiments revealed that in the supercooled state the polymer's extrudate exhibited significant die swell. In addition, the samples extruded in the supercooled region exhibited a more oriented fibrous texture compared to isothermal extrusion above the melting point.

In a recent study, Masuda and co-workers (179) investigated the effects of thermal history on the viscoelastic properties on samples of two different copolyesters (60-40 PHB/PET and 28-72 PHB/PET). Compression molded samples were used in the rheological measurements. The compression molding was performed at 280°C. Compression molded samples were thermal treated for 30 min at 210°C prior to rheological measurements. In the case of 60-40 PHB/PET, they observed a rheological transition at around 270°C. This behavior was explained, on the basis of X-ray diffraction and DSC analyses, by the melting of small amounts of crystallites generated during the thermal treatment at 210°C.. However, at temperatures above that of the rheological transition temperature the effects of thermal history on the viscoelastic properties disappeared. This was attributed to the complete melting of the crystallites and the formation of a liquid crystalline structure. On the other hand, thermal history had no effect on the viscolastic properties of the 28-72 PHB/PET copolyester. The high crystallinity observed in this copolyester coupled with a very distinct liquid crystal temperature transition was claimed to be the cause of such a behavior.

It is clear from the above findings that the rheology of thermotropic liquid crystalline polymers is extremely sensitive to the previous thermal history undergone by the material. As was shown, some thermotropic copolyester may exhibit supercooling behavior and show

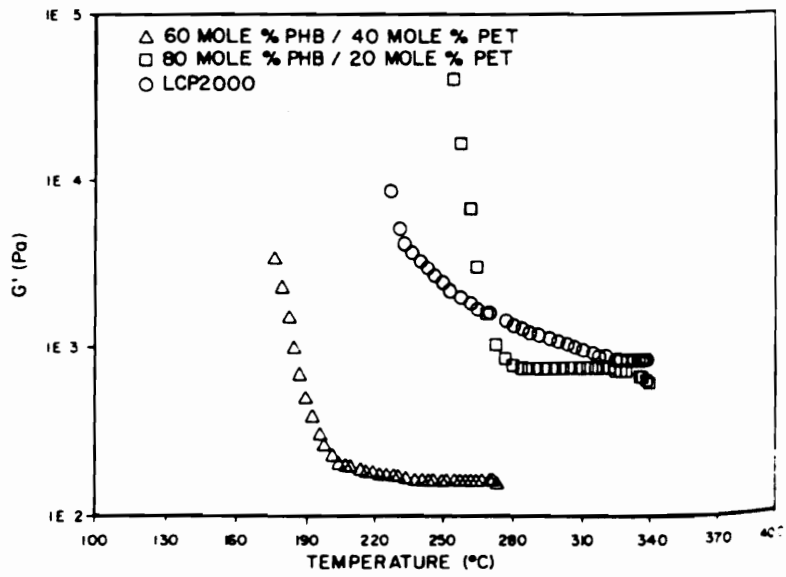

Figure 2.13. **G′ versus temperature during cooling from temperatures higher than flow temperatures, measured at a strain amplitude of 5% (178).**

fluidity at temperature as low as 30°C below their nominal melting temperatures (178). Such a phenomenon is very important to the development of in situ thermoplastic composite. In process where non-isothermal conditions are present, the matrix material will increase its viscosity at a faster rate than the thermotropic LCP. Consequently, varying conditions for fibrillition of the LCP phase as the system cools down. Such a feature could be of importance during, for example, the injection molding process where conditions such as the one described above appears during the molding filling step of the process.

2.4.3 Rheology/Shear History Dependence

In the previous parts of this section, some important rheological features of thermotropic liquid crystalline polymers have been discussed. The rheological behavior of thermotropic liquid crystalline polymers is different of that of flexible chain polymer in many aspects. Further, the rheology of thermotropic LCPs can be strongly dependent upon thermal history undergone by the material and most importantly, TLCPs may show supercooling behavior. In this section, a discussion of the effects of previous shearing history on the rheological behavior of TLCPs will be addressed.

Wissbrun and co-workers (171) have investigated the effects of shear rate history on the rheological properties of a HBA/HNA copolyester, commercially available as Vectra A900. The authors have used a cylindrical annulus to impose a uniform shear history on the material. The material was collected as a strand extruded at different temperatures and shear rates, followed by the melt flow index measurements. They have found that the effects of preshearing were more pronounced at low extrusion temperatures, and a four-fold increase in the material's fluidity, high melt flow index, could be induced. The authors have also noticed the appearance of a fibrous texture in the material upon shearing relative to the unsheared material.

In another study, Wisbrun and Griffin (180) have also reported on the effects of preshearing history on the rheological properties of a themotropic copolyester synthesized in their laboratories. The authors reported that a substantial decrease in the viscosity of the material as a function of increasing preshearing history (refer to Figure 2.14). The dependence of viscosity on the shear history was explained in terms of the polydomain structures assumption as proposed by Ogoni and Asada (174).

The effects of preshearing on the transient behavior (stress growth) of a thermotropic liquid crystalline polymer has been reported by Cogswell (181). The melt was presheared at 0.04 sec^{-1} until a steady state response was reached. The flow was then stopped and the stress allowed to relax below 200 Pa followed by a restart in shear at the same shear rate. The stress was seen to reach immediately its equilibrium value. However, if a much higher preshear rate was applied (1.14 sec^{-1}), and the same procedure repeated, a significant overshoot of the initial stress was observed before returning to its equilibrium value. The difference in the stress growth behavior was attributed to the reorganization of the texture due to the two different preshear rates. The author explained that relaxation to an equilibrium domain structure was fast enough after shearing at the higher rate and this structure had to be broken up again upon startup, resulting in the overshoot peak. Cogswell suggested that a range of rheological responses at a given shear rate are possible depending on the shear history of the material.

In summary, it has been shown that preshearing history reduces the viscosity of a thermotropic liquid crystalline polymer relative to the unsheard material. This change in behavior was explained in terms of changes in orientation and texture of the TLCP induced by preshearing (181) which aggress with the polydomain theory of Ogoni and Asada (174). Besides, appearance of a fibrous texture in the material upon shearing has also been detected (178). The above peculiar rheological characteristics of thermotropic liquid crystalline polymers have tremendous influence in the processing of these materials as will be seen in the next section.

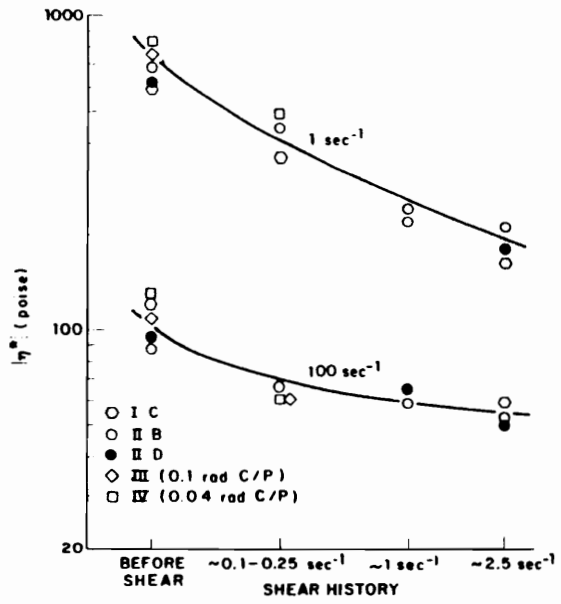

Figure 2.14. Effect of shear history on the viscosity of a thermotropic copolyester (180).

2.4.4 Processing of TLCPs

The rheology of thermotropic liquid crystalline polymers has been discussed briefly in the previous sections. The rheological behavior of TLCPs, as was shown, differs in many aspects from that of flexible chain polymers. One of the most striking differences relative to flexible chain polymers is the fact that TLCPs have the ability to easily orient into elongated fibrils upon application of an external strain, at temperatures above their melting temperatures. Further, the rheology of TLCPs is strongly dependent upon previous thermal and shearing histories. A reduction of the viscosity of TLCPs may be achieved by either previous heating treatment or mechanical shear. Moreover, orientability of the TLCP polydomains increases a the magnitude of shear rate applied to the material increases. In this section, a discussion about processing applications of these materials will be presented. As will be shown, thermotropic liquid crystalline polymers are processed in conventional polymer processing machinery without special adjustments or modifications. They may be melt spun in conventional melt spinning units into very strong and stiff fibers. TLCP fibers may even show specific properties compared to that of metals (46). Besides, they can also be injection molded, extruded into sheets, blow molded and blown into films. This section will review the most recent and/or relevant findings from the literature that are of interest to this research.

2.4.4.1 Extrusion and Melt Spinning of TLCPs

The flow induced orientation of thermotropic liquid crystalline polymers coupled with their long relaxation times (170) are the key properties that influence the processing of these materials. Both the level of orientation, and its distribution, are important for evaluating the mechanical properties of liquid crystalline polymers upon processing (65). However, as pointed out by Kenig (182), the level of orientability of a thermotropic LCP is also a function

of the chemical structure of the material. This orientation can then be preserved upon solidification leading to parts of high mechanical properties.

Because elongational flows are more effective than shear flows in imparting orientation to the TLCP molecules (182), much of the full potential of these materials have thus far been realized through melt spinning of highly oriented fibers of high modulus and strength (32-39), as was shown in Table 1. In the conventional melt spinning process, the polymer flows through a spinneret into air. A stretching force is then applied to the melt resulting in a strong orientation of the polymer molecules along the stretching direction. This orientation, depending on the material's relaxation time (39), may then be locked in upon cooling.

The effects of processing variables on the orientation and mechanical properties in the melt spinning of a thermotropic copolyester of 60-40 PHB/PET (LCP60) have been reported by several authors (33,39,183-185). Muramatsu and Krigbaum (184,185) have reported on the fiber spinning of LCP60 from the melt. They have found that some spin draw ratio was always required to optimize fiber properties and that the length/diameter (L/D) ratio of the capillary die used was another important parameter. They also reported that modulus of the fibers increased as the extrusion temperature was increased from 260°C and higher (185). Reports of Tealdi and Ciferri (186) on the melt spinning of LCP60 have shown an almost constant high modulus fiber as the extrusion temperature was raised from 260°C to 290°C.

Recently, Fujiwara and co-workers (187) compared the effectiveness of shear and elongational flow induced orientation on extrusion from capillaries and melt spinning of LCP60. Capillaries with L/D ratios ranging form 5 to 100, and temperatures from 240°C to 300°C were used in their experiments. Based upon wide angle X-ray scattering (WAXS) and mechanical measurements, they concluded that a highly oriented structure enough to show high modulus could not be obtained by means of shear flow through the capillary. The tensile modulus obtained for strands extruded at 285°C with a shear rate of 1.4×10^4 sec^{-1} and a L/D ratio of 20 was of only 2.0 GPa, whereas for filaments spun at the same temperature and L/D ratio the tensile modulus reached 40 GPa at a draw ratio of 100. In elongational flow produced by spinning, the dominant processing conditions to impart orientation to the melt were the

spin-draw ratio and the initial diameter of the filament. They could not observe, however, a significant effect of the processing conditions, such as spinning velocity, spinning temperature, and cooling on the orientation behavior of the material. The effect of filament diameter on the orientation was claimed to be due to the appearance of necking upon spinning which reduced the virtual spin-draw ratio.

Studies on the effects of shear and elongational flows on the properties and orientability of a thermotropic liquid crystalline copolymer of HBA/HNA (Vectra A900) have recently been investigated by Kenig (182,188). He used an Instron Capillary Rheometer along with a rotating spool to collect the extruded strand. Based upon experimental results accompanied by mathematical analyses, Kenig concluded that the orientation development in shear flows depended on the total shear strain applied to the material and not on the shear rate. Absolute values of shear strains of 170 to 700 were not as effective as elongational strains in the range of 2 to 10 in imparting orientation to the thermotropic copolymer. Furthermore, he pointed out that relative low shear rates did not affect orientation because of achieving enough high shear strains at low shear rates required a long shearing period and, at such durations, relaxation of the orientation contributed to the orientation decay.

2.4.4.2 Injection Molding of TLCPs

The fluid mechanics of the injection molding process is complicated compared to extrusion or melt spinning due to the unsteady and non-isothermal two-dimensional flow coupled with the existence of an advancing front (65). The polymer melt is subjected to both shear and elongational stresses during the filling stage of the injection molding process.

A schematic representation of the mold filling stage during the injection molding process is illustrated in Figure 2.15 (A). An initial analyses indicates that there are at least three major sources of orientation during the filling step of the process. These are (1) the spreading radial flow in the vicinity of the gate as the material enters the cavity, (2) interlayer

shear induced orientation at some distance from the mold walls downstream from the melt front, and (3) the fountain flow at the advancing melt front. These three flow regimes, coupled with non-isothermal and nonuniform shearing conditions, have fundamental importance to the development of orientation on the TLCP molecules in the injection molding process.

From the three flow regimes of the injection molding process the one with the most complicated flow pattern is undoubtedly the advancing front, which is known as "fountain flow". This is illustrated in Figure 2.15 (B). During this type of flow, the fluid elements from the center of the incoming melt are elongated while flowing along the streamlines towards the front. These fluid elements reach their maximum state of elongation at the moving front and are deposited on the wall of the mold cavity. Thus, the fountain flow pattern in the injection molding process generates an elongational flow in the advancing front. As will be seen from experimental works reviewed later, the complex flow pattern of the injection molding process gives rise to a layered structure along the thickness direction in injection molded parts. This structure, as will be seen, is made of a highly fibrillar oriented skin and a relative unoriented core regions (189).

Jackson and Kuffus (64), in their widely cited work, were among the first to experiment on the injection molding of thermotropic liquid crystalline polymers. In their studies on a series of thermotropic copolyesters, they were able to obtain injection molded parts of 40-60 PET/PHB copolyester with tensile strength as high as 200 MPa, and flexural modulus as high as 17 GPa in the direction of flow. However, they observed that the injection molded parts exhibited a very strong degree of mechanical anisotropy. The transverse to the flow flexural modulus was in the order 1.5 GPa, which was an order of magnitude lower than flow direction properties. This mechanical anisotropy, however, could be reduced by the increase in the part thickness (refer to Figure 1.4). Although morphological studies were not performed, it is clear from the mechanical property results that a strong orientation of the LCP domains along the injection molding flow direction was attained upon processing.

Studies of Joseph and co-workers (189) have indicated that the strong mechanical anisotropy exhibited by injection molded parts of 40-60 PET/PHB was due to the morphological

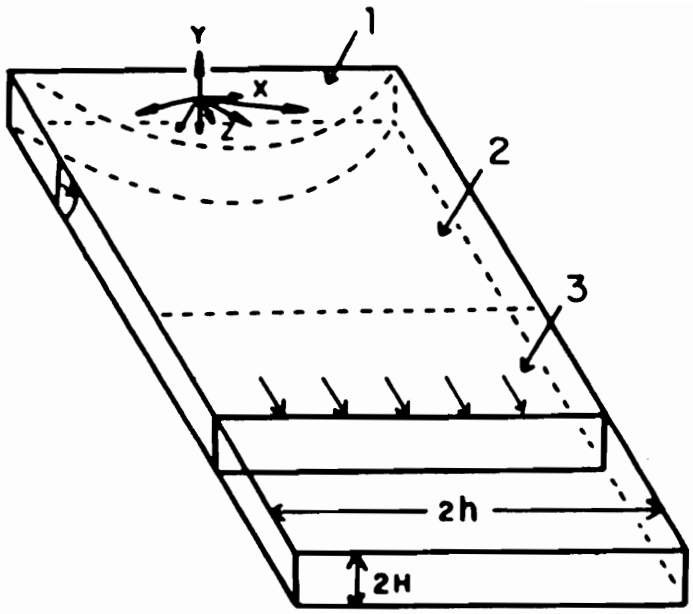

(A)

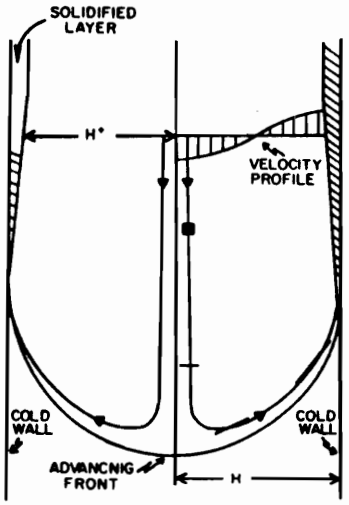

(B)

Figure 2.15. Schematic representation mold filling during the injection molding process (A) with different flow regions and (B) the fountain flow pattern (65).

structure attained by the material upon processing. They observed, based upon WAXS and scanning electron microscopy experiments, that a skin/core type of morphology was present in the injection molded parts. The skin exhibiting a highly fibrillar structure oriented in the injection molding flow direction and a relative unoriented central region was observed in the molded part.

Recently, Carg and Kenig (65) carried out extensive experimental work, coupled with mathematical flow analyses, on the injection molding of a thermotropic copolymer of HBA/HNA (Vectra A900). In their studies, they evaluated the residual orientation and the residual mechanical properties of an injection molded Vectra A900 sample as a function of the cross section part thickness using layer removal technique. This technique consists of symmetrically removing layers of a defined thickness from both sides of the molded sample by grinding on a fine grit diamond polished wheel. The modulus of the removed layers was calculated based on a simple two-component composite model in which the residual sample and the removed layer were taken as the components of the composite, using the equation $E_l = (L_0E - LE_r)/(L_0 - L)$, where E_l is the modulus of the removed layer, E is the initial modulus of the sample, E_r is the residual modulus, and L and L_0 are the residual and the initial thickness of the sample, respectively. The residual flow direction modulus of the injection molded Vectra A900 sample is shown in Figure 2.16, normalized to the initial modulus E. From the figure it can be concluded that the skin region of the sample, originated in the elongational fountain flow, is the part of the sample that contributes the most to the overall mechanical behavior of the sample. Another observation is the fact that the residual modulus decays amazingly fast towards the center region of the part. These differences in residual modulus confirms the fact that the outer layers of the injection molding part are the ones with the most fibrillation of the TLCP molecules. The figure also shows a peak in the modulus following the skin region at $L/L_0 = 0.85$. This peak suggests that interlayer shear orientation exists at regions closer to the mold wall. However, this orientation is not as high as the orientation originated in the elongational fountain flow.

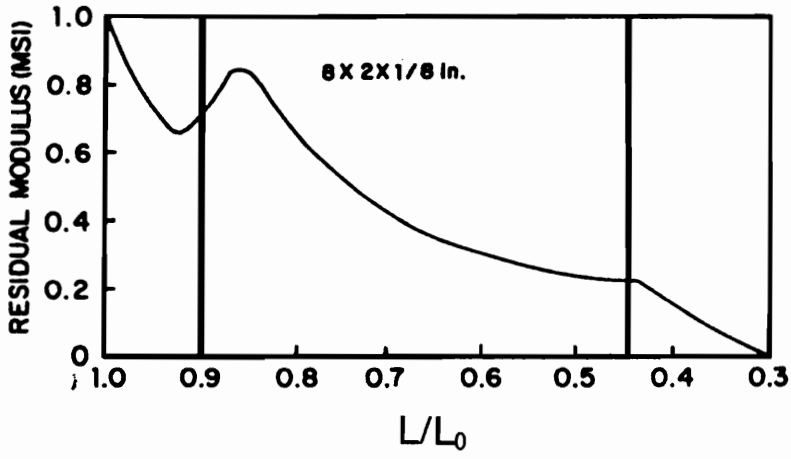

Figure 2.16. Tensile modulus as a function of removed fractional thickness for an injection molded sample of a HBA/HNA thermotropic copolyester (65).

Suokas and co-workers (190) have also studied the relationships between the microstructures and the physical properties of injection molded parts of Vectra A900. They used a especial designed injection mold in where several combinations of gate geometries and part profiles could be obtained. Variations in the injection molding conditions, such as holding pressure and injection speed, were also included in their work. From analyses of the mold filling process, they found that 5 different flow patterns could be observed. Mechanical properties measurements on the injection molded samples of Vectra A900 revealed that parts with tensile modulus as high as 11 GPa and tensile strength as high as 180 MPa, could be obtained.

The mechanical properties of an injection molded part, as was seen, do not approach those reported for melt spun fibers. The kinematics of the process give rise to a layered structure with thickness dependent orientation and consequently, giving to the molded part less than ideal flow direction properties. This apparent deficiency inherent to the process has motivated Blizard and co-workers (191) to further process injection molded plaques with the objective of improving their mechanical properties. In their studies, they have compression molded injection molded plaques of two different TLCPs, LCP60 and Vectra A900. The molded plaques were pressed at both isothermal and noisothermal conditions. Isothermal compression temperatures of 190°C and 205°C , and 210°C and 240°C were used for LCP60 and Vectra A900, respectively. Non-isothermal conditions were achieved by rapid cooling during the squeezing step of the process. Biaxial elongational deformations were generated during the compression molding experiments. Lubricated plates were used to minimize the effects of shear at the plate walls. Mechanical properties measurements have indicated an improvement of both tensile and flexural moduli of the LCP60 relative to the molded part. Tensile modulus could be increased by as much as 35% (from 3.2 GPa to 4.3 GPa) and flexural modulus could be increased by as much as 27% (from 10.5 GPa to 13.5) after nonisothermal compression. Based upon scanning electron microscopy observations, the increase in modulus was attributed to an increase in the fibrillar fraction of the part upon compression. Consequently, reducing the negative effect of the unoriented core to the mechanical properties of the part.

In summary, it has been shown that the flow induced orientation of thermotropic liquid crystalline polymers has a tremendous effect on the mechanical properties of these materials. Processes in where elongational flow fields are present, such as melt spinning, the TLCP polydomains attain a highly oriented fibrillar structure giving rise to high mechanical properties. Whereas in processing where nonuniform shear flow fields are present, such as extrusion, the polydomains orientation will vary accordingly to the magnitude of the interlayer shear strain induced. Further, it has been shown that in the injection molding process a skin/core type of structure arises in the molded part upon processing. Because of such a structure, the effectiveness of the process in achieving high mechanical properties compared to melt spinning process, is reduced. Nevertheless, the mechanical properties of injection molded TLCP parts can be improved by post processing of these parts such as, for example, compression molding.

Some aspects of the processing of thermotropic liquid crystalline polymers have been reviewed above. In the following section, the use of TLCPs as a reinforcing phase in blends with flexible chain polymers is discussed.

2.5 In Situ Thermoplastic Composites

Much of the fundamental aspects of the formation of in situ composites have been discussed in earlier Sections. Specifically, the theory of droplet deformation and breakup were discussed with some extent in Section 2.2. In addition, the phenomena of capillary instability and conditions under which the deformed fibrils would remain stable were reviewed in Section 2.3. As pointed out earlier, the phenomenon of fibrillation of a dispersed fluid in a matrix of another fluid are directly interconnected with microrheological aspects of the components. Thus, the rheologic characteristics of thermotropic liquid crystalline polymers

were reviewed in Section 2.4. Important aspects of TLCP rheology such as thermal and shear histories dependence were addressed.

A general introduction to the topic of in situ thermoplastic composites was presented in Chapter 1. As shown, blending of thermotropic TLCPs with flexible chain polymers may in fact improve the mechanical properties of the flexible chain polymer. Some examples were cited in where the properties of the flexible chain matrix could be increased by as much as 300%, depending on processing conditions, compared to the properties of the unreinforced matrix. In this section, a survey of the literature concerning to the development of in situ composites will be presented. Research on the development of in situ composites has been extremely active in the last several years and as a consequence the scientific literature available on this subject is quite vast. Thermotropic liquid crystalline polymers have taken part in blends with almost any commercially available thermoplastic. For instance, blends of TLCPs with polyamides (PA) (3,68,192-194), polycarbonate (PC) (3, 60, 192-197), poly(ethylene terephthalate) (PET) (198-202), polystyrene (PS) (47,53,203,204), poly(butylene terephathalate) (PBT) (3,192,193,205,206), polyetherimide (PEI) (3,50,58,61,81,208), polyarylates (PAR) (3,209) polyetherketone (PEEK) (3,57,210,211), poly(phenylene sulfide) (PPS) (59,198,199,212), poly(vinyl chloride) (PVC) (213,214), polypropylene (PP) (198,199), and others (3,53,215) have been recently appeared in the literature. Most of these researchers have concentrated on the use of LCPs as to obtain enhanced mechanical properties of the hosting matrix and reduced melt viscosity. Frequently studied are also phase behavior of TLCP/polymer blends and blend morphology. The scope of this review is to present the literature of most relevance to this research. However, when deemed necessary, references outside the scope of this research will be cited only as corroborative evidences to the reviewed subject.

The literature dealing with blends of flexible chain and thermotropic liquid crystalline polymers is divided below into two main categories. These categories are: rheology and processing. However, the processing section will be coupled with references on morphology and mechanical properties of these blends.

2.5.1 Rheology of TLCP/polymer blends

The rheology of polymer blends containing liquid crystalline polymers is discussed in this section. As will be shortly seen, the addition of a liquid crystalline polymer to a polymer matrix reduces the viscosity of the matrix at concentrations of as low as 5 w/w percent TLCP. Reduction of the matrix viscosity upon addition of a TLCP phase seems to be a common finding in the study of the rheology of TLCP/polymer. The following discussions will present some illustrative examples of the use of TLCPs as effective processing aids to thermoplastic materials.

Siegmann and co-workers (74) were among of the first researchers to report on blends of a thermotropic copolyesters based on HBA/HNA and a flexible chain polymer. The exact composition of the copolyester used in their work was not disclosed. The rheological behavior of the blends and pure polymers was analyzed only at high shear rates using a capillary rheometer at a temperature of 260°C, below the TLCP melting point. A significant reduction of the system's viscosity compared to that the pure polymers was reported. A minima in the viscosity composition curve was found to occur at 5% TLCP concentration.

Isayev and Modic (60) have studied the rheological behavior of blends of polycarbonate (PC) with two thermotropic polymers based on HBA/HNA copolyesters at temperatures of 280°C and 310°C. The copolyesters studied consisted of 25 and 30 mole percent HBA and 75 and 70 mole percent HBA, denominated as HBA/HNA and LCP2000, respectively. Blends of PC/TLCP were prepared by either extrusion through a six-element Koch static mixer or in a internal mixer with Banbury rotors. TLCP concentration in the blends was in the range of 2.5 to 50 weight percent. In the case of the pure components, they noticed that at each test temperature there was a shear rate in where a crossover in the viscosity of the pure components was found, i.e. a viscosity ratio of unity between the blends components. These crossover points of the viscosity of each blend component as a function of shear rate is of importance to the development of in situ composites because, as discussed in Section 2.3,

fibrillation of the reinforcing TLCP phase in the matrix polymer occurs most effectively at this particular viscosity ratio (23). The rheological behavior of the PC/(HBA/HNA) and PC/LCP-2000 blends have shown that at a 310°C, at high and low shear rates the viscosity curves of the blends at 25 w/w HBA/HNA and below were in between those of the individual polymers. In the range of intermediate shear rates the viscosity of the blends was lower than the viscosity of the components. However, a peculiar behavior was found for the system with a HBA/HNA concentration of 50 w/w percent. At this particular composition, the viscosity of the blend was found to be significantly higher than that of the each component for the whole shear rate range investigated. Based upon scanning electron microscopy (SEM) results, the authors concluded that the increase in the blend viscosity was because undeformed HBA/HNA spherical droplets were found in the PC matrix. Blends of PC/LCP-2000 revealed similar behavior of the PC/HBA-HNA blends but, however, the 50% w/w LCP-2000 in the PC matrix had a viscosity in between that of the pure components. The author have also observed that mixing history had no effect on the rheological behavior of PC/HBA-HNA at 97.5/2.5 w/w composition ratio. Thus, in the range of shear rate investigated the viscous behavior of the blend was apparently not perceptible to the method of mixing used. Similar blends of PC and HBA/HNA thermotropic copolyester have been studied by Malik and co-workers (52). They found that the melt viscosities of the blends were below and more shear thinning than that of pure PC. These authors have also investigated transient behavior of the blends by solid state relaxation measurements and found that the relaxation modulus increased with the addition of the TLCP.

The rheological behavior of blends containing HBA/HNA thermotropic copolyester and poly(ether imide) PEI, available as Ultem from GE Plastics, have also received attention by the research community. Most of these investigations have used a HBA/HNA thermotropic copolyester at a molar fraction of 73 mole percent HBA and 27 mole percent HNA. This specific copolyester is marketed by Hoechst-Celanese under the trade name Vectra A 900. Swaminathan and Isayev (216) have investigated the rheological behavior of blends of PEI and Vectra A 900 by the use of capillary rheometry. Their rheological measurements have indi-

cated that a reduction of the PEI viscosity was possible by the addition of as low as 2.5 w/w percent Vectra A 900.

Recent investigations of Sun and co-workers (50) have, among other things, studied the rheology of blends containing Vectra A900 and PEI (Ultem 1000). Their investigations are of particular interest to this research and will be reviewed in some detail next. The rheological studies were performed on a Rheometrics Mechanical Spectrometer (RMS 800) utilizing a parallel plate attachment. Temperature, frequency and time sweeps were investigated. The objective of the rheological investigations was to find a overlapping processing temperature in where the two materials would be rheologically stable. The lower limit of processing temperature of the pure materials was specified as the crossover in the storage, G′, and loss, G″, moduli and was defined as T_x. The upper limit of the processing temperature was taken as the most stable rheological temperature, defined as T_r This temperature was determined by the increase in the viscosity of the materials during isiothermal time sweeps. Based upon rheological results for the pure components the processing window of PEI/Vectra A900 blends was selected from 285°C to 350°C. The effects of the addition of Vectra A900 on the viscosity of the hosting PEI were determined by the changes in the complex viscosity, $\eta^{\star}$, monitored during cooling from the melt down to T_x temperature, as shown in Figure 2.17. For pure PEI, T_x was around 285°C. This temperature was lowered to 280°C with the addition of 10% w/w of Vectra A900. However, the viscosity of the blend did not decreased significantly from that of the pure PEI. The viscosity of the blend was still dominated by the PEI component. At 50% w/w Vectra A900 concentration $T_{x'}$ was reduced to 275°C. The viscosity of the blend at this composition was still dominated by the PEI phase and was a decade higher than that of the pure TLCP. Therefore, the supercooling behavior of the blends was increased as the Vectra concentration in the blend was increased, consequently bringing even farther down the lower limit of the processing temperature window.

Quite recently Berry and co-workers (197) have studied the shear and elongational viscosity of PC and Vectra A900 and their 80/20 w/w PC/TLCP blend using a capillary rheometer. Their investigation focused on experimental studies using two sets of capillaries.

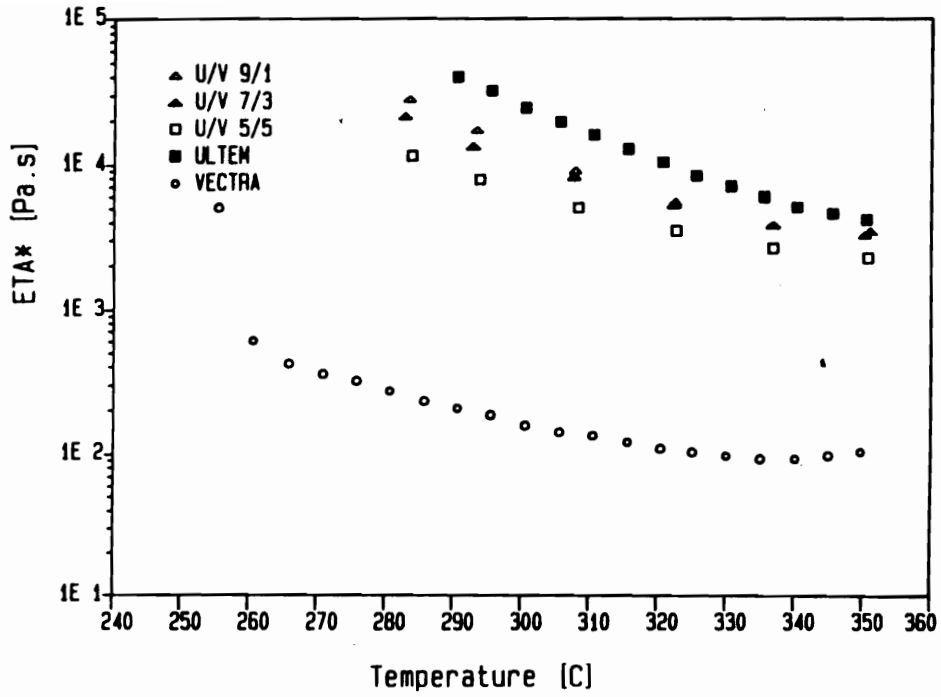

Figure 2.17. Complex viscosity vs. temperature for Ultem, Vectra A900 and Ultem/Vectra blends (90/10, 70/30 and 50/50) cooling from 350°C (50).

The first set comprised capillaries having a converging entrance followed by a cylindrical section. The second set, named "zero length" set, included capillaries having only the converging section. In the sets various entrance angles were used. Based upon experimental results they concluded that the shear viscosity and entrance pressure were practically independent of the entrance angle. The entrance pressure was small in the case of PC but it was appreciable in the case of PC/TLCP blends. The entrance pressure drop reached 50% of the total pressure drop for the pure TLCP and it was attributed to the TLCP orientability in the converging flow of the capillary entrance. Consequently, entrance pressure corrections are necessary to obtain the real shear viscosity of TLCPs. To estimate the elongation viscosity of the pure materials and their blend, the entrance pressure drop component due to elongational flow was treated separately from that of the shear component, following the approach proposed by Gibson (217). They have found that the pressure component due to elongational flow rather than the shear component dominates the entrance pressure drop. The elongational viscosities of the TLCP were higher than those of PC in the elongation rate range studied. The 80/20 PC/TLCP blend exhibited intermediate values of viscosities relative to the two pure components. A summary of their finding is presented in Figure 2.18. In the figure, the ratio of the elongational (λ) to shear viscosity (η) as a function of flow rate is presented. As one would notice, the viscosity ratio λ/η for LCP increases with flow rate while for the neat PC and 20%LCP blend this ratio decreases to minimum values. The higher elongational to shear viscosity ratio for LCP and the LCP blend was claimed to be due to orientation development of the LCP phase during elongational flow within the converging entry region. Further, one notices that the ratio of elongational to shear viscosities exceeds the value of 3, the expected ratio for Newtonian fluids, for all the three materials studied.

In summary, it can be seen from the few examples reviewed above that the addition of a TLCP phase to a polymer matrix may in fact reduce the viscosity of the matrix relative to the pure hosting material at a broad range of shear rates. The viscosity of a polymer may be strongly reduced by the addition of as little as 2.5% w/w TLCP., as was in the case of polyamides. On the other hand, this effect is not so strong observed as in the case of

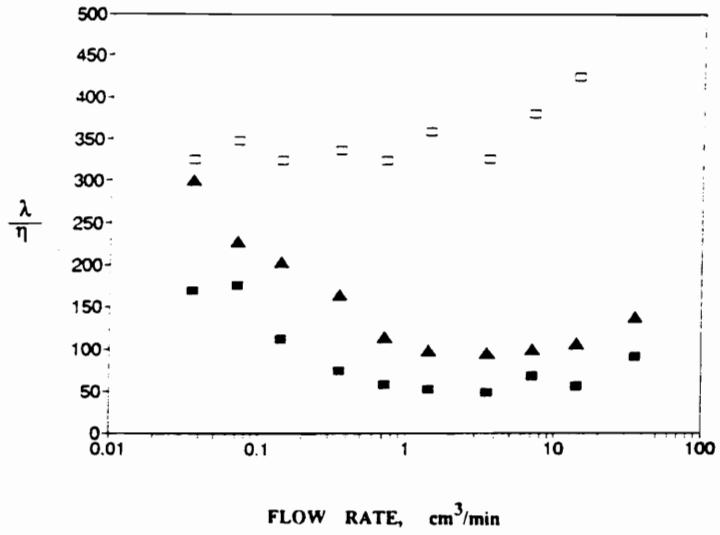

Figure 2.18. Ratio of elongational to shear viscosities of LCP (□), PC (■), and 20%/LCP/80%PC blend (▲) at a capillary entrance angle of 60° (197).

polyetherimides (50) in where blends of up to 50% w/w LCP exhibited a viscosity closer to that of the pure PEI. In the next section a discussion on the processing of TLPC/polymer blends will be presented.

2.5.2 Processing of TLCP/Polymer Blends

Earlier discussions highlighted the need to utilize extensional flow processes to impart maximum fibrillation and high mechanical properties to TLCPs. Reports on the fiber spinning of Vectra A900 have indicated that infinite aspect ratio fibers with tensile modulus as high as 65 GPa can be obtained (39). In processing TLCP/polymer blends, fibrillation of the TLCP domains in the matrix polymer to enhance the mechanical properties of the matrix material is also obtained through processes where strong elongational flows are involved. Thus, in processing such as fiber spinning and sheet extrusion where drawing of the polymer melt is obtained by the application of an external force, maximum orientation and consequently improved mechanical properties of the hosting matrix can be obtained. Nevertheless, injection molding of TLCP/polymer blends have also indicated that improvements in the mechanical properties of the matrix polymer may be achieved and sometimes synergism in the mechanical properties could also be verified. In this section, some examples of fiber spinning, sheet extrusion and injection molding of TLCP/polymer blends will be presented.

Recently, Li and co-workers (200) have investigated the morphology and mechanical properties during the fiber spinning of blends of Vectra A900 and PET over the entire composition range. The fibers were spun at 300°C, using different takeup speeds according to LCP concentration. Subsequently, The fibers were etched with a 40% by weight aqueous methylamine solution to remove excess PET and reveal the morphology attained by the LCP phase. The authors concluded, based upon experimental results, that discontinuous fibers of the LCP domains were found in fibers with 35 and 60% by weight LCP. By increasing the LCP concentration to 85 and 96%, the LCP phase was found as continuous fibers. Fibers diameters

where in the range of 0.5 μm. Further, they have noticed that the transition form discontinuous to continuous fibers were accompanied by an increase in modulus and strength with a change in the fracture mode from brittle fracture when the TLCP fibers where discontinuous to delamination fracture when the TLCP fibers where continuous. Besides, Vectra A900 revealed a tensile modulus of 70.7 GPa, whereas the pure PET revealed a value of 1.5 GPa. The tensile modulus for PET/Vectra blends followed those predicted by the rule of mixtures at high LCP concentrations. At low LCP concentrations the tensile modulus followed the predictions of particulate filled polymers. A maxima in the tensile strength was observed at 96% Vectra concentration. The authors claimed that the morphological changes from discontinuous to continuous LCP fibers affected the mechanical properties response of the blends.

Sun and co-workers (50) have investigated the morphology and mechanical properties variations during the sheet extrusion of PEI and Vectra A900 blends as a function of post extrusion draw ratio. The authors have used a single screw extruder to which was attached a 102 mm width sheet die to generate sheets of PEI, Vectra A900 and their blends at a temperature of 345°C. After extrusion the sheet was fed onto takeup rolls. The first roll placed at 15cm from the die and the second roll located at 20cmm from the first one. By controlling their relative speed, draw ratios ranging from 2 to 60 could be imposed to the extruded sheet. Wide angle X-ray diffraction (WAXD) was utilized to verify the effects of draw ratio on the molecular orientation of the TLCP phase. The effects of draw ratio on the morphology, obtained by scanning electron microscopy, and molecular orientation of PEI/Vectra 70/30 composition ratio is presented in Figure 2.19. The tensile moduls of the extruded sheets increased as the draw ratio increased, following the increase in the fibrillar structure of the TLCP domains with draw ratio (DR). As and example, PEI/Vectra 70/30 composition ratio revealed a tensile modulus of 2.7 GPa at a DR = 3.1. Increasing DR to 16, tensile modulus increased to 7.5 GPa. In contrast to the improvement in modulus, no improvement in the tensile strength was observed. The authors claimed that this may be due to poor adhesion between PEI matrix and the reinforcing Vectra fibrils. Pulled out Vectra fibrils could be observed after cryogenic fracture.

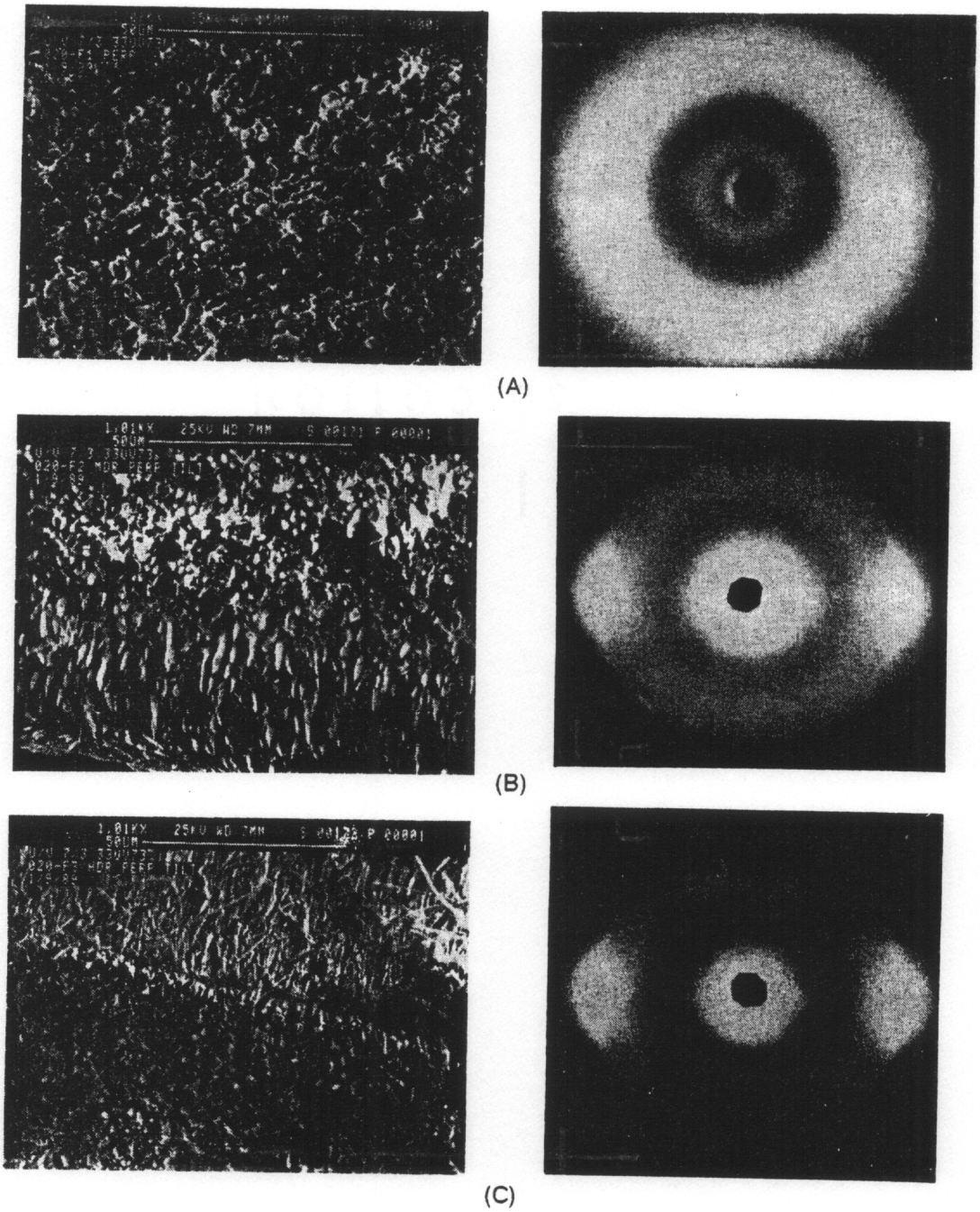

Figure 2.19. Effects of draw ratio (DR) on the morphology and molecular orientation of PEI/Vectra A900 70/30 w/w composition ratio: (A) DR = 1.8; (B) DR = 6.3; (C) DR = 19 (50).

The morphology and mechanical properties of injection molded and spun fibers of blends of PS and Vectra A900 and Vectra B950, were examined more recently by Crevecoeur and Groeninkx (53). The mechanical properties obtained for the blends showed that the dispersed LCP phase possessed moderate aspect ratio fibrils in the case of injection molding samples but nearly continuous fibrils for the spun fibers due to a more strong elongational flow field provided by the spinning process, as reviewed earlier. Further, the modulus and strength of the injection molded samples were observed to be below that predicted by the rule of mixtures. However, the spun fibers were observed to obey the rule of mixtures, which is the limiting case of the Tsai-Halpin equation for continuous fibrils reinforcement. The contribution of the LCP reinforcement was higher in the case of fibers compared to the injection molding process. This was attributed to both, finer morphology and higher molecular orientation of the LCP phase in the fibers.

A good illustration of the effects of viscosity ratio of the reinforcing LCP to the matrix material on the fibrillation of the LCP phase is found in the work of Isayev and Subramanian (211). These authors have studied the injection molding of blends of PEEK and a thermotropic liquid crystalline polymer based on paraoxy-benzoyl and oxy-biphenylene terephthalate units (Xydar SRT-300 from Amoco). Blends of these materials were prepared by using a single screw extruder with a static mixer attachment followed by injection molding into minitensile bars (ASTM D 638 type 5) at a temperature of 420°C. The authors have found that the mechanical properties, such as tensile strength and moldulus, revealed a slight increase at low LCP concentration which was attributed to the presence of ellipsoids of LCP in the PEEK matrix. At high LCP concentrations, phase inversion was observed in the blends with fibrillation of the PEEK phase in the matrix of the LCP. Consequently, the presence of the low modulus PEEK fibers contributed to the reduction of the mechanical properties of the blend. Injection molded minitensile bars of the neat Xydar showed a remarkable tensile modulus of about 30 GPa and a tensile strength of the order of 140 MPa.

Extensive studies on the injection molding of blends of Vectra A900 with polypropylene (PP), polyethylene terephthalate (PET), and polyphenylene sulfide (PPS) as

matrices have recently been performed by Sepala and co-workers (198,199). The processing temperatures for the pure materials were in accordance to manufactures recommendations. In the case of the blends PET/, PP/, and PPS/LCP an average injection molding temperature of 295°C, 285°C, and 325°C was used, respectively. A TLCP concentration of up to 50% w/w was used. Prior to injection molding, the blend components were melt blended in a twin screw extruder at temperatures ranging from 285 to 290°C. Blends were then injection molded into standard tensile bars according to ASTM 638. As a general conclusion, they have found that the mechanical properties of the matrix materials were increased by the addition of the TLCP phase. In the case of PET/LCP, the elastic modulus and the tensile strength increased linearly with LCP content. In the case of PP/LCP and PPS/LCP blends both systems revealed similar trends in the mechanical behavior. Tensile moduli increased quite steeply at low LCP content, almost leveling off at intermediate LCP concentrations and picking up again at 50% LCP concentration. An important observation from their work was the decrease in the linear thermal expansion coefficient of the matrix polymers with the addition of the liquid crystalline phase. This is illustrated in Table 2.1.

Berry and co-workers (192,193) have recently studied the effects of the viscosity ratio on microestructure and mechanical properties developed during the injection molding of LCP/polymer blends. They have used a HBA/HNA 70/30 mole percent thermotropic copolyester in blends with PC, PBT, Nylon-6 (N-6), and an amorphous Nylon (AN). A TLCP concentration up to 25% w/w was used in their blends. The authors have observed that, upon injection molding a distinct skin/core morphology appeared in the molded part, where elongated LCP fibrils comprised the skin and spherical and ellipsoidal particles composed the core region. Similarly to the findings of Joseph and co-workers (189). The highest aspect ratio LCP fibrils were obtained with AN/LCP system, followed by PC/LCP. PBT/LCP and N-6/LCP showed a coarser morphology. Consistent with the morphological observations, AN/LCP blends demonstrated the highest values of tensile moduli and again it was followed by PC/LCP, PBT/LCP and N-6/LCP. The morphological variations, consequently affecting the mechanical properties of the blends, were attributed to differences in the viscosity ratio be-

Table 2.1. Linear thermal expansion coefficients of PET/, PP/, and PPS/Vectra A900 blends (198).

Matrix/LCP %	α (10^{-5} K^{-1})
LCP	0.1
PET	5.0
PET/10	4.1
PET/30	3.0
PP	5.8
PP/10	4.5
PP/30	3.4
PPS/	3.6
PPS/10	3.3
PPS/30	3.1

tween the systems. The viscosity ratio of the dispersed LCP phase to that of the isotropic polymers, according to the authors, was the decisive factor determining the deformation and the structure development of the LCP phase in the matrix polymer. In the case of AN/LCP and PC/LCP, the viscosity ratio was about 1.0 at a shear rate of 540 sec^{-1}. At the same shear rate, PBT/LCP showed a viscosity ratio of 6.0 and N-6/LCP a viscosity ratio of 13. The effect of viscosity ratio on the fibrillation of the LCP domains during the injection molding process is illustrated in Figure 2.20 for PC/LCP and N-6/LCP, after etching of the matrix polymer. Figures 24 (A) and (B) represent the LCP particles after removal of the PC phase encountered in the skin and core regions, respectively. Figures 24 (C) and (D) represent the LCP particles after removal of the N-6 phase for the skin and core regions, respectively. A one observes, fibrillation of the LCP domains was more pronounced in the system were the viscosity ratio was closer to unity. These observations corroborate with the discussions of Section 2.2. Furthermore, the authors have noticed, upon SEM analyses, a strong interfacial adhesion between the AN and the LCP phase. This fact contributed to the enhancement of the tensile strength of the blend relative to the pure polymer.

Isayev and co-workers have carried out studies on the injection molding of several TLPC/polymer blends (57-60). They have used PEEK, PEI, PPS and PC as matrix materials and Vectra A900 as the reinforcing LCP phase. Synergistic effects in the tensile modulus on PEI/ and PEEK/ Vectra A900 blends have been observed (57,58). Figures 2.21 (A) and (B) show the modulus as a function of LCP concentration of PEKK/Vectra A900 and PEI/Vectra A900 blends, respectively. The authors have attempted to explain the causes of such a positive deviation from the rule of mixtures based upon fibrillation attained by the LCP domains during the injection molding process. Further, they have found that the elongation at break of both systems decreased with increasing LCP concentration. Based upon differential scanning calorimetry (DSC), they concluded that both systems were imminscible over the entire composition range. They also have found that the degree of mechanical anisotropy, machine versus transverse properties, increased as the LCP concentration was increased (57).

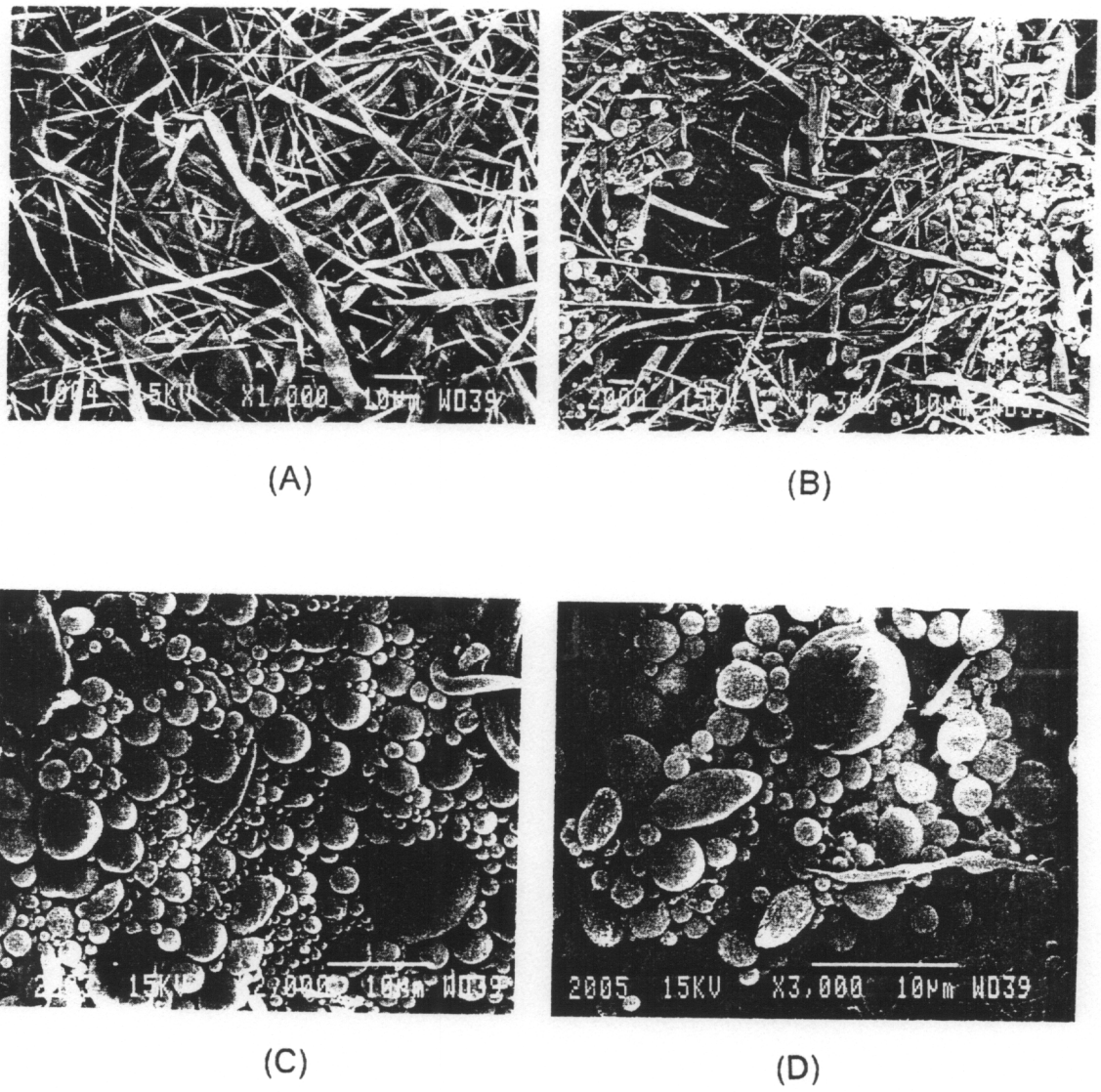

Figure 2.20. LCP particles after etching of the matrix polymer: PC/10% LCP taken from (A) skin and (B) core regions; N-6/10% LCP taken from the (C) skin and (D) core regions (193).

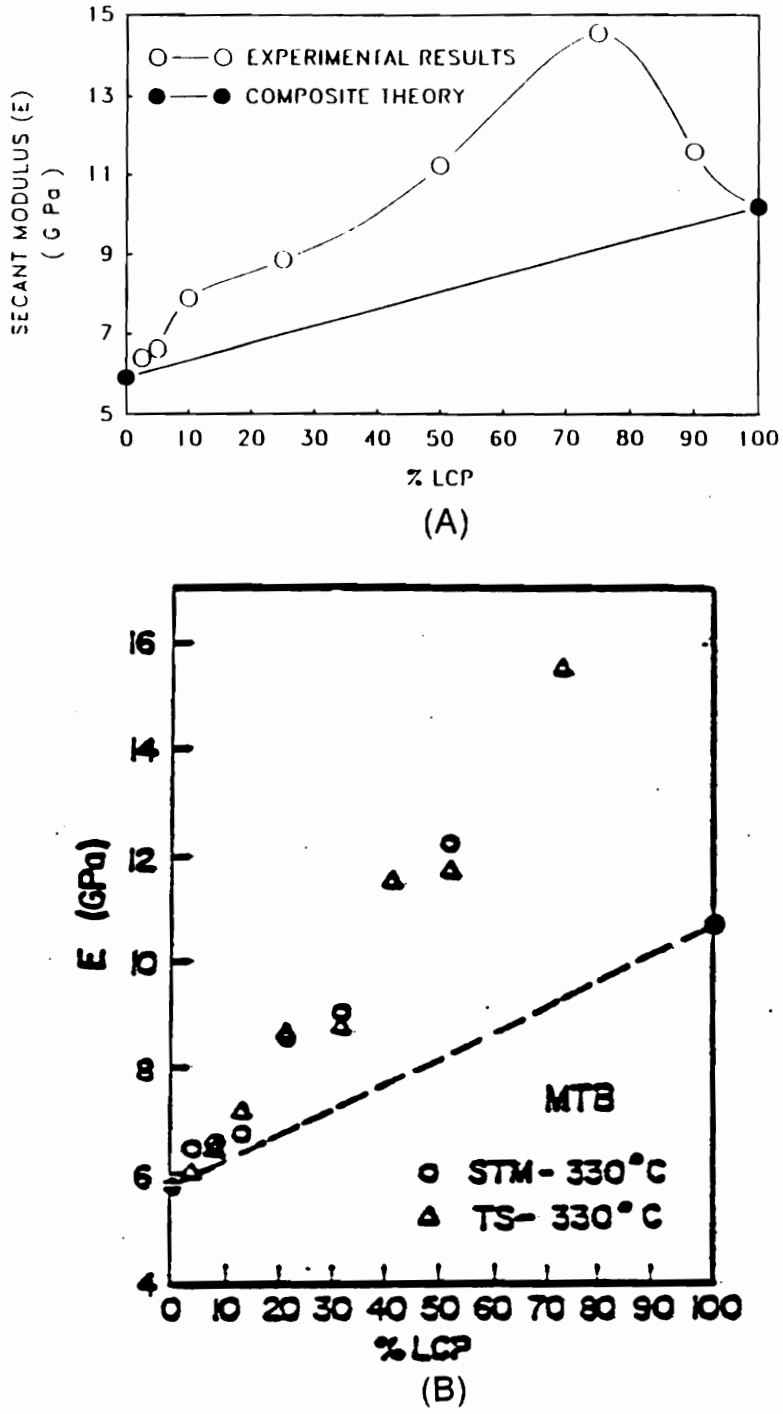

Figure 2.21. Modulus as a function of LCP concentration of (A) PEEK/Vectra A900 and (B) PEI/Vectra A900 blends (57-58).

The effects of miscibility of the matrix and reinforcing phases on the development of in situ composites has been studied by Zhuang and co-workers (218). In their study, PS, PET, and PC were used as the matrices and LCP60 as the reinforcing phase. Blends were prepared by both solution and melt blending. Based upon DSC, SEM, and dielectric thermal analyses (DETA), they concluded that PS was immiscible whereas both PC and PET were partially miscible with the LCP60, the PET being miscible to a higher degree than PC. The phase morphologies of these three systems reflected their differences in misciblity behavior. The PS/LCP60 blend had the coarsest and more distinct phase morphologies, and the PET/LCP60 blend had the finest and least distinctive morphology. Also, it was seen that for all the systems studied, there was a transition from ellipsoidal LCP particles to to long LCP fibrils with increasing shear rate in capillary extrudates as well as melt spun fibers. Mechanical properties enhancement of compression molded films, extrudates and melt spun filaments was observed for all the three blend systems studied.

Quite recently, Sun and co-workers (219) have reported studies on the miscibility of blends of PEI with an amorphous, referred to as HX1000, and a semicrystalline, referred to as Vectra A, liquid crystalline polymer. Dynamic thermal analysis (DMTA) and DSC tests were used to determine the degree of miscibility of the PEI/Vectra A and PEI/HX1000 systems. The degree of miscibility was assessed by measuring the shift in the glass transition temperature of the PEI rich phase in the blend. The DMTA results for the PEI/Vectra A system are reproduced in Figure 2.22, in where it is observed that the Tg's of PEI and Vectra A occurs at 228°C and 105°C, respectively. As one observes from Figure 2.22, when the Vectra A concentration in the blend is increased, the Tg of the PEI rich phase remains almost unchanged at 228°C. Meanwhile, a shoulder due to the Tg of the Vectra A phase can be observed for all blend compositions studied. The DMTA behavior observed for the PEI/Vectra A system suggests that this system is immiscible throughout the range of compositions studied.

DMTA results for the PEI/HX1000 system are shown in Figure 2.23 (219). The Tg's of both PEI and HX1000 individual components are found at 228°C and 185°C, respectively. However, for this system, the increase in the HX1000 concentration in the blend gives rise to

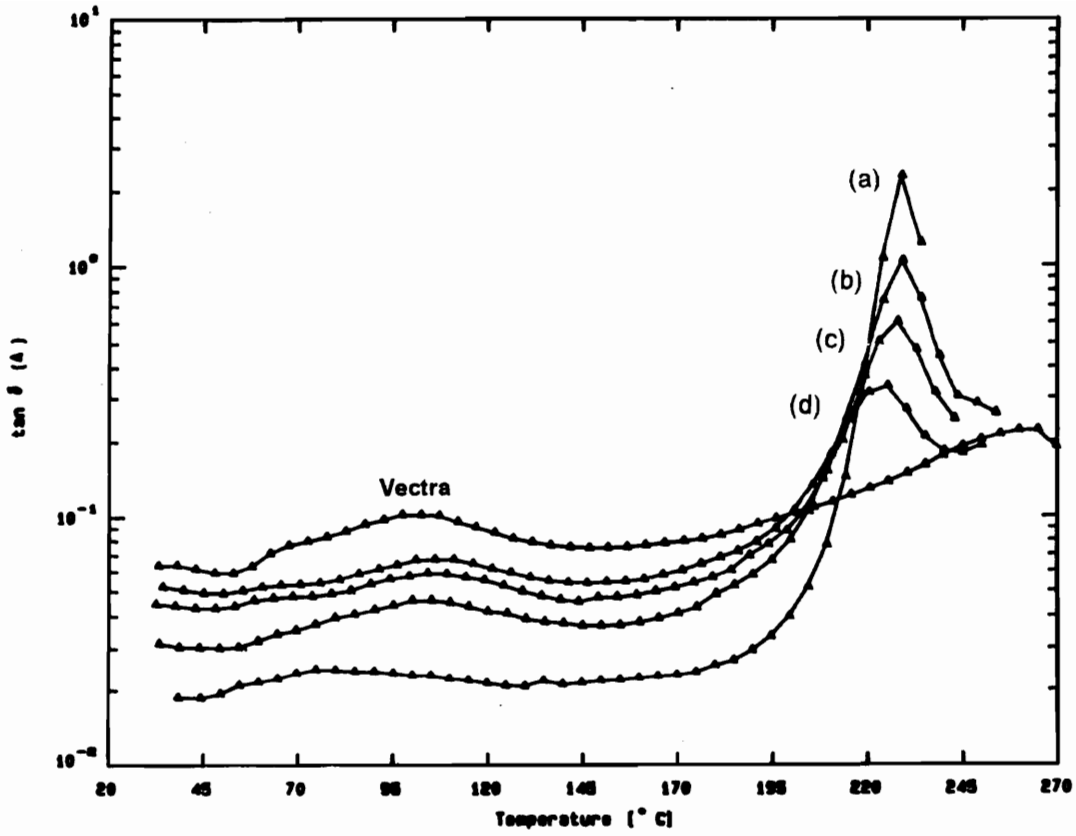

Figure 2.22. Loss Tangent (tan δ) vs. Temperature for PEI/Vectra A blends as a function of Vectra A concentration (219). (a) 100/0, (b) 70/30, (c) 50/50, (d) 30/70 and (e) 0/100.

a shift in the Tg of the PEI rich phase to lower temperatures. Once again, a shoulder due to the glass transition of the HX1000 phase appears at 185°C with the increase in the HX1000 concentration. The shift in the glass transition temperature of the PEI phase upon addition of HX1000, which is also observed in DSC tests (219), suggests that PEI/HX1000 blends are partially miscible. The partial miscibility suggests that it is possible that in this system two phases may coexist in the composite. One phase composed solely of HX1000 coexisting with another phase composed of a mixture rich in PEI with some HX1000 dissolved in it. This may account for the observed depression in the Tg of the PEI phase. Moreover, annealing and mixing history are also observed to affect the degree of shift in the glass transition temperature. However, Sun et al. (219) did not address how partial miscibility would affect the mechanical properties of the two systems.

In summary, liquid crystalline polymers have taken part in blends with most of thermoplastics currently available. The above reviews were just a few illustrations of the common findings of the literature regarding the use of TLCPs as processing aids and, sometimes, as effective reinforcements to the hosting polymer. One important aspect regarding the reinforcing capability of a thermotropic LCP seemed to be the viscosity ratio between the TLCP and the polymer matrix. As was shown, when the viscosity ratio was closer to unity, maximum fibrillation of the TLCP domains was achieved. Another consideration is the fact that miscibility between the phases was not always required to promote synergistic effects in the mechanical properties of the blends. For instance, blends of immiscible TLCP/polymer blends, such as PEEK/Vectra A900 (57), have shown a positive deviation from the rule of mixtures as function of LCP concentration.

The objective of this section was not to present a thorough review of the available literature in the subject of blends of liquid crystalline and flexible chain polymers. The examples reviewed in this section were meant to illustrate the common findings of the literature regarding the development of in situ composites. They were selected based upon one very important aspect. They would clearly illustrate the importance of adequate processing conditions to impart fibrillation to the LCP domains in the matrix polymer.

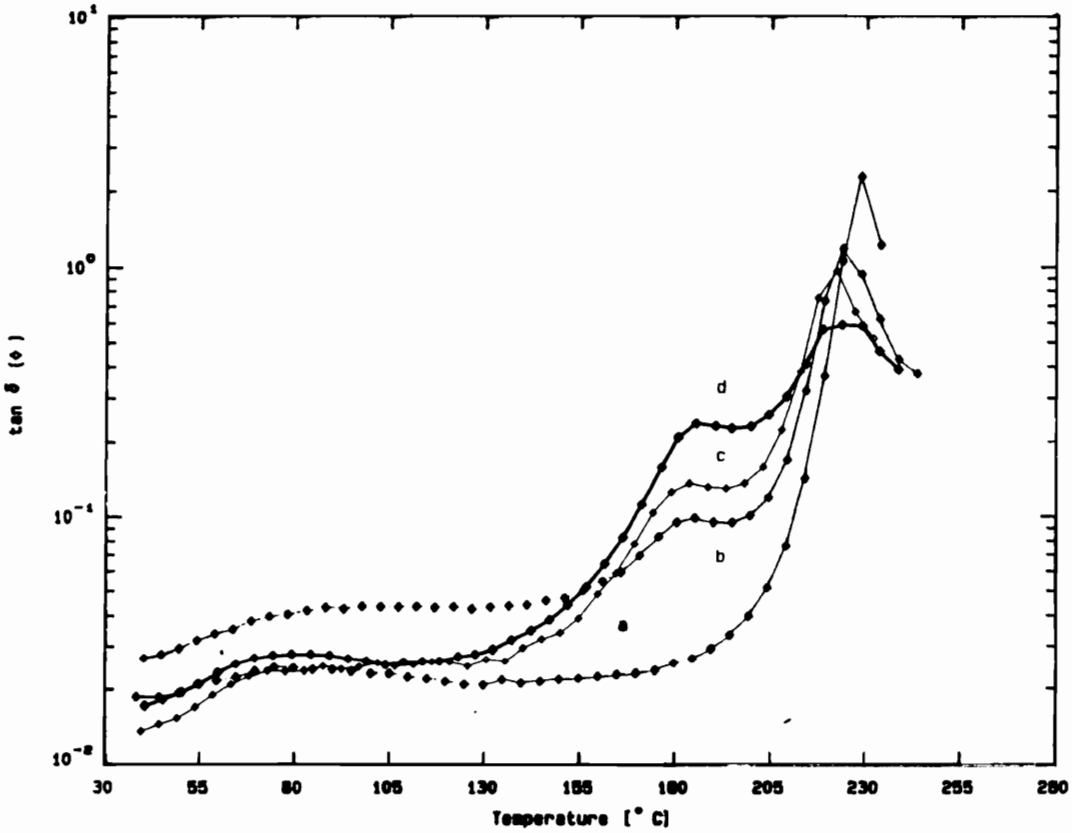

Figure 2.23. Loss Tangent (tan δ) vs. Temperature for PEI/HX1000 blends as a function of HX1000 concentration (219). (a) 100/0, (b) 70/30, (c) 50/50 and (d) 30/70.

2.6 Transverse Mechanical Properties

In the previous Section, the use of thermotropic liquid crystalline polymers as processing aids and reinforcement to thermoplastic materials have been discussed. Thermotropic liquid crystalline polymers may in fact improve the mechanical properties of thermoplastic polymers under adequate processing conditions for the fibrillation of the TLCP molecules. Further, it was shown that elongational flow fields are much more effective, due to their irrotation characteristics, in imparting fibrilation to the TLCP domains than are shear flow fields. Further, a skin/core type of morphology is always present during the injection molding of in situ composites. This characteristic morphology emerges because of the nonuniform shear flow conditions during the mold filling step of the process coupled with an elongational flow field in the advancing front and noinsothermal conditions.

The main objective of this research is to develop methods in where the transverse mechanical properties of in situ thermoplastics composites would be improved without any significant loss of the already outstanding flow direction properties. A review of the available literature regarding the enhancement of the transverse mechanical properties of TLCPs and TLCP/Polymer blends is discussed in this section.

Very few publications have dealt with the problem of mechanical anisotropy exhibited by thermotropic liquid crystalline polymers and TLCP/polymer blends. Farrel and Fellers (220) have developed a rotating annular die to control biaxial orientation in melt processed thermotropic liquid crystalline polymers from cellulose derivatives. This special die consisted of a rotating inner core and a simultaneously counter rotating outer cylinder. By controlling the inner core and outer cylinder speeds they were able to control the flow profile through the die. The materials used in their experiments were composed of two thermotropic liquid crystalline cellulose derivatives (hydroxypropyl cellulose (HPC) and ethyl cellulose (EC)), an isotropic cellulose derivative (cellulose acetate butyrate (CAB)), and an amorphous and a semicrystalline polymer (polystyrene and polyethylene, respectively) as reference materials.

The rotating die was mounted on a 3/4 inch single screw extruder. The inner core and outer cylinder were rotate at the same angular speed, ranging from 0 to 17.2 rpm giving values of the ratio of the tangential wall shear rates to the axial wall shear rates (R) from 0 to 410. Birefringence measurements, scanning electron microscopy, and pole figure analyses used in conjunction with White-Spruiell biaxial orientation factors were used to characterize the HPC films and extrudates. From experimental observations, the authors have concluded that the rotating annular die could be used successfully to control the molecular orientation in melt processed thermortropic liquid crystalline polymers. The control of the TLCP orientation was more effective than for the reference polymers due to the long relaxation times exhibited by LCPs, compared to polyolefins. By controlling the angular velocities of the rotating surfaces , the polymer chain axis could be placed at any desired position between the machine and the transverse directions. Consequently, the controlled molecular orientation affected directly the mechanical properties of the extrudates. The mechanical properties of the HPC and EC films at R = 0 where much greater in the machine direction than in the transverse direction. As the die rotation was increased, the mechanical properties decreased in the machine direction and increased in the transverse direction. Thus, the mechanical properties in the transverse direction increased at the expenses of the machine direction properties. Effects on the morphology of HPC films was also observed. HPC films produced without rotation formed coarse fibrillar structures with the fibers aligned in the machine direction. After rotation, the large fibrils were broken down into very fine fibrils and as the rotation increased the fibers orientation moved from machine to transverse direction.

Recently, Blizard and co-workers (43,221) have studied film blowing and blow molding of TLCPs with the objective of achieving biaxial properties. They have used both Vectra A900 and LCP60 in their experiments. They found that an increase in the blow up ratio, in the case of film blowing, improved the transverse mechanical properties of films from both TLCPs. However, as illustrated in Table 2.2, the increase in the film's transverse property was accompanied by an equivalent decrease of the flow direction properties for both TLCPs. In the case of blow molding, however, they reported that a range of properties and orientations was

found for bottles blown out of LCP60, ranging from uniaxial in the machine direction (MD) and transverse direction (TD), to biaxial with nearly equal properties in MD and TD directions, depending on the barrel and die temperatures used. They concluded that the LCP60 material tended to reorient from the initial axial orientation during the blowing process if the extruder temperature was below 260°C. On the contrary, the blowing of the Vectra A900 tended to remove any initial orientation generated during the extrusion. They pointed out that the viscosity and the elasticity of the material were sufficiently high to create enough stresses during the blowing process in the middle of the bottle to change the initial orientation during the planar deformation process occurred in that region.

The influence of glass fiber reinforcement on the mechanical anisotropy of liquid crystalline polymers has recently been investigated by Chivers and Moore (222). The thermotropic liquid crystalline polymers used in their studies were two copolyesters based on HBA/HNA and HBA/isophthalic acid (IA)/hydroquinone (HQ). LCP and LCP with 27% w/w glass reinforcement were injection molded into a rectangular plaque mold provided with a coathanger gate. Mechanical properties were evaluated in strips cut out perpendicularly and parallel to the injection molding flow direction. Based upon mechanical properties measurements, they have concluded that the mechanical anisotropy of the glass reinforced LCPs was a little less than the LCPs alone. For example, the flexural modulus of the HBA/HNA copolyester was 14.0 and 2.2 GPa in the flow and transverse directions, respectively. The addition of 27 w/w percent glass fibers to the HBA/HNA copolyester increased the parallel and the transverse to flow values of the flexural modulus to 15.4 and 3.5 GPa, respectively.

In summary, it was shown that thermotropic liquid crystalline polymers exhibit a very strong mechanical anisotropy when parallel and transverse to flow mechanical properties are compared. From the examples reviewed above, it was seen that the improvement of the transverse mechanical properties of TLCPs results in a reduction of the initial flow direction properties of the material. Further, the addition of glass fibers to LCP improves the transverse and the parallel to flow properties of the material. Consequently, the mechanical anisotropy of TLCPs reinforced with glass fibers remained practically similar to that of unreinforced LCPs.

Table 2.2. Tensile properties of blown films as a function of blowup ratio (BUR) in the machine (MD) and transverse (TD) directions (221).

Direction	T_b °C	BUR HBA/PET	E_t GPa	σ_{max} MPa
MD	267	1.45	11.2	171
MD	267	2.30	10.6	247
MD	267	3.10	9.16	297
MD	247	1.30	10.7	231
TD	267	1.45	1.13	20.6
TD	267	2.30	1.29	25.3
TD	267	3.10	1.86	36.7
TD	247	1.30	1.07	19.9
	T_b °C	BUR HBA/HNA	E_t GPa	σ_{max} MPa
MD	337	1.0	13.3	264
MD	337	1.95	14.8	360
MD	337	2.60	12.4	378
MD	319	1.35	12.4	342
MD	319	2.30	12.4	391
TD	337	1.0	1.08	16.1
TD	337	1.95	1.71	31.1
TD	337	2.60	3.08	69.8
TD	319	1.35	1.32	30.8
TD	319	2.30	1.93	57.5

Average standard deviations were 1.94 and 0.18 for the MD and TD moduli, respectively, and 37.0 and 2.37 for the MD and TD maximum stresses, respectively.

Research in this area is still needed in order to establish whether TLCP parts with good balance of transverse and flow direction properties can be obtained. Investigations on the enhancement of the transverse mechanical properties of TLCP/polymers blends appear to be lacking in the published literature. In the following section, a detailed discussion on the objectives of this research is presented.

2.7 Research Objectives

The literature pertaining to the current research has been reviewed in the previous sections. In this section the objectives of this research are given in detail after a brief discussion of the main points from the literature. This discussion is undertaken so that some key points from the literature review which have a direct bearing on the current research may be highlighted and so that the statement of the research objectives may be better appreciated.

In earlier sections it has been shown that an understanding of the droplet deformation and break up process gives an insight in the process of the fibrillation of a dispersed phase in a matrix polymer. In particular the importance of the Weber number and the viscosity ratio in determining the morphology of a two phase system was highlighted. From experimental results, it was seen that a viscosity ratio of unity or less is necessary for the formation of fibrils of the dispersed phase in the hosting matrix (193).

The rheology of TLCPs has shown very interesting features. One of the main features is the dependence of the LCP viscosity on the shear rate. Specifically, the viscosity of LCPs is dependent on the shear rate over many orders of magnitude of the shear rate. Further, preheating the LCP melt to a temperature much higher than its melting temperature and subsequently cooling to a lower test temperature results in a much lower viscosity than if the material had been brought to the test temperature from the solid state. The magnitude of such a decrease in viscosity increases with an increase in the preheating temperature. Such a be-

havior provides a handy processing tool in which the viscosity of the LCP melt may be altered by adequately changing thermal history of the material.

The review on blends of TLCPs with thermoplastics also revealed some important results. Blends of LCPs with thermoplastics may show higher mechanical properties than those of the pure matrix polymer. Moreover, the full reinforcing potential of TLPCs may be achieved in processings where high elongational flow fields are present, such as in melt spinning. In addition, elongational flows are capable of inducing high fibrillation and molecular orientation to the TLCP domains.

Very few are the studies on the enhancement of the transverse mechanical properties of TLPs and TLCP/polymer blends. It was shown that the flow direction mechanical properties of TLCPs usually decrease when transverse properties are improved. Research in this area is still needed in order to establish whether materials with good balance in the mechanical properties can be obtained. Lastly, it was shown that the role of partial miscibility on the structure and properties of TLCP/polymer blends is usually not fully understood. In some cases, partially miscible and immiscible TLCP/polymer blends may show synergism in mechanical properties regardless of the phase behavior exhibited by the system (58,59).

From the discussions above and keeping in mind the information obtained from the literature review, the objectives of this research work are:

1. **To determine the effects of shearfree elongational flows on the morphology and mechanical properties of TLCP/polymer blends.**

2. **To enhance the transverse mechanical properties of in situ composites, which could eventually reduce the mechanical anisotropy of the system.**

3. **To determine the effects of partial miscibility on the morphology and mechanical properties of TLCP/polymer blends.**

4. **To determine the contributing factors which lead to the maxima in the mechanical properties of TLCP based in situ composites.**

5. **To determine the suitability of in situ composites to other processing alternatives, such as thermoforming and compression molding.**

A review of the literature and the objectives of this research have been presented in this chapter. This chapter started out with a brief discussion on the general concepts of polymer/polymer blends. Next, fundamental aspects of the droplet deformation and breakup phenomena along with experimental observations from various sources were discussed. Following that a discussion of capillary instabilities was presented. A discussion on thermotropic liquid crystalline polymers along with considerations regarding their rheology and processing was presented in a subsequent section. Next, a review of the development of in situ composites was discussed. In particular aspects such as viscosity reduction of the matrix polymer by the addition of a TLCP phase, mechanical properties and processing of these blends were addressed. Finally, the research objectives were discussed. In the next chapters, the experimental procedure necessary to fulfill the objectives of this research along with results and discussions are presented.

2.8 References

1. A. Metha and A.I. Isayev, **Polym. Eng. Sci.**, 31(13), 971 (1991).
2. D. Acierno, M.R. Nobile, L. Nicolais and L. Incarnato in **Polymer Rheology and Processing**, A. Collyer and L.A. Utracki (eds). Elsevier Applied Science. New York, 1990.
3. G. Kiss, **Polym. Eng. Sci.**, 27(6), 410 (1987).
4. D.J. Williams, **Adv. Polym. Tech.**, 10(3), 173 (1991).
5. A. Siegmann, M. Narkis, M. Puterman, and A.T. DiBenedetto, **Polymer**, 20, 89 (1979)
6. A. Siegmann, M. Narkis, M. Puterman, and A.T. DiBenedetto, **J. Polym. Sci., Polym. Phys.**, 17, 225 (1979).
7. J.R. Joseph, J.L. Kardos, and L.E. Nielsen, **J. Appl. Polym. Sci.**, 12, 1151 (1968).
8. R.D. Stichler, E.J. Parks, and F.J. Linning, **Appl. Polym. Symp.**, 7, 143 (1968).
9. J.L. Kardos, W.L. MaDonnel, and J. Raisoni, **J. Macrom. Sci., Phys.**, B6, 397 (1972).
10. R.H. Baughman, H. Gleiter, and N. Sendfield, **J. Polym. Sci., Polym. Phys.**, 13, 1871 (1975).
11. R.H. Baughman, and E.A. Turi, **J. POlym. Sci., Polym. Phys.**, 11, 2453 (1973).
12. Y.R. Patell, and J.M. Schultz, **J. Macrom. Sci., Phys.**, B7, 433 (1973).
13. G. Wegner, E.W. Fisher, and A. Munoz-Escalona, **Makromol. Chem., Suppl.**, 1, 521 (1975).
14. I. Voigt-Martin, **Makromol. Chem.**, 175, 2669 (1974).
15. G. Kiss, A.J. Kovacs, and J.C. Wittmann, **J. Appl. Polym. Sci.**, 26, 2665 (1981).
16. R.H. Baughman, H. Gleiter, and N. Sendfield, U.S. Patent No. 4,255,535 (1981).
17. A.I. Isayev, and M.J. Modic, **Polym. Comp.**, 8, 158 (1987).
18. K.G. Blizard, and D.G. Baird, **Polym. Eng. Sci.**, 27, 653 (1987).
19. A. Siegman, A. Dagan, and S. Kenig, **Polymer**, 26, 1325 (1985).
20. R.A. Weiss, W. Huh, and L. Nicolais, **Polym. Eng. Sci.**, 27, 779 (1983).
21. G. Crevecoeur, and G. Groeninckx, **Polym. Eng. Sci.**, 30(9), 532 (1990).
22. T.S. Chung, **Plast. Eng.**, 43, 39 (1987).

23. D.G. Baird, and R. Ramanathan, in Contemporary Topics in Polymer Science, Vol. 6: Multiphase Macromolecular Systems; B.M. Culberton Ed., Plenum Press, New York (1989).
24. G. Vertogen, and W.H. de Jev, Thermotropic Liquid Crystals, Fundamentals. Springer-Verlag, Berlin (1988).
25. D. Demus, and L. Richter, Textures of Liquid Crystalline Polymers, Verlag Chemie, New York (1987).
26. D.G. Baird, in Liquid Crystalline Order in Polymers; A. Blumstein Ed., Academic Press, New York (1987).
27. S.L. Kwoleck, W. Memeger, and J.E. van Trump, in "Polymers for Advanced Technologies", L. Memachem Ed., VCH Publ., New York (1988).
28. W.J. Jackson, and H.F. Kuhfuss, **J. Polym. Sci., Polym. Chem. Ed.**, 14, 2043 (1976).
29. G.W. Calundann, in "High Performance Polymers: Their Origen and Development", R.B. Seymour, and G.S Kirshembaum Eds. Elsevier, Amsterdan (1986).
30. A.J. East, L.F. Charbonneau, and G.W. Calundann, **Mol. Cryst. Liq. Cryst.**, 157, 615 (1988).
31. M. Jaffe, in "Polymers for Advanced Technologies", L. Memachem Ed., VCH Publ., New York (1988).
32. E. Suokas, J. Sarlin, and P. Tormala, **Inst. Phys. Conf. Ser.**, 89(3), 155 (1988).
33. D. Acierno, F.P. La Mantia, G. Polizzoti, A. Ciferri, and B. Valenti, **Macromolecules**, 15, 1455 (1982).
34. K. Itoyama, **J. Polym. Sci., Polym. Let.**, 27, 369 (1989).
35. A.E. Zachariades, and J.A. Logan, **Polym. Eng. Sci.**, 23, 797 (1983).
36. H.N. Yoon, **Coll. Polym. Sci.**, 268, 230 (1990).
37. K.J. Itoyama, **J. Polym. Sci., Polym. Phys. Ed.**, 26, 1845 (1988).
38. A.T. Dibenedetto, L. Nicolais, E. Amendola, C. Carfagna, and M.R. Nobile, **Polym. Eng. Sci.**, 29, 153 (1989).
39. T. S. Chung, **J. Polym. Sci., Polym. Phys. Ed.**, 26, 1549 (1988).
40. T.S. Chung, P.E. McMahon, **J. Appl. Polym. Scie.**, 31, 965 (1986).
41. C.E. McChesney, and J.R. Dole, Modern Plastics, 112, Jan (1988).

42. A. Boldizan, **Plast. Rubber. Process. Apll.**, 10, 73 (1988).

43. K.G. Blizard and D.G. Baird, **Intern. Polym. Proc.**, 3, 172 (1989)

44. T.Y. Tam, M.B. Boone, and G.C. Weedon, **Polym. Eng. Sci.**, 28(13), 172 (1988).

45. W. Huh, R.A. Weiss, and L. Nicolais, SPE Antec, 306 (1986).

46. D.J. Williams, **Adv. Polym. Tech.**, 10(3), 173 (1991).

47. G. Crevecoeur, "In Situ Composites, Blends of Thermotropic Liquid Crystalline Polymers in a Thermoplastic Matrix", PhD Thesis, Catholic University of Leuven (1991).

48. A.M. Sukhadia, PhD dissertation, Virginia Polytechnic Institute and State University (1991).

49. A. Kohli, N. Chung, and R.A. Weiss, **Polym. Eng. Sci.**, 29(9), 573 (1989).

50. T. Sun, D.G. Baird, H.H. Huang, D.S. Done, and G.L. Wilkes, **J. Comp. Mat.**, 25, 788 (1991).

51. R.A. Weiss, W. Huh, and L. Nicolais, in "High Modulus Polymers", A.E. Zachariades and R.S. Porter Eds., Marcel Dekker Inc., New York (1988).

52. T.M. Malik, P.J. Careau, and N. Chapleau, **Polym. Eng. Sci.** , 29, 600 (1989).

53. G. Crevecoeur, and G. Groeninckx, **Polym. Eng. Sci.**, 30(9), 532 (1990).

54. T.S. Chung, **Plast. Eng.**, 43, 39 (1987).

55. D. Dutta, H. Fruitwala, A. Kohli, and R.A. Weiss, **Polym. Eng. Sci.** , 30, 1005 (1990).

56. R. Ramanathan, K.G. Blizard, and D.G. Baird, SPE 46th ANTEC, Conf. Proc., Atlanta, 1123 (1988).

57. A. Metha and A.I. Isayev, **Polym. Eng. Sci.**, 31(13), 971 (1991).

58. A.I. Isayev, and S. Swaminathan, U.S. Patent No. 4,835,047 (1989).

59. P.R. Subramanian, and I.A. Isayev, **Polymer**, 32(11), 1961 (1991).

60. A.I. Isayev and M. Modic, **Polym. Comp.**, 8(3), 158 (1987).

61. S.S. Bafna, J.P. de Souza, T. Sun and D.G. Baird, **Polym. Eng. Sci.**, 33 (13), 808 (1993).

62. J.P. de Souza, and D.G. Baird, Southeastern Graduate Polymer Conf., Atlanta (1991).

63. A. Kohli, N. Chung, and R.A. Weiss, **Polym. Eng. Sci.**, 29(9), 573 (1989).

64. W.J. Jackson, and H.F. Kuhfuss, **J. Polym. Sci., Polym. Chem. Ed.**, 14, 2043 (1976).

65. S.K. Carg and S. Kenig, in "High Modulus Polymers, approahes to design and development", A.E. Zachariades and R.S. Porter Eds., Marcel Dekker, New York, 71-103 (1988).

66. D. Berry, A Siegmann, and S. Kenig, **J. Mater. Sci. Let.**, 7, 1071 (1988).

67. M.R. Nobile, E. Amendola, L. Nicolais, D. Acierno, and C. Cartagna, **Polym. Eng. Sci.**, 29, 244 (1989).

68. F.P. La Mantia, A. Valenza, M. Paci, and P.L. Magagnini, **Polym. Eng. Sci.** , 30(1), 7 (1990).

69. K.G. Blizard, and D.G. Baird, **Polym. Eng. Sci.**, 27(9), 653 (1987).

70. P.R. Subramanian, and A.I. Isayev, SPE Antec, 489 (1990).

71. S.G. James, A.M. Donald, and W.A. McDonald, **Mol. Cryst. Liq. Cryst.**, 153, 491 (1987).

72. B. Lee, SPE Antec, 1088 (1988).

73. D. Acierno, E. Amendola, C. Carfagna, L. Nicolais, and R. Nobile, **Molec. Cryst. Liq. Cryst.**, 153, 533 (1987).

74. A. Siegmann, A. Dagan, and S. Kenig, **Polymer**, 26, 1325 (1985).

75. R.A. Weiss, W. Huh, and L. Nicolais, Int. Conf. Liq. Cryst. Polym., France, 8P8 (1987).

76. C. Kim, V. Sullivan, and G. Berry, SPE Antec, 990 (1988).

77. M. Amano, and K. Nakagawa, **Polymer**, 28, 263 (1987).

78. G.I. Taylor, **Proc. Roy. Soc.**, A146, 501 (1934).

79. B.J. Bentley, and L.G. Leal, **J. Fluid Mech.**, 167, 241 (1986).

80. R.G. Cox, **J. Fluid Mech.**, 37(3), 601 (1969).

81. D.G. Baird, S.S. Bafna, J.P. de Souza, and T. Sun, **Polym. Comp.** , 14 (3), 214 (1993).

82. Modern Plastics Encyclopedia 1992.

83. K. Shimamura, **Makromol. Chem.**, 4, 107 (1983).

84. S.L. Kwoleck, W. Memeger, and J.E. van Trump, in "Polymers for Advanced Technologies", L. Memachem Ed., VCH Publ., New York (1988).

85. D.R. Paul, in Polymer Blends, Chapter 1: Background and Perspectives. Vol.1, Academic Press, New York (1978).

86. O. Olabisi, L.M. Roberson, and T.M. Shaw, Polymer-Polymer Miscibility, Academic Press, New York (1979).

87. J.A. Mason and L.H. Sperling, "Polymer Blends and Composites", Plenum Press, New York (1977).

88. F. Ghuam. and J.L. White, **Polym. Eng. Sci.**, 31(2), 76 (1991).

89. C.D. Han, K.U. Kim, J. Parker, N. Siskovic, and C.R. Huang, **Appl. Polym. Symp.**, 20, 91 (1973).

90. W.J. Ho., and R. Salovey, **Polym. Eng. Sci.**, 21, 839 (1981).

91. K. Min, J.L. White, and J.F. Fellers, **J. Appl. Polym. Sci.**, 29, 2117 (1984).

92. P.M. Subramanian, and V. Mehra, **Polym. Eng. Sci.**, 27 (9), 663 (1987).

93. R.L. Scott, **J. Chem. Phys.**, 17, 279 (1949).

94. J.H. Hilderbrand and R.L. Scott, "The Solubility of Non-Electrolites", 3rd. edition, Van Nostrand Reinhold, Princeton, NJ (1950).

95. J.H. Hilderbrand and R.L. Scott, "Regular Solutions", Prentice Hall, Englewood Cliffs, NJ (1962).

96. P.J. Hoftyzer, and D.W. van Krevelen, in "Properties of Polymers", 2nd edition, Chapter 7, 152-155, Elesevier, New York (1976).

97. K.L. Hoy, "Tables of Solubility Parameter", Solvent and Coatings Materials Research and Development, Union Carbide Coorporation (1985).

98. K.L. Hoy, **J. Coated Fabrics**, 19, 53 (1989).

99. D.W. van Krevelen, "Properties of Polymers", 3rd edition, Elsevier, New York (1990).

100. R.S. Porter, J.M. Jonza, M. Kimura, C.R. Desper, and R.R. George, **Polym. Eng. Sci.**, 29(1), 55 (1989).

101. S. Wu, "Polymer Interface and Adhesion", Marcel Dekker, New York (1982).

102. F.M. Folkes, in "Treatise on Adhesion and Adhesives", vol. 1, R.L. Patrick Ed., Marcel Dekker, New York (1967).

103. R.J. Good, in "Treatise on Adhesion and Adhesives", vol. 1, R.L. Patrick Ed., Marcel Dekker, New York (1967).

104. M. Uzman, Investigations on Metallization of Acrylonitrile/Butadiene Copolymers, PhD Thesis, Technical University of Berlin (1983).

105. J.J. Bikerman, "Physical Surfaces", Academic Press, New York (1970).

106. C. Wake, "Adhesion and the Formulation of Adhesives", Appl. Sci. Publ., London (1976).

107. G.L. Gaines, **Polym. Eng. Sci.**, 12, 1 (1972).

108. R.J. Roe, V.L. Bacchetta, and P.M.G. Wong,**J. Phys. Chem.**, 71, 4190 (1967).

109. R.J. Roe, **J. Coll. Interf. Sci.**, 31, 228 (1969)

110. S. Wu, **J. Phys. Chem.**, 74, 632 (1970).

111. S. Meretz, M. Kwiatkowski, and G. Hinrichsen, **Intern. Polym. Proc.**, 6(3), 239 (1991).

112. G. Crevecoeur, "In Situ Composites, Blends of Thermotropic Liquid Crystalline Polymers in a Thermoplastic Matrix", PhD Thesis, Catholic University of Leuven (1991).

113. P.J. Flory and A. Abe, **Macromolecules**, 11(6), 1119 (1978).

114. A. Abe and P.J. Flory, **Macromolecules**, 11(6), 1122 (1978).

115. P.J. Flory and R.S. Frost, **Macromolecules**, 11(6), 1126 (1978).

116. R.S. Frost and P.J. Flory, **Macromolecules**, 11(6), 1134 (1978).

117. P.J. Flory, **Macromolecules**, 11(6), 1138 (1978).

118. P.J. Flory, **Macromolecules**, 11(6), 1141 (1978).

119. P.J. Flory, **Proc. R. Soc., London**, A 234, 73 (1956)

120. C.D. Han, "Multiphase Flow in Polymer Processing", Academic Press, New York (1981).

121. G.I. Taylor, **Proc. Roy. Soc.**, A138, 41 (1932).

122. G.I. Taylor, **Proc. Roy. Soc.**, A226, 289 (1954).

123. R.G. Cox, **J. Fluid Mech.**, 37(3), 601 (1969).

124. D. Barthes-Biesel and A. Acrivos, **J. Fluid Mech.**, 61, 1 (1973).

125. J.M. Rallison,**J. Fluid Mech.**, 109, 465 (1981).

126. Z. Zhang and J. Qiao, **Polym. Eng. Sci.**, 31(21), 1553 (1991).

127. H.B. Chin and C.D. Han, **J. Rheol.**, 23(5), 557 (1979).

128. S. Wu, **Polym. Eng. Sci.**, 27(5), 335 (1987).

129. G. Hetsroni and S. Haber, **Rheol. Acta**, 9, 488 (1970).

130. H.J. Karam and J.C. Bellinger, **Ind. Chem. Eng. Fundam.**, 7(4), 576 (1972).

131. R.W. Flumerfelt, **Ind. Chem. Eng. Fundam.**, 11(3), 312 (1972).

132. B.D. Favis and J.P. Chalifoux, **Polym. Eng. Sci.**, 27(20), 1591 (1987).

133. C.D. Han and K. Funatsu, **J. Rheol.**, 22(2), 113 (1978).

134. A. Einstein, **Ann. Physik**, 19, 289 (1906).

135. H.P. Grace, **Chem. Eng. Commun.**, 14, 225 (1982).

136. T. Tavgac, PhD Thesis University of Houston, Texas (1972).

137. S. Torza, R.G. Cox, and S. Mason, **J. Coll. Interf. Sci.**, 38, 395 (1972)

138. F.D. Rumscheidt, and S. Mason, **J. Coll. Interf. Sci.**, 16, 238 (1961).

139. C.E. Chaffey, and H. Brenner, **J. Coll. Interf. Sci.**, 24, 258 (1967).

140. B.M. Turner, and C.E. Chaffey, **Trans. Soc. Rheol.**, 13, 411 (1969).

141. S.J. Choi, and W.R. Showalter, **Phys. Fluids**, 18, 420 (1975).

142. J.P. Buckmater, **J. Fluid Mech.**, 55, 385 (1972).

143. J.P. Buckmater, **J. Appl. Fluid Mech.**, E40, 18 (1973).

144. A. Acrivos and T.S. Lo, **J. Fluid Mech.**, 86, 641 (1978).

145. H. van Oene, in "Polymer Blends", vol. I, D.R. Paul and S. Newman, eds., Academic Press, New York (1978).

146. H. van Oene, **J. Coll. Interf. Sci.**, 40(3), 448 (1972).

147. J.J. Elmendorp and R.J. Maalcke, **Polym. Eng. Sci.**, 25(16), 1041 (1985).

148. W.J. Milliken and L.G. Leal, **J. Non-Newt. Fluid Mech.**, 40, 335 (1991).

149. H.B. Chin and C.D. Han, **J. Rheol.**, 24(1), 1 (1980).

150. B.D. Favis and J.P. Chalifoux, **Polym. Eng. Sci.**, 27(20), 1591 (1987).

151. H.L. Goldsmith and S.G. Mason, **J. Coll. Sci.**, 17, 448 (1962).

152. I. Gauthier, H.L. Goldsmith and S.G. Mason, **Trans. Soc. Rheol.**, 15, 297 (1971).

153. G.I. Taylor, Proc. 11th Intern. Cong. Appl. Mech., Munich (1964).

154. H.A. Stone and L.G. Leal, **J. Fluid Mech.**, 220, 161 (1990).

155. D.L. Ballman, **Rheol. Acta**, 4, 137 (1965).

156. J.J. Elmendorp, Dispersive Mixing in Liquid Systems, Chap. 2.

157. S.L. Goren and M. Gottledb, **J. Fluid Mechan.**, 126, 245 (1982).

158. M. Plateau, Statistique des Liquid, Gauthe-Villars, Paris (1884).

159. J.W.S. Rayleigh, **Phylisoph. Mag.**, 34, 145 (1892).

160. S. Tomotika, **Proc. Roy. Soc., Ser. A**, 150, 332 (1935).

161. J.J. Elmendorp, **Polym. Eng. Sci.**, 26, 418 (1986).

162. F.D. Rumscheidt and S. Mason, **J. Colloid Sci.**, 17, 260 (1961).

163. M.V. Tsebrenko, **J. Non-Newt. Fluid Mech.**, 31, 1 (1989).

164. M. Goldin, J. Yerushelmi, R. Pfeffer, and R. Shinnar, **J. Fluid Mech.**, 38, 689 (1969).

165. M. Goldin, J. Yerushelmi, and R. Shinnar, **Trans. Soc. Rheol.**, 17, 303 (1973).

166. P. Schumer, and K. Tebel, **J. Non-Newt. Fluid Mech.**, 12, 231 (1983).

167. R. Buscall, D.J. Bye, and I. Miles, Gen. Rheol. Conference, Birmingham (1984).

168. T.M. Pakula, M. Grebowicz, and M. Kryzewski, **Polym. Bull.**, 2, 799 (1980).

169. C.K Ober, J.I. Jin, and R.W. Lenz, **Advan. Polym. Sci.**, 59, 103 (1984).

170. S. Chandrashekhr, "Liquid Crystals", Cambridge University Press, Cambridge (1977).

171. K.F. Wissbrun, G. Kiss, and F.N Cogswell, **Chem. Eng. Commun.**, 53, 149 (1987).

172. A.D. Gotsis, and D.G. Baird, **J. Rheol.**, 29, 539 (1985).

173. K.F. Wissbrun, **Br. Polym. J.**, 12, 163 (1980).

174. S. Ogoni and T. Asada, "Rheology and Rheo-optics of Polymer Liquid Crystals", 127-147, Rheology, Vol. I, Astarita, Marrucci and Nicolais, eds., Plenum Press, New York (1980).

175. G. Marruci, "Advances in Rheology", Vol. 1B, Mena A. Garcia-Rejon and C. Rangel-Nafaile, eds. Universidad Nacional Autonoma de Mexico (1984).

176. F. Cocchini, M.R. Nobile and D. Acierno, **J. Rheol.**, 35 (6), 1171 (1991).

177. D. Done and D.G. Baird, **Polym. Eng. Sci.**, 27 (11), 816 (1987)

178. D. Done and D.G. Baird, **Polym. Eng. Sci.**, 30 (16), 989 (1990).

179. T. Masuda, K. Fujiwara and M. Takahashi, **Intern. Polym. Process.**, 6 (3), 225 (1991).

180. K.F. Wissbrun and A.C. Griffin, **J. Polym. Sci., Polym. Phys. Ed.**, 24, 27 (1986).

181. F.N. Cogswell, in "Recent Advances in Liquid Crystalline Polymes", L.L. Chapoy, ed., Elsevier, London (1985).

182. S. Kenig, **Poly. Eng. Sci.** 27 (12), 887 (1987).

183. Y. Ide and Z. Ophir, **Polym. Eng. Sci.**, 23 (5), 261 (1983).

184. H. Muramatsu and W.R. Krigbaum, **J. Polym. Sci., Polym. Phys. Ed.**, 24, 1695 (1986).

185. H. Muramatsu and W.R. Krigbaum, **J. Polym. Sci., Polym. Phys. Ed.**, 25, 803 (1986).

186. A. Tealdi, and A. Ciferri, **Polym. Commun.**, 28, 22 (1987)

187. K. Fujiwara, M. Takahashi and T. Asuda, **Intern. Polym. Process.**, 6 (3), 232 (1991).

188. S. Kenig, **Polym. Eng. Sci.**, 29 (16), 1136 (1989).

189. E.G. Joseph, G.L. Wilkes, and D.G. Baird., **Polym. Eng. Sci.**, 25 (7), 377 (1985).

190. E. Suokas, J. Sarlin and P. Tormala, **Mol. Cryst. Liq. Cryst.**, 153, 515 (1987).

191. K.G. Blizard, D.G. Baird, and R. Ramanathan, Antec Tech. Papers, 585 (1987).

192. D. Berry, S. Kenig, and A. Sigmann, **Polym. Eng. Sci.**, 31 (6), 451 (1991).

193. D. Berry, S. Kenig, and A. Sigmann, **Polym. Eng. Sci.**, 31 (6), 459 (1991).

194. T.S. Chung, Antec Tech. Papers, 1404 (1987)

195. D. Acierno, E. Amendola, C. Carfagna, L. Nicolais, and R. Nobile, **Mol. Cryst. Liq. Cryst.**, 153, 553 (1987).

196. A. Valenza, F.P. La Mantia, M. Paci and P.L. Magagnini, **Intern. Polym. Process.**, 6 (3), 247 (1991).

197. D. Berry, S. Kenig, A. Sigmann and M. Narkis, **Polym. Eng. Sci.**, 32 (1), 451 (1992).

198. J. Seppala, M. Heino, and C. Kapanen, **J. Appl. Polym. Sci.**, 44, 1051 (1992)

199. M. Heino and J. Seppala, **J. Appl. Polym. Sci.**, 44, 2185 (1992)

200. J. Li, M. Silverstein, A. Hiltner, and E. Baer, **J. Appl. Polym. Sci.**, 44, 1531 (1992),

201. M. Amano and K. Nakagawa, **Polymer**, 28, 263 (1987)

202. B.Y. Shin, S.H. Jang, I.J. Chung and B.S. Kim, **Polym. Eng. Sci.**, 32 (1), 73 (1992).

203. B.R. Basset and A.F. Yee, **Polym. Comp.**, 11 (1), 10 (1990).

204. R.A. Weiss, W. Huh, and L. Nicolais, **Polym. Eng. Sci.**, 27 (6), 684 (1987).

205. A. Ajji, J. Brisson, and Y. Qu, **J. Polym. Sci., Polym. Phys. Ed.**, 30, 505 (1992).

206. T. Brinkmann, P. Hoeckk, and W. Michaeli, Antec Tech. Papers, 988 (1991).

207. C. Carfagna, et. al., **J. Appl. Polym. Sci.**, 43, 839 (1991).

208. M. Nobile, et. al., **J. Appl. Polym. Sci.**, 41, 2723 (1990).

209. R.S. Porter, **Thermochim. Acta**, 134, 251 (1988).

210. A. Mehta and A.I. Isayev., **Polym. Eng. Sci.**, 31 (13), 963 (1991).

211. A. I. Isayev and P.R. Subramanian, **Polym. Eng. Sci.**, 32 (2), 85 (1992).

212. L. Minkova, M. Paci, M. Pracella and P. Magagnini, **Polym. Eng. Sci.**, 32 (1), 57 (1992).

213. B. Lee, Antec Tech. Papers, 1088 (1988)

214. B. Lee, **Polym. Eng. Sci.**, 28, 1107 (1988).

215. J.F. Croteau and G.V. Lainvins, **J. Appl. Polym. Sci.**, 39, 2377 (1990).

216. S. Swaminathan and A.I. Isayev, **Polym. Mater. Sci. Eng.**, 57, 330 (1987).

217. A.G. Gibson and G.A. Williamson, **Polym. Eng. Sci.**, 25, 968 (1985).

218. P. Zhuang, T. Kyu, and J.L. White, **Polym. Eng. Sci.**, 28 (17), 1095 (1988).

219. S.S. Bafna, T. Sun, J.P. de Souza, and D.G. Baird, **Polymer**, 34 (4), 708 (1993).

220. G.W. Farrel and J.F. Fellers, **J. Polym. Eng.**, 6, 263 (1986).

221. K.G. Blizard, T.S. Wilson, and D.G. Baird, **Intern. Polym. Process.**, 5 (1), 53 (1990).

222. R.A. Chievers and D.R. Moore, **Polymer**, 32 (12), 2190 (1991).

In Situ Composites Based on Blends of a Polyetherimide and Thermotropic Liquid Crystalline Polymers under Injection Molding Conditions

To be submitted to **POLYMER**

3.0 EXPERIMENTAL RESULTS

3.1 Introduction

The addition of a thermotropic liquid crystalline polymer (TLCP) to a thermoplastic matrix is attractive in at least two ways. First, the TLCP may act as a processing aid by reducing the viscosity of the matrix material, so that materials exhibiting extremely high viscosities may be processed with lower energy expenditure (1-5). Secondly, the TLCP, under adequate processing conditions, deforms into elongated fibrils which often reinforce the thermoplastic matrix in a fashion analogous to glass fibers (6). Enhancement of the mechanical properties of several polymer matrices upon addition of TLCPs has been reported by several research groups (7-12).

In reinforcing a thermoplastic by the addition of a TLCP phase, the objective is to deform the dispersed TLCP phase into elongated fibrils that will reinforce the polymeric matrix. However, this is a a complex process that will depend primarily on the rheological and interfacial properties of the blend components, and the flow strength and volume fraction of the dispersed TLCP phase (13,14).

Theoretical treatment of this process has been lacking. Most often, Taylor's theory on the deformation of a Newtonian droplet suspended in a Newtonian medium is used to describe the morphology of in situ composites (15-17). According to Taylor (15), under uniform shearing or plane hyperbolic flows, a spherical droplet of initial radius, *a*, deforms into a spheroidal form. The shape of the droplet depends on the viscosity ratio of the droplet phase, μ_d, to the medium, μ_m, ($\lambda = \frac{\mu_d}{\mu_m}$), and the ratio of the product of the local shear stress and the droplet radius to the interfacial tension, often called Weber or Capillary number. This is defined as We $= \frac{\mu_m \dot{\gamma} a}{\sigma}$, where $\dot{\gamma}$ is the shear rate, *a* is the initial droplet radius, and σ is the interfacial tension. When the interfacial tension effect dominates the viscous effect, the deformation parameter D is given by:

$$D = We \frac{(19\lambda + 16)}{(16\lambda + 16)} \tag{3.1}$$

where D is defined as:

$$D = \frac{(L - B)}{(L + B)} \tag{3.2}$$

in which L and B are the length and breadth of the deformed droplet, respectively. Experimental data on the relation between the Weber number and viscosity ratio on the droplet deformation phenomena have been reported by several authors (18-21). According to these studies, a viscosity ratio between 0.1 and 1.0 will favor droplet deformation in simple shear flow conditions.

Dispersion, morphology, and adhesion of the component phases are greatly affected by interfacial energies important in determining the mechanical properties of the blend. Determining the interfacial properties of in situ composites is of great importance, since mechanical performance could be predicted. Interfacial tension studies on seven types of TLCPs in seven different matrices were recently carried out by Meretz et al. (22). By measuring contact angles on the individual solid samples, the authors were able to calculate differences

in polarities and surface tension and interfacial tension of the 49 possible TLCP/matrix combinations. This procedure led them to the selection of polyethylene terephthalate (PET) and a TLCP copolyester based on PET and hydroxybenzoic acid (HBA) as the most compatible TLCP/matrix pair. Minimized polarity and surface tension differences and interfacial tension were the criteria for compatibility. Through morphological studies they observed that very fine dispersions of the PET/HBA TLCP in the PET matrix could be achieved by blending the polymers through a piston mixer. The work of Meretz et al. (22) is significant because it shows that measurements of the contact angle on solid samples could be useful in predicting the compatibility of the blend components.

One of the most attractive properties of TLCPs is the intrinsic anisotropy of the mesophase, which can be used to create molecular orientation in fabricated articles (23). One application of such a feature is fiber spinning, in which the orientation in the fiber is created by the elongational flow field prevailing in the spinning line. The effectiveness in orienting a liquid crystalline phase under melt spinning conditions is usually observed in the increase of the elastic modulus as a function of draw down ratio (24-26). For example, in studying the melt spinning of a thermotropic copolyester (Vectra A950), Chung (24) observed that the elastic modulus would increase exponentially with molecular orientation (measured as the Herman's orientation function). He was able to obtain values of elastic modulus for this TLCP of as high as 65 GPa, corresponding to a value of the Herman's orientation function of 0.93.

However, in processes such as injection molding the effects of flow on the orientation of TLCPs is more complex. Due to the kinematics of the process, injection molded parts of TLCPs show a distribution in the molecular orientation along the thickness direction (27). The surface (skin) of the part is often formed of highly oriented fibrils, whereas in the center (core) region, a less orientated TLCP phase is usually found. Because of this, injection molded parts of TLCPs usually show lower values of mechanical properties relative to spun fibers. For instance, injection molded tensile bars (ASTM D638 type 5) of Vectra A950 show values of tensile modulus of about 12 GPa (28), which is considerably lower than the 65 GPa value obtained in fiber spinning (24).

Several studies have indicated that in the injection molding of TLCP/polymer blends a synergistic effect in the mechanical properties often appears (29-32). Positive deviation from the simple rule of mixtures (which predicts a linear variation of the composite stiffness with reinforcement content) has been observed in the elastic modulus for blends of PET (29), PEI (30,31) and PEEK (32) with several TLCPs. The reason for such a synergism is most often not completely understood. Furthermore, a maximum in the mechanical properties is usually found at intermediate TLCP concentrations (29-34).

In recent publications, Baird et al. (33,34) have studied blends of PEI with an amorphous and a semicrystalline TLCP. The authors have shown that the mechanical properties of the in situ composites studied were not only affected by the partial miscibility among the components of the blend, but also by the ultimate properties of the TLCP used. The authors have also observed that regardless of miscibility the mechanical properties of the blends (obtained from mini tensile bars) passed through a maximum at a TLCP concentration of 90 wt%. The authors have attempted to explain such a behavior in terms of blend morphology and partial miscibility (34).

In this paper, the work of Baird et al. (34) is extended and additional studies (x-ray diffraction, blend rheology and interfacial energies) are presented which will contribute to the understanding of the mechanical properties exhibited by TLCP/polymer blends. Therefore, the primary objective is to determine the contributing factors which lead to the observed maximum in the mechanical properties of TLCP-based in situ composites. Our studies are concentrated on blends of a polyetherimide (PEI) with an amorphous and a semicrystalline TLCP. In addition, the effects of partial miscibility on the rheolgy and interfacial and mechanical properties are also investigated. Morphological and molecular orientation analyses are presented with the intent of explaining the mechanical properties of these blends.

3.2 Experimental Procedure

3.2.1 Materials

The matrix material is polyetherimide (PEI), commercially available as Ultem 1000 from General Electric Plastics. PEI is an amorphous engineering thermoplastic with a glass transition temperature at about 228°C and a processing temperature ranging from 340 to 380°C (35). The semicrystalline TLCP is a thermortropic copolyester composed of 73 mol% of p-hydroxybenzoic acid and 27 mol% of 2-hydroxy-6-naphthoic acid. This TLCP is commercially available as Vectra A900 from Hoechst-Celanese. Vectra A900 (henceforth referred to as Vectra A) exhibits a glass transition temperature of 105°C, a crystal-mesophase transition at 283°C (36), and a maximum stable processing temperature of 370°C (35). The amorphous TLCP, supplied by DuPont, is based on hydroquinone (HQ), terephthalic acid (TA) and other hydroquinone derivatives. This amorphous TLCP, referred to as HX1000, has a glass transition temperature of 185°C (33) and a processing temperature ranging from 290 to 365°C. Proposed chemical structures for these TLCPs may be found in (37).

Vectra A and HX1000 were selected based upon the following criteria. First, they have an overlapping processing temperature relative to the engineering thermoplastic matrix used. Thus, thermal degradation of the TLCP is avoided. Secondly, HX1000, contrary to Vectra A, is partially miscible with PEI (33). Thus, by selecting these two TLCPs, the effects of partial miscibility on the structure and properties of the blends may be determined.

3.2.2 Blend Preparation and Processing

Before blending, pellets of the above materials were dried at 115°C in a convection oven for at least 48 hours. The dried pellets of PEI/Vectra A and PEI/HX1000 were then tumbled in a steel container on a weight percent (wt%) basis. In order to study the effects of TLCP concentration on the structure and properties of PEI/TLCP blends, the TLCP concentration was increased from zero to 100 wt% in 10 wt% intervals. After dry blending, the mixed pellets were stored in a hermetically sealed container.

The physically mixed pellets were then injection molded into mini-tensile bars (ASTM D638 type 5) and rectangular plaques (measuring approximately 75mm x 85mm x 1.75mm) using an Arburg 221-55-250 Allrounder Injection Molder. The temperature settings of the injection molding unit were 330, 345, 360, and 360°C for zones 1, 2, and 3 of the barrel and nozzle, respectively. The injection pressure was set at 7.0 MPa with a holding pressure of 3.5 MPa. The injection speed was set at a medium range, which gives a volumetric flow rate of 12 cm^3/sec. The mold was held at 110°C and a cooling time of 40 sec was used. The processing conditions were kept constant throughout all moldings.

It is important to point out, however, that the samples were generated through injection molding alone, without any previous melt blending of the tumbled pellets. Thus, all samples have only undergone the mixing history provided by the plasticating process in the injection molding unit. It should be emphasized that the effects of mixing history on the structure and properties of TLCP based in situ composites cannot be overlooked. The effect of mixing history on the morphology and mechanical properties displayed by a TLCP/polymer blend is very significant (34). To some extent, depending on the ratio of viscosities and interfacial tension, mixing improves dispersion of the minor phase component in the blend, and finer structures are often obtained by increasing passes through a single or twin screw extruder (33). However, depending on the system, improvement in the mechanical properties of TLCP/polymer blends are not always observed by the increase in the mixing history (34).

As mixing reduces the dispersed phase particle size, larger stresses, often not attained during processing, are necessary in order to elongate the droplet.

3.2.3 Rheological Characterization

Dynamic oscillatory shear viscosity data were obtained by means of a Rheometrics Mechanical Spectrometer (Model 800) for all blend compositions as well as for the individual components. The tests were performed in the frequency sweep mode on samples cut from injection molded plaques. Parallel plate fixtures were used with a gap between 1.0 and 1.25 mm. The test temperature was set a 360°C, which matches the maximum temperature the samples were exposed to during injection molding. Strain sweeps were conducted at a constant frequency to determine the limits of the linear viscoelastic region. Strain sweep experiments were carried out on the individual components and on 50/50 wt% blends to determine the limits of their linear viscoelastic behavior. Within the range of strains investigated, from 0.5 to 14.5%, PEI, PEI/Vectra A 50/50 wt% and PEI/HX1000 50/50 wt% exhibited linear viscoelastic response. Only a small deviation from the linear viscoelastic behavior was observed for Vectra A and HX1000 at strains greater than 10%. Hence, all the dynamic data were taken at 5% strain, which is well within the linear viscoelastic behavior of the materials.

3.2.4 Interfacial Tension

Interfacial tension calculations were performed in order to determine the degree of compatibility between the polymer pairs used. The harmonic mean method of calculating interfacial tension is utilized here to determine the interfacial energy between PEI and Vectra A, and PEI and HX1000 (38). Following Wu (38,39), the interfacial tension between two materials, γ_{12} may be estimated according to the equation:

$$\gamma_{12} = \gamma_1 + \gamma_2 - \frac{4\gamma_1^d\gamma_2^d}{\gamma_1^d + \gamma_2^d} - \frac{4\gamma_1^p\gamma_2^p}{\gamma_1^p + \gamma_2^p} \tag{3.3}$$

where γ_i is the surface tension of material i (i=1,2), γ_i^d and γ_i^p are the dispersive and polar components of the surface tension of material i. Combining the harmonic mean equation of the interfacial tension (Eq. 3.3) with the Young's equation for the contact angle (38) the result is:

$$(1 + \cos\Theta)\gamma_L = \frac{4\gamma_S^d\gamma_L^d}{\gamma_S^d + \gamma_L^d} + \frac{4\gamma_S^p\gamma_L^p}{\gamma_S^p + \gamma_L^p} \tag{3.4}$$

where the indices L and S characterize the liquid and the solid phase respectively. By measuring the contact angle of two test fluids with well known values of γ_L^d and γ_L^p, two simultaneous quadratic equations with γ_S^d and γ_S^p as unknown quantities can then be solved.

Two probe liquids (distilled water and formamid) were used to measure the equilibrium contact angle on solid samples of PEI, Vectra A and HX1000. The surface tension as well as its dispersive and polar components for distilled water are 72.6, 21.7 and 50.9 mN/m, respectively. For formamid the values are 58.3, 32.3 and 26.0 mN/m, respectively. Injection molded samples of PEI, Vectra A and HX1000 were used in the tests. The contact angle (Θ) of each sample was calculated by taking the average of at least eight measurements. Standard deviations were of order of 1.6 to 7.4%. The average values of the contact angle were placed into Equation 3.4 and the polar and dispersive components of the surface tension for each individual solid sample were determined. These results were then substituted into Equation 3.3 and the interfacial tension for each polymer pair was calculated.

3.2.5 Morphological Characterization and Mechanical Properties

The morphology of the injection molded parts (molded plaques and/or tensile bars) was investigated by means of scanning electron microscopy (SEM). A Cambridge Stereoscan-S200 Instrument with an accelerating voltage of 25 KV was used. The samples were cryogenically fractured along and across the injection molding flow direction after immersion in liquid nitrogen for at least 5 minutes. The samples were then mounted on aluminum stubs and sputter coated with gold for enhanced conductivity. The fracture surfaces were scanned from the surface to the center regions to determine the shape and size of the TLCP dispersed phase.

The mechanical properties of the injection molded tensile bars and rectangular strips (measuring approximately 12mm x 80mm) cut out from the injection molded plaques were evaluated using an Instron Universal Testing Instrument, model 4204. A cross-head speed of 1 mm/min was used. An extensometer was utilized to record the strain. Tensile strength and tensile (Young's) modulus were calculated from the stress-strain curves. The tensile modulus was determined from the best linear fit through the initial region of the stress-strain curve. Toughness was calculated as the area under the stress-strain curve through numerical integration. The mechanical properties reported are based on measurements made on at least five samples. In some cases, especially at high TLCP contents, the samples broke at the grips. In such cases, tensile strength and elongation at break are most probably underestimated. Error bars in the graphs indicate one standard deviation.

3.2.6 Molecular Orientation

The degree of molecular orientation, assessed by means of wide angle x-ray diffraction (WAXD) measurements, was specified by means of the Herman's orientation func-

tion, f^H, of the TLCP phase in the blend. An automated Philips diffractometer and nickel filtered CuKα radiation were used. 2θ data were collected in a fixed-time mode from 5 to 45° with a step size of 0.1°. The values of the Herman's orientation function, f^H, defined by:

$$f^H = \frac{3 < \cos^2\phi > - 1}{2} \tag{3.5}$$

were determined from azimuthal scan traces of the strong equatorial reflections. Calculated orientation functions were averaged over four quadrants, using both equatorial reflections. Background scattering was subtracted from the intensity profile. In Equation 3.5, ϕ is the angle between the director of the liquid crystalline phase or domain, and the reinforcing fibril axis. The brackets < > indicate the average over all possible configurations. For a perfect orientation of the domains in the fibril direction $f^H = 1$, and for a complete random orientation $f^H = 0$.

3.3 Results and Discussions

The methodology and experimental procedure used to fulfill the objectives of this paper have been discussed in the last section. In this section the experimental results along with the analysis and discussions will be presented. To make the following discussions as clear as possible, this section has been divided into several parts. First, in Section 3.3.1 the mechanical properties of PEI/Vectra A and PEI/HX1000 blends are presented. Following this, in Section 3.3.2 results from the interfacial tension analysis are presented. Next, in Section 3.3.3 rheological results of PEI/Vectra A and PEI/HX1000 blends are discussed. Finally, in Sections 3.3.4 and 3.3.5 morphological studies followed by molecular orientation analyses are presented which intend to explain the mechanical properties behavior observed.

3.3.1 Mechanical Properties

The results of mechanical tests performed on injection molded samples of PEI/Vectra A and PEI/HX1000 blends as a function of TLCP concentration are discussed in this section. Tensile and flexural properties are presented in order to illustrate the significance of partial miscibility and compatibility on the mechanical response of in situ composites. To better convey the findings of the mechanical tests, tensile properties are discussed first, followed by the results of flexural tests.

3.3.1.1 Tensile Properties

The effects of the addition of a thermotropic liquid crystalline phase on the tensile modulus (TM) of a PEI matrix are discussed first. Following this, the ultimate properties (strength, elongation at break and toughness) are discussed. In addition, transverse mechanical properties are presented which will provide additional understanding of the effects of partial miscibility on the properties of PEI/TLCP blends.

Tensile modulus (TM) values obtained from injection molded mini-tensile bars of PEI/Vectra A and PEI/HX1000 blends as a function of TLCP concentration are presented in Figure 3.1. As observed, blending PEI with either Vectra A or HX1000 leads to a significant increase in tensile modulus. The TLCP reinforcement increases the modulus of the PEI phase considerably. However, the degree of modulus increase obtained by the addition of HX1000 is larger than that for the addition of Vectra A, in spite of both TLCPs showing similar values of tensile modulus themselves. For instance, at 30 wt% TLCP reinforcement, PEI/HX1000 shows a tensile modulus of 8.70 GPa, whereas for PEI/Vectra, a value of 5.80 is observed. This represents an increase in the modulus of the PEI by a factor of 2 to 3 by the addition of either Vectra A or HX1000, respectively. Furthermore, a maximum in the tensile modulus, although of different magnitudes, is observed for both in situ composites at around 90 wt% TLCP con-

centration. The values of TM of the blends at this concentration are significantly higher than those of the neat TLCPs.

The fact that TLCPs can act as a reinforcing agent in a blend has led some investigators to model the mechanical behavior of TLCP/polymer blends according to composite theories (41-43). One of the relationships most commonly used to predict the modulus of a composite from the moduli of the individual components is the Tsai-Halpin equation (44):

$$E_c = E_m\left(\frac{1 + A\,B\,V_f}{1 - A\,V_f}\right) \tag{3.6}$$

with

$$A = \frac{E_f - E_m}{E_f + BE_m} \tag{3.7}$$

and, for the case of transversely isotropic composites, B is given by:

$$B = 2\left(\frac{L}{D}\right) \tag{3.8}$$

where E_c is composite modulus along the fiber direction, E_m is the modulus of the matrix, E_f is the modulus of the fiber, V_f is the volume fraction of fiber, and (L/D) is the aspect ratio of the fiber. For fibers with aspect ratios greater than 100, a linear relationship exists between the modulus of the composite and the volume fraction of reinforcement (41). This suggests that, for uniaxially reinforced systems, a simple rule of mixtures may conveniently be applied to predict the theoretical modulus of composites reinforced with fibers of aspect ratio greater than 100.

However, in addition to fiber aspect ratio, the modulus of the reinforcing fibers (more specifically E_f/E_m ratio) also plays an important role in the final modulus of the composite. In the case of TLCP/polymer blends, the difficulty lies in the proper selection of TLCP phase properties to use in the calculations. It is well known that the mechanical properties of TLCPs are significantly affected by the magnitude of the applied strain. Higher values of modulus

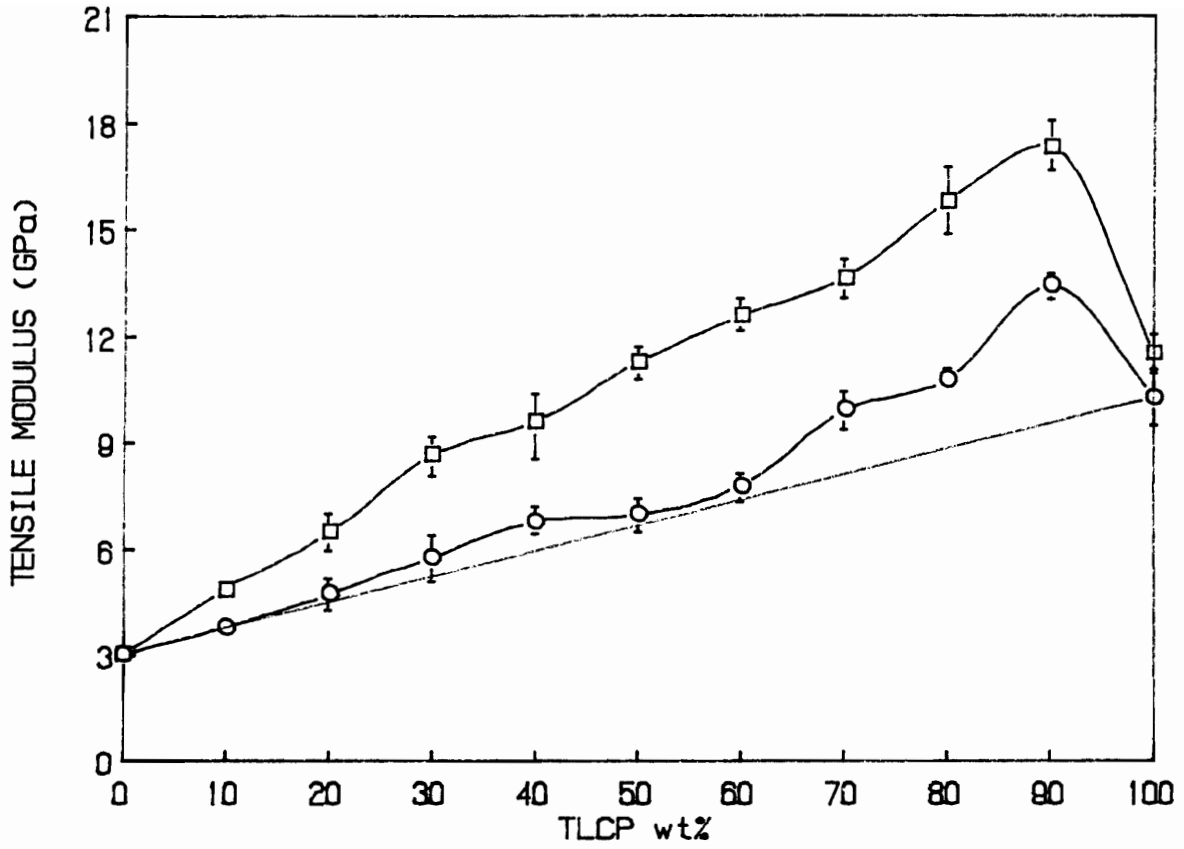

Figure 3.1. Tensile Modulus of injection molded tensile bars of PEI/TLCP in situ composites as a function of TLCP concentration ((○) PEI/Vectra A and (□) PEI/HX1000).

and strength are usually obtained through melt spinning or post-extrusion drawing (24,35). Therefore, in predicting the theoretical modulus of TLCP/polymer blends, one should be aware that the mechanical properties of TLCP/polymer blends are directly dependent upon processing history. Consequently, in estimating the TLCP/polymer blend properties, calculations should be performed with materials that have undergone comparable processing histories.

In Figure 3.1, the tensile moduli of the PEI/TLCP blends are compared to the moduli predicted by the simple rule of mixtures (indicated by the straight line). The modulus values used in calculations of the rule of mixtures are based on the modulus measurements made on injection molded samples of the individual blend components. Therefore, the processing histories of both individual components as well as the blends are alike. A positive deviation from the rule of mixtures is observed for both blends. In the case of PEI/Vectra A, the blend moduli follows the rule of mixtures up to a Vectra A concentration of 60 wt%. Above this concentration, a synergism in the tensile modulus is observed. In the case of PEI/HX1000, the synergism in the tensile modulus is observed in the whole range of compositions investigated.

However, for comparison the theoretical modulus of the blends was estimated using the modulus of spun TLCP fibers. If values of spun TLCP fibers were to be used and considering perfectly aligned fibers of aspect ratio of at least 100, the calculated theoretical modulus would be as follows. Using, for example, a tensile modulus for Vectra A fibers of 65 GPa (24) instead of 10.33 as obtained in injection molding, at 30 wt% Vectra A, which corresponds to 28 vol%, the theoretical modulus is estimated to be 20.4 GPa, which is considerably higher than the value of 5.83 GPa obtained in injection molding. It is apparent that if the moduli of spun fibers were to be used in the theoretical calculations, the experimental values would be considerably lower than the theoretical value.

We next turn our attention to the ultimate properties (strength, elongation at break and toughness) exhibited by the PEI/TLCP blends. The tensile strengths (TS) of PEI/Vectra A and PEI/HX1000 blends are presented in Figure 3.2. The tensile strength for all blend compositions are greater than that of the pure PEI. However, depending on the TLCP content, it seems that both partial miscibility and ultimate properties of the TLCP phase may play significant roles

in determining the tensile strength of the blend. At TLCP contents as high as 20 wt%, higher values of tensile strength are observed for the PEI/HX1000 system compared to PEI/Vectra A system. However, as the concentration of TLCP is increased, the ultimate properties of the TLCP overwhelms the effects of miscibility. Thus, at TLCP-rich concentrations, the ultimate properties of the TLCP phase dominates the tensile strength of the blend. The ultimate tensile strength of Vectra A (234 MPa) is almost twice that of HX1000 (126 MPa), and because of this, at TLCP-rich compositions, the tensile strengths of PEI/Vectra A blends are considerably higher than those of PEI/HX1000.

The transverse tensile strength is usually used as an indication of fiber/matrix adhesion in fiber composites (45). It is usually found that variations in thermal treatment can substantially affect the transverse properties and consequently fiber/matrix adhesion of a thermoplastic prepreg (45). In the case of in situ composites, it is expected that the transverse tensile strength would also be sensitive to the miscibility between the matrix and the reinforcing TLCP. With this in mind, transverse tensile strength measurements were performed on selected compositions of PEI/Vectra A and PEI/HX1000 blends. Transverse tensile strength values of PEI/HX1000 and PEI/Vectra A for TLCP contents of up to 30 wt% are presented in Table 3.1. As one notices, even though HX1000 shows a value of transverse strength significantly lower than Vectra A, the values of transverse tensile strength obtained for PEI/HX1000 blends are slightly higher than those of PEI/Vectra A blends at TLCP concentrations of up to 20 wt%. At 30 wt% TLCP content, both blends exhibit similar values of transverse tensile strength. As in the case of flow direction strength, it is observed that the higher compatibility (higher work of adhesion) between PEI and HX1000 phase is contributing significantly to the observed transverse strength response of the PEI/TLCP blends studied, especially at low TLCP concentrations.

The elongation at break (EB) for both in situ composites is illustrated in Figure 3.3. The elongation at break of PEI/TLCP blends falls drastically as the TLCP content is increased because of the dramatic difference in ductility between the PEI and the TLCPs. PEI usually shows an elongation at yield at 7% and an elongation at break at 60%, whereas Vectra A and HX1000

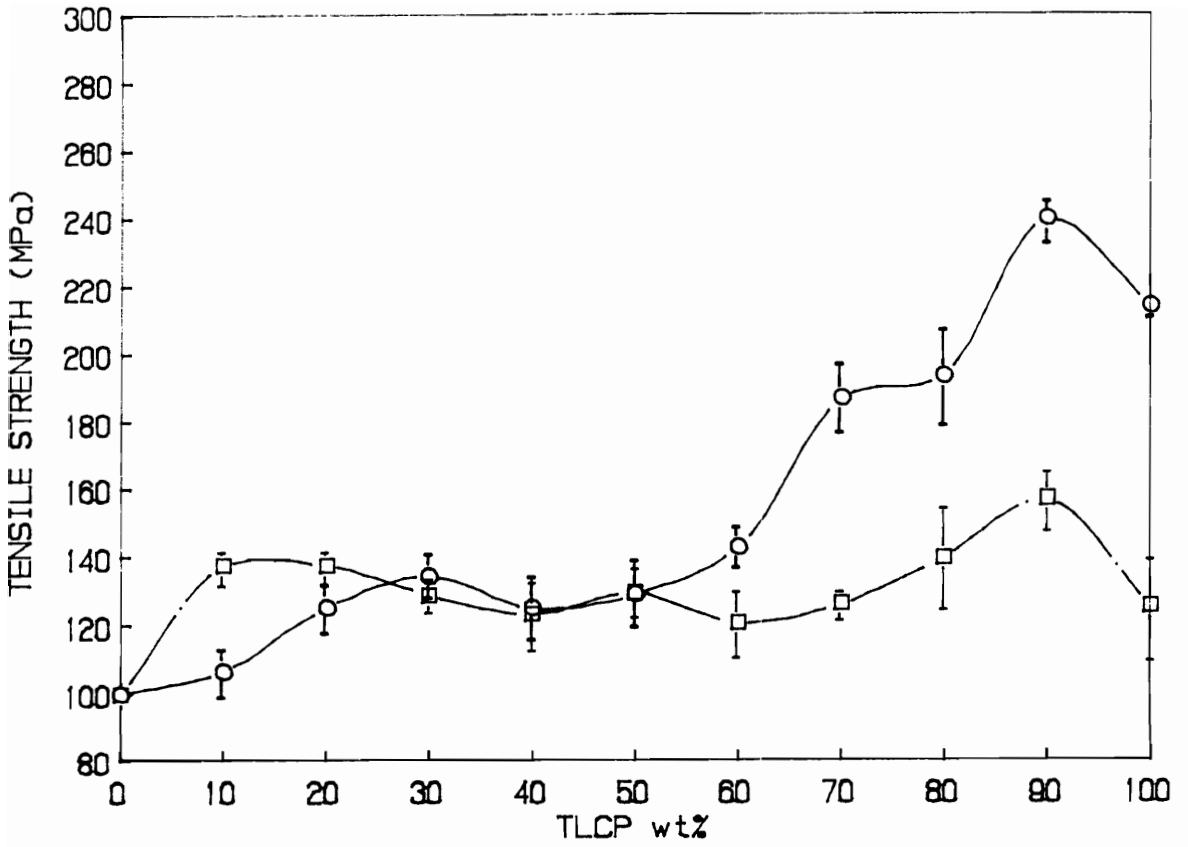

Figure 3.2. Ultimate Tensile Strength of injection molded tensile bars of PEI/TLCP in situ composites as a function of TLCP concentration ((○) PEI/Vectra A, (□) PEI/HX1000).

Table 3.1. Transverse tensile strength (MPa) of PEI/HX1000 and PEI/Vectra A blends.

COMPOSITION	PEI/HX1000	PEI/VECTRA A900
90/10	83.87 (3.59)	75.00 (3.90)
80/20	57.10 (3.92)	45.00 (4.10)
70/30	41.61 (2.74)	37.10 (3.30)
0/100	28.90 (2.01)	45.70 (1.80)

(*) standard deviations are given in parenthesis.

show an elongation at break of 4.4 and 1.7%, respectively. The elongation at break of PEI/Vectra A blends is much higher than that for PEI/HX1000 blends, especially at high TLCP contents, because Vectra A is more ductile than HX1000. It seems that the elongation at break of the PEI/TLCP systems studied is influenced much more strongly by the intrinsic properties of the TLCP used as a reinforcement than by partial miscibility.

The toughness of PEI/Vectra A and PEI/HX1000 blends, calculated as the area under the stress versus strain curve, is presented in Figure 3.4. Not shown in the figure is the toughness of neat PEI, which is in excess of 10 GJ/m^3. The toughness of the PEI/Vectra A blends is much greater than that of PEI/HX1000 blends. This is consistent with the fact that higher values of ultimate properties (strength and elongation at break) are observed for Vectra A. The values of toughness calculated for the neat Vectra A and HX1000 are of the order of 6 and 1.3 GJ/m^3, respectively. It is observed that the lower toughness of HX1000 is carried over to the PEI/HX1000 blends. For HX1000 concentrations greater than 20 wt%, the toughness of the blend is now dominated by the HX1000. PEI/Vectra A blends, on the other hand, exhibited a peculiar behavior. Once again, toughness of the blend decreased upon addition of Vectra A, but in this case, a minimum is observed at 40 wt% Vectra A concentration. Another important observation is the presence of the maxima at 90 wt% Vectra concentration, which is a consequence of the maxima in the tensile strength observed at this same concentration. The experimental data suggest that, as in the case of elongation at break, the toughness behavior of PEI/HX1000 and PEI/Vectra A blends is much more influenced by the properties of the TLCP used than by miscibility.

In summary, it is clear from the above results that although partial miscibility affects the tensile modulus of an in situ composite more strongly, the ultimate mechanical properties of the in situ composite are more strongly influenced by the ultimate properties of the TLCP used, especially for the TLCP-rich compositions. Therefore, it seems that the final decision in the selection of a TLCP to reinforce a polymeric matrix will be much more dependent upon the properties of the TLCP than on whether the TLCP has partial miscibility with the polymeric

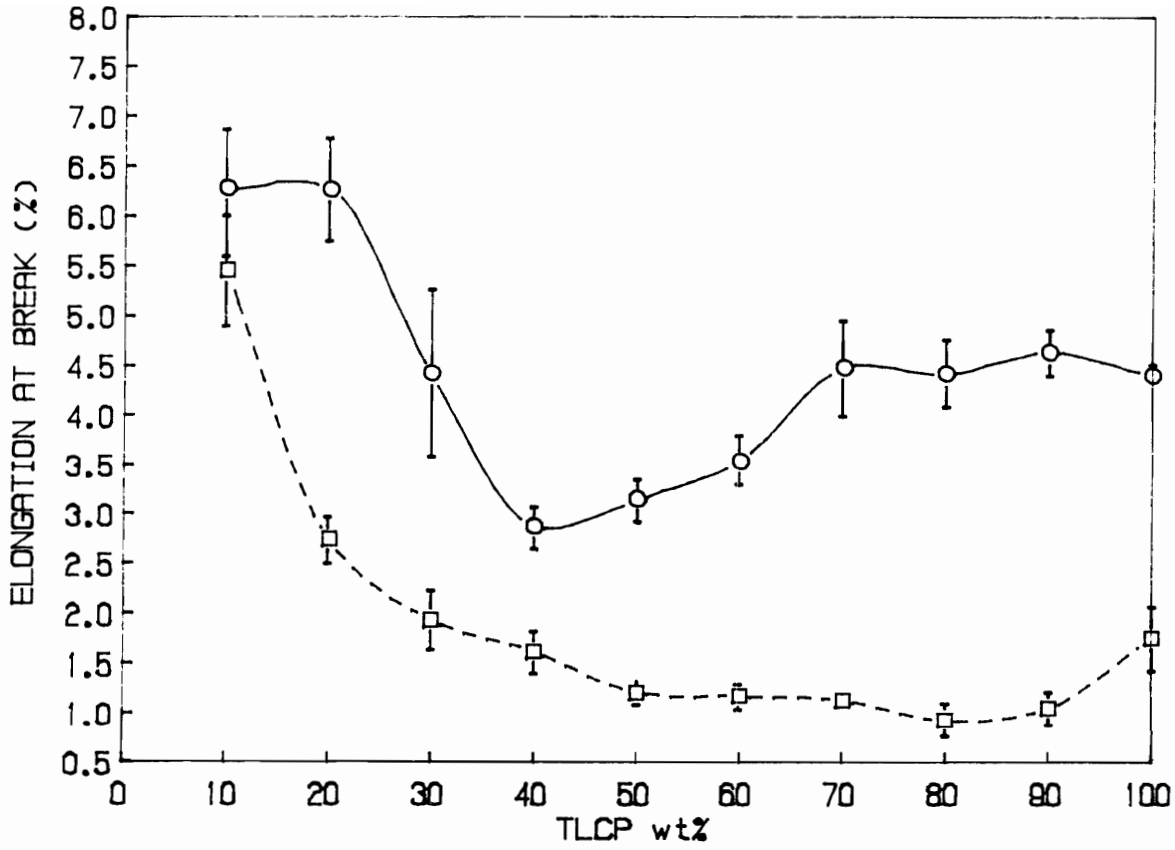

Figure 3.3. Elongation at break of injection molded tensile bars of PEI/TLCP in situ composites as a function of TLCP concentration ((○) PEI/Vectra A and (□) PEI/HX1000).

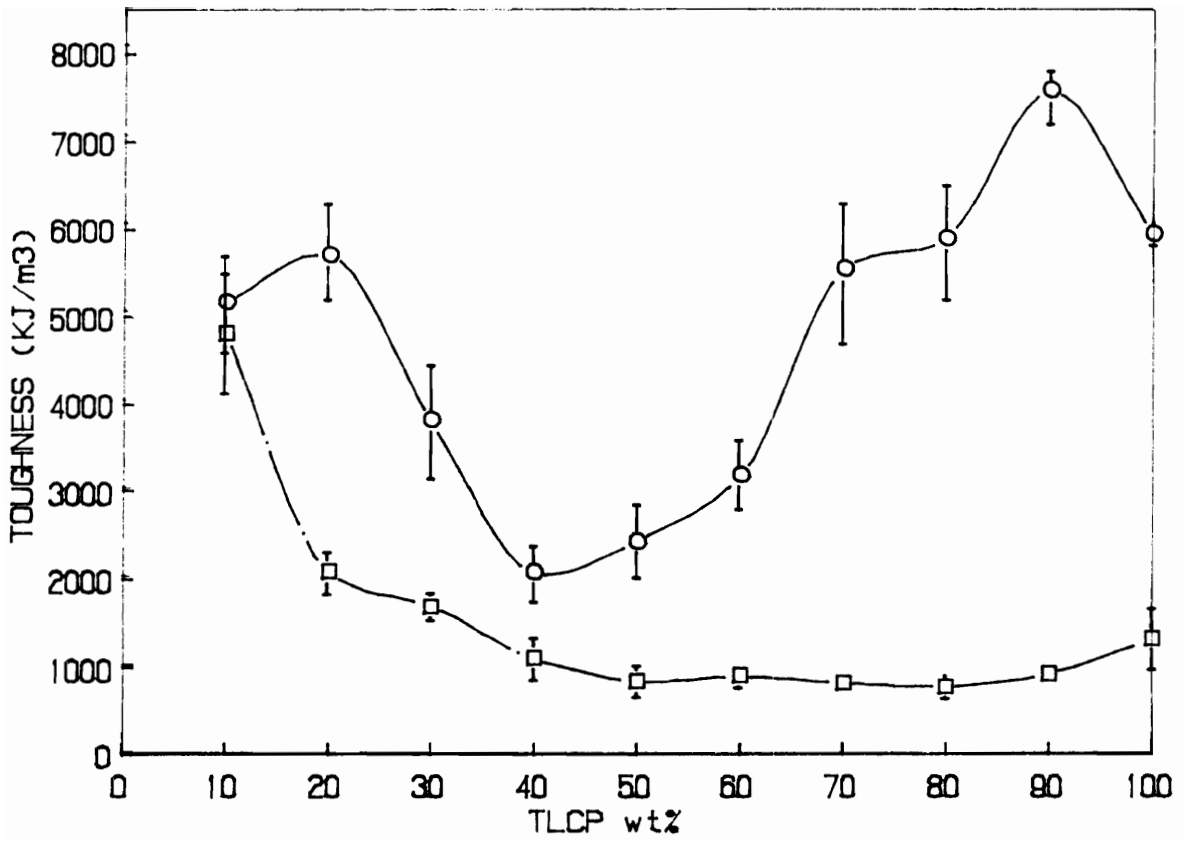

Figure 3.4. Toughness of injection molded tensile bars of PEI/TLCP in situ composites as a function of TLCP concentration ((○) PEI/Vectra A and (□) PEI/HX1000).

matrix. In addition, the ultimate mechanical property of the in situ composite is also dependent upon the TLCP concentration.

3.3.1.2 Flexural Properties

The flexural modulus and flexural strength for PEI/Vectra A and PEI/HX1000 blends are presented in Figures 3.5 and 3.6, respectively. Figure 3.5 shows that the flexural modulus of PEI/HX1000 blends show a positive deviation from the rule of mixtures (shown by the straight line) for all HX1000 concentrations. On the contrary, the flexural modulus of PEI/Vectra A follows the rule of mixturs for most of the Vectra A concentrations. A small synergism appears only at Vectra A concentrations of 80 wt% and above. Nevertheless, as in the case of tensile modulus, both blends once again show a maximum in modulus at 90 wt% TLCP concentration.

Flexural strength values plotted as function of TLCP concentration for PEI/Vectra A and PEI/HX1000 blends are presented in Figure 3.6. As one notices, the effect of partial miscibility on the flexural strength is very dramatic for TLCP concentrations up to 20 wt%. For instance, the addition of only 10 wt% HX1000 increases the flexural strength of the PEI matrix from 150 to about 210 MPa, representing a 40% increase. On the other hand, at the same concentration, Vectra A contributes to a lesser increase in the strength (from 150 to around 180 MPa), in spite of showing a higher flexural strength than HX1000. However, at 30 wt% TLCP concentration, the flexural strength of both blends drops to a value of around 140 MPa. When increasing the TLCP concentration above 30 wt%, a monotonic increase in the strength, up to the value of the neat TLCPs, is observed.

The mechanical properties of PEI/Vectra A and PEI/HX1000 blends have been presented in this section. It appears that partial miscibility has a greater effect on the modulus than on the ultimate properties of the in situ composite. In the case of ultimate properties, the effects of partial miscibility are limited by the TLCP content. It was observed that, for TLCP contents up to 20 wt%, partial miscibility affects ultimate properties. For example, even though

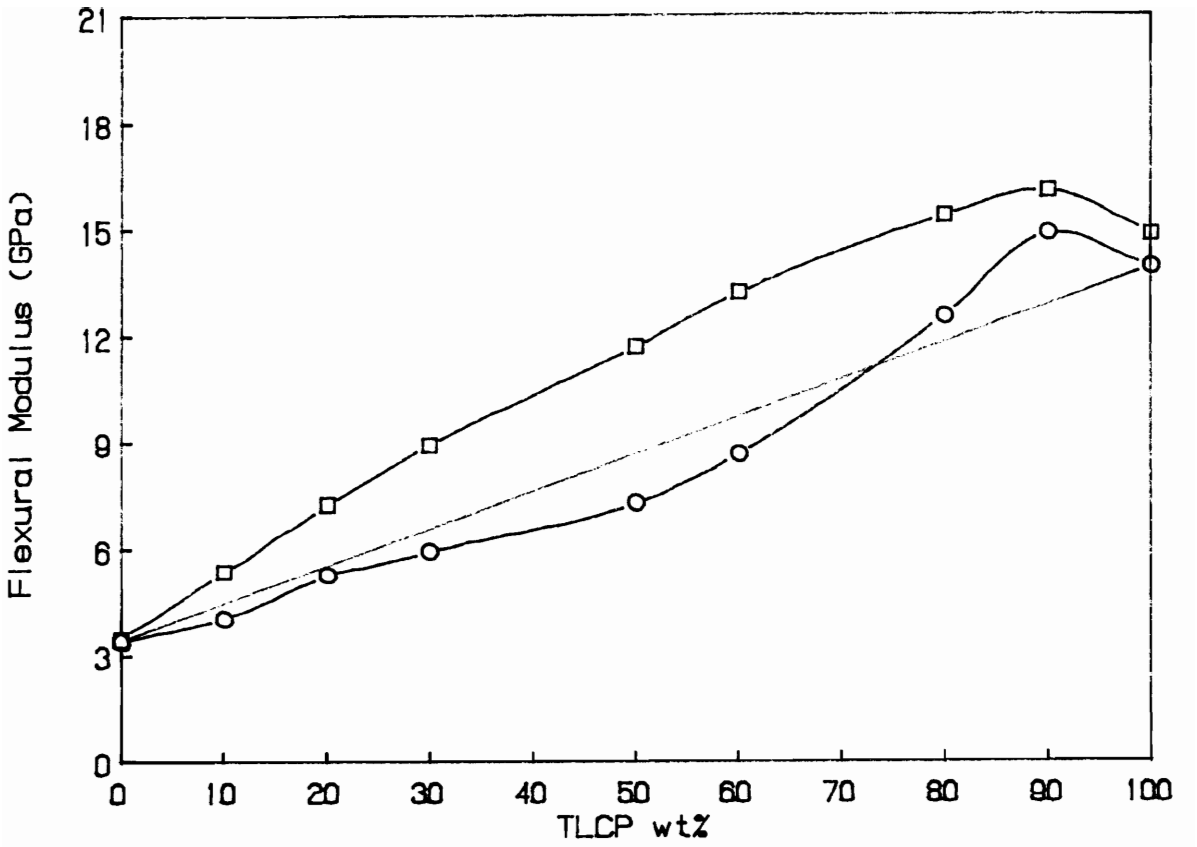

Figure 3.5. Flexural modulus of PEI/TLCP in situ composites as a function of TLCP concentration ((○) PEI/Vectra A and (□) PEI/HX1000).

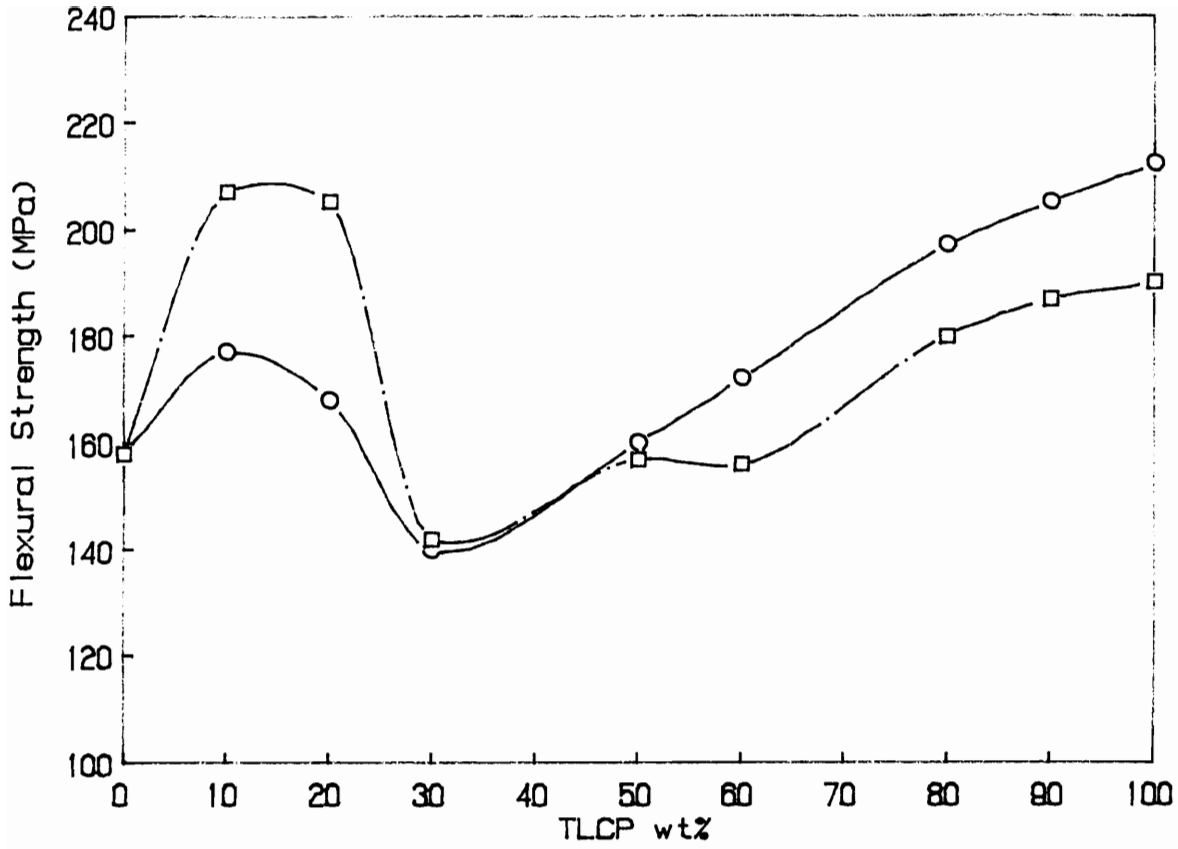

Figure 3.6. Flexural strength of PEI/TLCP in situ composites as a function of TLCP concentration ((○) PEI/Vectra A and (□) PEI/HX1000).

HX1000 shows a lower value of ultimate tensile strength than Vectra A, PEI/HX1000 blends exhibit a greater value of tensile strength than PEI/Vectra A blends for TLCP concentrations up to 20 wt%. However, for TLCP-rich compositions, the ultimate properties of the reinforcing TLCP dominate the ultimate properties of the composite.

3.3.2 Interfacial Tension Analysis

The mechanical performance of thermoplastic composites is usually affected by the interfacial adhesion of the reinforcing fiber to the thermoplastic matrix. Therefore, determining the interfacial adhesion between the reinforcing fibers and the matrix polymer is of great importance since mechanical properties could be predicted. Interfacial tension results for PEI/HX1000 and PEI/Vectra A are presented in Table 3.2. As seen, the PEI/HX1000 system exhibits a lower value of interfacial tension than the PEI/Vectra A system. This suggests that a greater degree of interfacial adhesion may be expected for the PEI/HX1000 system relative to the PEI/Vectra A system. The works of adhesion and cohesion are also presented in Table 3.2. For both in situ composites the work of interfacial adhesion is less than the work of matrix cohesion. This suggests that for both composites failure will most probably occur at the TLCP/matrix interface (46).

In Table 3.2, a lower interfacial tension and a higher work of adhesion are observed for PEI/HX1000 compared to PEI/Vectra A. Therefore, the ultimate mechanical properties of PEI/HX1000 and PEI/Vectra A at low TLCP contents correlate well with the observed differences in the interfacial adhesion. Hence, in spite of the neat HX1000 showing a lower value of ultimate mechanical properties than those of the neat Vectra A, the ultimate mechanical properties observed for the blends at low TLCP content is clearly influenced by the stronger interfacial adhesion encountered in the PEI/HX1000 relative to PEI/Vectra A.

In addition to the effect on ultimate properties, interfacial tension also plays an important role in the deformation of a TLCP phase into reinforcing fibrils. As seen from Equation

Table 3.2. Surface Energies (mN/m) for PEI, HX1000 and Vectra A.

Material	γ^d	γ^p	γ^t	X_p	γ_{12}	ΔX_p	W_a	W_c
PEI	10.50	42.30	52.80	0.801				105.60
Vectra A	20.59	11.57	32.16	0.360				
HX1000	13.00	23.10	36.10	0.640				
PEI/VA					20.80	0.441	64.16	
PEI/HX1000					7.20	0.161	81.70	

where: γ^d **= dispersive component of surface tension**
γ^p **= polar component of surface tension**
γ^t **= surface tension** ($\gamma^d + \gamma^p$)
X_p **= polarity** (γ^p/γ^t)
γ_{12} **= interfacial tension**
ΔX_p **= difference in polarities**
W_a **= work of adhesion**
W_c **= work of cohesion**

3.1, lower interfacial tension will result in lower values of the Weber number at the same stress. Consequently, a higher magnitude of the deformation parameter, D, may be observed. For TLCP/polymer blends, a low value interfacial tension may result in high aspect ratio TLCP fibers. Thus, one may expect that due to the lower value of interfacial tension HX1000 fibrils of higher aspect ratio than Vectra A fibrils could be formed during the injection molding of the blends. Furthermore, the values of interfacial tension may also suggest that lower magnitudes of deformation rates (lower We) are necessary in order to elongate the HX1000 phase into reinforcing fibrils compared to the Vectra A phase. However, in addition to interfacial tension, the deformation parameter D also depends on the viscosity ratio of the dispersed phase to the suspending medium. Studies have shown that, for Newtonian fluids, optimum fibrillation of the dispersed phase will result at a viscosity ratio between 0.1 and 1.0 (20). In light of the role of viscosity, the results of rheological experiments are discussed next.

3.3.3 Rheological Properties

Rheological tests were performed in order to determine the viscosity ratio between the components of the PEI/TLCP blends studied. The complex viscosity as a function of frequency of PEI, Vectra A and HX1000 are shown in Figure 3.7. The rheological behavior of PEI, for instance, shows a viscosity/frequency curve that is independent of frequency, similar to that of a Newtonian fluid. A slight deviation from Newtonian behavior is only observed for frequencies above 10 rad.s^{-1}. Vectra A, on the other hand, shows shear thinning behavior throughout the range of frequencies investigated. HX1000, however, shows the most interesting behavior of all. At low frequencies, up to 1 rad.s^{-1}, a pseudo-Newtonian plateau is observed. At frequencies above 1 rad.s^{-1}, the material shear thins at a rather high rate and a very steep slope is observed. The complex viscosity of HX1000 decreases monotonically from about 1000 Pa.s at 1 rad.s^{-1} to about 55 Pa.s at 100 rad.s^{-1}, which represents a reduction of over one order of magnitude of the viscosity over two decades of frequencies. In addition, the ratio

of viscosities of the TLCPs and PEI ($\frac{\eta_{TLCP}}{\eta_{PEI}}$) is observed to vary drastically with frequency. In the case of PEI/HX1000, for example, a viscosity ratio of about 0.80 is observed at a frequency of 0.1 rad.s^{-1}, and at 100 rad.s^{-1}, the viscosity ratio has dropped to 0.06. Therefore, for most of the range of frequencies investigated, a viscosity ratio exists in the PEI/TLCP blends, which is favorable for the deformation of the TLCP phase into reinforcing fibrils.

The effects of the addition of TLCP to the blend viscosity are considered next. The complex viscosity as a function of the frequency of PEI/Vectra A blends for Vectra A concentrations of 10, 50 and 90 wt% is presented in Figure 3.8. As shown, the addition of as little as 10 weight percent Vectra A to PEI reduces the viscosity of PEI by as much as 50% over the entire range of frequencies studied. Further, the dependence of the complex viscosity on the frequency for the 90/10 PEI/Vectra A blend resembles the behavior observed for the neat PEI (i.e. nearly Newtonian behavior over all frequencies). The reduction in the matrix viscosity upon addition of small amounts of a TLCP phase is typical behavior reported for other TLCP/polymer blends (47-51). Reasons for such a behavior have been attributed to: a) incompatibility between the two phases, and b) at small amounts, the low viscosity TLCP phase may act as lubricant to the polymeric matrix and reduce its viscosity (51).

At Vectra A concentrations of 50 and 90 wt%, however, a pseudo-plastic behavior is readily observed. The complex viscosity curves at high TLCP concentrations are, nonetheless, similar in shape to the one observed for the neat Vectra A. Due to the shape of the curves, one may speculate that for concentrations of Vectra A of 50 wt% and above the continuous phase is probably the TLCP. From this perspective, the increase in blend viscosity relative to the neat Vectra A could be related to the presence of a more viscous PEI phase.

The complex viscosity as a function of frequency of PEI/HX1000 blends for HX1000 concentrations of 0, 10, 20, 50, 90 and 100 wt% are illustrated in Figure 3.9. Once again, the addition of as little as 10 weight percent HX1000 considerably reduces the viscosity of the PEI matrix. The extent of viscosity reduction was greater than 65%, considerably greater than the 50% reduction observed for PEI/Vectra A blends. However, increasing the concentration of HX1000 in the blend does not necessarily mean that the viscosity of the blend will continue to

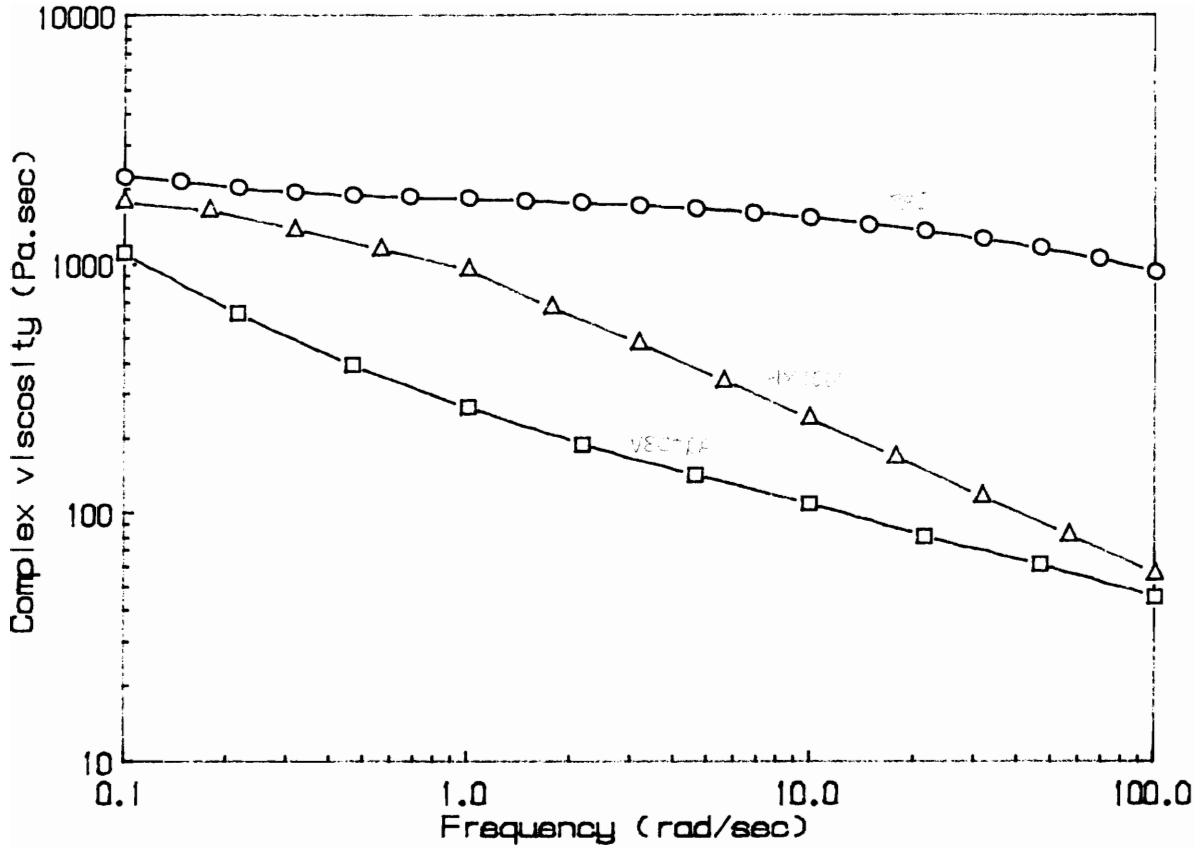

Figure 3.7. Complex viscosity vs frequency of (○) PEI, (□) Vectra A and (△) HX1000 measured at 360°C and 5% strain.

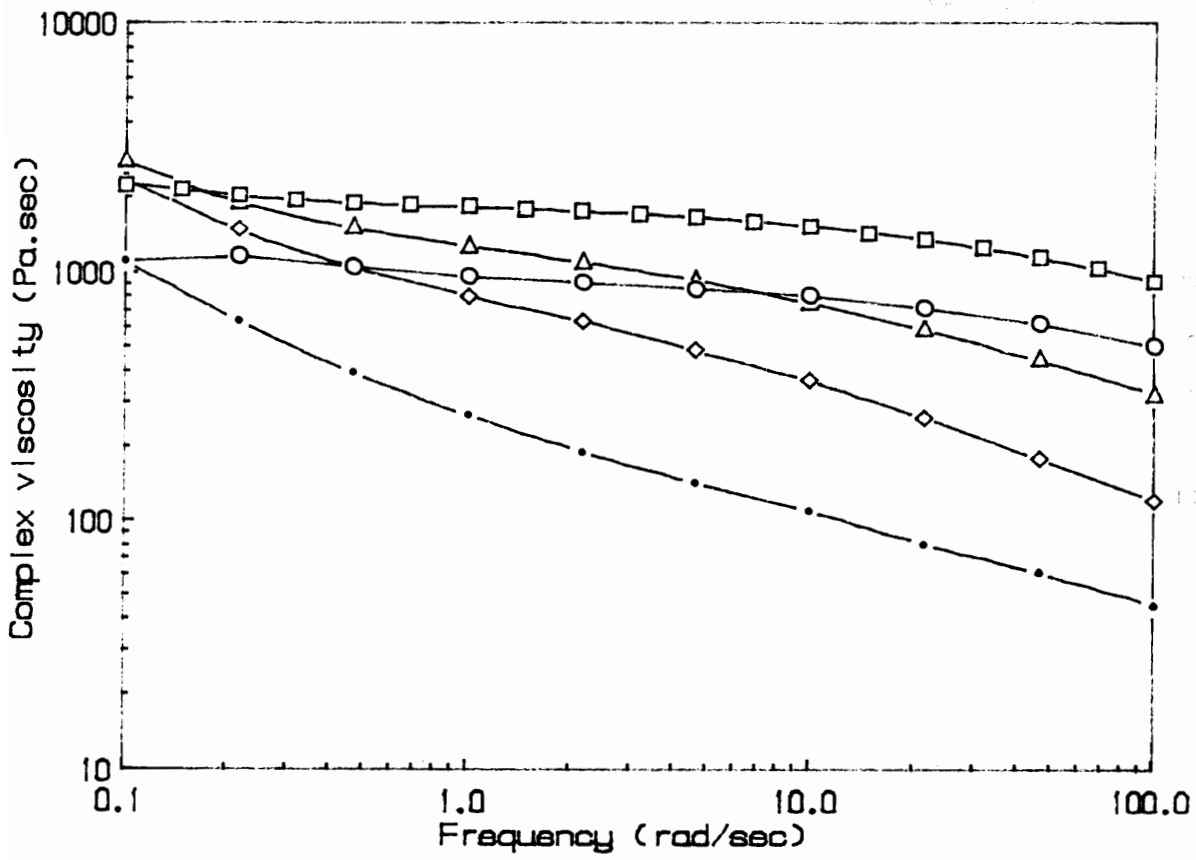

Figure 3.8. Complex viscosity vs frequency of PEI/Vectra A blends as a function of Vectra A concentration measured at 360°C and 5% strain ((□) 100/0, (○) 90/10, (△) 50/50, (◇) 10/90 and (•) 0/100).

decrease. As a matter of fact, the contrary is observed. The reduction in the viscosity of the PEI matrix by the addition of 20 wt% HX1000 was much less significant than the addition of 10 wt%. The viscosity of PEI/HX1000 80/20 is much closer to the pure PEI than the PEI/HX1000 90/10 blend. Nevertheless, the nearly Newtonian behavior observed in the neat PEI persists at HX1000 concentrations of as high as 20 wt%. This behavior indicates that the viscosity response of the system at this concentration is clearly dominated by the PEI phase. A transition in the rheological response (from Newtonian to shear thinning) of the PEI/HX1000 blends begins at an HX1000 concentration of around 50 wt%.

In summary, the rheological tests, although limited to dynamic shear measurements, have indicated that the viscosity ratio of the dispersed TLCP phase (HX1000 and Vectra A) to the PEI matrix falls within the optimum range for the deformation of the TLCP phase into reinforcing fibrils. In addition, the rhelogical tests have also shown that the addition of either Vectra A or HX1000 to the PEI phase greatly reduces its viscosity. However, even though Vectra A shows a lower viscosity than HX1000, the extent of viscosity reduction is more significant for PEI/HX1000 than for PEI/Vectra A, especially at 10 wt% TLCP. This may be explained according to the following. Sun et.al. (33) have observed that the maximum shift in the glass transition of the PEI phase in the PEI/HX1000 blend occurs at 10 wt% HX1000. Thus, it is believed that the reduction of PEI/HX1000 viscosity at this particular concentration may be due to the existence of a miscible PEI/HX1000 fraction having a lower viscosity than the neat PEI phase itself. The rheological tests also revealed that the blend viscosity for TLCP-rich compositions are significantly higher than the viscosity of the neat TLCPs.

3.3.4 Morphological Analysis

The morphology developed during the injection molding of PEI/Vectra A and PEI/HX1000 blends is discussed in this section. Knowledge of the structural development during injection molding is important in order to understand the mechanical properties of the

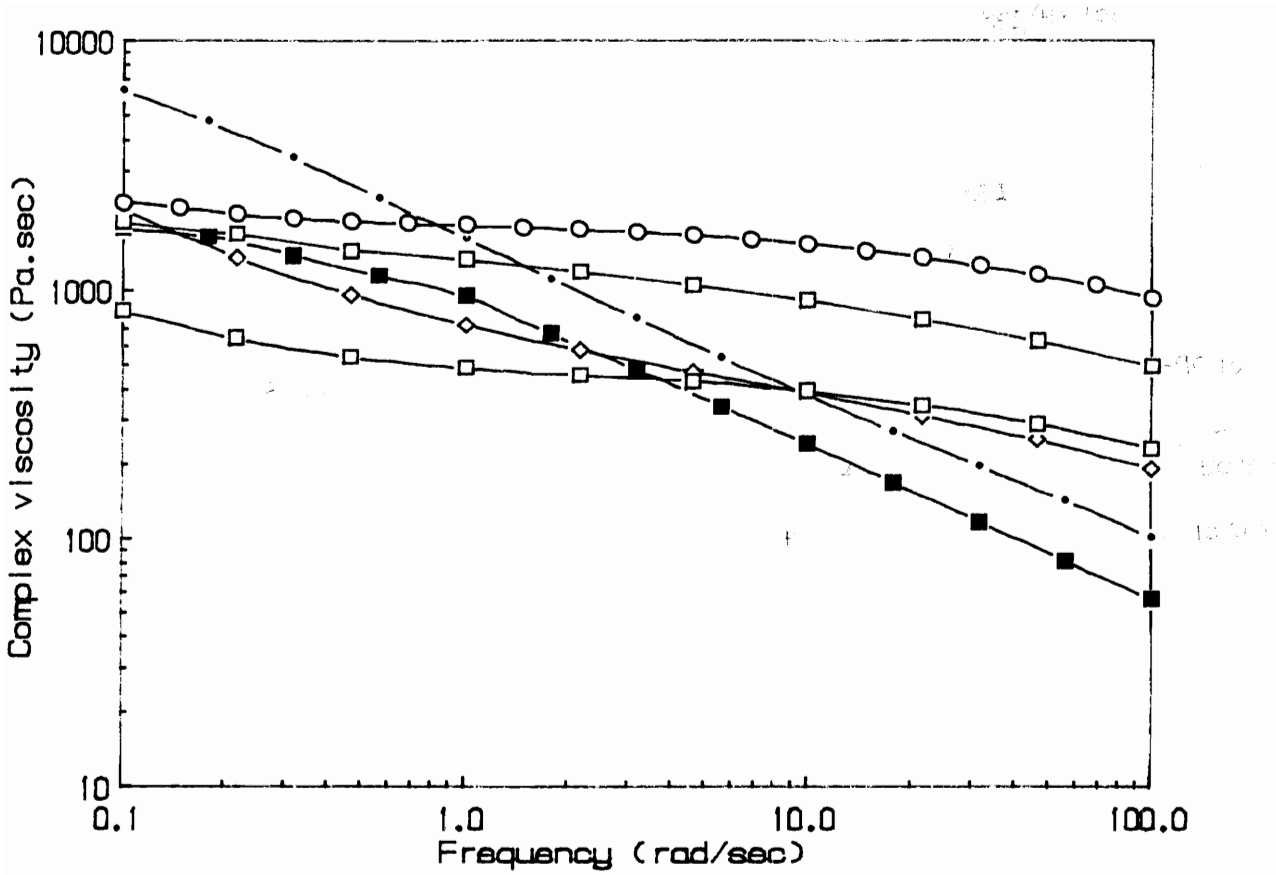

Figure 3.9. Complex viscosity vs. frequency of PEI/HX1000 blends as a function of HX1000 concentration measured at 360°C and 5% strain ((○) 100/0, (△) 90/10, (□) 80/20, (◇) 50/50, (•) 10/90, and (■) 0/100).

blends. First, the effects of the injection molding flow kinematics on the structure development of PEI/Vectra A blends are presented. Following this, studies on PEI/HX1000 blends are presented.

Scanning electron micrographs of fracture surfaces of injection molded plaques of PEI/Vectra A 80/20 wt% composition ratio are presented in Figures 3.10a and b. The samples were fractured along the flow direction. The effect of the kinematics of the injection molding process on the morphology of the in situ composite is apparent. The combination of elongational flow from the advancing front and strong shear gradients at regions closer to the mold walls leads to the formation of fibers of the Vectra A phase in the blend. Hence, in Figure 3.10a, fibers with considerably higher aspect ratios are observed in the skin region. On the other hand, approaching the center region of the molded part, the flow weakens and the TLCP phase remains as drops (Figure 3.10b). Near the center region, the shear stresses are not strong enough to overcome the interfacial tension forces, and undeformed TLCP drops are found. It should be noted that the adhesion between the PEI and Vectra A phase is poor. Large voids around the Vectra A phase are particularly observed in the core region.

As the concentration of Vectra A is increased, the morphological structure of the PEI/Vectra A in situ composite changes considerably. This is illustrated in Figure 3.11, where micrographs of fracture surfaces obtained by means of scanning electron microscopy (SEM) from injection molded tensile bars of PEI/Vectra A 60/40 wt% are shown. The sample has been fractured along the flow direction. One notices from Figure 3.11 that at a Vectra A concentration of 40 wt% a co-continuous structure is now observed. As detailed in Figure 3.11b, the structure is closely related to that of an interpenetrating network. This co-continuous morphology is of particular interest because mechanical tests have shown that a minimum in toughness for this particular composite appeared at this Vectra A concentration. This observation suggests that phase morphology also plays an important role in determining the mechanical performance of an in situ composite.

The morphology of a PEI/Vectra A 10/90 wt% composition ratio is presented in Figure 3.12. At this concentration, PEI is now the dispersed phase and Vectra A is the continuous

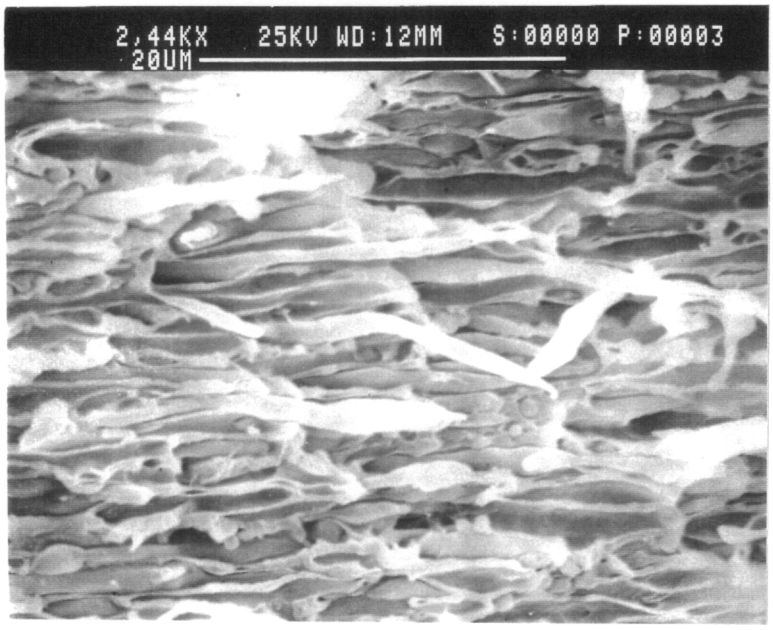

(A)

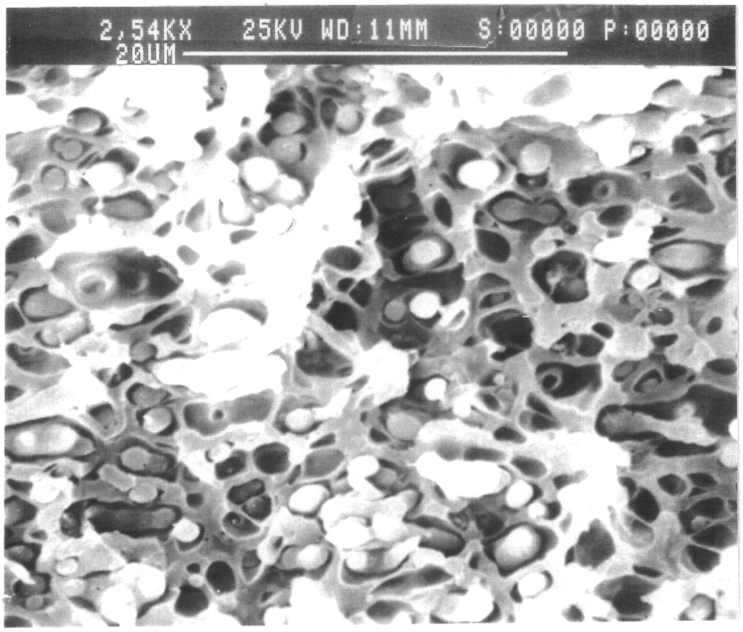

(B)

Figure 3.10. SEM photomicrographs of molded plaque of PEI/Vectra A 80/20 wt% composition ratio, a) skin and b) core regions.

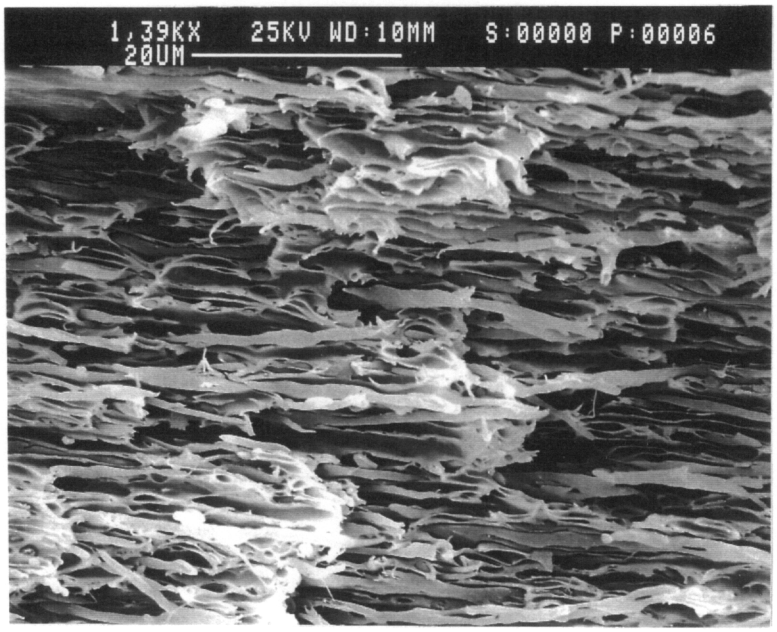

(A)

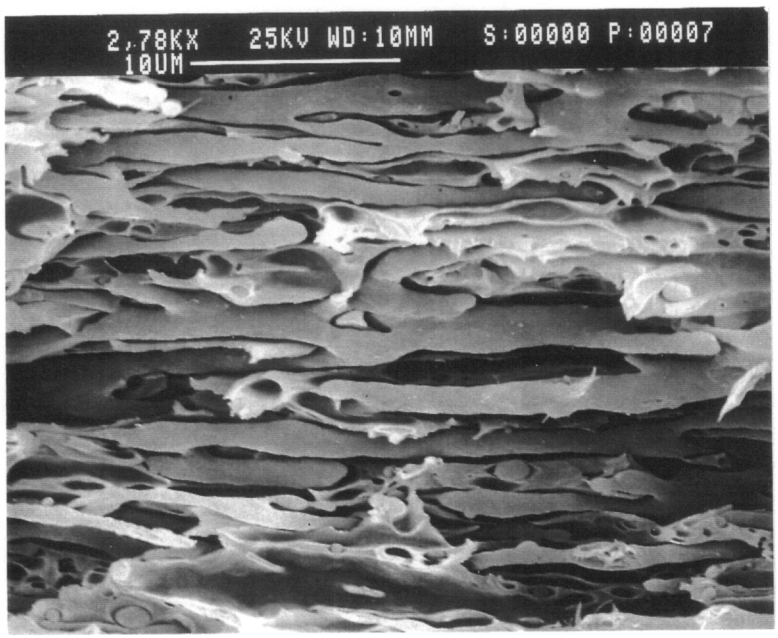

(B)

Figure 3.11. SEM photomicrographs of molded tensile bar of PEI/Vectra A 60/40 wt% composition ratio. Center region seen at a) 1390X and b) 2780X magnification.

phase. For this condition, the viscosity ratio between the PEI dispersed phase and the Vectra A continuous phase ($\frac{\eta_{PEI}}{\eta_{VA}}$) is much greater than 1. Nonetheless, even for this unfavorable viscosity ratio condition, deformation of the dispersed PEI phase into fibrils is evident in the skin region of the molded tensile bar as illustrated in Figure 3.12a. In the skin region, the flow is strong enough to overcome the extremely high viscosity ratio. However, as shown in Figure 3.12b, undeformed droplets of the PEI phase are apparent in the center region.

Scanning electron micrographs of a fractured surface of an injection molded tensile bar of PEI/HX1000 90/10 wt% composition ratio are shown in Figure 3.13. The sample was fractured along the flow direction. At this concentration, the PEI/HX1000 blend exhibits a morphological structure closely resembling a homogeneous system. In the skin region, illustrated in Figure 3.13a, very fine high aspect ratio fibers of at least 10 microns in length and less than one micron in diameter are observed. In the core region, illustrated in Figure 3.13b, submicron size drops are observed. In addition, the adhesion between the phases appears to be better than in the PEI/Vectra A system.

The effects of partial miscibility on the morphology of PEI/TLCP blends are better illustrated by a direct comparison of the morphologies exhibited by the PEI/Vectra A system and the PEI/HX1000 system. In Figure 3.14 a scanning electron micrograph of a fracture surface of PEI/HX1000 80/20 wt% composition ratio is shown. By comparing the morphologies observed in Figure 3.14 with that of Figure 3.10, the effects of partial miscibility on the morphologies of the blends are more apparent. The higher degree of compatibility of the PEI/HX1000 system which arises from the partial miscibility leads to a much finer structure than is observed for the PEI/Vectra A system. Furthermore, from Figure 3.14b one notices that HX1000 fibers can even be found in the core region of the molded tensile bar. This observation indicates that higher average aspect ratio HX1000 fibrils may exist in the PEI/HX1000 system compared to the PEI/Vectra A system.

The effect of partial miscibility on the morphology of the PEI/HX1000 system is also observed at high HX1000 concentrations. In Figure 3.15 a scanning electron micrograph of a fracture surface of PEI/HX1000 10/90 wt% composition ratio is presented. At this HX1000

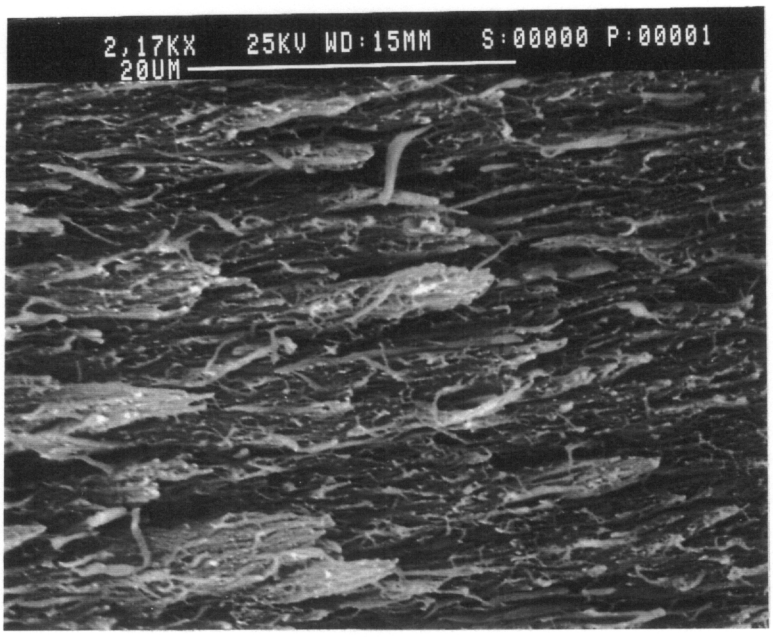

(A)

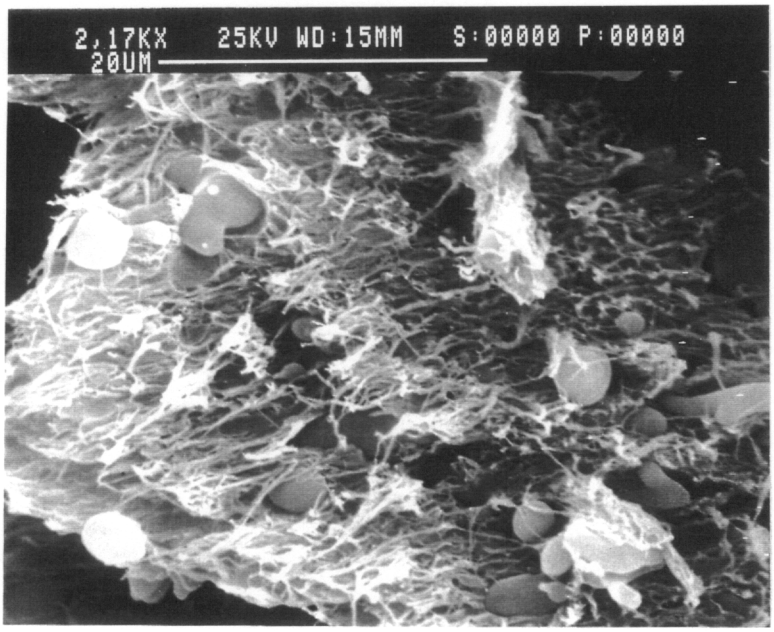

(B)

Figure 3.12. SEM photomicrographs of molded tensile bar of PEI/Vectra A 10/90 wt% composition ratio, a) skin and b) center regions.

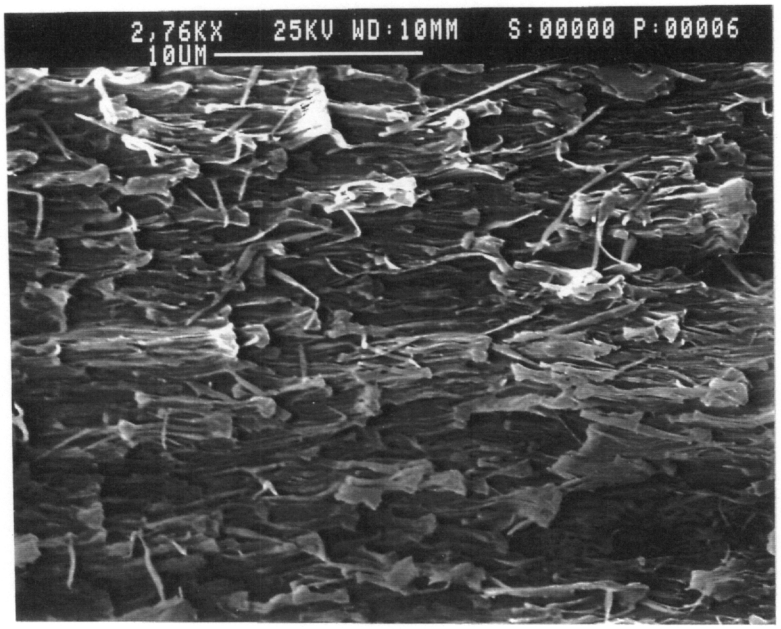

(A)

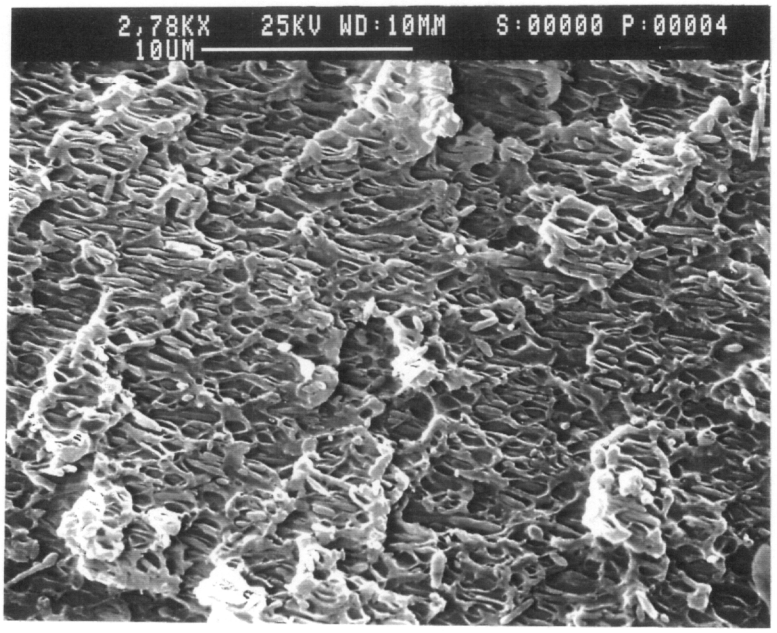

(B)

Figure 3.13. **Scanning electron micrographs of fractured surfaces of molded tensile bars of PEI/HX1000 90/10 wt% composition ratio.** The samples were fractured along the injection molding flow direction: a) skin and b) center regions.

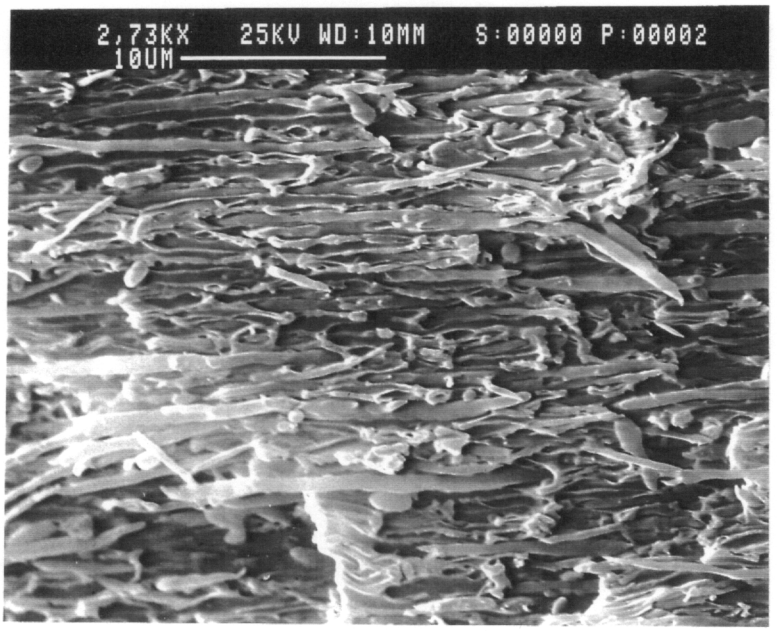

(A)

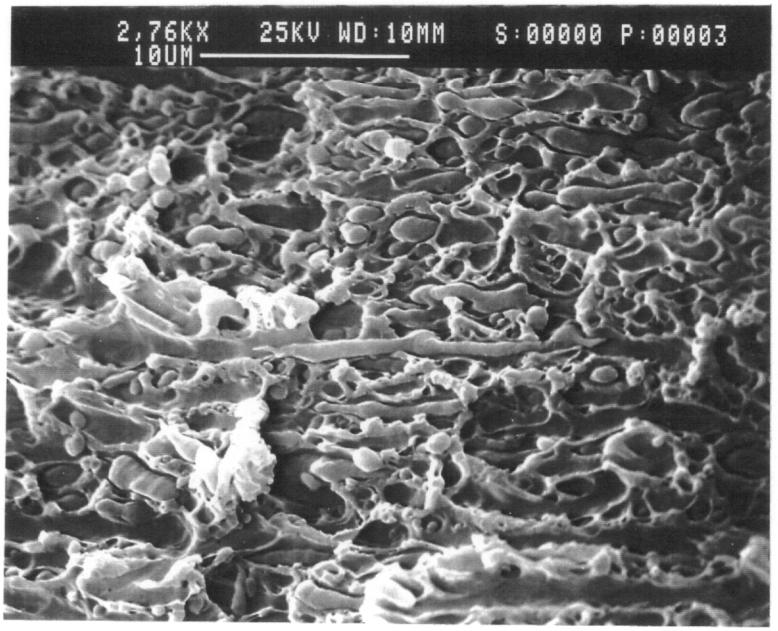

(B)

Figure 3.14. Scanning electron micrographs of fractured surfaces of molded tensile bars of PEI/HX1000 80/20 wt% composition ratio. The samples were fractured along the injection molding flow direction: a) skin and b) center regions.

concentration, the dispersed phase is that of the PEI phase, and the viscosity ratio between the dispersed PEI phase and the continuous HX1000 phase ($\frac{\eta_{PEI}}{\eta_{HX}}$) is again much greater than 1. Nevertheless, in Figure 3.15a, fibers of the PEI phase are observed in the skin region of the molded sample. This again emphasizes the effectiveness of the elongational flow in the advancing front in deforming the dispersed PEI phase into elongated fibrils, even at an unfavorable viscosity ratio. The core region, illustrated in Figure 3.15b, is again composed of undeformed PEI drops, but in this case the drops are considerably smaller.

3.3.5 Molecular Orientation

The orientation parameters, f^H, obtained for PEI/Vectra A and PEI/HX1000 blends are discussed in this section. The experiments were performed with the intent of determining whether the observed tensile modulus of the blends could be correlated to the degree of molecular orientation of the TLCP phase. Injection molded plaques were used in these studies. Values of molecular orientation were obtained from the skin, core and full sample thickness. The results from these studies are presented next.

The tensile modulus of thermotropic liquid crystalline polymers is observed to increase with the increase in the draw down ratio, as for example in fiber spinning (24,52). Chung (24) has shown that along with modulus molecular orientation (measured as the Herman's orientation function) also increases with draw ratio. Chung (24) observed that in fibers of Vectra A, the orientation of the TLCP varied exponentially with modulus. For instance, an orientation factor of 0.88 correlated with a modulus of 40 GP, and for an orientation of 0.93 a modulus of 65 GPa was observed. This suggests a direct correlation between molecular orientation and modulus. With this in mind, molecular orientation analyses were performed on selected samples of PEI/Vectra and PEI/HX1000 blends to determine whether the maximum in the tensile modulus observed at 90 wt% TLCP could be related to a higher molecular orientation of the TLCP phase in the blend compared to the neat TLCP.

(A)

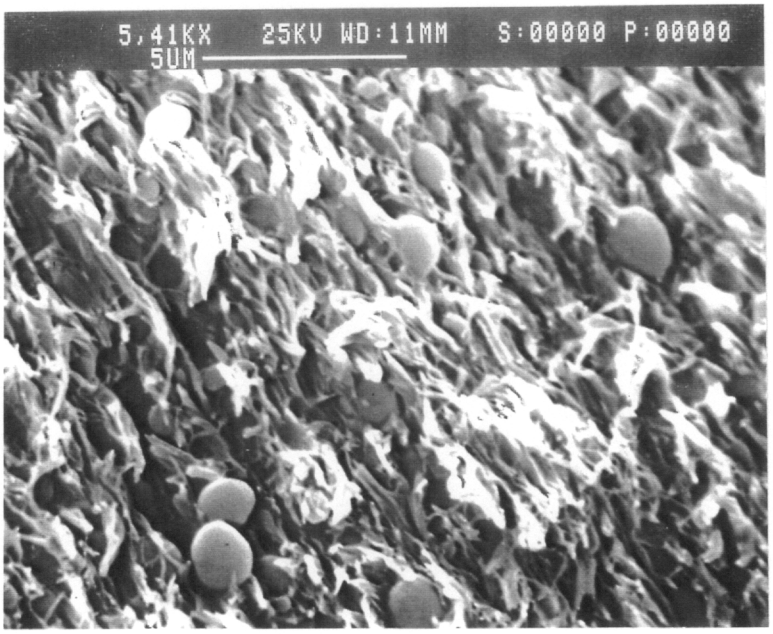

(B)

Figure 3.15. Scanning electron micrographs of fractured surfaces of molded tensile bars of PEI/HX1000 10/90 wt% composition ratio. The samples were fractured along the injection molding flow direction: a) skin and b) center regions.

The values of the orientation parameter measured for PEI/Vectra A and PEI/HX1000 blends are presented in Table 3.3. As one observes, the overall values of the orientation function (skin, core and full) of the PEI/TLCP blends at 90 wt% TLCP are significantly higher than those of the neat TLCPs. Further, one also observes that PEI/HX1000 shows a slightly higher degree of overall molecular orientation than PEI/Vectra A. However, the values of molecular orientation obtained from the skin indicate that highly oriented Vectra A fibrils have been formed in the outer layers of the molded plaque. However, this orientation drops drastically in the center regions of the sample. From the molecular orientation analysis presented above, it is clear that the maximum in the modulus found in the PEI/TLCP blends at 90 wt% TLCP concentration is a consequence of the higher molecular orientation shown by the blends at this concentration.

The differences in molecular orientation between the blends and neat TLCPs may be related to the following. Rheological tests have revealed that the values of complex viscosity of PEI/Vectra A and PEI/HX1000 at 90 wt% TLCP concentration were significantly higher than those of the pure TLCPs. In addition, the processing conditions were kept constant during the injection molding of the samples. Consequently, since the samples must have experienced similar rates of deformation during processing, the stresses generated must depend directly upon the viscosity of the system. Hence, materials exhibiting higher values of viscosity will experience higher magnitudes of stress. Therefore, it is believed that stress induced molecular orientation of the TLCP phase may have occurred at 90 wt% TLCP concentration. This suggests that the criterion for the maximum in properties observed in TLCP/polymer blends is related to the viscosity of the flexible chain polymer relative to that of the TLCP.

Table 3.3. Orientation Parameters for PEI/Vectra A900 and PEI/HX1000 blends.

COMPO-SITION	PEI/VECTRA A			PEI/HX1000		
	skin	core	full	skin	core	full
0/100	0.82	0.66	0.67	0.79	0.67	0.70
10/90	0.82	0.65	0.75	0.80	0.72	0.77
20/80	0.75	0.64	0.73	0.77	0.68	0.75

3.4 Conclusions

In the injection molding process, the deformation of the TLCP phase into reinforcing fibrils will depend upon its position in the flow. Closer to the mold walls, where elongational flow from the advancing front and strong shear gradients exist, the TLCP phase deforms to a higher extent than in the center regions of the molded part, where weaker shear flows are present. In addition, partial miscibility plays an important role in determining the final structure of the molded part. Finer higher aspect ratio TLCP fibrils were observed in the PEI/HX1000 system, where higher partial miscibility exists, relative to the PEI/Vectra A system. Tensile and flexural moduli were found to correlate well with the observed morphology. For instance, tensile and flexural moduli of PEI/HX1000 blends were greater than those of PEI/Vectra A blends throughout the range of compositions investigated.

For both blends a maximum in the tensile modulus, which has also been observed in other systems (29-34), occurred at a TLCP concentration of approximately 90 wt%. This maximum in tensile modulus at 90 wt% TLCP concentration was attributed to a higher molecular orientation of the TLCP phase in the blend than in the neat TLCP, as revealed in the WAXD measurements. It is believed that due to a higher blend viscosity at this concentration stress induced molecular orientation of the TLCP phase may have occurred. The higher molecular orientation would lead to higher modulus TLCP fibers in the blend relative to the pure TLCP.

In addition, tensile strength properties, depending on the TLCP concentration, were affected by either interfacial adhesion or ultimate tensile strength of the TLCP. At low TLCP concentrations, up to 20 wt%, interfacial adhesion was important. In such cases, PEI/HX1000 blends, which have shown greater interfacial adhesion, exhibited higher tensile strengths than PEI/Vectra A blends. For instance, at 10 wt% TLCP concentration, tensile strengths of about 110 and 140 MPa were observed for PEI/Vectra A and PEI/HX1000, respectively. However, at TLCP concentrations of 70 wt% and above, the tensile strength properties were dominated by the ultimate strength of the TLCP. The TLCPs used, Vectra A and HX1000, show tensile

strengths of about 215 and 126 MPa, respectively. Therefore, PEI/Vectra A blends have shown, at these concentrations, considerably higher values of tensile strength than PEI/HX1000.

However, PEI/HX1000 blends have also shown, at low TLCP concentrations, a higher value of transverse tensile strength than PEI/Vectra A blends. This agrees with the fact that a higher interphase adhesion was observed for the PEI/HX1000 system compared to the PEI/Vectra A system.

Although partial miscibility has a strong effect on the stiffness of an in situ composite, the ultimate properties of a TLCP strongly dominate the ultimate properties of the TLCP/polymer composite. Therefore, PEI/Vectra blends have shown higher values of toughness throughout the range of compositions studied compared to the PEI/HX1000 blends. Consequently, the selection of a TLCP to reinforce a polymer matrix will not only depend upon whether partial miscibility between the TLCP and the matrix polymer exists, but also on the overall mechanical properties of the TLCP.

3.5 Acknowledgements

The author would like to express his greatest appreciation to Kenn Gardner, at DuPont Experimental Station for his collaboration with the X-ray analysis. Support from the DuPont Company and the Army Research Office (Grant No. DAAL03-91-G-0166) is greatly appreciated.

3.6 References

1. A. Siegmann, A. Dagan, and S. Kenig, **Polymer**, 26, 1325 (1985).
2. A.I. Isayev, and M. Modic, **Polym. Comp.**, 8 (3), 158 (1987).
3. T.M. Malik, P.J. Carreau, and N. Chapleau, **Polym. Eng. Sci.**, 29, 600 (1989).
4. T. Sun, D.G. Baird, H.H. Huang, D.S. Done, and G.L. Wilkes, **J. Comp. Mat.**, 25, 788 (1991).
5. D. Beery, S. Kenig, A. Sigmann, and M. Narkis, **Polym. Eng. Sci.**, 32 (1), 73 (1992).
6. D.G. Baird, and R. Ramanathan, in *Contemporary Topics in Polymer Science*, Vol. 6: Multiphase Macromolecular Systems; B.M. Culberton, ed., Plenum Press, NY (1989).
7. J. Li, M. Silverstein, A. Hiltner, and E. Baer, **J. Appl. Polym. Sci.**, 44, 1531 (1992).
8. T.S. Chung, **J. Polym. Sci., Polym. Phys. Ed.**, 26, 1549 (1988).
9. G. Crevecoeur, and G. Groeninckx, **Polym. Eng. Sci.**, 30 (9), 532 (1990).
10. A.I. Isayev, and P.R. Subramanian, **Polym. Eng. Sci.**, 32 (2), 85 (1992).
11. J. Seppala, M. Heino, and C. Kapanen, **J. Appl. Polym. Sci.**, 44, 1051 (1992).
12. G. Kiss, **Polym. Eng. Sci.**, 27 (6), 410 (1987).
13. J.J. Elmendorp and A.K. Van der Vegt, in *Two-Phase Polymer Systems*, L.A. Utracki, ed., Hanser, Munich, Germany (1991).
14. L.A. Utracki, *Polymer Alloys and Blends, Thermodynamics and Rheology*, Hanser, Munich, Germany (1989).
15. G.I. Taylor, **Proc. Roy. Soc.**, A146, 501 (1934)
16. G.I. Taylor, **Proc. Roy. Soc.**, A138, 41 (1932)
17. G.I. Taylor, **Proc. Roy. Soc.**, A226, 289 (1954)
18. B.J. Bentley and L.G. Leal, **J. Fluid Mech.**, 167, 241 (1986)
19. H.L. Goldsmith and S.G. Mason, **J. Coll. Sci.**, 17, 448 (1962)
20. H.P. Grace, **Chem. Eng. Commun.**, 14, 225 (1982)
21. J.J. Elmendorp and R.J. Maalke, **Polym. Eng. Sci.**, 25 (16), 1041 (1985)
22. S. Meretz, M. Kwiatkowski and G. Hinrichsen, **Intern. Polym. Proc.**, 6 (3), 239 (1991)

23. G. Marrucci, in *Thermotropic Liquid Crystal Polymer Blends*, F.P. La Mantia, ed., Technomic, Lancaster, Pa (1993)
24. T.S. Chung, **J. Polym. Sci., Polym. Phys. Ed.**, 26, 1549 (1988)
25. A.M. Sukhadia, PhD dissertation, Virginia Polytechnic Institute and State University (1991)
26. D. Dutta, H. Fruitwala, A. Kohli, and R.A. Weiss, **Polym. Eng. Sci.**, 30, 1005 (1990)
27. E.G. Joseph, D.G. Baird and G.L. Wilkes, **Polym. Eng. Sci.**, 25 (7), 377 (1985)
28. A. Metha and A.I. Isayev, **Polym. Eng. Sci.**, 31 (13), 971 (1991)
29. K.G. Blizard, A.M. Sukhadia, J.P. de Souza and D.G. Baird, **Poly. Commun.**, (1990)
30. J.P. de Souza and D.G. Baird, SPE Antec Technical Papers XXXIX, 1716 (1993).
31. A.I. Isayev and S. Swaminathan, U.S. Patent No. 4,835,047 (1990)
32. A. Metha and A.I. Isayev, **Polym. Eng. Sci.**, 31 (13), 971 (1991)
33. S.S. Bafna, T. Sun, J.P. de Souza, and D.G. Baird, **Polymer**, 34 (4), 708 (1993)
34. D.G. Baird, S.S. Bafna, J.P. de Souza, and T. Sun, **Polym. Comp.**, .14 (3), 214 (1993)
35. T. Sun, D.G. Baird, H.H. Huang, D.S. Done, and G.L. Wilkes, **J. Comp. Mat.**, 25, 788 (1991)
36. M.Y. Cao and B. Wunderlich, **J. Polym. Sci., Polym. Phys. Ed.**, 23, 521 (1985)
37. P. Magagnini, in *Thermotropic Liquid Crystal Polymer Blends*, F.P. La Mantia, ed., Technomic, Lancaster, Pa (1993)
38. S. Wu,*Polymer Interface and Adhesion*, Marcel Dekker, New York (1982)
39. S. Wu, **J. Phys. Chem.**, 74, 632 (1970)
40. G.R. Mitchel and A.H. Windle, in *Developments in Crystalline Polymers*, D.C. Basset, ed., Elsevier, London (1988)
41. G. Crevecoeur, and G. Groeninckx, **Polym. Eng. Sci.**, 30 (9), 532 (1990).
42. A.I. Isayev and M. Modic, **Polym. Comp.**, 8, 158 (1987)
43. A. Kohli, N. Chung and R.A. Weiss, **Polym. Eng. Sci.**, 29, 573 (1989).
44. J.C. Halpin and J.L. Kardos, **Polym. Eng. Sci.**, 16, 344 (1976)
45. J. Kelly, Ph.D. dissertation, Virginia Polytechnic Institure and State University (1991).
46. M.J. Folkes, *Short Fiber Reinforced Thermoplatics*, John Wiley and Sons, New York (1982)
47. K.G. Blizard and D.G. Baird, **Polym. Eng. Sci.**, 27 (9), 653 (1987).

48. P. Zhuang, T. Kyu, and J.L. White, **Polym. Eng. Sci.**, 28 (17), 1095 (1989)

49. M.R. Nobile, E. Amendola, L. Nicolais, D. Acierno, and C. Carfagna, **Polym. Eng. Sci.**, 27 (9), 244 (1989)

50. A. Valenza, F.P. La Mantia, M. Paci and P.L. Magagnini, **Int. Polym. Proc.**, 6 (3), 247 (1991)

51. Q. Lin, J. Jho and A.L. Yee, **Polym. Eng. Sci.**, 33 (13), 789 (1993)

The Effects of Shearfree Deformation on the Morphology and Mechanical Properties of In Situ Composites Based on Blends of Polyetherimide and Thermotropic Liquid Crystalline Polymers.

To be submitted to **International Polymer Processing**

PREFACE

One of the aspects of considerable importance in the development of thermotropic liquid crystalline polymer (TLCP) blends is the control of the morphology during the processing which, in turn, affects the overall mechanical performance of the system. The deformation of the TLCP phase into highly oriented high aspect ratio fibers is usually necessary in order for the TLCP to act as an effective reinforcement to the polymeric matrix. However, this complex process depends primarily on the rheological and interfacial properties of the blend components, flow strength and the volume fraction of dispersed TLCP phase. Several studies addressing the necessary conditions for the deformation of the TLCP phase into reinforcing fibers have been published (1-3). Most of these studies, though, have dealt with the development of in situ composites in process where shear or uniaxial flow dominate, such as injection molding (4-7), strand extrusion (8-10) and fiber spinning (11-14).

In the series of studies presented here, the focus is on the effects of shearfree elongational flows on the morphology and mechanical properties of blends of thermotropic liquid crystalline polymers (TLCPs) with an engineering thermoplastic. The work is concentrated on three specific modes of shearfree deformations: uniaxial, planar and biaxial. The experimental results obtained from each specific mode of shear free deformation are presented and discussed separately. Thus in Chapters 4, 5 and 6, respectively, the effects of uniaxial, planar and biaxial elongational deformation on the structure and properties of TLCP/polymers are presented.

From the experimental results, it is observed that each particular mode of shear free deformation has a distinct effect on the final morphology and mechanical properties of the TLCP based in situ composite. For instance, the dispersed TLCP particles can be deformed into elongated fibrils by the application of uniaxial elongation, deformed into an elongated ribbon-like structure after planar deformation, or even the TLCP phase can be deformed into a disk-like shape by the application of equal biaxial deformation. The mechanical properties after each mode of shearfree deformation follow the variations in the morphology accordingly.

Eventually, the results from this work can be used to develop processing methods in which a specific morphology and, consequently mechanical properties, may be obtained in order to meet applications demand.

4.0 UNIAXIAL ELONGATION

4.1 Introduction

Blends of thermotropic liquid crystalline polymers (TLCPs) with thermorplastics have attracted considerable interest over the last few years due to their potential in generating in situ composites (4-14). As a result of the active research in this field, the scientific literature available on this subject is quite vast. In this paper, we review only studies pertinent to the scope of this work, i.e. the effects of elongational flows on the structure and properties of TLCP/polymer blends. The reader is referred to the reviews of Dutta et al. (15), Weiss et al. (2), Baird and Ramanathan (3) and La Mantia (16) for a more complete and detailed look at this subject.

In reinforcing a thermoplastic by the addition of a TLCP phase, the TLCP is dispersed in a thermoplastics matrix in a conventional mixing step and in a subsequent processing step involving strong shear or preferably extensional flow, the TLCP domains are elongated into fibrils that reinforce the matrix in a fashion analogous to glass fibers (17). Thus the reinforcing fibrils are formed in situ during the processing. However, in addition to the flow history, this

complex process depends strongly on the rheological and interfacial properties of the blend components, and the volume fraction of the dispersed TLCP phase (18).

The morphology formation during the processing of polymer blends is often explained in terms of the theories of droplet deformation and breakup for Newtonian fluids (19-22). According to Taylor (19), a dispersed phase subject to either shear or elongational flow will deform into an elongated thread-like form, provided that the disruptive stresses of viscous drag overcome the effects of the interfacial forces that resist this deformation. The viscous forces supporting this deformation will depend on the deformation rate and the rheological properties of the two components, while the interfacial forces that resist this deformation will depend on the surface tension between the two phases (19). In the case of a system undergoing homogeneous uniaxial elongational flow at a constant elongation rate, the deformation may be described as (22):

$$\frac{L}{L_o} - 1 = 1.5 \frac{\eta_m \dot{\varepsilon} a}{\sigma} \frac{(19\lambda + 16)}{(16\lambda + 16)} \tag{4.1}$$

where L_o and L are, respectively, the length of the undeformed and deformed droplet. $\dot{\varepsilon}$ is the elongation rate, λ is the viscosity ratio of the dispersed droplet phase to the matrix, η_m is the matrix viscosity, σ is the interfacial tension and a is the initial droplet radius.

Studies relating the effects of flow history to the development of a fibirillar morphology in TLCP based in situ composites have indicated the following. In general, shear flows are capable of deforming the TLCP domains into elongated fibrils, provided the magnitude of applied shear stress exceeds a critical value. Otherwise, dispersed droplets of the TLCP phase are usually found (23). Elongational flow causes the formation of a fibirillar morphology over a broad range of viscosity ratios (1,11-14). In complex flows, as in the case of injection molding, the deformation of the TLCP into elongated fibrils will depend upon the position of the TLCP phase in the flow. Closer to the mold walls, where elongational flow from the advancing front and strong shear gradients exist, the TLCP phase deforms more than in the center regions of the molded part, where weaker shear flows are present (4-7,24,25).

The mechanical properties of TLCP/polymer blends directly correlate to the degree of orientation of the TLCP phase (26,27). Consequently, flow strength, which affects the deformation and orientation of the TLCP phase, will also affect the mechanical properties of the TLCP polymer blends. Mechanical properties of TLCP/polymer blends processed by means of fiber spinning, where elongational flow prevails, are superior to those obtained from, for example, injection molding. Fibers with moduli as high as 65 GPa have been obtained through the spinning of a thermotropic copolyester (26), whereas injection molded samples of the same copolyester have reached moduli of only 12 GPa (6). This illustrates that the reinforcing potential of TLCPs is greatly affected by the processing history.

Post-processing of injection molded plaques of TLCPs has led to the improvement of their initial mechanical properties. This was shown by Blizard and co-workers (28) who studied the compression molding of TLCP plaques. Molded plaques of two different TLCPs, based on polyethylene terephthalate (PET)/p-hydroxybenzoic acid (HBA), LCP60, and HBA/hydroxynaphthoic acid (HNA), Vectra A, were pressed at both isothermal and non-isothermal conditions. Isothermal compression temperatures of 190°C and 205°C and 210°C and 240°C were used for LCP60 and Vectra A, respectively. Non-isothermal conditions were achieved by rapid cooling during compression molding. Biaxial elongational deformations were generated during the compression molding experiments by lubricating the plates to minimize the effects of shear at the plate walls. Mechanical property measurements have indicated an improvement in both tensile and flexural moduli of the LCP60 relative to the molded part. The tensile modulus could be increased by as much as 35% (from 3.2 GPa to 4.3 GPa) and the flexural modulus could be increased by as much as 27% (from 10.5 GPa to 13.5 GPa) after nonisothermal compression molding. Based upon scanning electron microscopy observations, the increase in modulus was attributed to an increase in the amount of TLCP in the form of fibers, especially in the core region, upon compression molding.

The effects of draw down ratio (DR) on the mechanical properties of TLCP based in situ composite have been investigated by several authors (10-13,29). Recently, Sun and co-workers (10) have studied the effects of post-extrusion drawing on the morphology and cor-

responding mechanical properties of PEI/Vectra A blends. The authors have used a single screw extruder to which was attached a 102 mm width sheet die to generate sheets of PEI, Vectra A and their blends at a temperature of 345°C. After extrusion the sheet was fed onto takeup rolls. The first roll was placed 15 cm from the die and the second roll at 20 cm from the first. By controlling their relative speeds, draw ratios ranging from 2 to 60 could be introduced to the extruded sheet. Wide angle X-ray diffraction (WAXD) was utilized, although qualitatively, to verify the effects of draw ratio on the molecular orientation of the TLCP phase. The tensile modulus of the extruded sheets increased as the draw ratio increased, following the increase in the fibrillar structure of the TLCP domains with draw ratio (DR). As an example, the PEI/Vectra 70/30 composition ratio revealed a tensile modulus of 2.7 GPa at a DR = 3.1. Increasing DR to 16, the tensile modulus increased to 7.5 GPa. In contrast to the improvement in modulus, no improvement in the tensile strength was observed. The authors claimed that this was due to poor adhesion between the PEI matrix and the reinforcing Vectra fibrils. Vectra fibrils which were pulled out from the matrix were observed after cryogenic fracture.

Further support for the importance of drawing to the enhancement of the mechanical properties of TLCP based in situ composites was given by Baird and co-workers (30,31). Films based on blends of engineering thermoplastics, including polyetheretherketone (PEEK) and polyphenylyne sulfide (PPS), and a variety of TLCPs, were generated. In general, concentration of TLCP was in the range of 20 to 30 wt%, and draw ratios as high as 50 led to films with moduli in the range of 14 GPa.

The flow induced orientation of TLCPs represents a key property that influences the processability of these materials. Although this very important property may be used to generate controlled morphologies, it also leads to some drawbacks. One of the most significant is mechanical anisotropy (32). That is, the properties parallel to the principal direction of orientation are significantly greater than the properties transverse to the orientation direction. Several techniques have been used to reduce the mechanical anisotropy of in situ composites. For example, the addition of glass fibers (32-34), cross lamination in a manner similar to composite prepregs (35), coinjection molding (24,36) and processing modifications such as

push-pull injection molding (37) have been studied. However, glass fibers tend to orient along the flow direction, contributing to a further increment of the flow direction properties of the TLCP/polymer blend and, therefore, doing little in terms of reducing anisotropy. In the case of the use of TLCP/polymer blends as prepregs, isotropic mechanical properties have usually been observed, but the mechanical properties of the cross plies were lower than the average obtained from the initial flow and transverse properties. This is usually attributed to fiber buckling during compression. On the other hand, coinjection molding seems attractive, not only due to the potential of reducing anisotropy, but because it may also contribute to lower overall part cost by the use of a less expensive material to make up the core region of the molded part. Push-pull injection molding has given attractive results, but thick parts are usually required.

In summary, flow induced orientation of thermotropic liquid crystalline polymers has a tremendous effect on the mechanical properties of these materials. In processes in which elongational flow fields are present, such as melt spinning and post-extrusion drawing, the TLCP polydomains attain a highly oriented fibrillar structure, giving rise to high mechanical properties, whereas in processes such as injection molding a skin/core structure arises, and overall molecular orientation is reduced, affecting overall mechanical properties. However, the flow induced orientation of TLCPs creates mechanical anisotropy in molded articles and consequently limits potential applications of these materials. Techniques often studied to reduce mechanical anisotropy, such as addition of glass fibers, have not yet proven totally successful.

The objective of this study is to determine the effects of elongational flows on the mechanical properties and morphology of TLCP/polymer blends. As part of the overall objective, we are interested in developing methods in which controlled morphologies can be developed in TLCP/polymer blends. Ultimately, the findings from the fundamental studies presented here will be used to develop processing methods in which morphology and mechanical properties of TLCP/polymer blends may conveniently be tailored to fulfill the needs of a particular application. In addition, we investigate the effectiveness of elongational flows

in reducing the mechanical anisotropy of TLCP based in situ composites. In an attempt to present the results as clearly as possible, this work has been divided into three parts. In each part, attention is focused on a specific mode of shearfree deformation: uniaxial, planar and biaxial. A description of the kinematics and expected changes in the deformation and molecular organization generated by these types of shearfree flows may be found elsewhere (38,39). In this paper we are concerned with the effects of uniaxial elongational flow on the morphology and properties of TLCP polymer blends.

4.2 Experimental Procedure

4.2.1 Materials

The matrix material is a polyetherimide (PEI), commercially available as Ultem 1000 from General Electric Plastics. PEI is an amorphous engineering thermoplastic with a glass transition temperature at about 228°C and a processing temperature ranging from 330 to 365°C (10). The semicrystalline TLCP is a thermortropic copolyester composed of 73 mol% of p-hydroxybenzoic acid and 27 mol% of 2-hydroxy-6-naphthoic acid. This TLCP is commercially available as Vectra A900 from Hoechst-Celanese. Vectra A900 (henceforth referred to as Vectra A) exhibits a glass transition temperature at 105°C, a crystal-mesophase transition at 283°C (40), and a maximum stable processing temperature of 370°C (10). The amorphous TLCP, supplied by DuPont, is based on hydroquinone (HQ), terephthalic acid (TA) and other hydroquinone derivatives. This amorphous TLCP, referred to as HX1000, has a glass transition temperature of 185°C (5) and a processing temperature ranging from 290 to 365°C. Proposed chemical structures for these TLCPs may be found elsewhere (41).

4.2.2 Blend Preparation and Processing

Before blending, pellets of the above materials were dried at 115°C in a convection oven for at least 48 hours. The dried pellets of PEI/Vectra A and PEI/HX1000 at composition ratios of 90/10, 80/20 and 70/30 wt% were then tumbled in a steel container. The physically mixed blends of PEI/Vectra A and PEI/HX1000 were then injection molded into rectangular plaques and extruded into sheets.

Rectangular plaques (measuring approximately 75mmx85mmx1.75mm) of PEI/Vectra A and PEI/HX1000 plaques were injection molded utilizing a Arburg Allrounder injection molding unit. The injection molding conditions were as follows. The temperature settings of the injection molding unit were 330, 345, 360 and 360°C for zones 1, 2, and 3 of the barrel and nozzle, respectively. The injection pressure was set at 7.0 MPa with a holding pressure of 3.5 MPa. The injection speed was set at a medium range, which gives a volumetric flow rate of 12 cm^3/sec. The mold was held at 110°C, and a cooling time of 40 sec was used. The processing conditions were kept constant throughout all moldings.

Sheets of PEI/Vectra A and PEI/HX1000 blends were extruded utilizing a 2.54 cm (1 inch) diameter single screw extruder. A 10.16 cm (4 inches) wide film die was used. The sheets were extruded without any post-extrusion drawing. The objective was to obtain a sheet in which only undeformed droplets of the TLCP phase would be found. The extruder temperature settings were 290, 310, 315, 315, 230 and 245°C for zones 1, 2, 3, clamp ring, adaptor and die, respectively. The extruder speed was set at 12.4 RPM. The melt temperature and pressure, measured at the screw head, were 334°C and 1410 psi, respectively.

The use of injection molded plaques and extruded sheets of PEI/TLCP blends in the shearfree flow experiments was based upon the following. It is well known that injection molded parts develop a layered structure (skin/core) morphology during processing. The skin of the sample is comprised of long, high aspect ratio fibrils of the TLCP phase, whereas in the core region, undeformed droplets of the TLCP phase is usually found. In the extrusion process,

on the other hand, external drawing is usually necessary in order to deform the TLCP phase into elongated fibrils. Hence, by controlling the post-extrusion drawing, undeformed droplets of the TLCP phase can be obtained in the extruded sheets. Therefore, with the use of injection molded samples and extruded sheets, the effects of shearfree deformations on samples showing two distinct initial morphologies (skin/core and drops) can be determined.

4.2.3 Dynamic Mechanical Experiments

Dynamic mechanical tests were carried out to determined the transition temperatures of the materials used. Dynamic analysis in the torsional mode was carried out using a Rheometrics Mechanical Spectrometer (Model RMS 800). Rectangular samples measuring approximately 42 mm x 12 mm were cut from injection molded plaques. The storage modulus (G′) and loss tangent (tan δ) for PEI, Vectra A and HX1000 were monitored and recorded as a function of temperature. The frequency of oscillation was 10 rad/sec, and the strain was varied from 0.05 to 1.0%. The experimental temperature was raised at a rate of 5°C/min from 40°C to a temperature at which the modulus of a given sample dropped significantly.

4.2.4 Morphological Characterization and Mechanical Properties

The morphologies of the injection molded plaques and extruded sheets were investigated by means of scanning electron microscopy (SEM). A Cambridge Stereoscan-S200 Instrument with an accelerating voltage of 25 KV was used. The samples were cryogenically fractured along and across the injection molding flow direction after immersion in liquid nitrogen for at least 5 minutes. The samples were then mounted on aluminum stubs and sputter coated with gold for enhanced conductivity. The fracture surfaces were scanned from the surface to the center regions to determine the shape and size of the TLCP dispersed phase.

The mechanical properties were evaluated on rectangular strips (measuring approximately 12mm x 80mm) cut out from the deformed molded plaques and sheets by means of an Instron Universal Testing Instrument, model 4204. A cross-head speed of 1 mm/min was used. An extensometer was utilized to record the strain. Tensile strength and tensile (Young's) modulus were calculated from the stress-strain curves. The tensile modulus was determined from the best linear fit through the initial region of the stress-strain curve. Toughness was calculated as the area under the stress-strain curve through numerical integration. The mechanical properties reported are based on measurements made on at least five samples.

4.2.5 Generation of Uniaxial Elongational Deformation

The kinematics of homogeneous uniaxial elongational flow are given by the velocity field (38):

$$V_x = -\frac{1}{2}\dot{\varepsilon}x \tag{4.1}$$

$$V_y = -\frac{1}{2}\dot{\varepsilon}y \tag{4.2}$$

$$V_z = +\dot{\varepsilon}z \tag{4.3}$$

where $\dot{\varepsilon}$ is the strain rate, given by $\dot{\varepsilon}=(1/z)(\partial z/\partial t)$. V_z is the velocity along the principal axis of deformation (in this case z). V_x and V_y are the velocities perpendicular to the deformation direction. The Hencky strain is defined as $\varepsilon = \ln(\lambda_z)$, in which λ_z is the principal elongation ratio defined as $\lambda_z = z/z_0$, with z_0 and z being, respectively, the initial and instantaneous length of the sample. For incompressible fluids $\lambda_x\lambda_y\lambda_z = 1$, and for uniaxial elongation $\lambda_x=\lambda_y=\sqrt{\lambda_z^{-1}}$.

Stretching experiments were performed by the use of an Instron Universal Testing Machine, model 4204, coupled with a forced convection oven, manufactured by Russells

Technical Products model HD-3-300. The sample's ends were clamped to the fixed and movable cross-head grips and placed inside the working area of the oven. Because of this way of fixing the sample ends, necking would appear towards the center of the sample, therefore, making the deformation highly inhomogeneous. The temperature reached the set point after about 25 minutes of heating. Equilibrium in the temperature across the working area of the oven was reached with an additional 6 minutes of heating. The temperature inside the oven was monitored with the aid of two external thermocouples placed within 30 cm from each other. Strain and initial strain rate were controlled by selecting the total displacement and speed of the Instron's crosshead. Injection molded plaques were stretched both parallel and transverse to the initial injection molding flow direction. Extruded sheets were stretched parallel to the extrusion direction. PEI/TLCP blends with TLCP concentrations as high as 30 wt% were successfully stretched. Above 30 wt% TLCP, the samples did not show enough melt strength to withstand the deformation and rupture occurred. Therefore, the studies were limited to samples with TLCP concentrations of up to 30 wt%. In our experimental procedure, a constant stretching velocity was used to deform the sample and, consequently, the strain rate was not constant during the deformation.

The deformation under the test condition is highly inhomogeneous. The clamped ends constrained the contraction of the sample at the grips and necking is observed towards the center region of the sample and, because of this, the elongation strain (ε) and principal elongation ratio (λ_z) along the stretch direction would vary from the center to the edges of the sample. This inhomogeneity in the deformational strains will have a tremendous implication in the overall deformation of the dispersed TLCP phase.

4.3 Results and Discussions

The methodology and experimental procedure necessary to fulfill the objectives of this paper were given in the previous section. In this section the experimental results along with the analysis and interpretations will be given. Before discussing the experimental results, however, the aspects of the mechanical anisotropy found in TLCP based in situ composites are discussed in Section 4.3.1. We have selected flow and transverse tensile moduli obtained from molded plaques of PEI/Vectra A900 and PEI/HX1000 blends to illustrate the mechanical anisotropy found in TLCP composites. Following this, in Section 4.3.2, the results from dynamic torsion tests are presented. From the dynamic tests, the stretching temperatures were selected. After these preliminary discussions, experimental results obtained from the uniaxial stretching of PEI/TLCP blends are presented. In Section 4.3.3 is discussed the experimental results related to the effects of uniaxial elongation on the morphology and mechanical properties of injection molded plaques, whereas in Section 4.3.4 the results from extruded sheets are discussed.

4.3.1 Mechanical Anisotropy

One of the objectives of this study is to determine whether shearfree deformation can be used as an effective means to reduce the mechanical anisotropy found in TLCP/polymer blends. Thus, in order to illustrate this problem we have selected, as an example of anisotropy, to show tensile moduli obtained from molded plaques of PEI/Vectra A blends, measured along (MD) and transverse (TD) to the direction of the fibers. Some comments regarding mechanical anisotropy are given next.

The flow induced orientation of TLCPs, coupled with their long relaxation times, are important properties that distinguish these materials from conventional thermoplastics. Al-

though these very important characteristics make it possible to develop in situ composites, it also introduces mechanical anisotropy to TLCP based in situ composites. This is illustrated in Figure 4.1 by the MD and TD tensile moduli obtained from injection molded plaques of PEI/Vectra A blends. It is apparent that, as the concentration of Vectra A increases, a significant increase in the MD tensile modulus follows. However, the TD tensile modulus remains constant at around 3 GPa regardless of TLCP concentration. The observed anisotropy in the tensile moduli is the result of a strong orientation of the TLCP phase along the injection molding flow direction (25).

4.3.2 Dynamic Mechanical Analysis

The main objective of this work is to determine whether uniaxial elongational flow may be used as an effective method to control the morphology and mechanical properties of in situ composites. However, in order to perform such studies, a temperature must be selected at which both the matrix and dispersed TLCP phases would be deformable. Therefore, by performing dynamic mechanical thermal analysis (DMTA) the transition temperatures of the blend components (PEI, Vectra A and HX1000) can be determined.

In Figure 4.2 the DMTA results, performed in the dynamic torsional mode, are presented. The shear storage modulus (G′) and loss tangent (tan δ) for PEI, Vectra A and HX1000 are plotted as a function of temperature. In the DMTA test, the peak in tan δ is usually associated with the glass transition temperature (Tg) of a material (42). Thus, from Figure 4.2-a it can be seen that the peaks in tan δ, which correspond to the glass transition temperature of PEI, Vectra A and HX1000 are around 228, 105 and 185°C, respectively. The corresponding variation in the shear storage modulus (G′) as function of temperature for PEI, Vectra A and HX1000 is illustrated in Figure 4.2-b. It is apparent that at Tg, PEI shows a very sharp transition from the glassy to the rubbery state. A decrease of over two decades in G′ is observed over

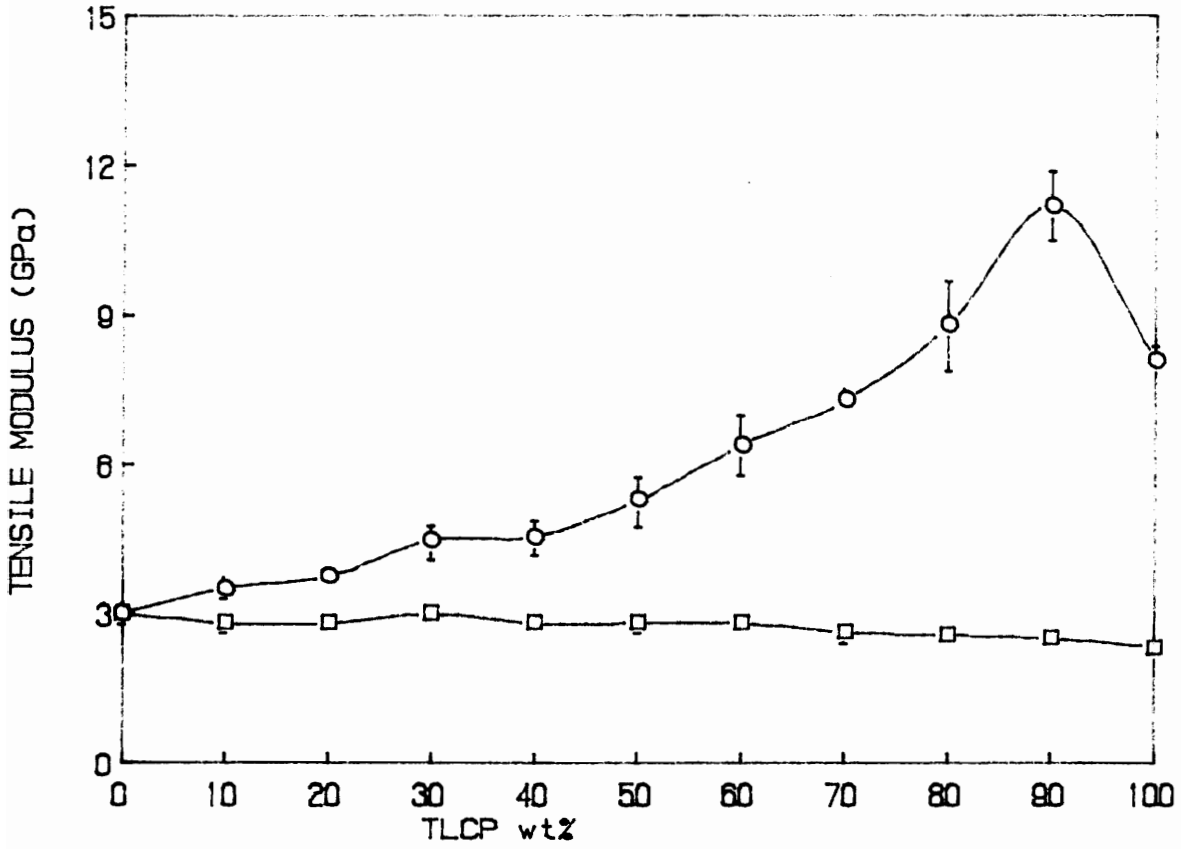

Figure 4.1. Tensile Modulus of PEI/Vectra A blends as a function of Vectra A concentration, (○) along and (□) transverse to the direction of the fibers.

only 20°C around its glass transition temperature. On the other hand, in the case of the TLCPs the decrease in G′ occurs at a much broader range of temperatures.

In an attempt to determine the effects of the temperature on the structure development and corresponding mechanical properties of the PEI/TLCP blends upon stretching, two temperatures have been selected at which to perform the stretching experiments. Based upon the DMTA results, a temperature of 240°C, which is above the glass transition temperature of the PEI matrix, and a temperature of 265°C, which is closer to the melting temperature of the TLCPs, were selected. However, it is apparent that at the selected temperatures both TLCPs, Vectra A and HX1000, have a higher value of shear modulus than the PEI matrix. Due to the higher modulus, it is apparent that at the stretching temperatures both TLCPs show higher rigidity than the PEI matrix.

4.3.3 Molded Plaques Subjected to Uniaxial Elongation

We next turn our attention to the effects of uniaxial stretching on the structure and corresponding mechanical properties of PEI/TLCP blends. However, as two sets of samples, each one corresponding to a different initial morphology, were used in the experiments the following discussions are divided into two sections. First, we start, in Section 4.3.3, by presenting the results of uniaxial stretching performed on injection molded plaques, in which the initial morphology is that of fibers. Following this, in Section 4.3.4, experimental results obtained from extruded sheets, in which the initial morphology is that of drops, are discussed. In addition, the effects of stretching temperature are also included in the discussions.

The experimental results obtained from the uniaxial elongation of injection molded plaques of PEI/Vectra A and PEI/HX1000 blends at concentration ratios of 90/10, 80/20 and 70/30 wt% are presented in this section. However, due to the similarities in the results and also to avoid repetition, the discussions presented here will concentrate primarily on PEI/TLCP blends with a TLCP concentration of 20 wt%. Results for the other blend compos-

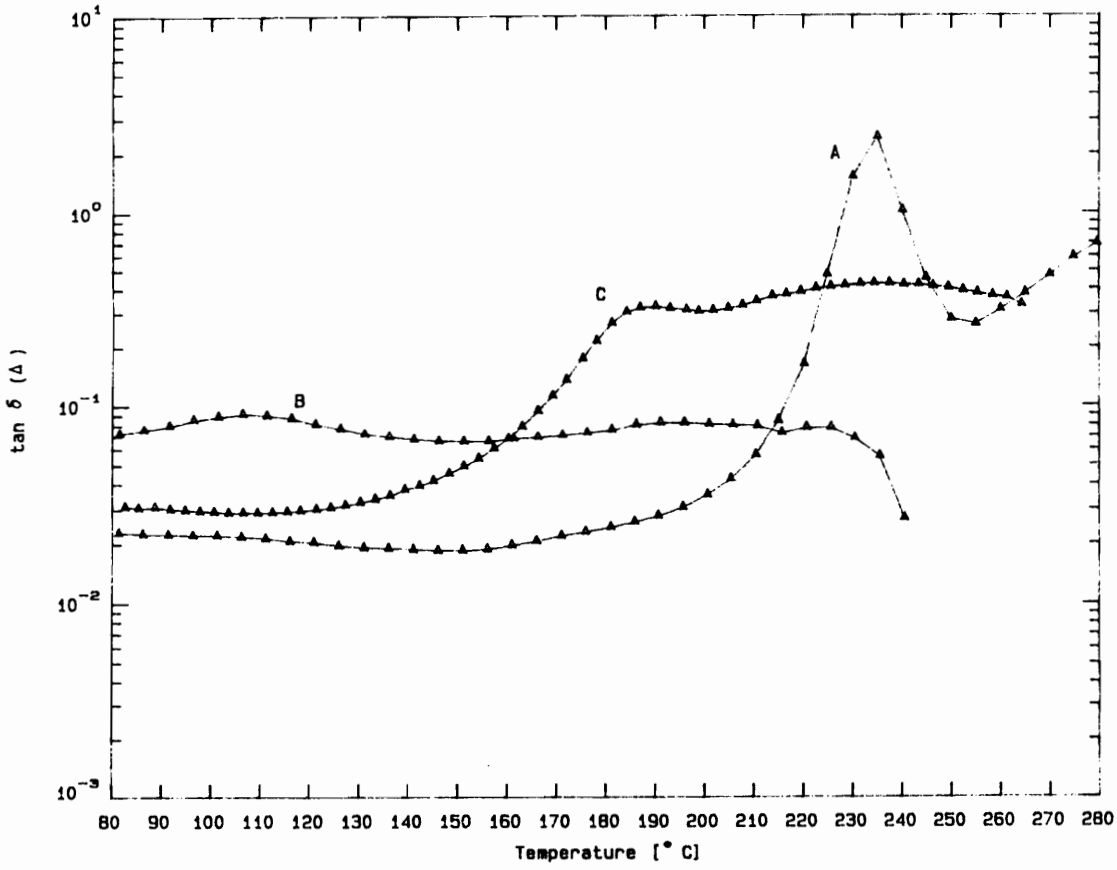

(A)

Figure 4.2. **(A) Loss tangent (tan δ) and (B) Shear Storage Modulus (G') as a function of Temperature for (a) PEI, (b) Vectra A and (c) HX1000** measured at a frequency of 10 rad. sec^{-1} and 0.05-1% strain.

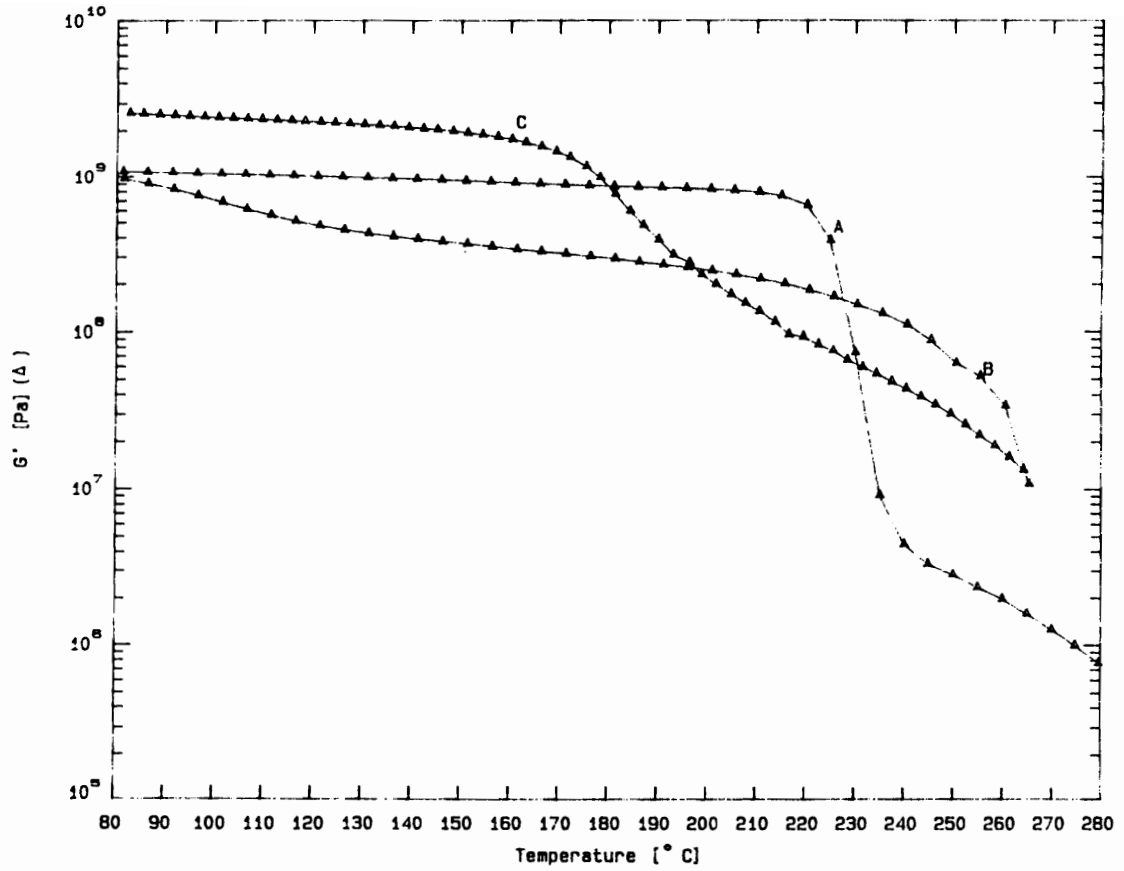

(B)

Figure 4.2. continues

itions are included elsewhere (43). Because of the orientation of the TLCP fibers in the injection molded samples is parallel to the flow direction, uniaxial stretching experiments were performed both along and perpendicular to the initial flow direction. Therefore, the effect of uniaxial stretching applied in a direction parallel and transverse to the initial fiber direction is assessed. In order to present the results of these experiments as clearly as possible, the variations in morphology and mechanical properties of injection molded plaques subjected to uniaxial elongation along the initial flow direction are presented first. Results from transverse stretching follow.

The effects of uniaxial stretching applied along the initial flow direction of the plaques on the morphology of PEI/Vectra A 80/20 wt% samples are discussed next. However, in order to compare the morphologies before and after deformation, the structure developed during the injection molding of a PEI/Vectra A blend at 80/20 wt% composition ratio is presented first in Figure 4.3. It is apparent that, due to the kinematics of the injection molding process, a layered structure develops in the sample upon molding. A high degree of deformation of the TLCP phase into fibrils is found at regions closer to the mold walls (skin) as indicated in Figure 4.3-a. Closer to the mold walls the elongational stresses from the advancing front overcome the interfacial stresses, and the TLCP phase is deformed into elongated fibrils. Towards the center region (Fig. 4.3-b), however, where shear flow dominates, the interfacial stresses resist the deformation and droplets of the TLCP phase are found. Therefore, due to the flow kinematics, the structure developed during the injection molding of TLCP polymer blends is very complex. Depending on the position of the TLCP particle in the flow, both elongated fibers and undeformed drops of the TLCP phase are found.

The effect of uniaxial stretching on the morphology of the molded plaque of PEI/Vectra A 80/20 is presented in Figure 4.4. The applied uniaxial strain is 0.5 units (corresponding to a λ_z of 1.65) at an initial elongation rate of 0.014 sec^{-1}. The fracture surface is taken along the stretching direction, that is parallel to the initial orientation of the fibers. A comparison of the micrographs presented in Figure 4.3 with these shows that further stretching of the molded sample in the flow direction increases the deformation of the TLCP phase into reinforcing

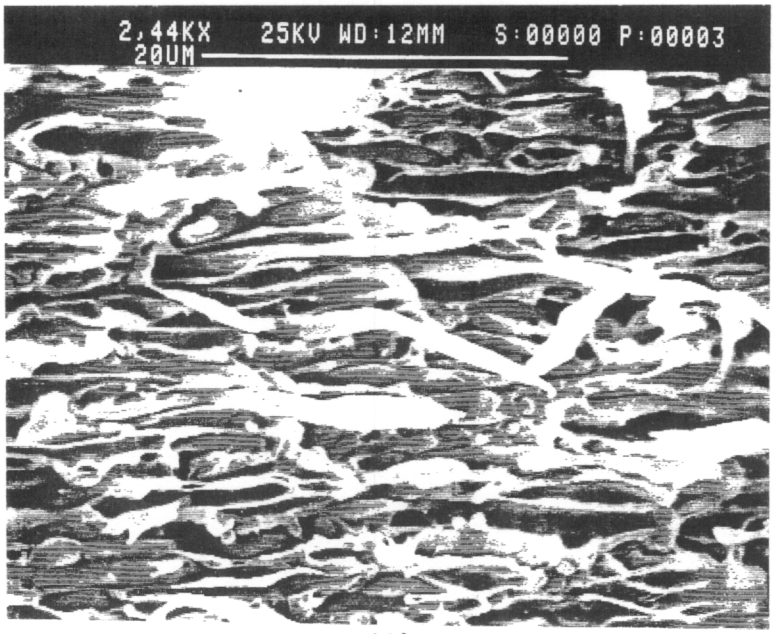

(A)

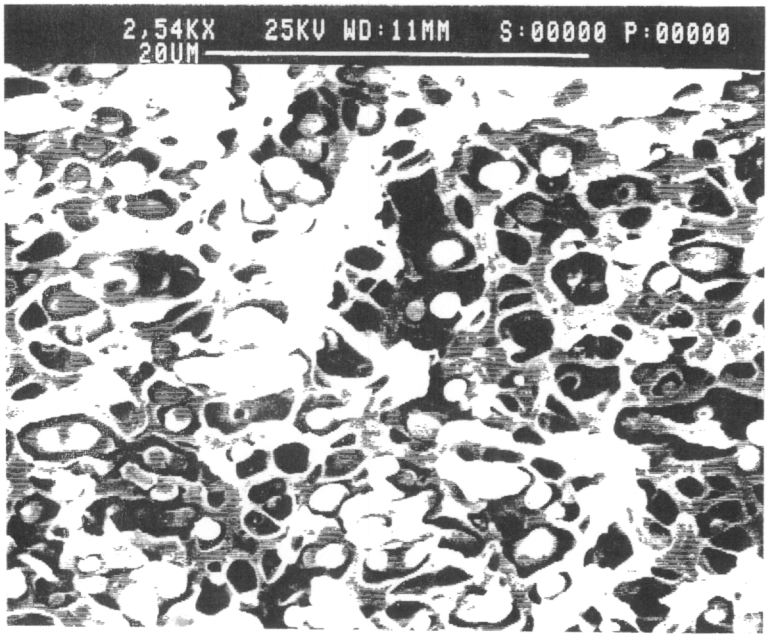

(B)

Figure 4.3. Scanning electron micrographs from injection molded plaque of PEI/Vectra A900 80/20 wt%, fractured parallel to the flow direction, a) skin and b) core regions.

fibrils. This is shown by the presence of elongated TLCP fibers in the core region (Fig. 4.4-b) which initially were in the form of drops (Fig. 4.3-b). Moreover, the TLCP fibers initially present in the skin (Fig. 4.3-a) appear much finer and more elongated after stretching (Fig. 4.4-a). Therefore, it is believed that an increase in the average aspect ratio of the reinforcing TLCP fibers may have occurred after stretching. Further, it is observed that even though the TLCP phase shows a greater rigidity than the PEI matrix (greater G′) at the stretching temperature, the flow is strong enough to further elongate and increase the average aspect ratio of the TLCP fibrils. The effect of this morphology on the mechanical properties of the blends is seen next.

The effects of uniaxial stretching applied parallel to the initial fiber direction on the mechanical properties of molded plaques of PEI/Vectra A and PEI/HX1000 blends at 80/20 wt% are considered next. From the morphological discussions above, we have seen that after uniaxial deformation, an increase in the average aspect ratio of the TLCP fibers may have occurred. The corresponding variations in the mechanical properties of the PEI/Vectra A and PEI/HX1000 blend, both flow and transverse direction, as a function of applied uniaxial strain are presented in Tables 4.1. and 4.2, respectively. It is apparent that after stretching the mechanical properties, including modulus, strength and elongation, of both blends have increased considerably along the direction of the applied deformation. This corresponds well with the observed increase in the average aspect ratio of the reinforcing TLCP fibrils upon stretching. However, in the case of the initial transverse direction (which is perpendicular to the stretching direction) the mechanical properties have only significantly decreased at a values of uniaxial strain (ε_u) approaching 0.75 units ($\lambda_z = 2.11$), that is, the sample being stretched to over twice its initial length. This observation is important because it shows that while the flow direction properties of the blends increased upon uniaxial stretching, the transverse properties did not decrease until the magnitude of the applied uniaxial strain (ε_u) approached 0.75 units. The benefit of this is that processing methods could be designed in which the mechanical properties of the TLCP polymer blends could be increased along the

(A)

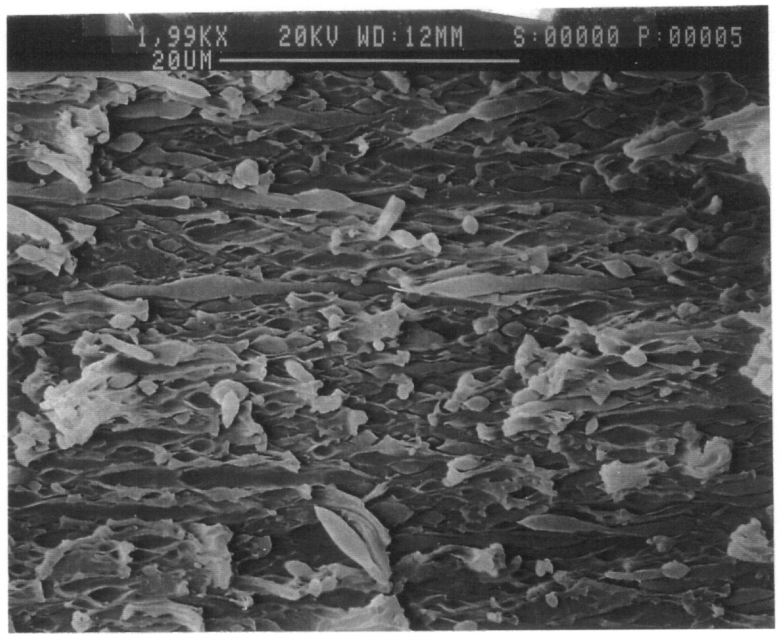

(B)

Figure 4.4. Scanning electron micrographs of injection molded plaque of PEI/Vectra A900 80/20 wt% after uniaxial deformation applied along the initial flow direction. The fracture surface is parallel to the stretching direction, a) skin and b) core regions. ($T = 240°C$, $\varepsilon_U = 0.5$ units and $\dot{\varepsilon}_I = 0.014\ sec^{-1}$)

stretching direction without affecting (at least at small strains) the initial transverse direction properties of the blend.

Another important observation from the data presented in Tables 4.1 and 4.2 is that the extent of increase of mechanical properties after stretching is higher for the PEI/HX1000 blends than for the PEI/Vectra A blends. In the case of PEI/Vectra A, no further gain in the tensile modulus is observed after 0.5 units of strain. In the case of PEI/HX1000, however, a monotonic increase in the modulus is found up to 0.75 units. This is better illustrated in Figure 4.5, where the tensile modulus is plotted as a function of uniaxial strain for both PEI/HX1000 and PEI/Vectra A 80/20 blends. Under the above stretching conditions, it is possible that the molecular orientation of the Vectra A phase may have reached its maximum value, and no further increase in the molecular orientation (supported by the no increase in modulus) was achieved by the increase in the uniaxial strain. On the hand, PEI/HX1000 blend continues to show an increase in the flow direction properties with the increase in the uniaxial strain. No asymptotic value is observed at the strains applied. In Figure 4.7 are also included the transverse direction properties as a function of uniaxial strain applied along the injection molding flow direction. As seen, although the tensile modulus in the transverse direction only drops at high values of strain, the mechanical anisotropy of the blend (indicated by the flow and transverse moduli) increases upon stretching.

The discussions thus far reflect the effects of uniaxial stretching on the structure and corresponding mechanical properties of PEI/TLCP blends at a temperature of 240°C. As observed, an increase in the deformation of the TLCP phase into reinforcing fibrils occurred upon stretching. Moreover, it was observed that the mechanical properties of the blends along the direction of the deformation increased, although to a different extent, upon stretching. This corresponded well with the observed increase in the average aspect ratio of the TLCP fibrils upon stretching. However, in order to compare the effects of stretching temperature on the structure and corresponding mechanical properties of PEI/Vectra A and PEI/HX1000 blends, results from stretching experiments performed at 265°C are discussed next.

Table 4.1. Effects of uniaxial stretching[1,2] applied parallel to the flow direction on the mechanical properties of molded plaques of PEI/Vectra A 80/20 wt%.

FLOW DIRECTION PROPERTIES			TRANSVERSE DIRECTION PROPERTIES			UNIAXIAL STRAIN
Modulus (GPa)	Strength (MPa)	Elongation (%)	Modulus (GPa)	Strength (MPa)	Elongation (%)	
3.80 (0.10)	81.90 (3.80)	3.10 (0.40)	2.80 (0.10)	45.00 (9.10)	2.20 (0.10)	0.0
4.21 (0.21)	113.57 (11.65)	2.86 (0.18)	2.68 (0.24)	53.17 (6.76)	2.95 (0.06)	0.25
4.53 (0.18)	120.05 (11.41)	3.10 (0.24)	2.45 (0.16)	47.18 (6.20)	2.02 (0.10)	0.50
4.48 (0.18)	134.67 (11.15)	4.42 (0.58)	2.30 (0.20)	30.98 (2.55)	1.54 (0.14)	0.75

1. **Stretching Temperature: 240°C.**
2. **Initial Strain Rate: 0.014 sec^{-1}**

(★) Standard deviations are given in parenthesis.

Table 4.2. Effects of uniaxial stretching[1,2] applied parallel to the flow direction on the mechanical properties of molded plaques of PEI/HX1000 80/20 wt%.

FLOW DIRECTION PROPERTIES			TRANSVERSE DIRECTION PROPERTIES			UNIAXIAL STRAIN
Modulus (GPa)	Strength (MPa)	Elongation (%)	Modulus (GPa)	Strength (MPa)	Elongation (%)	
5.13 (0.47)	105.36 (4.15)	2.38 (0.15)	2.84 (0.14)	57.10 (3.92)	2.57 (0.23)	0.0
7.89 (0.21)	142.64 (8.01)	1.86 (0.26)	3.06 (0.52)	64.84 (6.17)	2.88 (0.24)	0.25
8.91 (0.73)	180.70 (16.65)	3.50 (0.42)	2.64 (0.12)	54.30 (7.86)	2.34 (0.37)	0.50
10.40 (0.34)	198.79 (18.30)	3.64 (0.38)	2.47 (0.23)	30.21 (6.97)	1.12 (0.16)	0.75

1. **Stretching Temperature: 240°C.**
2. **Initial Strain Rate: 0.014 sec^{-1}**

(★) Standard deviations are given in parenthesis.

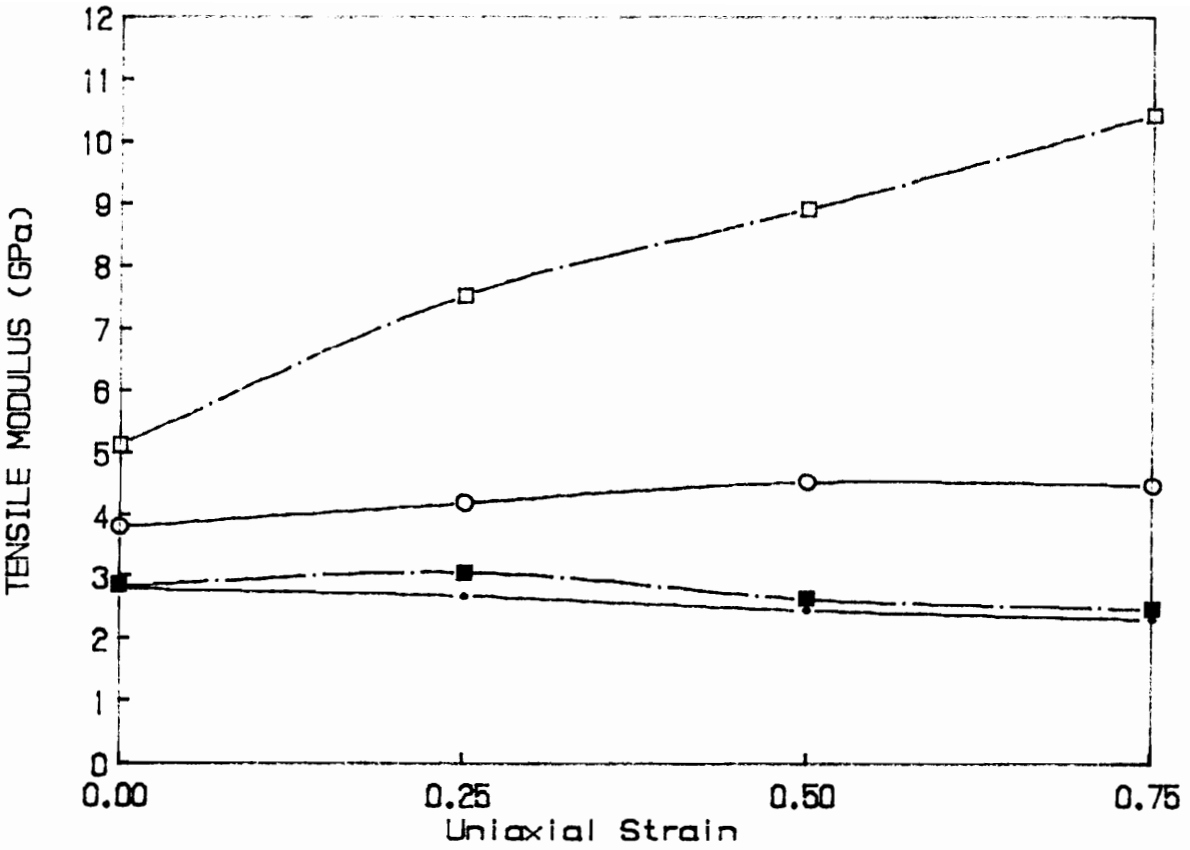

Figure 4.5. Tensile modulus as a function of uniaxial strain, applied along the fiber direction, for (○,•) PEI/Vectra A and (□,▪) PEI/HX1000 80/20 wt% blends. (open symbols = flow direction, filled symbols = transverse direction).

The effect of the temperature at which the sample was stretched on the morphology of PEI/Vectra A 80/20 wt% is shown in Figure 4.6. The applied uniaxial strain is 0.5 units at an initial strain rate of 0.014 sec^{-1}. In Figure 4.6-a is shown a fracture surface of PEI/Vectra A 80/20 stretched at 240°C, and in Figure 4.6-b the stretching temperature is 265°C. The surfaces were fractured along the stretching direction, i.e. parallel to the initial direction of the fibers. Comparing the micrographs of Figure 4.6-a and b, it appears that the extent of deformation of the TLCP phase is greater at 265°C than at 240°C. One reason for this may be that at 265°C, due to a more liquid-like characteristic of the TLCP at this temperature (lower magnitude of G′), the Vetra A phase is more easily deformable than at 240°C. A closer look at the deformed TLCP phase, which is shown in Figure 4.7, reveals the following. It appears that at 265°C (shown in Figure 4.7-b), due to again a more fluid-like nature of the TLCP, the TLCP phase tended to flatten and elongate to a greater extent compared to the deformation at 240°C (shown in Figure 4.7-a).

The mechanical properties of PEI/Vectra A and PEI/HX1000 80/20 wt% blends stretched along the initial direction of the fibers and at a temperature of 265°C are presented, respectively, in Tables 4.3 and 4.4. As in the case of uniaxial stretching at 240°C, the mechanical properties of the blends along the direction of deformation increased upon stretching. However, even though the deformation of the TLCP phase into fibrils appeared to be favored at 265°C, the magnitude of the increase in the mechanical properties along the stretching direction was less than that observed at 240°C. It is possible that due to the more liquid-like nature of the TLCPs at 265°C, relaxation of the molecular orientation may have occurred and, therefore, affected the mechanical properties. In the case of the transverse mechanical properties, one observes that the properties have not decreased at all upon stretching at 265°C. It is possible that, due to the observed flattening of the fibers upon stretching at 265°C, the in increase the surface area of the reinforcing TLCP phase in the plane of deformation is contributing to the observed behavior in the transverse mechanical properties upon deformation.

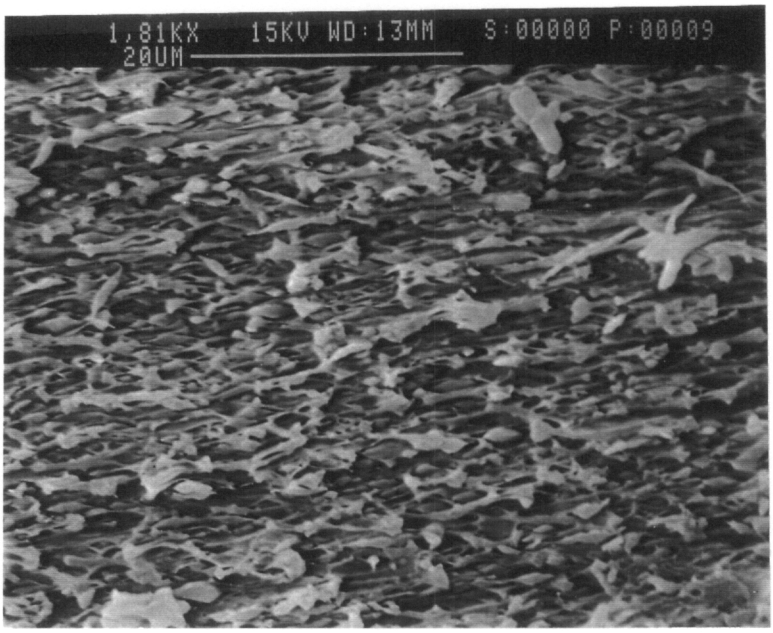

(A)

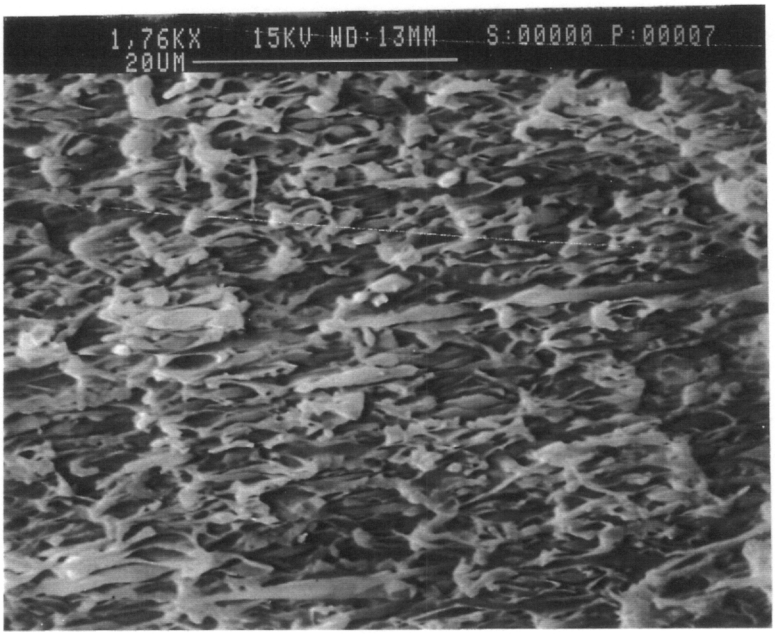

(B)

Figure 4.6. Scanning electron micrographs of injection molded plaque of PEI/Vectra A900 80/20 wt% after uniaxial deformation applied along the initial flow direction. The fracture surface is parallel to the stretching direction, a) T = 240°C and b) T = 265°C ($\varepsilon_u = 0.5$ units and $\dot{\varepsilon}_i = 0.014\ sec^{-1}$)

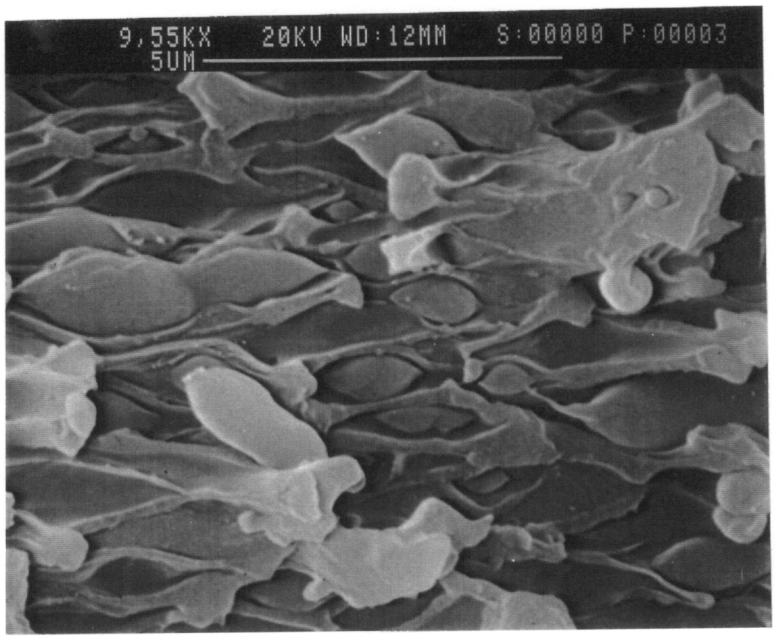

(A)

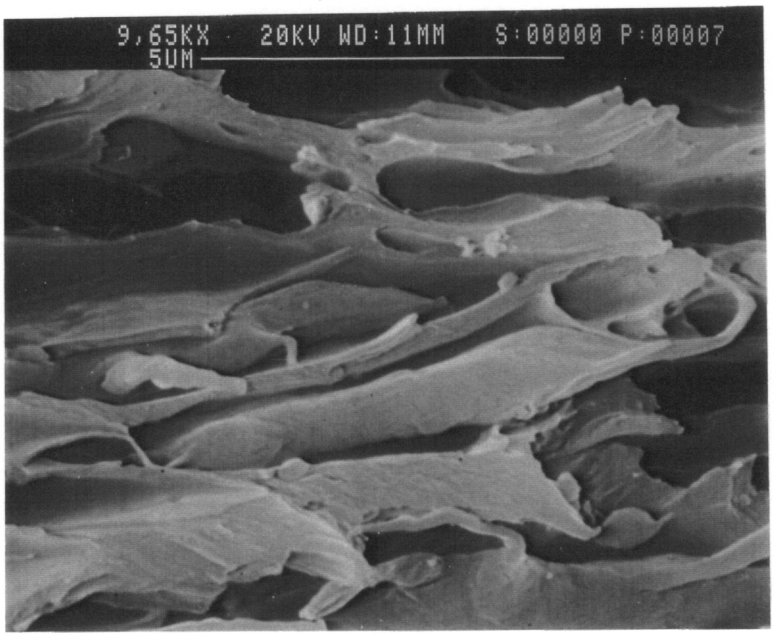

(B)

Figure 4.7. **Scanning electron micrographs of injection molded plaque of PEI/Vectra A900 80/20 wt% after uniaxial deformation applied along the initial flow direction.** The fracture surface is parallel to the stretching direction. Closer look at the deformed TLCP phase, a) T = 240°C and b) T = 265°C ($\varepsilon_U = 0.5$ units and $\dot{\varepsilon}_i = 0.014\ sec^{-1}$)

Table 4.3. Effects of uniaxial stretching[1,2] applied parallel to the fiber direction on the mechanical properties of molded plaques of PEI/Vectra A 80/20 wt%.

FLOW DIRECTION PROPERTIES			TRANSVERSE DIRECTION PROPERTIES			UNIAXIAL STRAIN
Modulus (GPa)	Strength (MPa)	Elongation (%)	Modulus (GPa)	Strength (MPa)	Elongation (%)	
3.80 (0.10)	81.90 (3.80)	3.10 (0.40)	2.80 (0.10)	45.00 (9.10)	2.20 (0.10)	0.0
4.27 (0.38)	104.47 (3.94)	2.66 (0.37)	2.99 (0.40)	57.51 (4.63)	3.39 (0.15)	0.25
4.36 (0.10)	121.40 (10.47)	4.05 (0.56)	2.83 (0.10)	59.74 (7.31)	2.92 (0.57)	0.50
4.85 (0.48)	126.78 (8.86)	3.86 (0.32)	2.64 (0.10)	57.10 (0.62)	3.56 (0.25)	0.75

1. **Stretching Temperature: 265°C.**
2. **Initial Strain Rate: 0.014 sec^{-1}**

(★) Standard deviations are given in parenthesis.

Table 4.4. Effects of uniaxial stretching[1,2] applied parallel to the fiber direction on the mechanical properties of molded plaques of PEI/HX1000 80/20 wt%.

FLOW DIRECTION PROPERTIES			TRANSVERSE DIRECTION PROPERTIES			UNIAXIAL STRAIN
Modulus (GPa)	Strength (MPa)	Elongation (%)	Modulus (GPa)	Strength (MPa)	Elongation (%)	
5.13 (0.47)	105.36 (4.15)	2.38 (0.15)	2.84 (0.14)	57.10 (3.92)	2.57 (0.23)	0.0
6.61 (0.54)	118.40 (7.50)	2.11 (0.18)	2.74 (0.21)	52.00 (8.66)	2.10 (0.22)	0.25
7.03 (0.33)	135.45 (1.41)	2.50 (0.17)	2.73 (0.14)	59.30 (2.06)	2.40 (0.24)	0.50
7.20 (0.43)	146.46 (2.83)	2.49 (0.27)	2.66 (0.13)	57.97 (3.46)	1.06 (0.10)	0.75

1. **Stretching Temperature: 265°C.**
2. **Initial Strain Rate: 0.014 sec^{-1}**

(★) Standard deviations are given in parenthesis.

In summary, it was observed that uniaxial elongation applied in a direction parallel to the initial flow direction of the molded plaques is effective in improving the deformation of the TLCP phase into reinforcing fibrils and, thus, enhancing the mechanical properties of the blends in the direction of the deformation. However, the magnitude of the increase in the mechanical properties upon deformation was found to be a function of both the type of TLCP used and the stretching temperature. Stretching the samples at a temperature which was closer to the melting temperature of the TLCP (at 265°C), the competing effects of deformation and relaxation of molecular orientation tended to reduce the effectiveness of the deformation in improving the mechanical properties in the stretching direction. In addition, it was observed that the mechanical properties transverse to the stretching direction were only slightly affected by the applied uniaxial strain. Only at considerable values of uniaxial strains (approaching 0.75 units), were the transverse mechanical properties decreased from their initial values. However, in terms of the mechanical anisotropy, it was found that uniaxial elongation applied in a direction parallel to the initial flow direction of the plaque tended to increase the overall mechanical anisotropy of the system.

Next, the effects of uniaxial elongation applied in a direction perpendicular to the initial injection molding flow direction, that is, transverse to the initial TLCP fiber direction are discussed. We present first the effects of transverse uniaxial deformation on the morphology of PEI/TLCP blends, followed by the effects of transverse stretching on the mechanical properties.

The effect of transverse uniaxial elongation on the morphology of a molded plaque of PEI/Vectra A 80/20 composition ratio is presented in Figure 4.8. The stretching temperature was 240°C, and the transverse uniaxial strain applied was 0.50 units at an initial elongation rate of 0.014 sec^{-1}. The sample was fractured along the direction of the deformation, that is perpendicular to the initial injection molding flow direction. It should be emphasized that the direction of applied deformation was perpendicular to the initial direction of the fibers. It is apparent that after transverse stretching elongated fibrils along the stretching direction have appeared. This observation can only mean that after deformation the TLCP fibrils, especially

the fibers located in the skin region of the plaque, which were initially oriented perpendicular to the stretching direction, have followed the stretch and performed a 90° rotation. One also observes that in the core region, which initially contained undeformed drops, small fibers of the TLCP phase have started to appear. Therefore, it appears that after transverse stretching, a complete inversion of the initial sample's morphology has occurred. As will be seen next, the change in the fiber's alignment after transverse stretching will tremendously affect the mechanical properties of the blend.

The effects of transverse stretching on the mechanical properties of molded plaques of PEI/Vectra A and PEI/HX1000 80/20 blends are presented in Table 4.5 and 4.6, respectively. It is apparent that as the magnitude of transverse uniaxial strain increases, a monotonic decrease of the initial flow direction mechanical properties (perpendicular to the deformation direction) is observed. On the other hand, the initial transverse direction properties seem to increase considerably upon deformation. One even notices that a complete inversion in the mechanical properties has taken place after a transverse strain of about 0.75 units is applied. The reason for this inversion in the mechanical properties is clearly the result of the morphological changes that have occurred after the deformation, that is the rotation of the fibers following the transverse deformation. However, it is expected that, with the inversion of the mechanical properties upon transverse stretching, there must be a point at which both the flow and transverse mechanical properties are similar, that is a point of equal flow and transverse mechanical properties. This is illustrated in Figure 4.9 with the tensile modulus of PEI/Vectra A and PEI/HX1000 blends being plotted as a function of transverse strain. As one notices, equal flow and transverse properties appear at about 0.5 units of transverse uniaxial strain. This is a very important observation because it illustrates that transverse uniaxial deformation may be used as an effective method to impart equal flow and transverse properties to molded plaques of TLCP polymer blends.

The effects of stretching temperature on the mechanical properties of molded plaques of PEI/Vectra A 80/20 and PEI/HX1000 80/20 blends are discussed next. In Tables 4.7 and 4.8 are shown, respectively, the variations in the mechanical properties of the PEI/Vectra A and

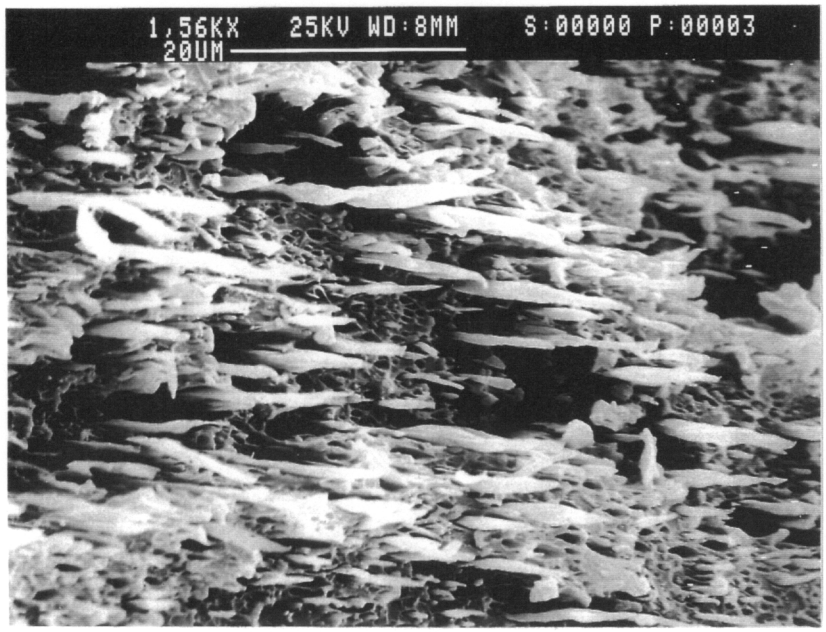

(A)

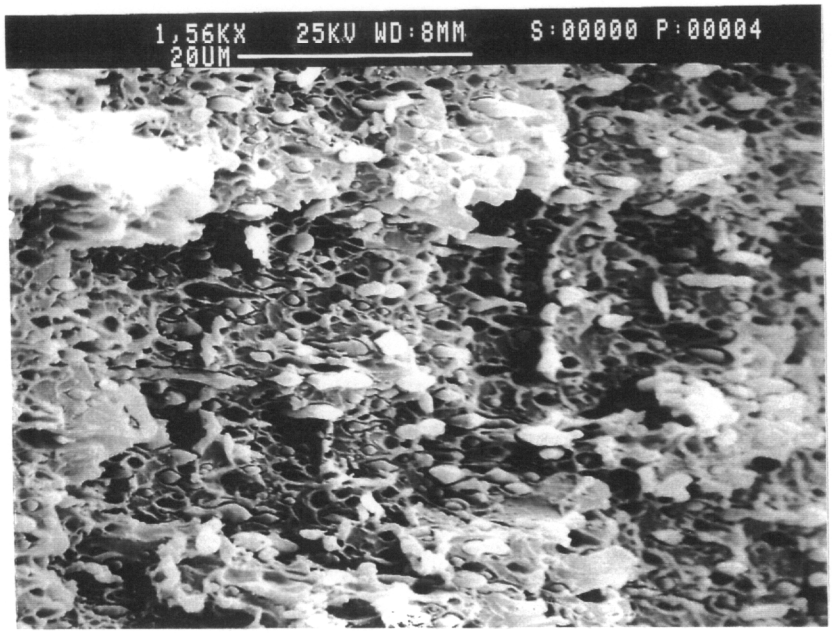

(B)

Figure 4.8. **Scanning electron micrographs of injection molded plaque of PEI/Vectra A900 80/20 wt% after transverse uniaxial deformation.** The fracture surface is parallel to the stretching direction, a) skin and b) core regions. ($T = 240°C$, $\varepsilon_u = 0.5$ units and $\dot{\varepsilon}_i = 0.014\ sec^{-1}$)

Table 4.5. Effects of uniaxial stretching[1,2] applied parallel to the flow direction on the mechanical properties of molded plaques of PEI/HX1000 80/20 wt%.

FLOW DIRECTION PROPERTIES			TRANSVERSE DIRECTION PROPERTIES			UNIAXIAL STRAIN
Modulus (GPa)	Strength (MPa)	Elongation (%)	Modulus (GPa)	Strength (MPa)	Elongation (%)	
5.13 (0.47)	105.36 (4.15)	2.38 (0.15)	2.84 (0.14)	57.10 (3.92)	2.57 (0.23)	0.0
6.61 (0.54)	118.40 (7.50)	2.11 (0.18)	2.74 (0.21)	52.00 (8.66)	2.10 (0.22)	0.25
7.03 (0.33)	135.45 (1.41)	2.50 (0.17)	2.73 (0.14)	59.30 (2.06)	2.40 (0.24)	0.50
7.20 (0.43)	146.46 (2.83)	2.49 (0.27)	2.66 (0.13)	57.97 (3.46)	1.06 (0.10)	0.75

1. **Stretching Temperature: 265°C.**
2. **Initial Strain Rate: 0.014 sec^{-1}**

(★) Standard deviations are given in parenthesis.

Table 4.6. Effects of uniaxial stretching[1,2] applied transverse to the initial flow direction on the mechanical properties of molded plaques of PEI/Vectra A900 80/20 wt%.

FLOW DIRECTION PROPERTIES			TRANSVERSE DIRECTION PROPERTIES			UNIAXIAL STRAIN
Modulus (GPa)	Strength (MPa)	Elongation (%)	Modulus (GPa)	Strength (MPa)	Elongation (%)	
3.80 (0.10)	81.90 (3.80)	3.10 (0.40)	2.80 (0.10)	45.00 (9.10)	2.20 (0.10)	0.0
3.45 (0.06)	67.57 (5.89)	2.42 (0.21)	2.95 (0.12)	72.25 (7.10)	3.30 (0.26)	0.25
3.08 (0.09)	55.78 (2.23)	1.91 (0.29)	3.40 (0.21)	80.50 (6.77)	2.87 (0.23)	0.50
2.56 (0.24)	49.52 (2.53)	2.22 (0.21)	3.70 (0.26)	91.40 (8.90)	3.27 (0.35)	0.75

1. **Stretching Temperature: 240°C.**
2. **Initial Strain Rate: 0.014 sec^{-1}**

(★) Standard deviations are given in parenthesis.

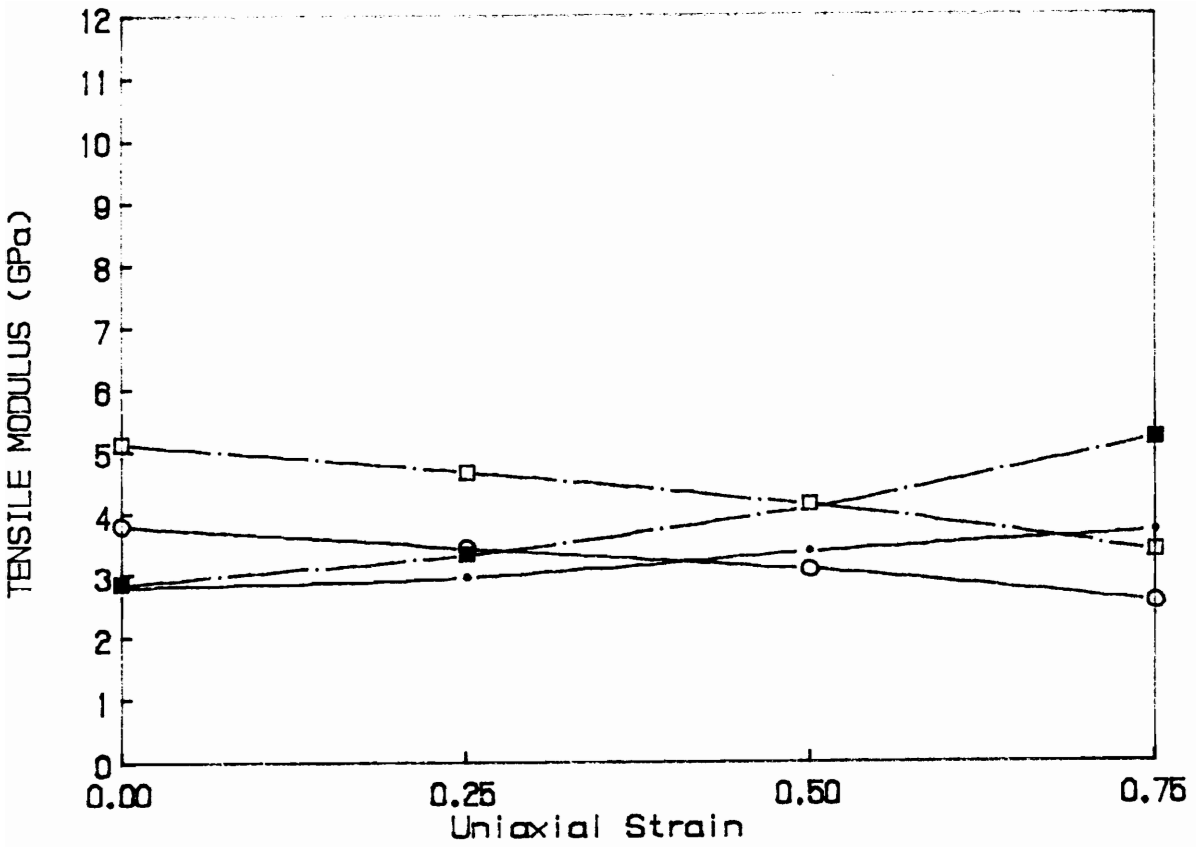

Figure 4.9. Tensile modulus as a function of transverse uniaxial strain for (○,•) PEI/Vectra A and (□,▪) PEI/HX1000 80/20 wt% blends. (open symbols = flow direction, filled symbols = transverse direction).

PEI/HX1000 blend as function of transverse uniaxial strain in which the samples were stretched at a temperature of 265°C. Here again one observes that, the initial flow direction properties decrease as the transverse uniaxial strain increases. However, once again it appears that the PEI/HX1000 blend is more sensitive to the stretching temperature than the PEI/Vectra A blend. That is, the increase in the transverse mechanical properties of PEI/HX1000 80/20 blend following transverse stretching was less than that at 240°C. On the other hand, a similar increase in transverse properties appears to occur for the PEI/Vectra A blends at both stretching temperatures.

The effects of uniaxial elongation, applied both parallel and transverse to flow direction, on the morphology and mechanical properties of injection molded plaques of PEI/Vectra A and PEI/HX1000 blends have been discussed. We have found that the direction of the applied deformation relative to the initial direction of the TLCP fibrils was an important factor in affecting the resultant morphology and corresponding mechanical properties of the blends. If the direction of the applied uniaxial deformation was parallel to the initial fiber direction, the deformation tended to increase the average aspect ratio of the the TLCP fibers and mechanical properties were enhanced along the direction of deformation. However, if the deformation was applied transverse to the initial fiber direction, the fibers tended to follow the deformation and a 90° rotation was observed. In terms of mechanical properties after transverse deformation, it was observed that a complete inversion occurred after a strain of 0.75 units was applied transversely to the initial flow direction. It has been also found that the stretching temperature had a greater effect on the mechanical properties of the PEI/HX1000 blends than for the PEI/Vectra A blends. It is believed, stretching at a temperature of 265°C may promote relaxation of the molecular orientation and, consequently, reducing the effectiveness of the deformation. However, wide angle x-ray diffraction experiments have not been performed in order to support such a conclusion.

Table 4.7. Effects of transverse uniaxial stretching applied at 265°C on the mechanical properties of molded plaques of PEI/Vectra A 80/20 wt%.

FLOW DIRECTION PROPERTIES			TRANSVERSE DIRECTION PROPERTIES			UNIAXIAL STRAIN
Modulus (GPa)	Strength (MPa)	Elongation (%)	Modulus (GPa)	Strength (MPa)	Elongation (%)	
3.80 (0.10)	81.80 (3.80)	3.10 (0.40)	2.80 (0.10)	45.00 (9.10)	2.20 (0.10)	0.0
3.55 (0.28)	63.71 (4.94)	2.40 (0.17)	3.10 (0.14)	73.96 (5.96)	3.60 (0.38)	0.25
3.23 (0.23)	71.93 (6.20)	3.28 (0.12)	3.24 (0.32)	96.28 (2.19)	4.58 (0.37)	0.50
2.98 (0.10)	75.71 (6.59)	3.78 (0.26)	3.73 (0.20)	103.10 (6.17)	4.64 (0.42)	0.75

1. **Stretching Temperature: 265°C.**
2. **Initial Strain Rate: 0.014 sec^{-1}**

(★) Standard deviations are given in parenthesis.

Table 4.8. Effects of transverse uniaxial stretching applied at 265°C on the mechanical properties of molded plaques of PEI/HX1000 80/20 wt%.

FLOW DIRECTION PROPERTIES			TRANSVERSE DIRECTION PROPERTIES			UNIAXIAL STRAIN
Modulus (GPa)	Strength (MPa)	Elongation (%)	Modulus (GPa)	Strength (MPa)	Elongation (%)	
5.13 (0.47)	105.36 (4.15)	2.38 (0.15)	2.84 (0.14)	57.10 (3.92)	2.57 (0.23)	0.0
5.30 (0.21)	82.86 (3.74)	2.01 (0.10)	3.00 (0.12)	72.21 (6.44)	2.88 (0.19)	0.25
4.91 (0.37)	76.30 (7.30)	1.80 (0.36)	3.45 (0.14)	88.45 (9.05)	2.76 (0.18)	0.50
3.00 (0.12)	56.16 (3.44)	1.04 (0.10)	3.63 (0.17)	93.96 (1.61)	3.14 (0.21)	0.75

1. **Stretching Temperature: 265°C.**
2. **Initial Strain Rate: 0.014 sec^{-1}**

(★) Standard deviations are given in parenthesis.

4.3.4 Extruded Sheets Subjected to Uniaxial Elongation

In this section, we complete the objectives of this paper by presenting the effects of uniaxial deformation on the structure and mechanical properties of extruded sheets of PEI/Vectra A and PEI/HX1000 blends. The effects of uniaxial stretching on the morphology and mechanical properties of PEI/Vectra A blends are discussed first, followed by results for PEI/HX1000 blends. However, because the initial morphology of the extruded sheets is that of undeformed TLCP droplets, stretching experiments were performed only in a direction parallel to the extrusion direction. In addition, all experiments were carried out at at 240°C and at an initial elongation rate of 0.014 sec^{-1}.

The morphology obtained during the extrusion of a PEI/Vectra A 90/10 blend is shown in Figure 4.10 where scanning electron micrographs of samples fractured along the extrusion direction are presented. As described in the experimental section, the sheets were extruded without any post extrusion drawing with the objective of obtaining undeformed TLCP drops. As shown in Figure 4.10, with this procedure we were successful in obtaining an extrudate in which only underformed TLCP drops were found. However, as one notices from Figure 4.10, a distribution in droplet size across the thickness of the extrudate is observed. It is possible that this might be due to the following. Closer to the die walls, where higher shear stress gradients exist, a higher rate of droplet breakup is induced and, therefore, small drops are found (Figure 4.10-a). At regions closer to the center, where weak shear flows dominate, the extent of breakup is reduced and large drops of the TLCP phase are found (Figure 4.10-b).

The variations in the initial morphology of the PEI/Vectra A 90/10 extruded sheet as a function of uniaxial strain are presented in Figures 4.11 and 4.12. In Figure 4.11 the total uniaxial strain applied was 0.25 units, whereas in Figure 4.12 the uniaxial strain was 0.50 units. The samples were fractured along the stretching direction. As one would expect, increasing the deformation strain increases the deformation of the TLCP phase into reinforcing fibrils along the direction of deformation. However, one notices that the extent of droplet deforma-

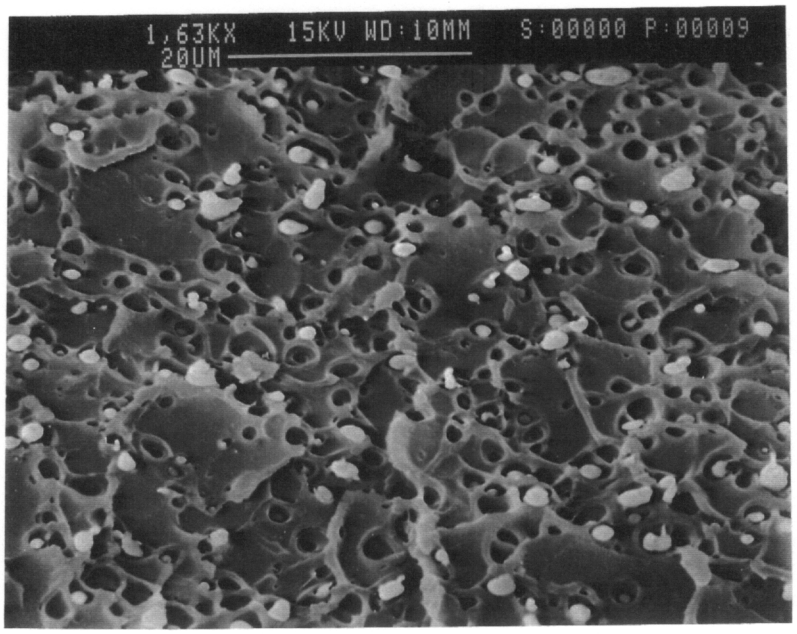

(A)

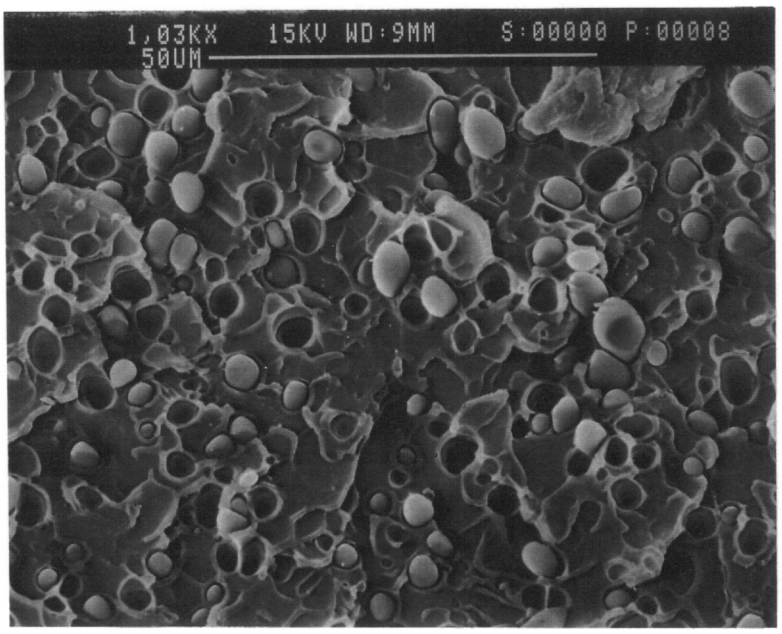

(B)

Figure 4.10. Scanning electron micrographs of as extruded sheets of PEI/Vectra A 90/10 composition ratio, fractured along the extrusion direction, a) skin and b) core regions.

tion was higher for the drops closer to the skin region of the sheet than for the ones found in the core. We believe that this may be attributed to the inhomogeneity of the deformation. As discussed in the experimental section, because of the way the samples were clamped to the Instron's grips necking occurs upon stretching and, therefore, the deformation strains are higher at the edges of the sample compared to the strains at the center. Thus, the droplets found at the outer regions (surface) of the sample are actually experiencing higher magnitudes of strains than the ones in the center. Consequently, the extent of droplet deformation, following the variations in strain, becomes a function of the relative position of the drop in the flow.

Next, the effects of uniaxial elongation on the mechanical properties of extruded sheets of PEI/Vectra A blends are addressed. In Table 4.9 are presented the mechanical properties of PEI/Vectra A 90/10 extruded sheets after uniaxial deformation. In the Table are also included, for the sake of comparison, the mechanical properties obtained from injection molded samples of PEI/Vectra A 90/10. The data shows that, as the applied uniaxial strain increases the overall mechanical properties of the extruded sheet increase considerably. This correlates well with the observed increase in the deformation of the TLCP phase into reinforcing fibrils upon stretching. One also observes that at small magnitudes of uniaxial strain the mechanical properties of the extruded sheets are much better to those obtained from injection molded samples. One important aspect pertaining to this work is the increase in the toughness of the extruded sheet upon stretching. This is a valuable observation because it shows that the mechanical performance of PEI/TCLP composites may be increased upon uniaxial stretching at temperatures below the melting temperature of the TLCP.

Next, attention is given to PEI/HX1000 blends. In Figure 4.13 are shown scanning electron micrographs obtained from extruded sheets of a PEI/HX1000 90/10 blend. As in the case of PEI/Vectra A, a distribution in droplet size is found across the thickness of the extrudate. However, compared to PEI/Vectra A, the size of the droplets found here is much smaller. This might possibly be due to the following. According to Sun et al. (44), a higher degree of miscibility exist in the PEI/HX1000 system compared to the PEI/Vectra A system.

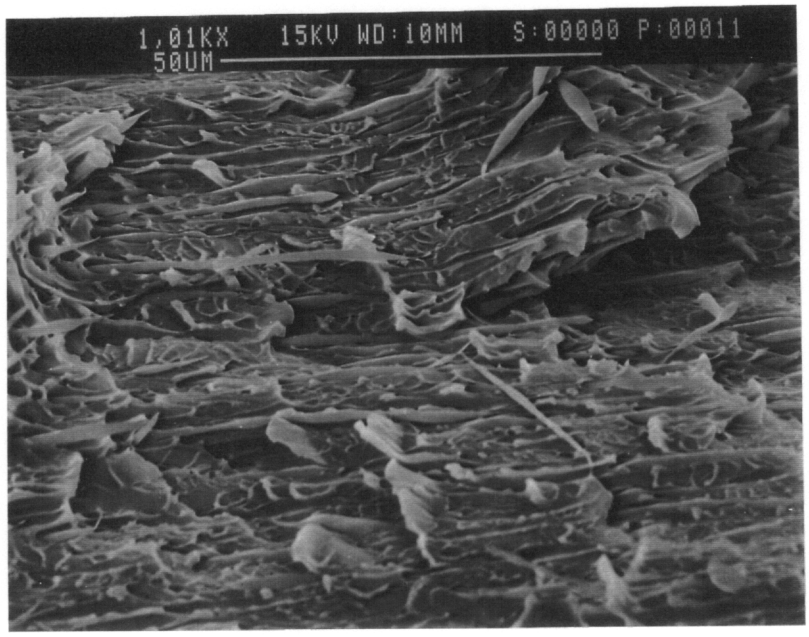

(A)

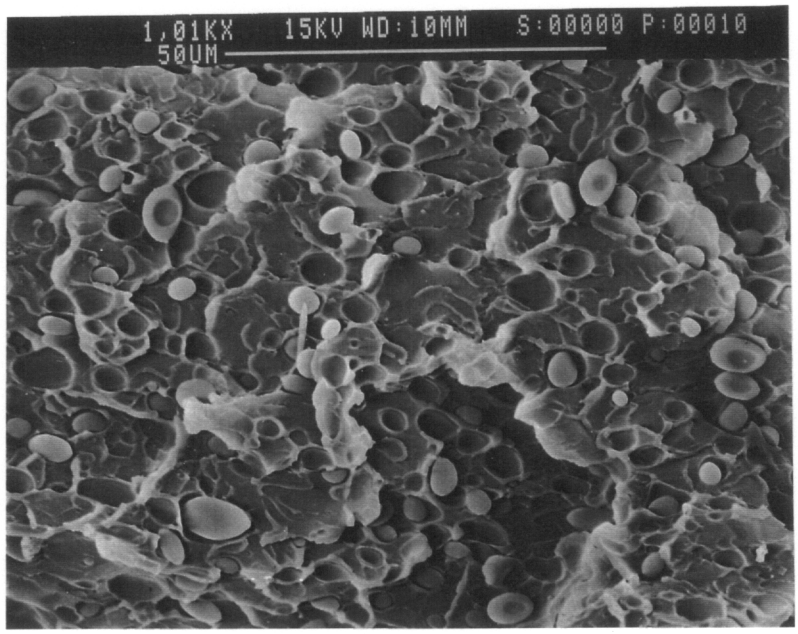

(B)

Figure 4.11. **Scanning electron micrographs of extruded sheets of PEI/Vectra A 90/10 composition ratio after uniaxial elongation deformation** fractured along stretching direction a) skin and b) core regions ($T = 240°C$, $\varepsilon_U = 0.25$ units and $\dot{\varepsilon}_I = 0.014\ sec^{-1}$).

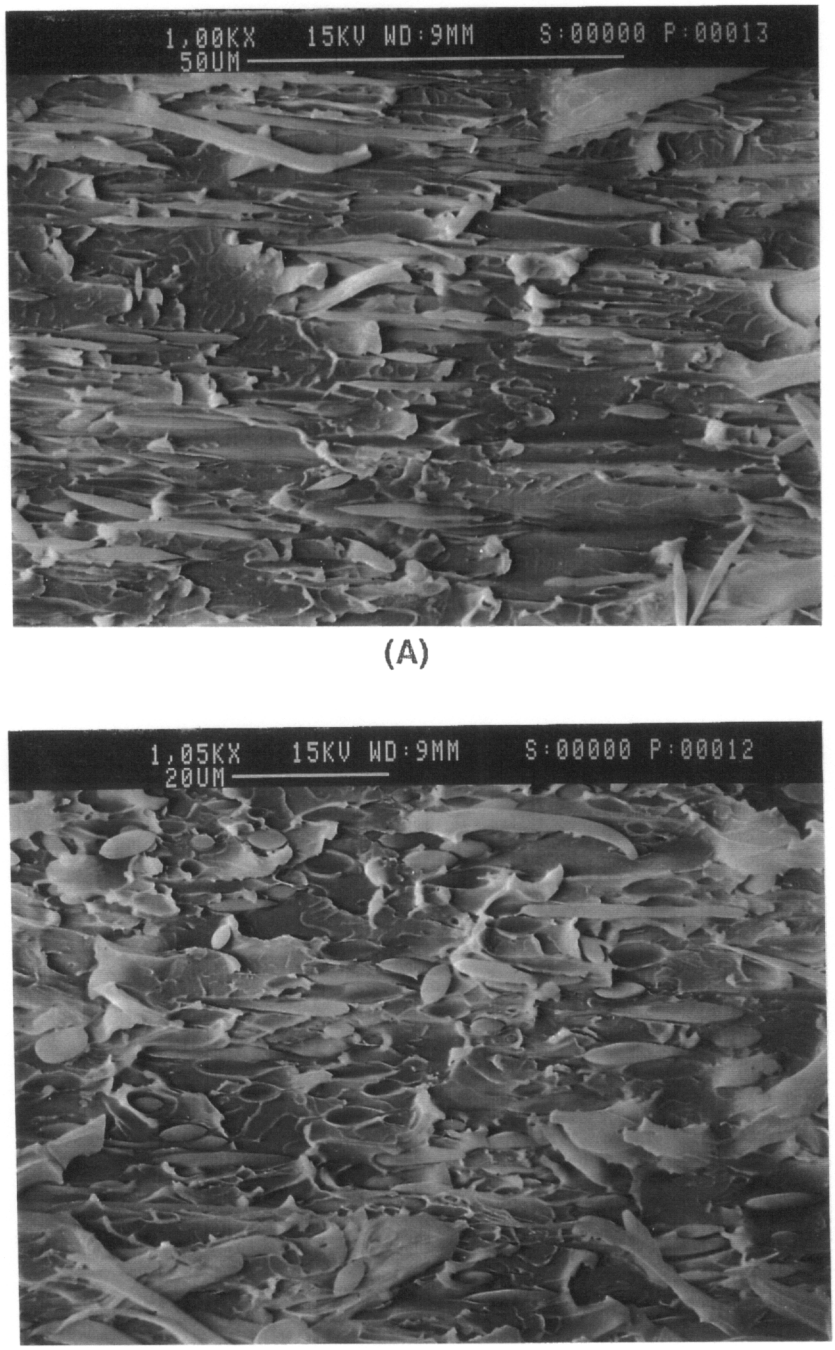

Figure 4.12. Scanning electron micrographs of extruded sheets of PEI/Vectra A 90/10 composition ratio after uniaxial elongation deformation fractured along stretching direction a) skin and b) core regions ($T = 240°C$, $\varepsilon_u = 0.50$ units and $\dot{\varepsilon}_i = 0.014\ sec^{-1}$).

Table 4.9. Effects of uniaxial stretching on the mechanical properties of extruded sheets of PEI/Vectra A 90/10 blend.

TENSILE MODULUS (GPa)	TENSILE STRENGTH (MPa)	ELONGATION BREAK (%)	TOUGHNESS[3] (KJ/m^3)	UNIAXIAL STRAIN
3.65 (0.29)	111.98 (3.27)	4.64 (0.52)	3510 (380)	0.0
3.69 (0.44)	130.64 (10.66)	5.35 (0.33)	4250 (340)	0.25
3.74 (0.21)	135.77 (6.35)	5.90 (0.43)	5230 (230)	0.50
4.30 (0.30)	143.50 (11.00)	6.00 (0.26)	6215 (480)	0.75
3.50 (0.20)	92.40 (2.10)	4.10 (0.30)	2554 (128)	MP[4]
3.82 (0.09)	106.77 (7.44)	6.28 (0.59)	5180 (620)	MTB[5]

1. **Stretching Temperature: 240°C.**
2. **Initial Strain Rate: 0.014 sec^{-1}**
3. **Calculated as the area under the stress vs. strain curve**
4. **Injection molded plaques**
5. **injection molded tensile bars (ASTM D 638 TYPE 5)**

(★) Standard deviations are given in parenthesis.

Therefore, due to the partial miscibility, lower interfacial tension is found between PEI/HX1000 than between PEI/Vectra A (25). Thus, due to lower interfacial tension and assuming that the blends must have experienced similar magnitudes of shear stress during processing, in blends with PEI the tendency of the HX1000 phase is to breakup into smaller drops compared to Vectra A phase. The distribution in the droplet size across the thickness of the extrudate is, once again, due to the gradient in shear stresses across the extrusion die.

The effects of uniaxial strain on the initial morphology of a PEI/HX1000 90/10 extruded sheet are presented in Figures 4.14. The total uniaxial strain applied was 0.50 units. Here again, increasing the strain increases the deformation of the TLCP phase into reinforcing fibrils along the direction of deformation. However, due to the lower interfacial tension, stress induced fiber breakup has started to appear. This is evidenced by the characteristic end-pinched shape of the fiber upon deformation. Once again, due to the inhomogeneity of the deformation, thickness dependent deformation is observed.

In Table 4.10 are presented the effects of uniaxial deformation on the mechanical properties of PEI/HX1000 90/10 extruded sheets as function of strain. In Table 4.10 are also included the mechanical properties obtained from injection molded samples of PEI/HX1000 90/10 blend. The data shows that as the applied uniaxial strain increases, the overall mechanical properties of the extruded sheet remained practically unchanged. That is, the increase in the mechanical properties upon deformation was not significant. An explanation for this is found in the morphological analysis just presented. Due to the lower interfacial tension of the PEI/HX1000 system, the deformed HX1000 fibrils would breakup into smaller shapes before reaching any appreciable length required to improve the mechanical properties. Therefore, it appears that, in the case of extruded sheets, the PEI/Vectra A system is more stable during stretching than is the PEI/HX1000 system. Perhaps due to a higher interfacial tension of the PEI/Vectra A system higher magnitudes of stresses are required to induce fiber breakup.

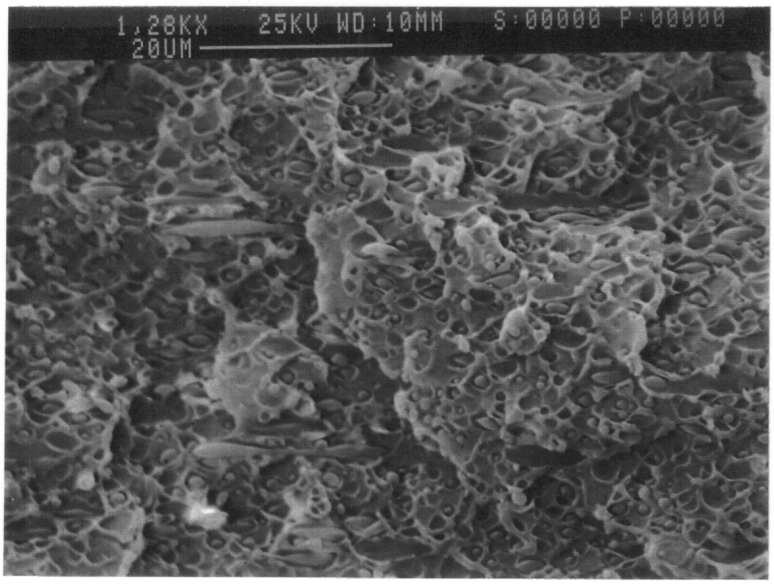

(A)

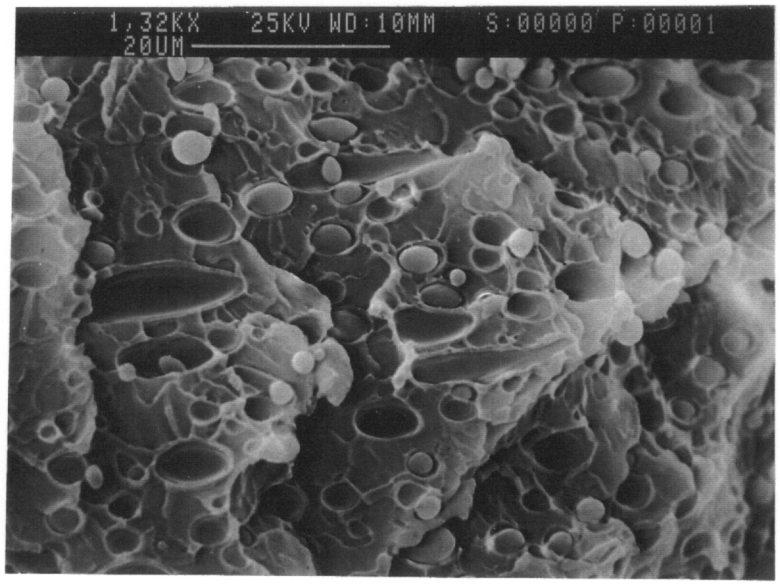

(B)

Figure 4.13. **Scanning electron micrographs of as extruded sheets of PEI/HX1000 90/10 composition ratio, a) skin and b) core regions.** The sample was fractured along the extrusion direction.

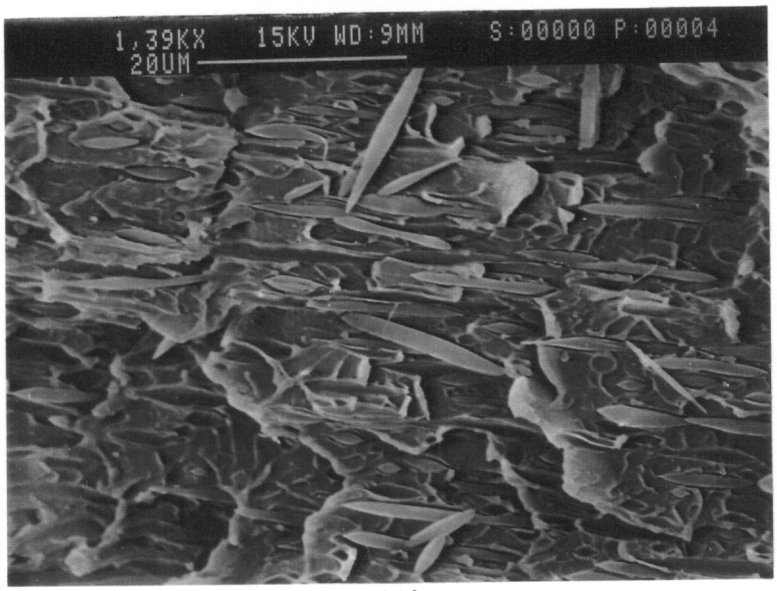

(A)

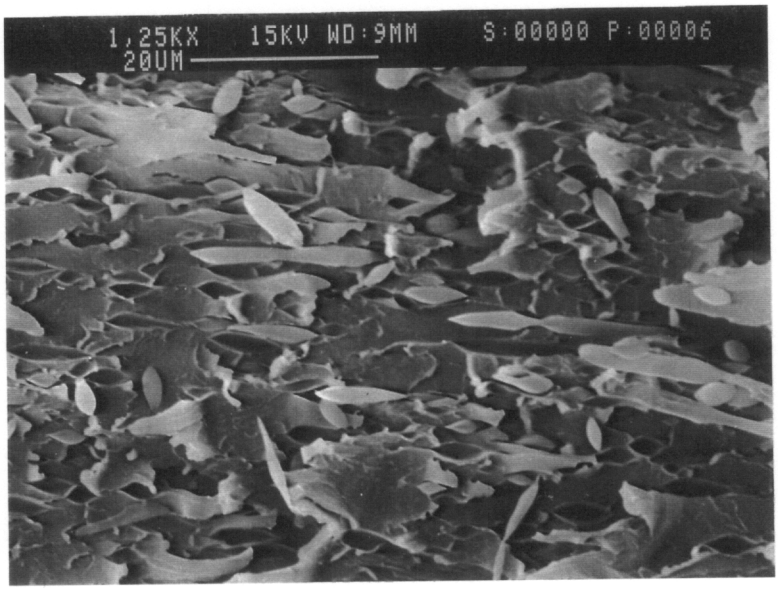

(B)

Figure 4.14. **Scanning electron micrographs of extruded sheets of PEI/HX1000 A 90/10 composition ratio after uniaxial elongation deformation** fractured along stretching direction, a) skin and b) core regions ($T=240°C$, $\varepsilon_U=0.50$ units and $\dot{\varepsilon}_I=0.014$ sec^{-1}).

Table 4.10. Effects of uniaxial stretching on the mechanical properties of extruded sheets of PEI/HX1000 90/10 blend.

TENSILE MODULUS (GPa)	TENSILE STRENGTH (MPa)	ELONGATION BREAK (%)	UNIAXIAL STRAIN
3.29 (0.25)	98.65 (2.21)	4.04 (0.40)	0.0
4.43 (0.25)	106.81 (4.93)	3.82 (0.46)	0.25
4.16 (0.25)	108.64 (5.78)	4.85 (0.10)	0.50
4.19 (0.21)	104.04 (4.81)	3.55 (0.43)	0.75
4.94 (0.15)	103.46 (6.96)	2.99 (0.33)	MP[3]
4.88 (0.24)	137.68 (4.83)	5.45 (0.56)	MTB[4]

1. **Stretching Temperature: 240°C.**
2. **Initial Strain Rate: 0.014 sec^{-1}**
3. **Injection molded plaques**
4. **injection molded tensile bars (ASTM D 638 TYPE 5)**

(★) Standard deviations are given in parenthesis.

4.4 Conclusions

The effects of uniaxial elongation on the morphology and mechanical properties of injection molded plaques and extruded sheets of PEI/Vectra A and PEI/HX1000 blends were investigated. It was found the in the case of injection molded samples, the effect of uniaxial elongation on the morphology and properties was dependent upon the relative direction of the deformation with respect to the initial direction of the fibers. If the direction of the applied uniaxial deformation was parallel to the initial fiber direction, the deformation tended to increase the average aspect ratio of the the TLCP fibers and mechanical properties along the deformation direction were enhanced. On the other hand, if the direction of the applied deformation was transverse to the initial fiber direction, the fibers tended to follow the deformation and a 90° rotation was observed. A corresponding increase in the transverse direction properties accompanied by a decrease in the flow direction properties followed the realignment of the fibers. In addition, equal flow and transverse mechanical properties were found after 0.5 unit of uniaxial strain.

The stretching temperature appeared to have a greater effect on the mechanical properties of the PEI/HX1000 blends compared to PEI/Vectra A blends. The magnitude of increase of the mechanical properties was less for PEI/HX1000 at 265°C than for 240°C It is believed, stretching at a temperature of 265°C, which is closer to the melting temperature of TLCP, the competing effects of deformation and relaxation of the molecular orientation reduced the effectiveness of the deformation in enhancing the mechanical properties of the blend.

Uniaxial stretching of extruded sheets have also indicated that the initial mechanical properties are significantly increased upon stretching. However, the stability of the fibers upon deformation seemed to be a function of the compatibility between the TLCP and the PEI phase. Highly stable and elongate TLCP fibrils were observed in the case of PEI/Vectra A relative to PEI/HX1000, in where breakup occurred.

4.5 Acknowledgements

Support from the Center for Innovative Technology of Virginia (Grant No. MAT-91-004-02) and the DuPont Company is greatly appreciated.

4.6 References

1. K. Blizard and D.G. Baird, **Polym. Eng. Sci.**, 27 (9), 653 (1987).
2. R.A. Weiss, H. Huh, and L. Nicolais, in , *High Modulus Polymers*, A.E. Zachariedes and R.S. Porter, eds., Marcel Dekker, New York (1988).
3. D.G. Baird and R. Ramanathan, in *Contemporary Topics in Polymer Science*, vol. 6, B.M. Culberston, ed., Plenum Press (1990).
4. D. Beery, S. Kenig, and A. Siegmann, **Polym. Eng. Sci.**, 31 (6), 459 (1991).
5. D.G. Baird, S.S. Bafna, J.P. de Souza, and T. Sun, **Polym. Comps.**, 31 (6), 459 (1993).
6. A. Metha and A.I. Isayev, **Polym. Eng. Sci.**, 31 (3), 971 (1991).
7. J. Seppala, M. Heino, and C. Kapanen, **J. Appl. Polym. Sci.**, 44, 1051 (1992).
8. G. Kiss, **Polym. Eng. Sci.**, 27 (9), 410 (1987).
9. A.I. Isayev and M. Modic, **Polym. Comp.**, 8 (3), 158 (1987).
10. T. Sun, D.G. Baird, H.H. Huang, D.S. Done, and G.L. Wilkes, **J. Comp. Mat.**, 25, 788 (1991).
11. R.A. Weiss, W. Huh, and L. Nicolais, **Polym. Eng. Sci.**, 27 (9), 684 (1987).
12. G. Crevecoeur and G. Groenickx, **Polym. Eng. Sci.**, 30 (9), 532 (1990).
13. S.H. Jung and S.C. Kim, **Polym. J.**, 20 (1), 73 (1988).
14. A. Valenza, F.P. La Mantia, M. Paci, and P.L. Magagnini, **Int. Polym. Proc.**, 6 (3), 247 (1991).
15. D.Dutta, H. Fruitwala, A. Kohli, and R.A. Weiss, **Polym. Eng. Sci.**, 30, 1005 (1990).
16. F.P. La Mantia, *Thermotropic Liquid Crystal Polysmer Blends*, Technomic, Lancaster, PA (1993).
17. G. Crevecouer, *In Situ Composites, Blends of Thermotropic Liquid Crystalline Polymers in a Thermoplastic Matrix*, PhD Thesis, Catholic University of Leuven (1991).
18. J.J. Elmendorp and A.K. Van der Vegt, in *Two-Phase Polymer Systems*, L.A. Utracki, ed., Hansen, Munich (1991).

19. G.I. Taylor, **Proc. Roy. Soc.**, A146, 501 (1934).

20. G.I. Taylor, **Proc. Roy. Soc.**, A138, 41 (1932).

21. G.I. Taylor, **Proc. Roy. Soc.**, A226, 289 (1954).

22. R.G. Cox, **J. Fluid Mech.**, 37 (3), 601 (1969).

23. S. Kenig, **Polym. Eng. Sci.**, 29, 1136 (1989).

24. E.G. Joseph, D.G. Baird, and G.L. Wilkes, **Polym. Eng. Sci.**, 25 (7), 377 (1985).

25. Chapter 3.0 of this dissertation.

26. T.S. Chung, **J. Polym. Sci., Polym. Phys. Ed.**, 26, 1549 (1988).

27. Q. Lin, J. Jho, and A.F. Yee, **Polym. Eng. Sci.**, 33 (13), 789 (1993).

28. K.G. Blizard, R. Ramanathan, and D.G. Baird, Antec Tech. Papers, 585 (1987).

29. A.M. Sukhadia, PhD dissertation, Virgina Tech (1991).

30. K. Blizard and D.G. Baird, **Polym. Eng. Sci.**, 27 (9), 653 (1987).

31. R. Ramanathan, K.G. Blizard and D.G. Baird, Antec Tech. Papers, Atlanta, 1123 (1988).

32. S.S. Bafna, J.P. de Souza, T.S. Sun, and D.G. Baird, **Polym. Eng. Sci.**, 33 (13), 808 (1993).

33. R.A. Chivers and D.R. Moore, **Polymer**, 21, 2190 (1991).

34. K. Friedrich and H. Voss, in *Engineering Applications of New Composites*, S.A. Paipetis and G.C. Papanicolou, eds., Omega Scientific, Oxford, England (1988).

35. G. Crevecoeur and G. Groenickx, **Polym. Eng. Sci.**, 33 (15), 937 (1993).

36. D.G. Baird and G.L. Wilkes, **Polym. Eng. Sci.**, 25 (7), 377 (1985).

37. *Modern Plastics*, 12, January (1990).

38. R.B. Bird, R.C. Armstrong and O. Hassager, *Dynamics of Polymeric Liquids*, Vol. 1, 2nd. ed., Wiley-Interscience, New York (1987).

39. J.M. Dealy and K.F. Wissbrun, *Melt Rheology and its Role in Plastics Processing*, Van Nostrand Reinhold, New York (1990).

40. M.Y. Cao, and B. Wunderlich, **J. Polym. Sci., Polym. Phys. ed.**, 23, 521 (1985).

41. P. Magagnini, in *Thermotropic Liquid Crystal Polymer Blends*, F.P. La Mantia, ed., Chapt. 1, Technomic, Lancaster, PA (1993).

42. L.H. Sperling, *Introduction to Physical Polymer Science*, 2nd. Ed., pp. 323-327, John Wiley and Sons, New York (1992).

43. Appendix section of this dissertation.

44. S.S. Bafna, T. Sun, J.P. de Souza and D.G. Baird, **Polymer**, 34 (4), 708 (1993).

5.0 PLANAR DEFORMATION

5.1 Introduction

In the first part of this study, the effects of uniaxial elongation on the structure and mechanical properties of molded plaques and extruded sheets of blends of thermotropic liquid crystalline polymers (TLCP) with a polyetherimide (PEI) were investigated (1). We found that the direction of the applied uniaxial deformation relative to the direction of the TLCP fibers is an important factor in affecting the resulting morphology and mechanical properties of the samples. For instance, in the case of injection molded plaques, in which the initial morphology is formed of both fibers and droplets, uniaxial elongation applied parallel to the direction of the fibers tended to increase the aspect ratio of the fibers and, as a result, the mechanical properties increased along the deformation direction. However, if uniaxial elongation was applied transverse to the direction of the fibers, the fibers followed the stretching and a 90° rotation was observed. A corresponding increase in the transverse properties, accompanied by a decrease of the initial flow direction properties, followed the realignment of the fibers upon transverse stretch. In addition, isotropic mechanical properties appeared at 0.5 units of transverse uniaxial strain. In the case of extruded sheets, in which the initial morphology is

that of drops, a fibrillar TLCP morphology developed after uniaxial deformation and the overall mechanical properties of the sheet increased upon stretching. However, we found that the stability of the deformed TLCP fibrils depended upon the degree of miscibility between the PEI matrix and the TLCP used. For a PEI/TLCP blend showing partial miscibility, stress induced fiber breakup occurred upon stretching.

In this paper we continue with the investigations of shearfree flows and report on the effects of planar deformation on the structure and mechanical properties of TLCP based in situ composites. Eventually, the findings of this fundamental study will be used to develop processing methods in which controlled morphologies and consequently mechanical properties can be obtained. In addition, we investigate the effectiveness of planar deformation in reducing the mechanical anisotropy of TLCP based composites.

5.2 Experimental Procedure

5.2.1 Materials and Processing

The matrix material is a polyetherimide (PEI), commercially available as Ultem 1000 from General Electric Plastics. PEI is an amorphous engineering thermoplastic with a glass transition temperature at about 228°C and a processing temperature ranging from 330 to 365°C (4). The semicrystalline TLCP is a thermotropic copolyester commercially available as Vectra A900 from Hoechst-Celanese. Vectra A900 (henceforth referred to as Vectra A) has a glass transition temperature at 105°C and a crystal-mesophase transition at 283°C (5). The amorphous TLCP, supplied by DuPont and referred to as HX1000, has a glass transition temperature at 185°C and a processing temperature ranging from 290 to 365°C (6).

The selection of the TLCPs and engineering thermoplastic used in this study was based upon the following criteria. First, because the PEI matrix has a glass transition temperature much higher than either TLCPs, at the stretching temperature of 240°C, both the PEI matrix and the TLCPs would be deformable (1). In addition, contrary to PEI/Vectra A, PEI/HX1000 forms a partially miscible blend (7) and, due to this, PEI/HX1000 blends exhibit a higher degree of compatibility when compared to PEI/Vectra A blends (8). This is supported by the interfacial tension values calculated from equilibrium contact angle measurements (8). The interfacial tension for PEI/Vectra A and PEI/HX1000 pairs are, respectively, 20.80 and 7.20 mN/m. Therefore, with the use of these TLCPs in blends with PEI, the role partial miscibility on the deformation of a TLCP phase upon planar extensional flow can be assessed.

Pellets of PEI, Vectra A and HX1000 were dried at 115°C in a convection oven for at least 48 hours prior to processing. After dry blending, the physically mixed pellets of PEI/Vectra A and PEI/HX1000 blends with TLCP concentration of up to 30 wt% were injection molded into rectangular plaques and extruded into sheets. The processing conditions for the injection molding and the extrusion processes are given elsewhere (1).

The use of injection molded plaques and extruded sheets of PEI/TLCP blends in the planar deformation experiments is based upon the following. In injection molding, the kinematics of the process impart a layered structure morphology to the sample upon molding. That is, at the outer surfaces (skin) of the sample long high aspect ratio fibrils of the TLCP phase are usually found, whereas in the center regions (core), undeformed droplets of the TLCP phase are usually found (8-12). In the extrusion process, on the other hand, external drawing is usually necessary in order to deform the TLCP phase into elongated fibrils (13-16). Hence, by controlling post-extrusion drawing, undeformed droplets of the TLCP phase can be obtained (1). Therefore, with the use of injection molded samples and extruded sheets, the effects of planar deformation on samples showing either a more fibrillar or a droplet morphology may be determined.

5.2.2 Morphological Characterization and Mechanical Properties

Morphological studies were performed by means of scanning electron microscopy (SEM). A Cambridge Stereoscan-S200 Instrument with an accelerating voltage of 25 KV was used. The samples were cryogenically fractured along and across the principal deformation direction after immersion in liquid nitrogen for at least 5 minutes. The samples were then mounted on aluminum stubs and sputter coated with gold for enhanced conductivity.

The mechanical properties were evaluated on rectangular specimens (measuring approximately 12mm x 80mm) by means of an Instron Universal Testing Instrument, model 4204. A cross-head speed of 1 mm/min was used. The mechanical properties reported are based on measurements made on at least five samples.

5.2.3 Generation of Planar Elongational Deformation

The kinematics of planar deformation are given by the velocity field (2):

$$V_x = -\dot{\varepsilon}\, x \tag{5.1}$$

$$V_y = 0 \tag{5.2}$$

$$V_z = +\dot{\varepsilon} z \tag{5.3}$$

where $\dot{\varepsilon}$ is the Hencky strain rate, and the Hencky strain ε is defined as $\varepsilon = \ln(\lambda_z)$, in which λ_z is the principal elongation ratio defined as $\lambda_z = z/z_0$, with z_0 and z being, respectively, the initial and instantaneous length of the sample. For incompressible fluids $\lambda_x\lambda_y\lambda_z = 1$, and for planar deformation $\lambda_y = 1$ and $\lambda_x = 1/\lambda_z$. Thus, in planar deformation, there is stretching in the z direction, compression in the x direction and no displacement in the y direction. Polymer processing operations that may involve planar deformation are, for example, thermorforming

when matching molds are used, and in the stretching of a tube while sufficient internal pressure is supplied to keep a constant diameter (3).

The kinematics of planar deformation were experimentally generated by two methods. One method used was constrained lubricated compression molding. In this procedure, a picture frame mold was used in conjunction with metallic blocks that were used to constrain the flow of the polymer in one specific direction. Thus, the material flowed through the rectangular channel bounded by the metallic blocks and planar elongation kinematics were obtained. The mold (containing the sample) was then placed between heated plates and after equilibrium of the temperature, it was transferred to a hydraulic press. The compression force used was about 90 KN. The extent of compression, or planar strain, was controlled with the aid of metallic shims placed in the mold. However, the disadvantage of this procedure was that with the manual operation of the press, estimation of the deformation rates was difficult. After compression, the mold was water cooled to room temperature. High temperature silicone oil (based on diphenyldimethyl siloxane) was used to lubricate the mold and sample surfaces in order to minimize the effects of shear flow. The compression temperature was set a 240°C. At this temperature both the PEI matrix and the TLCPs were deformable (1).

A procedure similar to that of the stretching experiments described in a previous paper (1) was also used as a means to obtain planar deformation. The exception here was that specially designed side clamps were used to constrain the contraction (necking) of the sample upon stretching, as seen in Figure 5.1. The advantage of using the Oven/Instron combination to generate planar deformation was that, in addition to the possibility of applying higher values of planar strains to the sample, the deformation, in terms of temperature and deformation rates, was better controlled compared to compression molding. However, in order to maintain the kinematics as close as possible to planar deformation, planar strains were applied at increments of 0.25 units. This procedure eliminated slippage of the side clamps which, consequently, would make the kinematics diverge from a true planar deformation.

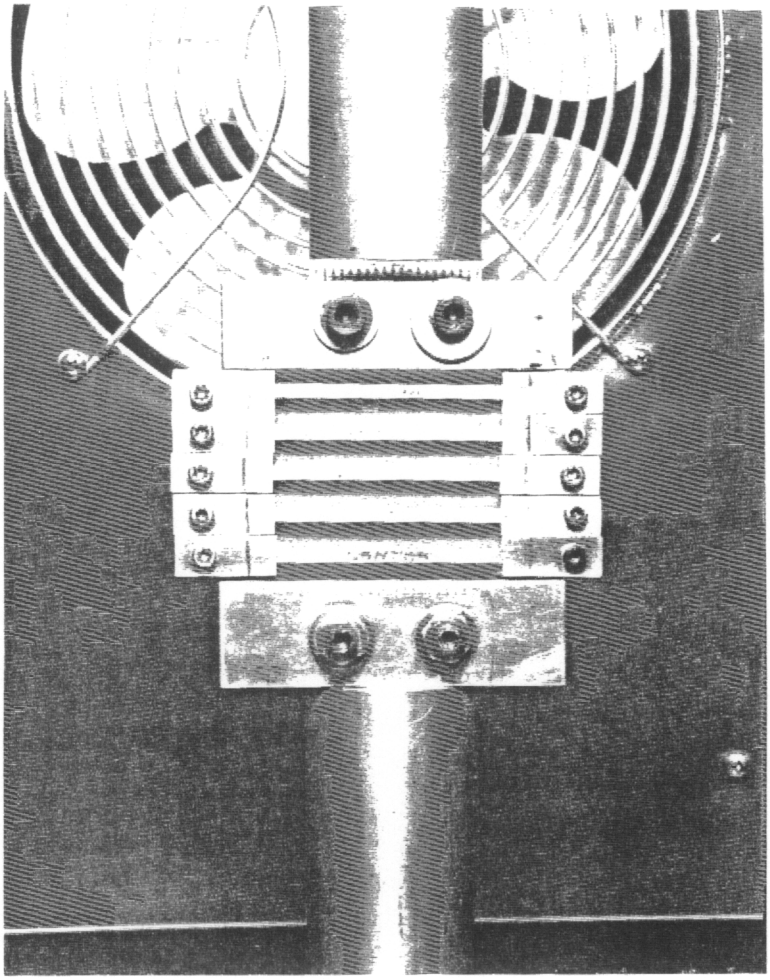

Figure 5.1. Clamping assembly used to obtain planar deformation upon stretching

5.3 Results and Discussions

The methodology and experimental procedure necessary to fulfil the objectives of this paper were given in the previous section. In this section the experimental results along with the analysis and interpretations are given. In order to present the results of this study as clearly as possible, this section is divided into two parts. In the first part, Section 5.3.1, the experimental results obtained from injection molded samples are presented. Following this, in Section 5.3.2, the results from extruded sheets are discussed. Due to the fact that the orientation of the TLCP fibers in the molded plaque is parallel to the direction of the flow, planar deformation was applied both parallel and perpendicular to the initial direction of the fibers. In the case of extruded sheets, in which the initial morphology was that of drops, planar deformation was applied parallel to the original extrusion direction.

5.3.1 Molded Plaques Subjected to Planar Deformation

Planar deformation results obtained from injection molded plaques of PEI/Vectra A and PEI/HX1000 blends with TLCP concentrations of up to 30 wt% are presented in this section. However, even though the analyses of morphological and mechanical properties were carried out on almost all compositions, the discussions presented here will concentrated primarily on a few representative samples. Additional results are included elsewhere (17).

The effects of planar compression molding applied parallel to the initial direction of the fibers (constrained in the transverse) on the morphology of molded plaques of PEI/Vectra A 80/20 blend are discussed next. However, for the sake of comparison, the initial morphology developed during the injection molding of the blend is shown first in Figure 5.2 in where scanning electron micrographs of PEI/Vectra A 80/20 blend are presented. The fracture surfaces were obtained both parallel and perpendicular to the injection molding flow direction.

As one clearly notices, a layered structure strongly oriented in the direction of flow developed upon molding. For regions closer to the mold walls (skin), the TLCP phase deforms into a highly fibrillar structure oriented along the direction of flow. This is observed by comparing Figures 5.2-a and c. As shown in Figures 5.2-b and d, towards the center region (core) the TLCP phase is less fibrillar than in the skin, and droplet shapes are found. Therefore, one observes that the structure developed during the injection molding of a TLCP/polymer blend is very complex. The kinematics of the process gives rise to a layered structure in the sample, and the deformation of the TLCP phase becomes dependent upon the position of the TLCP drop in the flow (8).

The effect of planar deformation (constrained lubricated compression molding) on the morphology of a molded plaque of PEI/Vectra A 80/20 blend is illustrated in Figure 5.3. The surface was fractured along the deformation direction, that is parallel to the initial flow direction. A comparison of the micrographs presented in Figure 5.2 with these reveals that, after planar compression molding, an increase in the aspect ratio of the TLCP phase along the direction of the deformation is observed. This is seen by the presence of elongated TLCP fibrils in the core region of the sample (Figure 5.3-b) which initially were in the form of drops. The mechanical properties along the direction of the deformation as shown later will be affected by planar deformation.

However, in order to obtain a better insight into the effects of planar deformation on the morphology of the blends, a fracture surface as shown in Figure 5.4 was taken in the plane of deformation (y-z plane). The direction of the planar elongational flow was parallel to the initial direction of the fibers, and the planar strain applied was 0.34 units. One observes that not only were the TLCP fibers deformed along the direction of the planar flow, as indicated in Figure 5.3, but also a flattening of the fibers occurred after planar deformation. Hence, it is apparent that planar deformation applied in a direction parallel to the initial direction of the fibers, tends to deform the initial TLCP fibers into a ribbon-like structure. This may be of advantage because not only may the mechanical properties increase along the direction of the

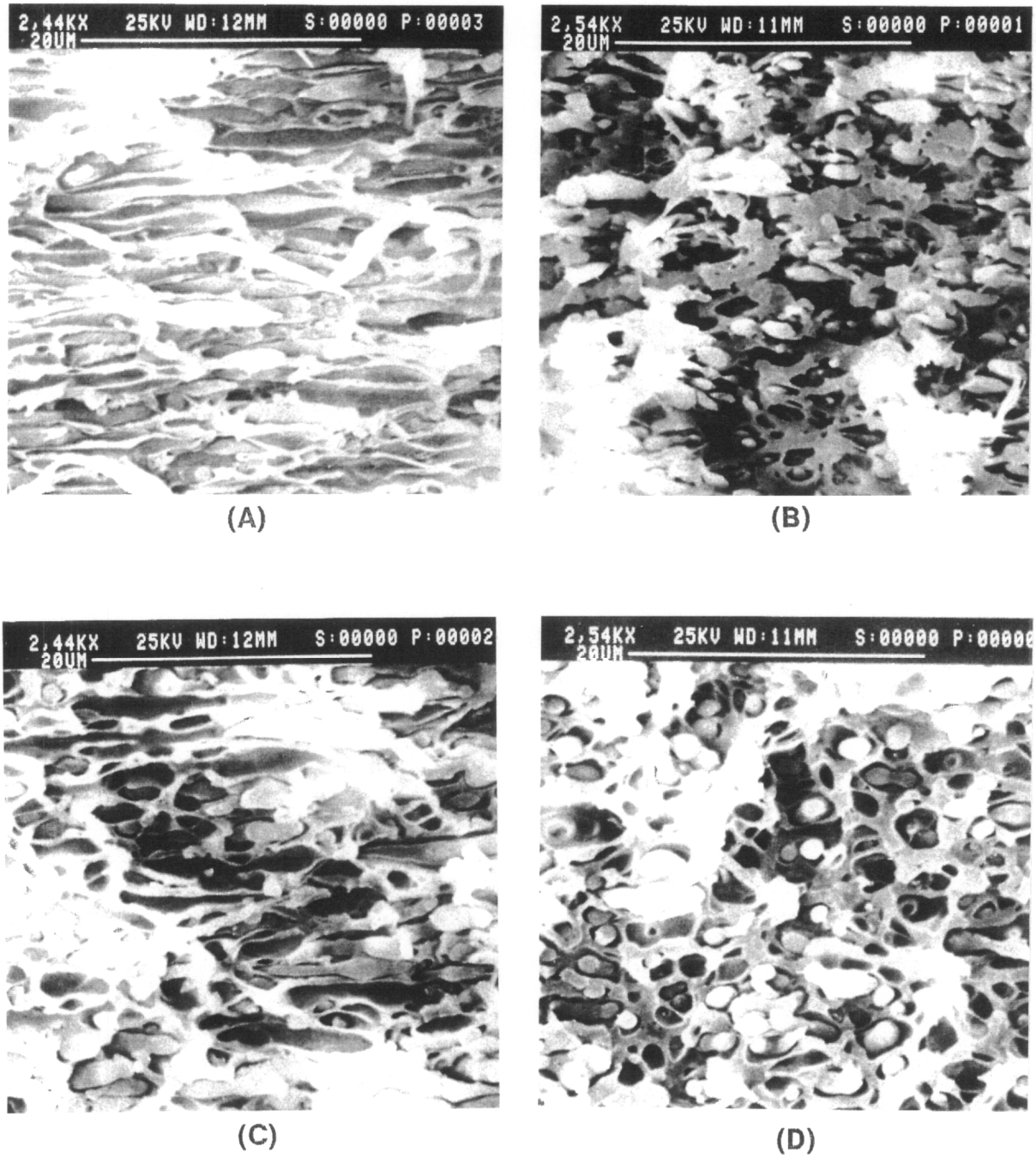

Figure 5.2. Scanning electron micrographs of a molded plaque of PEI/Vectra A 80/20 wt%. The fracture surfaces were taken parallel (a) skin and b) core) and perpendicular (c) skin and d) core) to the initial flow direction.

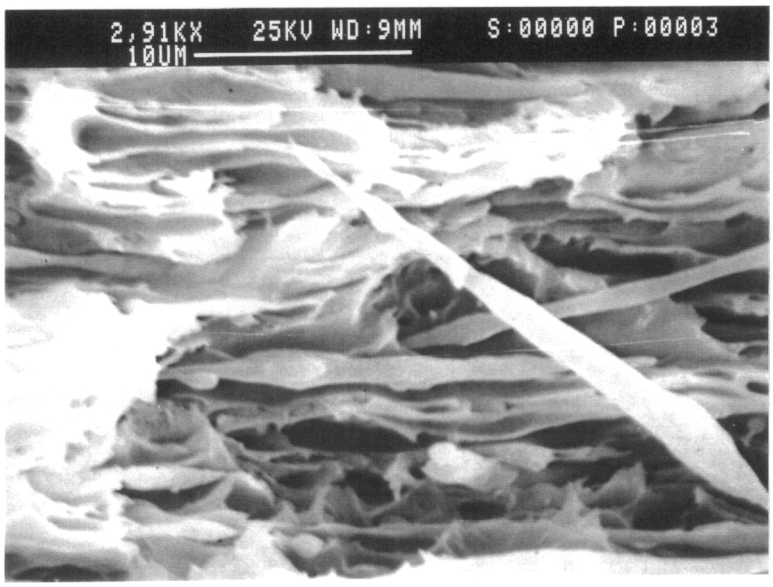

(A)

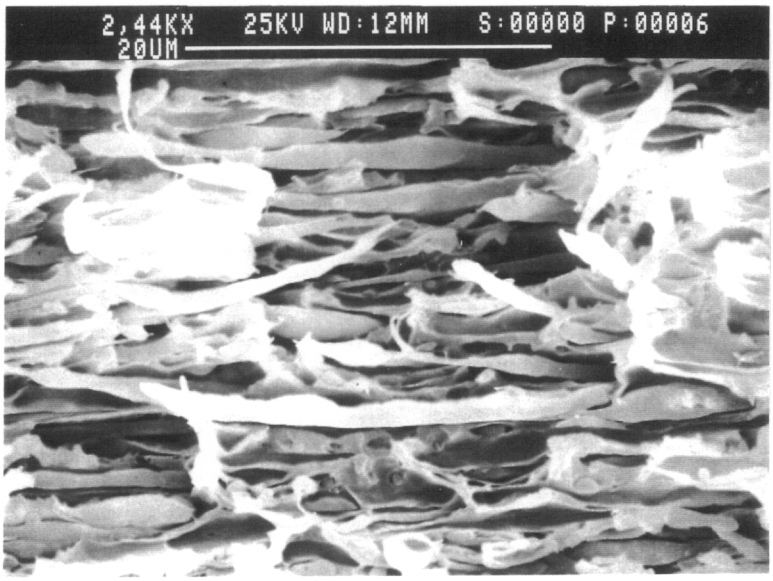

(B)

Figure 5.3. Scanning electron micrographs of a molded plaque of PEI/Vectra A 80/20 wt% after planar deformation parallel to the flow direction (constrained in the transverse direction). The fracture surfaces were taken parallel to the deformation direction: a) skin and b) core regions. ($\varepsilon_p = 0.23$ units and $T = 240°C$).

planar deformation, but also, due to the flattening of the fibers into ribbons, barrier properties may be enhanced.

The discussions thus far have illustrated the effects of planar compression molding on the morphology of PEI/TLCP blends. However, as indicated in the experimental section, injection molded plaques were also submitted to planar stretching deformation, and the results from these experiments are considered next. In Figure 5.5 is shown a scanning electron micrograph of a PEI/Vectra A 80/20 wt% blend after planar stretching along the flow direction. The fracture surface was taken perpendicular to the deformation direction. The applied planar strain was 0.5 units at an initial strain rate of 0.014 sec^{-1}. It is apparent that, even though flattening of fibers has occurred, the interfacial contact between the TLCP and the PEI matrix has worsened after planar stretching. This is indicated by the excessive fiber pull-out and voids around the TLCP phase. It is believed that the stresses generated during compression molding tend to promote fiber/matrix contact and, therefore, it is possible that interface adhesion may even be increased upon planar compression. On the other hand, the elongational stresses, due to the weakness of the PEI/Vectra A interface, tend to pull the fiber/matrix interface apart and, therefore, increasing the voids around the TLCP phase. As will be seen shortly, the method selected to apply the planar deformation, stretching or compression molding, will have a significant effect on the mechanical properties of the samples.

The effects of planar deformation, applied parallel to the initial fiber direction, on the mechanical properties of molded plaques of PEI/Vectra A 90/10 and 80/20 wt% are considered next. The morphological studies just discussed have revealed that, after planar deformation, the TLCP fibers tended to deform into high aspect ratio ribbons. That is, in addition to an increase in the aspect ratio of the TLCP fibers along the direction of the deformation, the TLCP fibers also tended to flatten in the plane of the deformation, consequently, originating a ribbon-like structure. Moreover, it seems that the TLCP fiber and PEI matrix interface is better preserved during planar compression than when planar stretching is used. The corresponding variations in the mechanical properties of the PEI/Vectra A blends as a function of TLCP concentration and mode of planar deformation are given in Table 5.1. It is apparent that after

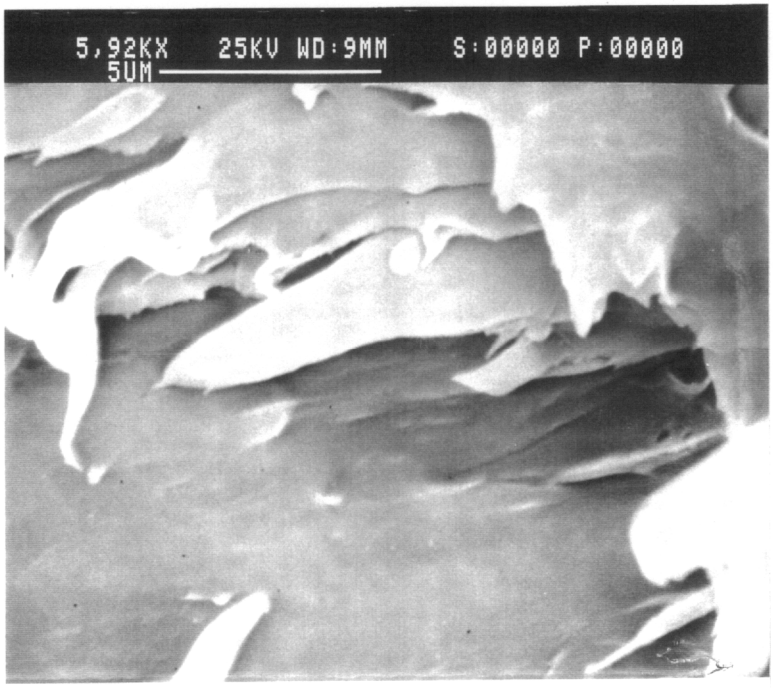

Figure 5.4. **Scanning electron micrograph of a molded plaque of PEI/Vectra A 80/20 wt% after planar compression molding parallel to the initial direction of the fibers** (constrained in the transverse direction). The fracture surface was taken in the plane of deformation ($\varepsilon_p = 0.34$ units and $T = 240°C$).

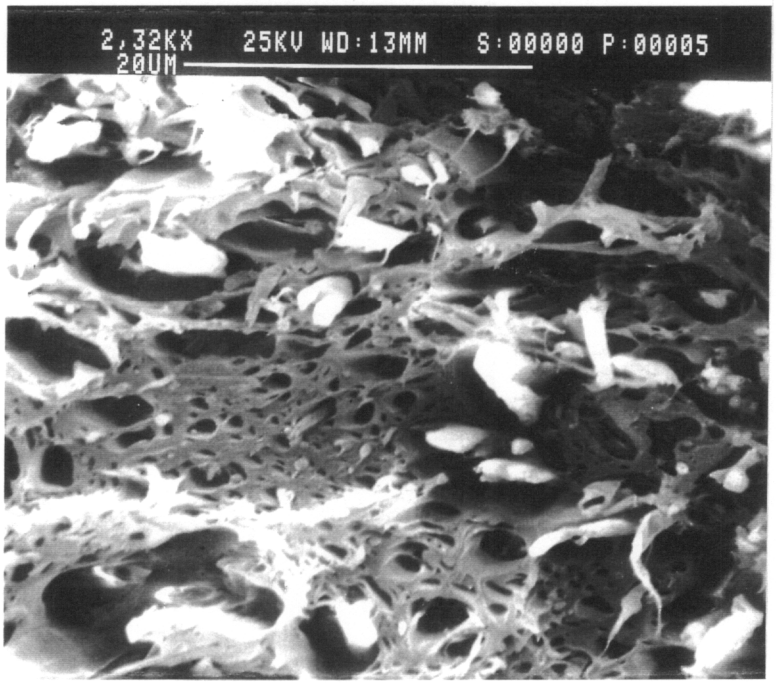

Figure 5.5. **Scanning electron micrograph of a molded plaque of PEI/Vectra A** 80/20 wt% after planar stretching parallel to the flow direction (constrained in the transverse direction). The fracture surface was taken perpendicular to the deformation direction. ($\varepsilon_p = 0.50$, $\dot{\varepsilon}_l = 0.014$ sec^{-1} and T = 240°C).

planar deformation the mechanical properties of the blends have increased considerably in the direction of the deformation. However, it seems that planar compression, in spite of the low magnitude of strains achieved, shows a greater magnitude of increase in the mechanical properties relative to planar stretching. For instance, considering the PEI/Vectra A 90/10 blend, an increase of both the tensile modulus and strength of over 35 and 45%, respectively, was achieved after 0.35 units of planar strain was applied parallel to the initial direction of the fibers. However, in the case of planar stretching, even though the magnitude of applied strain was much higher, the increase in the tensile modulus and strength was not as dramatic. After 0.50 units of planar stretching, an increase of about 15 and 30% was observed for the tensile modulus and strength, respectively. A more significant effect of the mode of applied planar deformation on the properties of the sample is seen in the elongation at break. It is evident from the values of the elongation at break obtained after deformation that a significant loss in interfacial adhesion results upon planar stretching compared to planar compression. The elongation at break of the blend is much closer to that of the neat PEI (7%) upon planar stretching than it is after planar compression. One also notices that, due perhaps to the flattening of the fibers in the plane of deformation, the mechanical properties perpendicular to the direction of the deformation have been preserved; that is, they have not substantially varied from their initial values.

In the experimental results discussed above only the effects of planar deformation applied in a direction parallel to the initial direction of the fibers have been considered. It was found that the TLCP fibrils tended to deform into high aspect ratio ribbon-like structures upon planar deformation. This contributed to an increase in the mechanical properties along the direction of the deformation while maintaining the initial transverse properties of the blend. Next, the effects of planar deformation applied in a direction perpendicular to the initial direction of the fibers on the morphology and mechanical properties of the TLCP blends are presented.

In Figures 5.6-a and b are shown scanning electron micrographs of injection molded plaques of PEI/Vectra A 80/20 wt% after planar compression molding. The direction of the

Table 5.1. Effects of planar deformation applied parallel to the initial fiber direction on the mechanical properties of molded plaques of PEI/Vectra A blends

COMPOSITION	FLOW DIRECTION PROPERTIES			TRANSVERSE DIRECTION PROPERTIES			PLANAR STRAIN
	Modulus (GPa)	Strength (MPa)	Elongation (%)	Modulus (GPa)	Strength (MPa)	Elongation (%)	
90/10	3.50 (0.20)	92.40 (2.10)	4.10 (0.30)	2.80 (0.20)	75.00 (10.30)	5.00 (0.90)	0.0
	4.69 (0.25)	131.21 (6.03)	3.98 (0.41)	3.06 (0.10)	78.01 (6.37)	3.88 (0.17)	0.35 (PC)
	4.00 (0.10)	119.82 (2.98)	6.02 (0.34)	3.32 (0.45)	72.63 (8.28)	3.58 (0.49)	0.50 (PS)
80/20	3.80 (0.10)	81.90 (3.80)	3.10 (0.40)	2.80 (0.10)	45.00 (9.10)	2.20 (0.10)	0.0
	5.30 (0.13)	132.89 (7.60)	2.73 (0.13)	2.85 (0.15)	57.35 (6.39)	2.14 (0.12)	0.42 (PC)
	4.53 (0.18)	120.05 (11.41)	3.10 (0.24)	2.45 (0.16)	47.18 (6.20)	2.62 (0.10)	0.50 (US)

Note: **Stretching Temperature: 240°C.**
PC = planar compression
PS = planar stretching
US = uniaxial stretching
Initial Strain Rate for US and PS = 0.014 sec^{-1}
(★) Standard deviations are given in parenthesis.

planar elongational flow in this case is transverse to the initial direction of the fibers; that is,the sample is constrained in the initial flow direction. The micrographs were taken from surfaces fractured perpendicular (Fig. 5.6-a) and parallel (Fig.5.6-b) to the deformation direction. A planar strain of 0.20 units was applied. It is apparent that after transverse planar deformation the TLCP fibrils originally oriented perpendicular to the compression direction have once again spread into a ribbon-like structure, as indicated in Figure 5.6-b. In addition, one observes that the initial flow direction orientation of the fibers was preserved upon deformation (Fig. 5.6-a). Therefore, it is observed that planar deformation, applied either parallel or transverse to the initial direction of the fibers, tends to deform (spread) the TLCP fibers into a ribbon-like structure. However, at comparative values of planar strain, planar deformation applied transversely to the direction of the fibers will tend to spread the fibers to a greater extent compared to planar deformation applied along the fiber direction. This is an important observation because it shows that by simply changing the relative direction of the applied planar deformation to the initial direction of the TLCP fibers, an increase in the surface area of the TLCP phase in the plane of the deformation may be achieved.

The effect of transverse planar stretching on the morphology of PEI/TLCP blends is considered next. In Figures 5.7 and 5.8 are shown, respectively, photomicrographs of injection molded plaques of PEI/Vectra A and PEI/HX1000 80/20 wt% blends subjected to transverse planar stretching. The constraint was imposed parallel to the initial direction of the fibers. The applied transverse planar strain was 0.5 units and the initial strain rate was 0.014 sec^{-1}. As one notices, a very interesting morphology has developed upon transverse planar stretching. It appears that after the deformation the TLCP droplets originally found in the center region of the molded plaque have attained a fibrillar-like structure upon transverse planar strain, as seen in Figure 5.8-b. In addition, the initial TLCP fibers, which were constrained during the deformation, tended to spread into a ribbon-like structure after transverse planar stretching. This is shown in Figure 5.7. Therefore, it appears that a morphology showing a fibrillar-like structure in both flow and transverse directions has developed after transverse planar

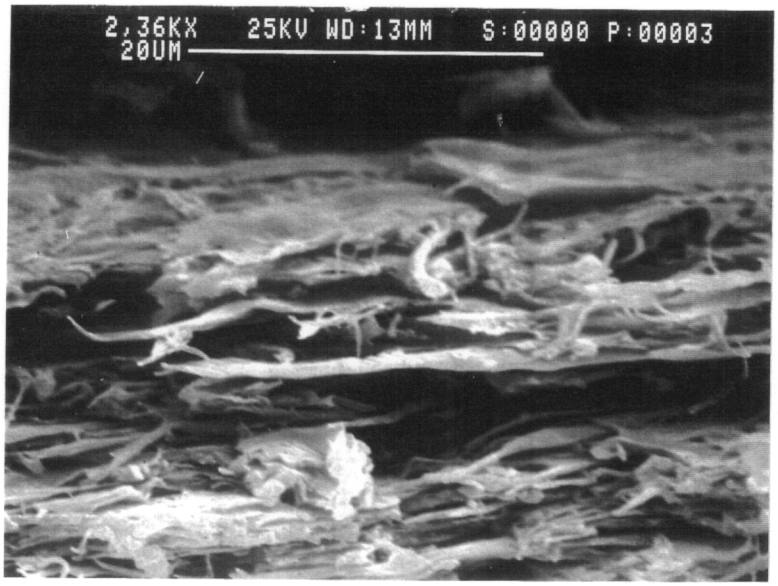

(A)

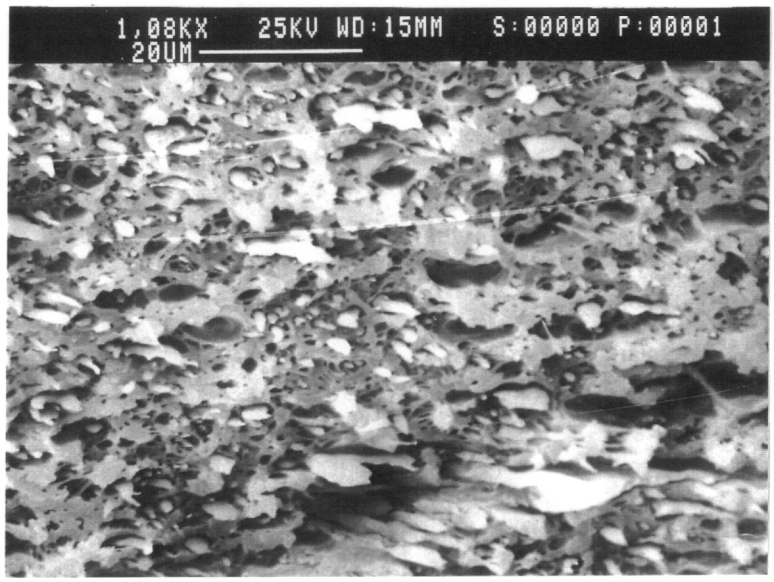

(B)

Figure 5.6. **Scanning electron micrographs of a molded plaque of PEI/Vectra A 80/20 wt% after planar compression deformation applied transversely to the initial direction of the fibers** (constrained in the flow direction). The surfaces were fractured a) perpendicular and b) parallel to the deformation direction ($\varepsilon_p = 0.20$ and $T = 240°C$).

stretching. Hence, it is expected that a good balance in the mechanical of the sample may develop after transverse planar stretching.

The effects of transverse planar stretching on the mechanical properties of molded plaques of PEI/Vectra A and PEI/HX1000 80/20 blends are presented in Tables 5.2 and 5.3, respectively. The morphological analysis just discussed has shown that after transverse planar stretching a fibrillar-like structure appears both in along and transverse to the deformation direction. Therefore, as observed from Tables 5.2 and 5.3, the variations in the mechanical properties after deformation seem to reflect the morphological changes just seen. It is apparent from the data presented in Tables 5.2 and 5.3 that a good balance in the mechanical properties has developed in the molded plaque after transverse planar stretch. One observes that, completely isotropic properties have appeared for magnitudes of transverse planar strain greater than 0.5 units. For example, at 0.75 units of strain, PEI/HX1000 80/20 blend show an isotropic tensile modulus of over 5 GPa. Therefore, planar deformation applied in a direction perpendicular to the initial TLCP fibers direction has effectively produced a material in which isotropic mechanical properties are found.

5.3.2 Extruded Sheets Subjected to Planar Deformation

The effects of planar compression molding on the morphology of extruded sheets of PEI/Vectra A and PEI/HX1000 90/10 wt% blends are presented in Figures 5.9 and 5.10, respectively. The morphology obtained in the extrusion of a PEI/Vectra A 90/10 blend is shown in Figure 5.9-a where a scanning electron micrograph of a sheet fractured along the extrusion direction is presented. The droplet morphology shown in Figure 5.9-a was obtained by extruding a sheet without any post-extrusion drawing (1). The variation in the morphology of the extruded sheets after 0.49 units of planar strain was applied is shown in Figure 5.9-b. The fracture surface was taken perpendicular to the deformation direction. It appears that, after

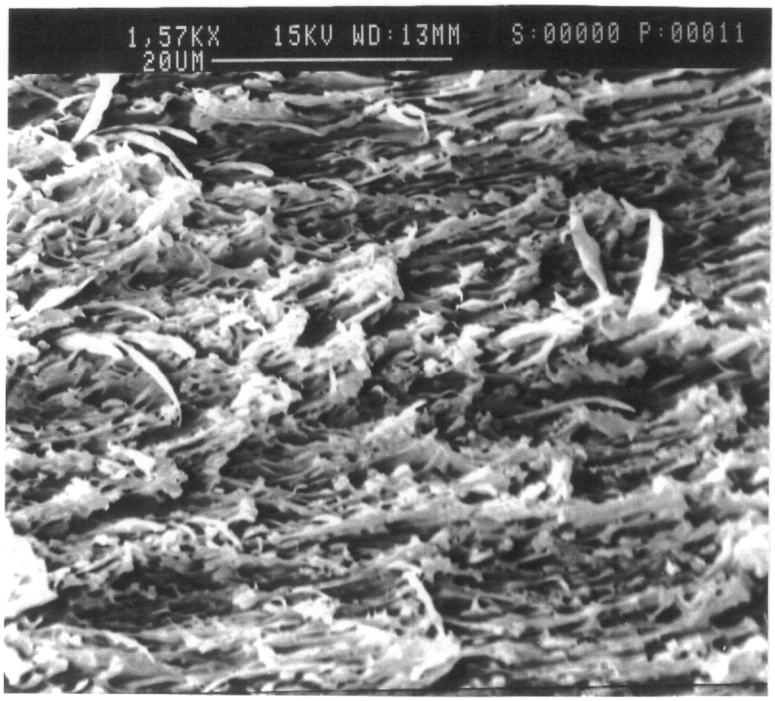

Figure 5.7. Scanning electron micrographs of a molded plaque of PEI/Vectra A 80/20 wt% after transverse planar stretching (constrained in the flow direction). The fracture surface was taken parallel to the deformation direction ($\varepsilon_p = 0.50$, $\dot{\varepsilon}_l = 0.014$ sec^{-1} and T = 240°C).

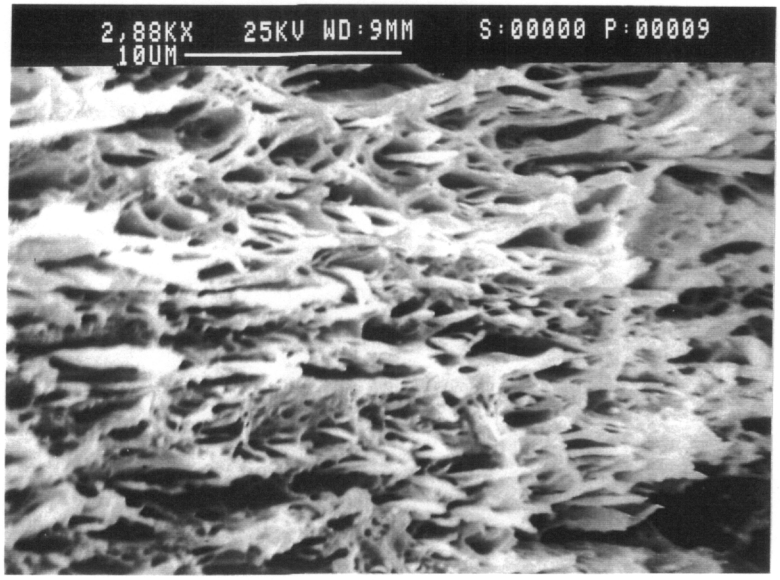

(A)

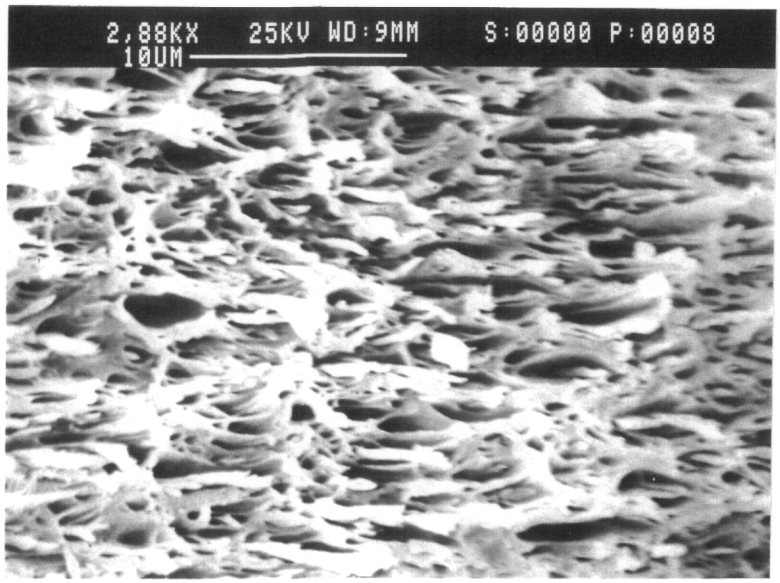

(B)

Figure 5.8. Scanning electron micrographs of a molded plaque of PEI/HX1000 80/20 wt% after transverse planar stretching (constrained in initial flow direction). The fracture surfaces were taken parallel to the stretching direction: a) skin and b) core regions ($\varepsilon_p = 0.50$, $\dot{\varepsilon}_l = 0.014$ sec^{-1} and T = 240°C).

Table 5.2. Effects of transverse planar stretching on the mechanical properties of molded plaques of PEI/Vectra A 80/20 wt%.

FLOW DIRECTION PROPERTIES			TRANSVERSE DIRECTION PROPERTIES			PLANAR STRAIN
Modulus (GPa)	Strength (MPa)	Elongation (%)	Modulus (GPa)	Strength (MPa)	Elongation (%)	
3.80 (0.10)	81.90 (3.80)	3.10 (0.40)	2.80 (0.10)	45.00 (9.10)	2.20 (0.10)	0.0
4.15 (0.35)	69.21 (8.49)	2.05 (0.17)	3.61 (0.25)	66.43 (7.79)	2.66 (0.25)	0.25
3.98 (0.61)	62.63 (8.49)	1.98 (0.11)	3.77 (0.23)	81.21 (7.12)	2.81 (0.28)	0.50
3.68 (0.17)	57.03 (2.56)	1.70 (0.10)	3.93 (0.26)	84.95 (4.32)	2.33 (0.10)	0.75

1. **The sample was constrained in the initial flow direction**
2. **Stretching Temperature: 240°C.**
3. **Initial Strain Rate: 0.014 sec^{-1}**

(★) Standard deviations are given in parenthesis.

Table 5.3 Effects of transverse planar stretching on the mechanical properties of molded plaques of PEI/HX1000 80/20 wt%.

FLOW DIRECTION PROPERTIES			TRANSVERSE DIRECTION PROPERTIES			PLANAR STRAIN
Modulus (GPa)	Strength (MPa)	Elongation (%)	Modulus (GPa)	Strength (MPa)	Elongation (%)	
5.13 (0.47)	105.36 (4.15)	2.38 (0.15)	2.84 (0.14)	57.10 (3.92)	2.57 (0.23)	0.0
6.31 (0.89)	74.21 (6.91)	1.55 (0.13)	3.75 (0.10)	67.57 (5.22)	2.31 (0.16)	0.25
5.78 (0.61)	67.16 (6.49)	1.35 (0.10)	4.14 (0.24)	67.11 (8.94)	2.26 (0.16)	0.50
5.16 (0.64)	61.59 (2.19)	1.25 (0.16)	5.05 (0.14)	78.97 (8.33)	1.87 (0.17)	0.75

1. **The sample was constrained in the initial flow direction**
2. **Stretching Temperature: 240°C.**
3. **Initial Strain Rate: 0.014 sec^{-1}**

(★) Standard deviations are given in parenthesis.

planar compression molding, the Vectra A phase which initially was in the form of droplets, spread into what seems a ribbon-like structure.

The effect of planar compression molding on the morphology of extruded sheets of PEI/HX1000 90/10 blend is discussed next. In Figures 5.10-a through c are shown the variations in the initial morphology of a PEI/HX1000 90/10 sheet as a function of planar deformation strain. It is observed that, at lower magnitudes of planar strains, the HX1000 phase, originally in the form of drops, deforms into a fibrillar-like structure, as shown is Figure 5.10-b. However, as the planar strain increases, breakup of the fibers into smaller drops is observed (Figure 5.10-c). We believe, due to the higher degree of compatibility exhibited by the PEI/HX1000 system relative to PEI/Vectra A system (1), stress induced fiber breakup may have occurred as the planar strain increased.

5.4 Conclusions

The effects of planar deformation on the structure and properties of injection molded plaques and extruded sheets of PEI/Vectra A and PEI/HX1000 have been investigated. It was found that in the case of injection molded samples, planar deformation leads to the spreading of the fibers in the plane of deformation and a ribbon-like morphological structure develops upon planar deformation. However, the extent of fiber spreading is dependent upon the relative direction of the applied planar deformation to the fiber direction. At comparative magnitudes of planar strains, it appears that transverse planar compression tends to promote a greater spreading of the fibers relative to planar stretching parallel to the initial direction of the fibers.

In the case of extruded sheets, it appears that the degree of compatibility between the PEI matrix and the TLCP phase is an important factor in affecting the morphology. For the immiscible PEI/Vectra A system, the initial TLCP drops tended to spread into a more stable

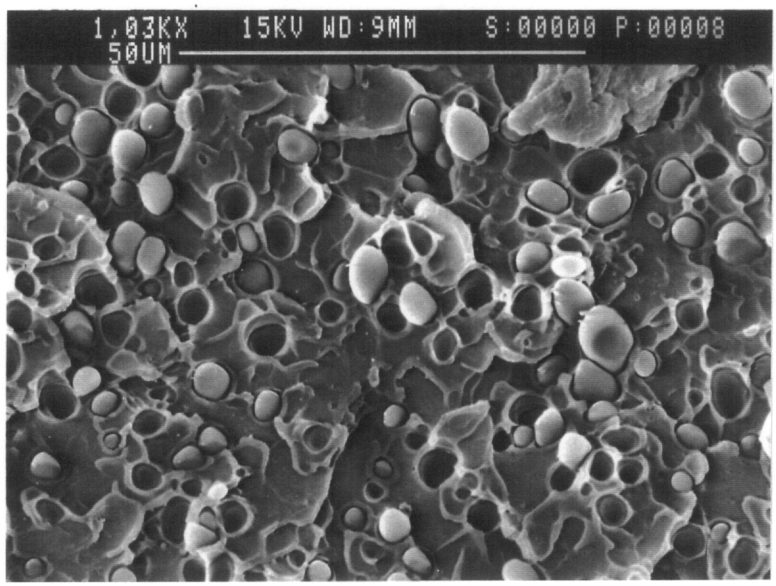

(A)

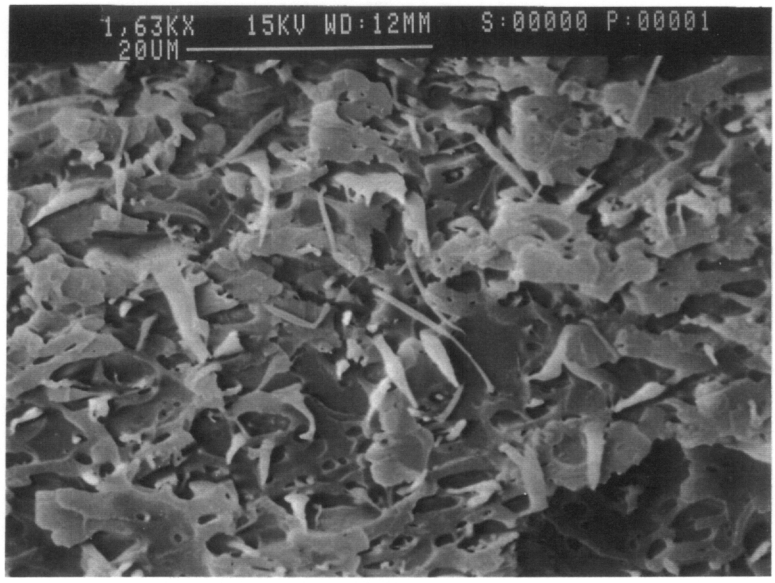

(B)

Figure 5.9. Scanning electron micrographs of extruded sheets of PEI/Vectra A 90/10 after planar compression molding at T=240°C. The fracture surfaces were taken a) parallel and b) perpendicular the deformation direction. Values of planar strains applied are: a) 0.0 and b) 0.49 units.

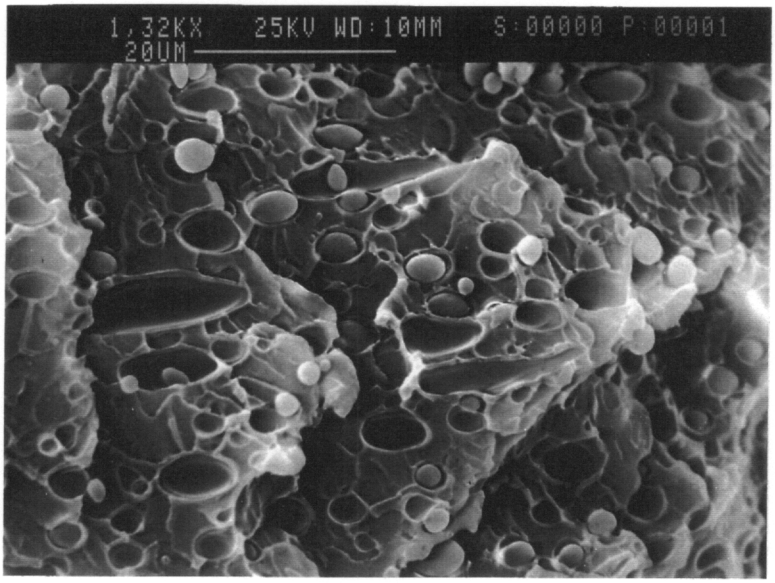

(A)

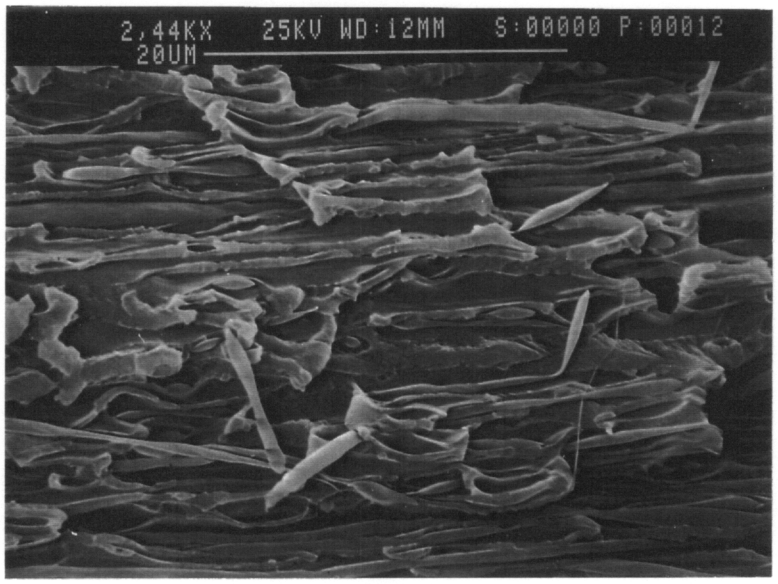

(B)

Figure 5.10. Scanning electron micrographs of extruded sheets of PEI/HX1000 90/10 after planar compression molding at T=240°C. The fracture surfaces were taken parallel to the deformation direction. Values of planar strains applied are: a) 0.0 and b) 0.21 and c) 0.53 units.

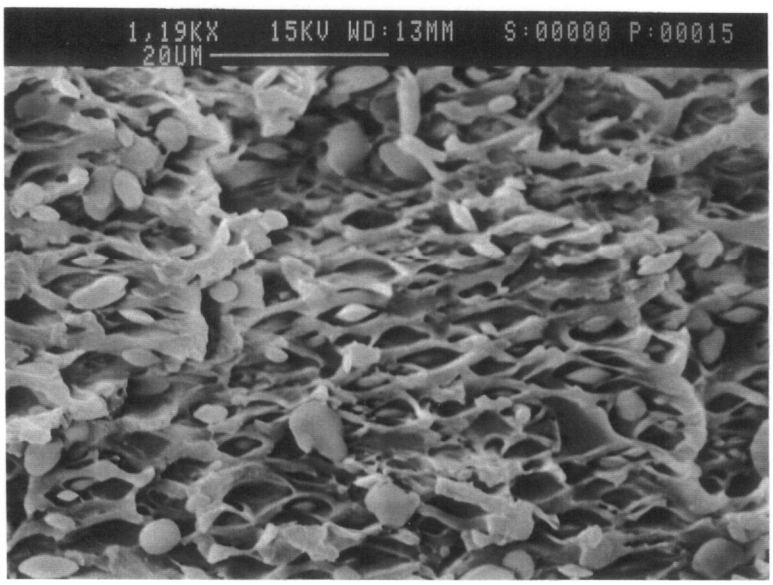

(C)

Figure 5.10. Continues

ribbon-like structure. For the partially miscible PEI/HX1000 system, stress induced fiber breakup occurred with planar strain.

In addition, it is found that planar stretching applied in a direction perpendicular to the initial direction of the TLCP fibers is effective in reducing the mechanical anisotropy of the molded plaques. PEI/Vectra A and PEI/HX1000 80/20 wt% blends showing equal properties in both flow and transverse directions were developed when planar strains, greater than 0.5 units, were applied in a direction perpendicular to the initial direction of the TLCP fibers.

5.5 *Acknowledgements*

Support from the Center for Innovative Technology of Virginia (Grant No. MAT-91-004-02) and the DuPont Company is greatly appreciated.

5.6 References

1. Chapter 4.0 of this dissertation.
2. R.B. Bird, R.C. Armstrong and O. Hassager, *Dynamics of Polymeric Liquids*, Vol. 1, 2nd. ed., Wiley-Interscience, New York (1987).
3. J.M. Dealy and K.F. Wissbrun, *Melt Rheology and its Role in Plastics Processing*, Van Nostrand Reinhold, New York (1990).
4. T. Sun, D.G. Baird, H.H. Huang, D.S. Done, and G.L. Wilkes, **J. Comp. Mat.**, 25, 788 (1991).
5. M.Y. Cao, and B. Wunderlich, **J. Polym. Sci., Polym. Phys. Ed.**, 23, 521 (1985).
6. S.S. Bafna, T. Sun, J.P. de Souza and D.G. Baird, **Polymer**, 34 (4), 708 (1993).
7. D.G. Baird, S.S. Bafna, J.P. de Souza, and T. Sun, **Polym. Comp.**, 14 (3), 214 (1993).
8. Chapter 3.0 of this dissertation.
9. E.G. Joseph, G.L. Wilkes, and D.G. Baird, **Polym. Eng. Sci.**, 25 (7), 377 (1985).
10. A.I. Isayev and M. Modic, **Polym. Comp.**, 8 (3), 158 (1987).
11. K.G. Blizard and D.G. Baird, **Polym. Eng. Sci.**, 27 (9), 653 (1987).
12. D. Beery, S. Kenig, and A. Siegmann, **Polym. Eng. Sci.**, 31 (6), 459 (1991).
13. D. Beery, S. Kenig, and A. Siegmann, **Polym. Eng. Sci.**, 31 (6), 451 (1991).
14. Q. Lin, J. Jho, and A. F. Yee, , **Polym. Eng. Sci.**, 33 (13), 789 (1993).
15. M. Kyotani, A. Kaito, and K. Nakayama, **Polymer**, 33 (22), 4756 (1992).
16. A.M. Sukhadia, D. Done, D.G. Baird, , **Polym. Eng. Sci.**, 30 (9), 519 (1990).
17. Appendix Section of this dissertation.

6.0 BIAXIAL DEFORMATION

6.1 Introduction

In the first two parts of this work, the effects of uniaxial (1) and planar (2) elongational flows on the structure and mechanical properties of molded plaques and extruded sheets of blends of thermotropic liquid crystalline polymers (TLCP) with a polyetherimide (PEI) were investigated. Experimental results led us to conclude the following. In the case of uniaxial elongation, we found that the relative direction of the applied uniaxial stretching to the initial direction of the TLCP fibers is an important factor in affecting the final morphology and mechanical properties of the blends. For injection molded plaques, in which the initial morphology is formed of both fibers and droplets, uniaxial elongation applied parallel to the direction of the fibers tends to increase the aspect ratio of the fibers and, as a result, the mechanical properties increase along the stretching direction. However, if uniaxial elongation is applied transversely to the direction of the fibers, the fibers follow the stretching and a 90° rotation is observed. A corresponding increase in the transverse properties accompanied by a decrease of the initial flow direction properties follows the realignment of the fibers upon transverse stretching. For extruded sheets, in which the initial morphology is that of drops,

a fibrillar TLCP morphology develops after uniaxial stretching and the overall mechanical properties of the sheet increase upon stretching. However, it appears that the stability of the deformed TLCP fibrils depends upon the degree of miscibility between the PEI matrix and the TLCP used. For a PEI/TLCP blend showing partial miscibility and, therefore, small value of interfacial tension, stress induced fiber breakup occurs upon stretching.

In the case of planar deformation, the tendency is for the TLPC fibers to spread into a ribbon-like structure upon planar strain. However, it seems that the extent of spreading is a function of the relative direction of the applied planar deformation to the initial direction of the fibers. The TLCP fibers spread to a higher extent when planar deformation was applied transversely to the initial direction of the fibers compared to parallel to the initial direction of the fibers. As in the case of uniaxial stretching, it appears that partial miscibility is again an important factor in affecting the final morphology of the sample. More stable ribbon-like structures were observed in the case of the immiscible PEI/Vectra A system relative to the partially miscible PEI/HX1000 system. One very important observation from the planar elongation experiments was that isotropic mechanical properties could be obtained after planar strains greater than 0.5 units were applied in a direction perpendicular to the initial direction of the TLCP fibers.

In this paper we continue with the investigations of shearfree flows and report on the effects of biaxial elongational deformation on the structure and mechanical properties of TLCP/polymer blends. The findings of this study will eventually be used to develop processing methods in which controlled morphologies and mechanical properties can be obtained. In addition, the effectiveness of biaxial deformation in reducing the mechanical anisotropy of the PEI/TLCP blends is addressed.

6.2 Experimental Procedure

6.2.1 Materials and Processing

The matrix material is a polyetherimide (PEI), commercially available as Ultem 1000 from General Electric Plastics. PEI is an amorphous engineering thermoplastic with a glass transition temperature at about 228°C and a processing temperature ranging from 330 to 365°C (3). The semicrystalline TLCP is a thermotropic copolyester commercially available as Vectra A900 from Hoechst-Celanese. Vectra A900 (henceforth referred to as Vectra A) has a glass transition temperature at 105°C and a crystal-mesophase transition at 283°C (4). The amorphous TLCP, supplied by DuPont and referred to as HX1000, has a glass transition temperature at 185°C and a processing temperature ranging from 290 to 365°C (5).

The selection of the TLCPs and engineering thermoplastic used in this work was based upon the following criteria. First, because the PEI matrix has a glass transition temperature much higher than either TLCPs, at the stretching temperature of 240°C, both the PEI matrix and the TLCPs would be deformable (1). In addition, contrary to PEI/Vectra A, PEI/HX1000 forms a partially misicible blend (6) and, due to this, PEI/HX1000 blends exhibit a higher degree of compatibility when compared to PEI/Vectra A blends. This is supported by the interfacial tension values calculated from equilibrium contact angle measurements (7). The interfacial tension for PEI/Vectra A and PEI/HX1000 pairs are, respectively, 20.80 and 7.20 mN/m. Therefore, with the use of these TLCPs in blends with PEI, the role partial miscibility on the deformation of a TLCP phase upon planar extensional flow can be assessed.

Pellets of PEI, Vectra A and HX1000 were dried at 115°C in a convection oven for at least 48 hours prior to processing. After dry blending, the physically mixed pellets of PEI/Vectra A and PEI/HX1000 blends with TLCP concentration of up to 30 wt% were injection molded into rectangular plaques and extruded into sheets. The processing conditions for the

injection molding and the extrusion processes are given elsewhere (1). With the use of injection molded plaques and extruded sheets, the effects of planar deformation on samples showing either a more fibrillar or a droplet morphology can be determined.

6.2.2 Morphological Characterization and Mechanical Properties

Morphological studies were performed by means of scanning electron microscopy (SEM). A Cambridge Stereoscan-S200 Instrument with an accelerating voltage of 25 KV was used. The samples were cryogenically fractured after immersion in liquid nitrogen for at least 5 minutes. The samples were then mounted on aluminum stubs and sputter coated with gold for enhanced conductivity.

The mechanical properties were evaluated on rectangular specimens (measuring approximately 12mm x 80mm) by means of an Instron Universal Testing Instrument, model 4204. A cross-head speed of 1 mm/min was used. The mechanical properties reported are based on measurements made on at least five samples.

6.2.3 Generation of Biaxial Elongational Deformation

The kinematics of biaxial deformation are given by the velocity field (8):

$$V_x = \frac{1}{2}\,\dot{\varepsilon}\,x \tag{6.1}$$

$$V_y = \frac{1}{2}\,\dot{\varepsilon}\,y \tag{6.2}$$

$$V_z = -\,\dot{\varepsilon}\,z \tag{6.3}$$

where $\dot{\varepsilon}$ is the strain rate. The Hencky strain in the compression direction is defined as $\varepsilon_z = \ln(\frac{H}{H_0})$, in which H and H_0 are the instantaneous and the initial thickness of the sample respectively, and in the case of equal-biaxial deformation, the strains in the plane of deformation are given by $\varepsilon_x = \varepsilon_y = \frac{\varepsilon_z}{2}$. The reported values of biaxial strain (ε_B) refer to the strains in the plane of deformation (ε_x and ε_y). Examples of polymer processing operations that may involve biaxial elongational deformation include blow molding, film blowing and vacuum forming (9).

The kinematics of biaxial deformation were experimentally generated by means of lubricated squeezing flow and step-biaxial stretching. In the case of lubricated squeezing flow two different procedures were used. First, we used lubricated compression molding with the aid of a picture frame mold. This procedure was similar to that described in a previous paper (2), however, in this case unconstrained compression molding was used. Second, we have used a parallel plates fixture mounted to the Rheometrics Mechanical Spectrometer (RMS-800).

In order to determine whether the kinematics of unconstrained compression molding were those of equal-biaxial deformation, a grid was drawn on the sample and the principal elongation ratios in the plane of deformation (λ_x and λ_y) were measured before and after compression molding. With this procedure, the true kinematics after compression could be determined. We noticed that after unconstrained compression, the extent of deformation did not truly follow equal-biaxial flow. The tendency was for the material to flow preferentially in a direction transverse to the initial direction of the fibers. Consequently, the kinematics of the deformation deviated from a true equal-biaxial deformation. With the use of the parallel plates fixture in the RMS this problem was eliminated. In the RMS, due to perhaps a perfect alignment of the plates, a true equal-biaxial deformation was obtained. However, in order to not exceed the safety limit of the transducer, lubricated squeezing compression in the RMS was performed at 265°C instead of 240°C. The increase in the temperature reduced the compression force to within the safety range of the transducer. The advantages of using the RMS were numerous. In addition to providing much better control of the test temperature, the RMS also provided a constant compression velocity of 0.00004 m/sec. Therefore, estimation of the

initial deformation rates were possible. However, the only disadvantage of using the RMS to generate equal-biaxial deformation was that very small samples (less than 1 inch in diameter) had to be used and, consequently, the variations in the mechanical properties after equal-biaxial deformation were difficult to assess. The mechanical properties reported in later section were obtained from unconstrained compression molded samples with the use of the frame-type mold. High temperature silicone oil (based on diphenyldimethyl siloxane) was used to lubricate the plates and sample surfaces in order to minimize the effects of shear flow.

Another procedure used to generate biaxial deformation was step-biaxial stretching. This procedure was similar to that of the planar stretching experiments described in a previous paper (2). However, in this case each additional step increment in strain was applied at 90° from the step before. That is, the sample would first be stretched in a direction transverse to the initial direction of the fibers, then rotated 90° and a subsequent step of 0.25 units of strain would be applied parallel to the initial direction of the fibers. Additional strain increments would follow the same procedure. The stretching temperature in this case was 240°C and the initial strain rate was 0.014 sec^{-1}.

6.3 Results and Discussions

The methodology and experimental procedure necessary to fulfil the objectives of this paper were given in the previous section. In this section the experimental results along with the analysis and interpretations are given. In order to present the results of this study as clearly as possible, this section is divided into two parts. In the first part, Section 6.3.1, the effects of biaxial deformation on the morphology of extruded sheets and injection molded plaques are presented. Following this, in Section 6.3.2, the corresponding variations in the mechanical properties after unconstrained compression molding and step-biaxial stretch are discussed.

6.3.1 Morphology Variations Upon Biaxial Flow

The effects of lubricated squeezing flow on the morphology of extruded sheets of PEI/Vectra A and PEI/HX1000 90/10 wt% blends are presented in Figures 6.1 and 6.2, respectively. The parallel plates procedure to obtain equal-biaxial deformation was the method used here. The initial morphology obtained in the extrusion of a PEI/Vectra A 90/10 blend is shown in Figure 6.1-a where a scanning electron micrograph of a sheet fractured along the extrusion direction is presented. The droplet morphology shown in Figure 6.1-a was obtained by extruding a sheet without any post-extrusion drawing (1). The effects of equal biaxial deformation on the initial morphology of the extruded sheet is shown in Figure 6.1-b. The applied biaxial strain (ε_B) was 0.39 units and the initial deformation rate ($\dot{\varepsilon}_{Bi}$) was 0.0132 sec^{-1}. The surface was fractured transversely to the initial extrusion direction. By comparing Figures 6.1-a and b, one notices that the TLCP phase initially in the form of droplets spread into what it seems a flake-like structure. Therefore, this may suggest that equal-biaxial deformation, as obtained in the RMS, tends to deform the initial drops of TLCP phase into a two dimensional disc-like structure.

We next turn our attention to the effects of equal-biaxial deformation on the morphology of extruded sheets of a PEI/HX1000 90/10 blend. In Figures 6.2-a through c are shown the variations in the initial morphology of a PEI/HX1000 90/10 sheet as a function of biaxial strain (ε_B). It is apparent that a different behavior from that of the PEI/Vectra A system is observed in this case. As one notices, increasing the biaxial strain, the HX1000 phase originally in the form of drops breaks up into much smaller drops, as shown in Figure 6.2-b and c. We believe that, due to the higher degree of compatibility exhibited by the PEI/HX1000 system relative to PEI/Vectra A system (1), stress induced fiber breakup may have occurred with biaxial strain.

The estimation of the biaxial elongational stresses during compression is presented next. In order to determine the magnitude of the elongational stresses generated during

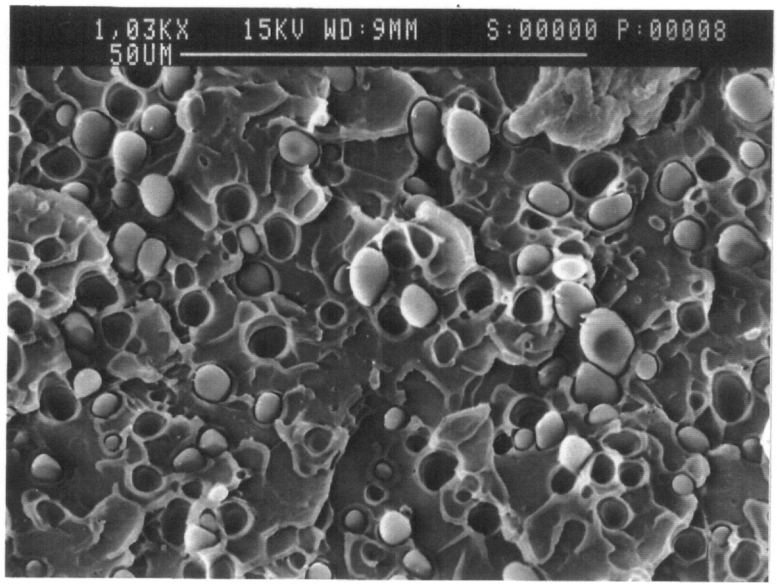

(A)

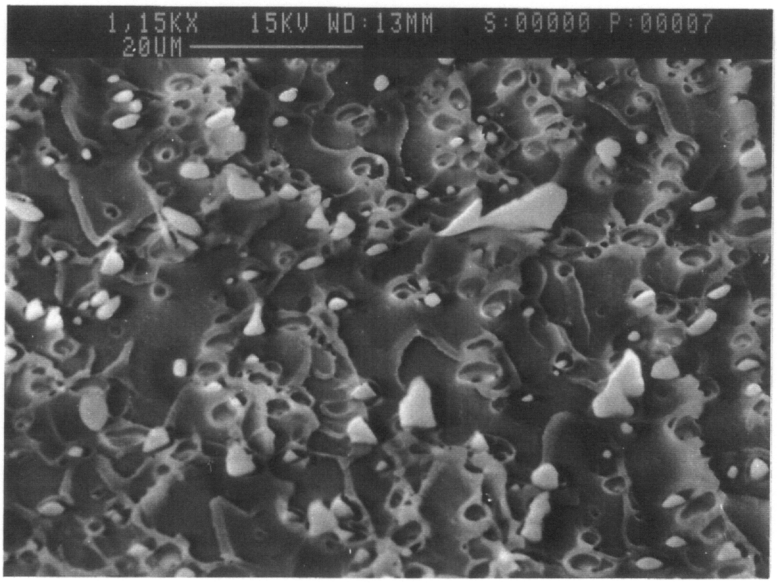

(B)

Figure 6.1. **Scanning electron micrographs of extruded sheets of PEI/Vectra A 90/10 after lubricated squeezing flow in the RMS at a temperature of 265°C.** The fracture surfaces were obtained a) parallel and b) perpendicular to the initial extrusion direction. Values of applied biaxial strains are: a) 0.0 and b) 0.39 units.

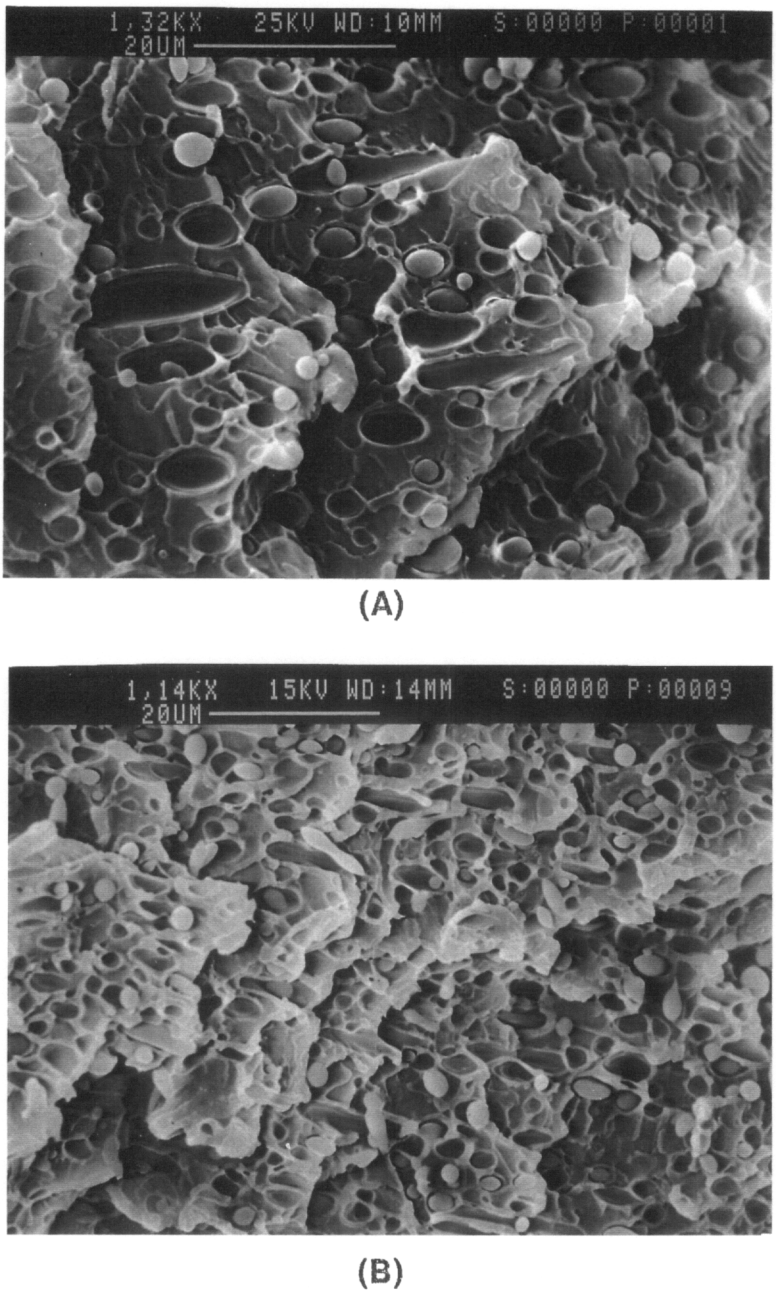

Figure 6.2. Scanning electron micrographs of extruded sheets of PEI/HX1000 90/10 after equal-biaxial deformation at T=265°C. The fracture surfaces were taken parallel to the initial extrusion direction. Values of biaxial strains applied are: a) 0.0 and b) 0.34 and c) 0.81.

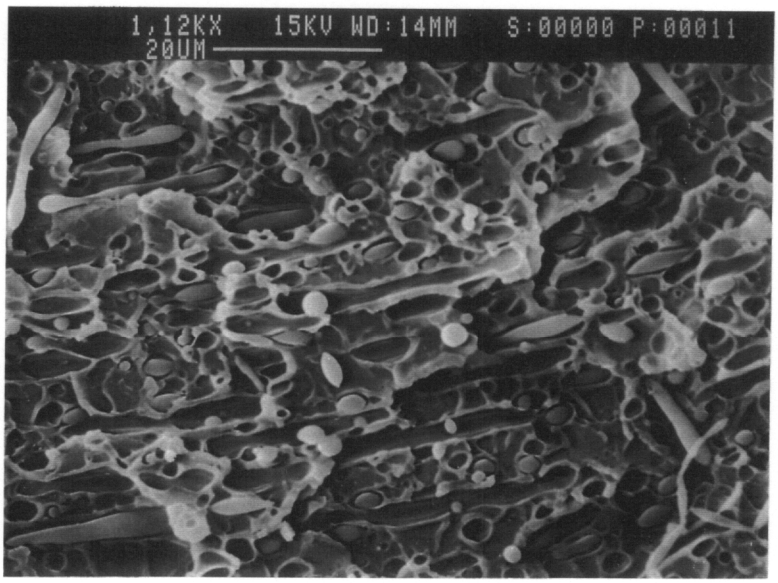

(C)

Figure 6.2. continues

compression and also to find out whether a critical stress for fiber breakup is reached in the case of the PEI/HX1000 system the following calculations are performed. It should be pointed out that, due to the lack of a more specific theory for droplet deformation and breakup in TLCP systems, the theories of droplet deformation for Newtonian fluids are used. From the theories of droplet deformation and break up for Newtonian fluids, it is known that a critical shear or elongational stress must be reached for fiber breakup to occur (10-14). According to Taylor (10) the critical shear stress at which breakup will occur is given by:

$$\tau = \frac{\sigma}{2a}\left(\frac{16\lambda + 16}{19\lambda + 16}\right) \tag{6.4}$$

where τ is the shear stress, σ is the interfacial tension, a is the droplet diameter, and λ is the viscosity ratio of the dispersed phase to the matrix phase.

Assuming that the relationship shown in Eq. 6.4 may be applied to the equal-biaxial deformation discussed here, the critical biaxial elongational stress for breakup may be written as:

$$\sigma_B = \frac{\sigma}{2a}\left(\frac{16\lambda + 16}{19\lambda + 16}\right) \tag{6.5}$$

where σ_B is the biaxial elongation stress defined as $\sigma_B = \eta_B \dot{\varepsilon}_B$, in which η_B is the biaxial elongational viscosity and $\dot{\varepsilon}_B$ is the biaxial strain rate. In the limit of small strain rates, linear viscoelastic behavior is usually observed and the biaxial elongational viscosity of a material may be approximated as $\eta_B = 6\eta_0$, in which η_0 is the zero shear viscosity. Thus, we assume that the biaxial viscosity of the blend components at 265°C may be given by $\eta_B(\dot{\varepsilon}) = 6\eta(\dot{\gamma})$. Therefore, η_B for PEI, Vectra A and HX1000 were estimated as 1.8, 9.0 and 9.0 MPa.sec. Additionally, the dispersed phase particle size is also needed in the calculations. Based upon the morphological structures shown in Figures 6.1-a and 6.2-a, the average droplet diameter the the Vectra A and HX1000 phases are, respectively, 4.42 and 3.20 μm. Thus, taking in consideration the above assumptions, the critical biaxial elongational stress (σ_{Bc}) for fiber breakup in the PEI/Vectra A and PEI/HX1000 systems were calculated as 2.03 and 0.97 KPa,

respectively. During the biaxial compression experiments, the biaxial elongational stresses generated during compression were of the order of 1.19 KPa. Thus, it is apparent that during the compression experiments in the RMS, the biaxial stresses generated during compression were greater than the critical stresses required for breakup of the HX1000 phase in the PEI/HX1000 system. In the case of the PEI/Vectra A system, the biaxial stresses generated during the experiments were below the critical elongational stress necessary for breakup. Therefore, one may attribute to stress induced structure breakup the reason for the morphological variations observed upon compression molding of PEI/Vectra A and PEI/HX1000 blends.

As discussed in the experimental procedure section, the kinematics generated during unconstrained compression molding in where a picture-frame mold was used were not truly equal-biaxial. The tendency during the compression was for a slightly preferred flow in a direction transversely to the initial direction of the fibers. However, due to fact that these samples were used for mechanical properties evaluations, it is important to discuss the variations in the sample's morphology after unconstrained compression molding, and this is done next.

The morphology obtained after unconstrained compression molding of an extruded sheet of PEI/HX1000 90/10 blend is shown in Figure 6.3. It is apparent that due to the tendency of the material to flow preferentially in one direction, the HX1000 phase, which were originally in the form of drops, has deformed into a fibrillar structure instead of the disc-like structure observed in equal-biaxial deformation. This clearly illustrates that the morphology attained by the TLCP phase upon processing is very sensitive to the flow kinematics the material is subjected to. Therefore, one observes that the control of the flow kinematics during processing is a very important factor in affecting the final morphology of a TLCP/polymer blend.

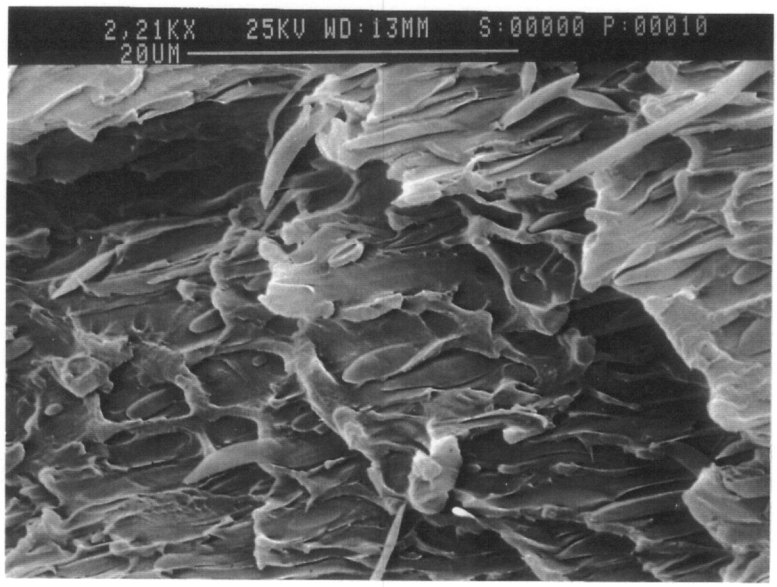

Figure 6.3. Scanning electron micrograph of an extruded sheet of PEI/HX1000 90/10 blend after unconstrained compression molding. The fracture surface was taken perpendicular to the initial extrusion machine direction. The strain applied was 0.23 units at a temperature of 240°C.

6.3.2 Effects of Biaxial Deformation on the Mechanical Properties

The effects of unconstrained compression molding and step-biaxial stretching on the mechanical properties of molded plaques and extruded sheets of PEI/Vectra A and PEI/HX1000 blends are presented in this section. However, even though unconstrained compression molding experiments were performed on molded plaques and sheets with TLCP concentration of up to 30 wt%, the discussions presented here will concentrate primarily on a few representative samples. Additional compositions may be found elsewhere (15).

The effects of unconstrained compression molding on the mechanical properties of molded plaques of PEI/Vectra A and PEI/HX1000 80/20 blends are presented in Tables 6.1 and 6.2, respectively. However, due to the fact that the kinematics of the deformation were not truly of equal-biaxial elongation, both biaxial elongational strains in the plane of deformation, ε_x and ε_y, are included in the Tables. Thus, the deformation history undergone by the sample upon unconstrained compression can be easily identified. It is apparent that the initial mechanical properties presented by the molded plaques is highly anisotropic; that is, the properties along the direction of the fibers (shown as flow direction properties) are much greater than the properties transverse to the direction of the fibers. As one notices after unconstrained compression, the mechanical properties transverse to the initial direction of the fibers have increased considerably. For example, the initial transverse direction tensile strengths for PEI/Vectra A and PEI/HX1000 80/20 were about 45 and 57 MPa, respectively. After unconstrained compression the transverse tensile strength of the blends increased to 63 and 73 MPa, respectively; that is, an increase in the transverse tensile strength of about 40 and 28%. One also notices that no significant changes in the flow direction properties of the blends has occurred upon unconstrained compression. The values of mechanical properties before and after compression are essentially identical. We believe that this may be attributed to the inhomogeneity of the deformation, as indicated by the inequality of the values of ε_x and ε_y.

Table 6.1. Effects of Unconstrained Compression Molding on the Mechanical Properties of Injection Molded Plaques of PEI/Vectra A 80/20 blend.

FLOW DIRECTION PROPERTIES			TRANSVERSE DIRECTION PROPERTIES			STRAIN
Modulus (GPa)	Strength (MPa)	Elongation (%)	Modulus (GPa)	Strength (MPa)	Elongation (%)	(ε_x/ ε_y)
3.80 (0.10)	81.90 (3.80)	3.10 (0.40)	2.80 (0.10)	45.00 (9.10)	2.20 (0.80)	0.0/0.0
3.64 (0.22)	80.02 (6.90)	2.30 (0.28)	2.70 (0.04)	58.33 (2.89)	2.38 (0.22)	0.11/0.14
3.78 (0.20)	79.30 (7.68)	2.06 (0.12)	2.96 (0.04)	63.09 (1.78)	2.48 (0.28)	0.28/0.33

Unconstrained compression molding at 240°C.
(★) Standard deviations are given in parenthesis.

Table 6.2. Effects of Unconstrained Compression Molding on the Mechanical Properties of Injection Molded Plaques of PEI/HX1000 80/20 blend

FLOW DIRECTION PROPERTIES			TRANSVERSE DIRECTION PROPERTIES			STRAIN (ε_x/ ε_y)
Modulus (GPa)	Strength (MPa)	Elongation (%)	Modulus (GPa)	Strength (MPa)	Elongation (%)	
5.13 (0.47)	105.36 (4.15)	2.38 (0.15)	2.84 (0.14)	57.10 (3.92)	2.57 (0.23)	0.0/0.0
4.54. (0.29)	93.57 (5.96)	2.24 (0.22)	2.90 (0.07)	52.79 (2.74)	2.00 (0.14)	0.09/0.12
5.16 (0.26)	94.90 (9.13)	1.87 (0.19)	2.96 (0.18)	67.33 (7.09)	2.65 (0.34)	0.14/0.17
5.10 (0.16)	78.18 (5.18)	1.53 (0.12)	3.20 (0.13)	73.10 (7.10)	2.70 (0.33)	0.21/0.25

Unconstrained compression molding at 240°C.
(★) Standard deviations are given in parenthesis.

The effects of unconstrained compression molding on the mechanical properties of extruded sheets of a PEI/HX1000 90/10 blend are presented in Table 6.3. It is apparent that the initial mechanical properties of the extruded sheets, in spite of lower values, show a much lower degree of mechanical anisotropy than the injection molded plaques. After biaxial deformation, both machine and transverse direction properties increase with biaxial strain. However, one notices that the magnitude of the increase in the mechanical properties of the extruded sheets corresponds well with the magnitude of the applied strain in the plane of deformation. It is apparent that the tendency of the mechanical properties of the sheets after unconstrained compression molding is towards a more isotropic behavior compared to that observed for the injection molded plaques.

The effects of step-biaxial stretching on the mechanical properties of injection molded plaques of PEI/Vectra A and PEI/HX1000 80/20 blends are shown in Tables 6.4 and 6.5, respectively. The samples were first stretched transversely to the initial direction of the fibers, followed by a subsequent stretch parallel to the initial direction of the fibers. Therefore, the biaxial strain indicated in the Tables reflect the magnitude of elongational strain each sample experienced in both flow and transverse directions. It is apparent that the overall mechanical properties of the molded plaques increased as the step-biaxial strain increased. However, a greater increment in the mechanical properties is observed for the PEI/HX1000 system compared to the PEI/Vectra A system. For example, an increase of over 34% in the flow and transverse directions tensile moduli of the PEI/HX1000 was observed after 0.50 units of strain. In the case of the PEI/Vectra A system, a much less significant improvement in the mechanical properties was observed.

Table 6.3. Effects of Unconstrained Compression Molding on the Mechanical Properties of Extruded Sheets of PEI/HX1000 90/10 blend

FLOW DIRECTION PROPERTIES			TRANSVERSE DIRECTION PROPERTIES			STRAIN
Modulus (GPa)	Strength (MPa)	Elongation (%)	Modulus (GPa)	Strength (MPa)	Elongation (%)	($\varepsilon_x/\varepsilon_y$)
3.29 (0.25)	98.65 (2.12)	4.04 (0.40)	3.10 (0.37)	95.80 (3.61)	3.20 (0.19)	0.0/0.0
3.40 (0.30)	99.55 (2.55)	4.67 (0.35)	3.28 (0.16)	100.19 (5.61)	4.04 (0.28)	0.08/0.11
4.41 (0.29)	101.64 (9.15)	2.60 (0.28)	3.96 (0.30)	98.52 (4.40)	3.53 (0.20)	0.21/0.24

Unconstrained compression molding at 240°C.
(★) Standard deviations are given in parenthesis.

Table 6.4. Effects of Step-Biaxial Stretching on the Mechanical Properties of Injection Molded Plaques of PEI/Vectra A 80/20 blend

FLOW DIRECTION PROPERTIES			TRANSVERSE DIRECTION PROPERTIES			STRAIN
Modulus (GPa)	Strength (MPa)	Elongation (%)	Modulus (GPa)	Strength (MPa)	Elongation (%)	
3.80 (0.10)	81.90 (3.80)	3.10 (0.40)	2.80 (0.10)	45.00 (9.10)	2.20 (0.80)	0.0
4.54 (0.22)	100.23 (11.25)	2.61 (0.25)	2.76 (0.16)	58.07 (3.53)	2.68 (0.25)	0.25
4.55 (0.14)	119.65 (6.90)	3.40 (0.37)	2.62 (0.28)	68.45 (3.36)	3.60 (0.36)	0.50

1. **Step-Biaxial Elongation (90°/0°), 0.25 strain/step**
2. **Stretching Temperature: 240°C.**
3. **Initial Strain Rate: 0.014 sec^{-1}**

(★) Standard deviations are given in parenthesis.

Table 6.5. Effects of Step-Biaxial Stretching on the Mechanical Properties of Injection Molded Plaques of PEI/HX1000 80/20 blend

FLOW DIRECTION PROPERTIES			TRANSVERSE DIRECTION PROPERTIES			STRAIN
Modulus (GPa)	Strength (MPa)	Elongation (%)	Modulus (GPa)	Strength (MPa)	Elongation (%)	
5.13 (0.47)	105.36 (4.15)	2.38 (0.15)	2.84 (0.14)	57.10 (3.92)	2.57 (0.23)	0.0
6.83 (0.37)	102.74 (9.27)	1.73 (0.10)	3.52 (0.44)	69.34 (7.46)	2.28 (0.22)	0.25
7.00 (0.39)	129.03 (9.85)	1.93 (0.27)	3.76 (0.19)	65.68 (2.59)	1.47 (0.18)	0.50

1. **Step-Biaxial Elongation (90°/0°), 0.25 strain/step**
2. **Stretching Temperature: 240°C.**
3. **Initial Strain Rate: 0.014 sec^{-1}**

(★) Standard deviations are given in parenthesis.

6.4 Conclusions

The effects of biaxial elongational flow on the structure and properties of injection molded plaques and extruded sheets of PEI/Vectra A and PEI/HX1000 were investigated. It was found that in the case of extruded sheets, equal-biaxial deformation tended to deform the TLCP phase, which initially was in the form of drops, into a two dimensional disc-like structure. However, it appeared that the extent of the deformation was a function of the elongational stress generated during compression. For the PEI/HX1000 system the elongational stresses generated during compression exceeded the critical elongational stress for fiber breakup and breakup of the dispersed HX1000 phase into much smaller drops were observed. In the case of the PEI/Vectra A system, the elongational stresses during compression were below the critical stresses for breakup and the Vectra A phase deformed into a flake-like structure.

In the case of unconstrained compression molding, the inhomogeneity of the deformation caused the TLCP phase to deform into a fibrillar structure rather than the flake-like structure observed in the equal-biaxial deformation. In terms of mechanical properties, it was observed that the magnitude of increase in the properties followed the variaions in the elongational strains in the plane of deformation. Nevertheless, for extruded sheets, unconstrained compression molding tended to induce isotropy in the mechanical properties compared to molded plaques.

6.5 Acknowledgements

Support from the Center for Innovative Technology of Virginia (Grant No. MAT-91-004-02) and the DuPont Company is greatly appreciated.

6.6 References

1. Chapter 4.0 of this dissertation.
2. Chapter 5.0 of this dissertation.
3. T. Sun, D.G. Baird, H.H. Huang, D.S. Done, and G.L. Wilkes, **J. Comp. Mat.**, 25, 788 (1991).
4. M.Y. Cao, and B. Wunderlich, **J. Polym. Sci., Polym. Phys. ed.**, 23, 521 (1985).
5. S.S. Bafna, T. Sun, J.P. de Souza and D.G. Baird, **Polymer**, 34 (4), 708 (1993).
6. D.G. Baird, S.S. Bafna, J.P. de Souza, and T. Sun, **Polym. Comp.**, 14 (3), 214 (1993).
7. Chapter 3.0 of this dissertation.
8. R.B. Bird, R.C. Armstrong and O. Hassager, *Dynamics of Polymeric Liquids*, Vol. 1, 2nd. ed., Wiley-Interscience, New York (1987).
9. J.M. Dealy and K.F. Wissbrun, *Melt Rheology and its Role in Plastics Processing*, Van Nostrand Reinhold, New York (1990).
10. G.I. Taylor, **Proc. Roy. Soc.**, A146, 501 (1934)
11. G.I. Taylor, **Proc. Roy. Soc.**, A138, 41 (1932)
12. G.I. Taylor, **Proc. Roy. Soc.**, A226, 289 (1954)
13. R.G. Cox, **J. Fluid Mech.**, 37 (3), 601 (1969).
14. Appendix section of this dissertation.

STRUCTURE DEVELOPMENT AND MECHANICAL PROPERTIES OF IN SITU THERMOPLASTIC COMPOSITES SUBJECTED TO THERMOFORMING CONDITIONS

to be submitted to **Polymer Engineering and Science**

7.0 THERMOFORMING OF IN SITU THERMOPLASTIC COMPOSITES

7.1 Introduction

Thermotropic liquid crystalline polymers (TLCPs) are materials with sufficient molecular rigidity to form a mesophase above the crystalline melting point. This is a phase which is intermediate to the solid crystalline and the isotropic liquid state. In this mesophase phase, the molecules are aligned in a preferential direction, called the director. Different types of mesophases can be distinguished. The most familiar are (1,2): nematic (molecules that possess only orientational order), smetic (molecules that possess orientational and positional orders) and cholesteric (local scale order similar to nematic, but on a larger scale the structure appear to be formed by twisting a series of parallel nematic layers, resulting in a periodic helical structure). The existence of the mesophase leads to a combination of properties that are both of scientific and technological importance (3,5).

One of the most important features of TLCPs is their ability to orient during flow. This very important feature offers the possibility of generating materials with outstanding me-

chanical properties in the direction of the orientation (6). TLCPs are processed in conventional polymer processing operations into parts with excellent stiffness and strength. They can be spun into high strength/high stiffness fibers with typical tensile moduli in the range of 40 to 100 GPa and tensile strengths of up to 1 GPa (6-12). They can be injection molded into stiff parts with tensile moduli of over 20 GPa (13-15) and can be even blow molded (16). In addition to their high stiffness and strength, TLCPs also offer a host of other attractive properties such as high use temperatures, excellent chemical resistance, low melt viscosity, low coefficient of thermal expansion, good dielectric properties and heat stability (17).

The remarkable combination of properties exhibited by TLCPs has motivated the development of thermoplastic composites in where the TLCP phase, under adequate processing conditions, deforms in situ into fibrils that may reinforce the thermoplastic matrix (18-22). The aspects of the development of in situ composites based upon the addition of a TLCP to a polyetherimide (PEI) subjected to injection molding conditions have been recently investigated. It was found that TLCPs may be used as an effective reinforcement to PEI. An increase in the tensile modulus and tensile strength of the PEI upon addition of the TLCP phase was observed (22).

In a series of studies presented recently, the effects of shearfree elongational flows on the morphology and corresponding mechanical properties of in situ composites based on blends of a polyetherimide with an amorphous and a semicrystalline TLCP were investigated (23-25). It was shown that under uniaxial elongation conditions the dispersed TLCP phase could be deformed into high aspect ratio fibers that reinforced the thermoplastics matrix (23). On the other hand, planar elongational deformation tended to deform the TLCP phase into an elongated ribbon-like structure (24), and equal-biaxial deformation tended to impart a disc-like morphology to the dispersed TLCP phase (25). In addition, it was observed that shearfree elongational flows, specially transverse planar elongation, were effective in reducing the mechanical anisotropy of molded plaques of TLCP based composites. Values of flow and transverse tensile moduli greater than 5.0 GPa were obtained when planar deformation was applied in a direction transversely to the initial direction of the fibers (25).

Most of the recent investigations in the processing of TLCP/polymer blends are concerned primarily with the development of in situ composites in the areas of either fiber spinning or injection molding. Very little attention is being placed on the development of TLCP/polymer blends in processes such as blow molding, compression molding and thermoforming. In these processes elongational flows usually prevails which, as many studies have pointed out (26-30), are very effective in deforming the dispersed TLCP phase into reinforcing fibrils. In this study, the use of TLCP based in situ composites in the thermoforming process is explored. A comparison of the thermoforming performance between in situ and glass fiber reinforced composites is performed which will illustrate the advantages of using in situ composites relative to glass reinforced composites in the thermoforming process. However, before discussing the results of this study, a brief review of the literature concerning with the use of thermoplastic composites in the thermoforming process is presented.

Thermoforming can be described as a processing technique in which a heat softened polymer sheet is subjected to a pressure differential causing the sheet to deform to the definition of a mold (31). In most thermoforming operations, the thermoplastic sheet is heated to a temperature above its glass transition temperature in order to render the material to a soft or rubbery state. Due to the relative low pressure requirements which leads to reduced tooling costs, thermoforming offers an advantage over competitive processes such as injection molding, blow molding and rotational molding. A detailed description of the many processing techniques and process technology may be found elsewhere (31,32).

Very limited are the studies dealing with the use of fiber reinforced composites in the thermoforming process (33-37). Furthermore, most of this studies have only used APC-2 (a carbon fiber reinforced poly(ether ether ketone) (PEEK)-based composite) as the thermoforming material (33-35). In the thermoforming of fiber reinforced composites, it is found that it is particularly important to avoid compressive stresses which can induce either buckling or breakage of the fibers (33). Very limited extensional deformations can be applied during forming due to the small elongation to break of the reinforcing fibers. Exceeding this limit may induce failure and permanent damages are observed in the formed article. More-

over, composite laminates have the tendency to delaminate during thermoforming and therefore requiring reconsolidation. In such cases the cycle is usually extended to account for the reconsolidation of the material. Forming cycles in the excess of 10 minutes have been reported in the thermoforming of APC-2 composites (33).

Therefore, considering the forming problems of fiber reinforced composites briefly discussed above, it is of technological advantage to develop a system in where the reinforcing phase can be either preserved or generated during forming which would maintain or even enhance the mechanical integrity of a formed article. In this paper, the thermoforming of thermoplastic composites in which the reinforcing phase is developed from a liquid crystalline polymer is investigated. The structure development and mechanical properties of in situ composites in the thermoforming process are reported. The main goal of this study is to illustrate the potential of in situ composites in thermoforming applications. Additionally, a comparison of the thermoforming performance of situ and glass reinforced composites is presented.

7.2 Experimental Procedure

7.2.1 Materials and Processing

The matrix material used is a polyetherimide (PEI), commercially available as Ultem 1000 from General Electric Plastics. PEI is an amorphous engineering thermoplastic with a glass transition temperature at about 228°C and a processing temperature ranging from 330 to 365°C (38). The semicrystalline TLCP used was a thermotropic copolyester composed of 73 mol% of p-hydroxybenzoic acid and 27 mol% of 2-hydroxy-6-naphthoic acid. This TLCP is commercially available as Vectra A900 from Hoechst-Celanese. Vectra A900 (henceforth re-

ferred to as Vectra A) shows a glass transition temperature at about 105°C, a crystal-mesophase transition at 283°C (39), and a maximum stable processing temperature of 370°C (38). The amorphous TLCP, supplied by DuPont, is based on hydroquinone (HQ), terephthalic acid (TA) and other hydroquinone derivatives. This amorphous TLCP, referred to as HX1000, has a glass transition temperature at about 185°C (40) and a processing temperature ranging from 290 to 365°C. Proposed chemical structures for these TLCPs may be found elsewhere (41).

Before blending, pellets of the above materials were dried at 115°C in a convection oven for at least 48 hours. The dried pellets of PEI/Vectra A and PEI/HX1000 were then tumbled in a steel container on a weight percent (wt%) basis. The mixed pellets were then injection molded into rectangular plaques (measuring approximately 75mm x 85mm x 1.75mm) using an Arburg 221-55-250 Allrounder Injection Molder. The temperature settings of the injection molding unit were 330, 345, 360, and 360°C for zones 1, 2, and 3 of the barrel and nozzle, respectively. The injection pressure was set at 7.0 MPa with a holding pressure of 3.5 MPa. The injection speed was set at a medium range, which gives a volumetric flow rate of 12 cm^3/sec. The mold was held at 110°C and a cooling time of 40 sec was used. The processing conditions were kept constant throughout all moldings.

Sheets of PEI/Vectra A and PEI/HX1000 blends were extruded utilizing a 2.54 cm (1 inch) diameter single screw extruder. A 10.16 cm (4 inches) wide film die was used. The sheets were extruded without any post-extrusion drawing. The objective was to obtain a sheet in which only undeformed droplets of the TLCP phase would be found. The extruder temperature settings were 290, 310, 315, 315, 230 and 245°C for zones 1, 2, 3, clamp ring, adaptor and die, respectively. The extruder speed was set at 12.4 RPM. The melt temperature and pressure, measured at the screw head, were 334°C and 1410 psi, respectively.

7.2.2 Thermoforming

Thermoforming of extruded sheets and injection molded plaques was performed using a Hydro-Trim Corporation model Labform II-B thermoformer. The machine essentially consists of two (top and bottom) vertically movable platens driven pneumatically. Between the platens, a horizontal movable clamp frame is located, which can slide in and out of an infrared oven. The oven is equipped with two 24inx18in planar heaters, each comprising of twenty-four 1in wide resistive strip heaters.

During thermoforming operation, the sample is clamped onto the clamping frame. The entire clamping assembly then slides into the oven, which is maintained at a preset temperature. For uniform heating of the sample, the heating surfaces are equidistant (about 4in) from the top and bottom of the sample. After a predetermined heating time (pre-heating) in the oven, the clamping frame slides out and locates itself between the mold halves. The soften sheet is then formed by closing the mold halves. After a predetermined cooling time (holding time), the mold is then opened and the part removed. Silicone oil was used to lubricated the mold surfaces in order to minimize friction at the mold walls. Thus, assuming a perfect slip condition at the mold walls, the maximum elongational strain upon forming will appear at the bottom of the formed tray. Two 0.75inx1.5in molds having depths of draw of 1/2in (0.70 maximum strain) and a 1in (1.10 maximum strain) were used in the experiments. All the experiments were carried out with a mold temperature of 110°C.

One of the most important and probably the most difficult aspect in the thermoforming process is the selection of the optimum pre-heating temperature. The material has to be heated until it becomes pliable enough to be effectively shaped while avoiding overheating which may result in sagging. From dynamic mechanical thermal analysis (DMTA) (23) it is found that the PEI/TLCP blends used in this study would reach a rubbery plateau at temperatures above the glass transition temperature of the PEI matrix (228°C). It is also noticed from the DMTA results that the rubbery plateau in these blends spans for about 35°, up to 265°C.

Above this temperature, the presence of viscous flow is detected. Therefore, considering the rubbery plateau (as detected in the DMTA tests) as the optimum thermoforming temperature for the PEI/TLCP blends, a thermoforming window ranging from about 230 to 265°C exists at which forming may be accomplished successfully. In order to determined the infrared oven operation temperature and pre-heating time, a mathematical model based on a one-dimensional heat transfer with a radiation heat flux at the sample surface was used. The model uses a finite difference scheme and predicts the temperature profile (nodal values) across the thickness of the sample as it is being heated (42). From the mathematical analyzes, it was found that an oven temperature of 280°C would be necessary to bring the sample to an optimum forming temperature of around 240°C with a pre-heating time of 90 sec. By selecting this condition, the temperature gradient across the thickness of the sample was minimized. The predictions of the numerical simulations may be found in the appendix.

7.2.3 Stretch-Thermoforming Process

The basic steps of a conventional thermoforming process, as describe in 7.2.2, are followed it the stretch-thermoforming process. This procedure, however, takes advantage of the sliding movement of the clamping assembly to impart an additional uniaxial stretching to the sample as it slides out of the infrared oven just prior to the closing of the mold halves. A photograph of the modified clamping assembly designed to perform the stretch-thermoforming process is shown in Figure 7.1. The pre-stretching, applied additionally to the deformation inherent to the thermoforming process, is applied by sliding the guiding rods outwards and positioning them at the desired strain position (the sample is stretched from both ends). The guiding rods are mounted independently from of the clamping assembly. One end of the rod is placed inside the infrared oven (mounted on a metallic crossbar) and the other is mounted on a wooden ruler marked with the strain positions. Pre-stretching strains of as high as 1.10 units are possible to be applied with this technique. The advantage of the stretch-

thermoforming process compared to conventional thermoforming process is that it not only enables the pre-stretching of the sample prior to forming, which would lead to the deformation of the TLCP phase into reinforcing fibrils, but also allows the combination of the relative directions of strains applied during the pre-stretching and the one inherent to the thermoforming process which would lead to a large range of morphological and mechanical properties variations that can be developed with the method.

7.2.4 Morphological Characterization

The morphology of the thermoformed parts was investigated by means of scanning electron microscopy (SEM). A Cambridge Stereoscan-S200 Instrument with an accelerating voltage of 25 KV was used. The samples were cryogenically fractured after immersion in liquid nitrogen for at least 5 minutes. The samples were then mounted on aluminum stubs and sputter coated with gold for enhanced conductivity.

7.2.5 Mechanical Properties

Due to the reduced size of the thermoformed trays, it was not possible to perform any conventional mechanical testing on the thermoformed samples. However, a mechanical testing procedure was designed, shown in Figure 7.2, in where the deflection resistance (measured as applied load over sample thickness) of the thermoformed samples could be assessed. The load was applied at a descending cross-head speed of 1 mm/min, utilizing an Instron Universal Testing Instrument, model 4204. A probe having a 1/2 in diameter head was used as the indenter. The applied load was monitored as a function of crosshead displacement. Failure was characterized by the appearance of cracks on the surface of the sample (picked

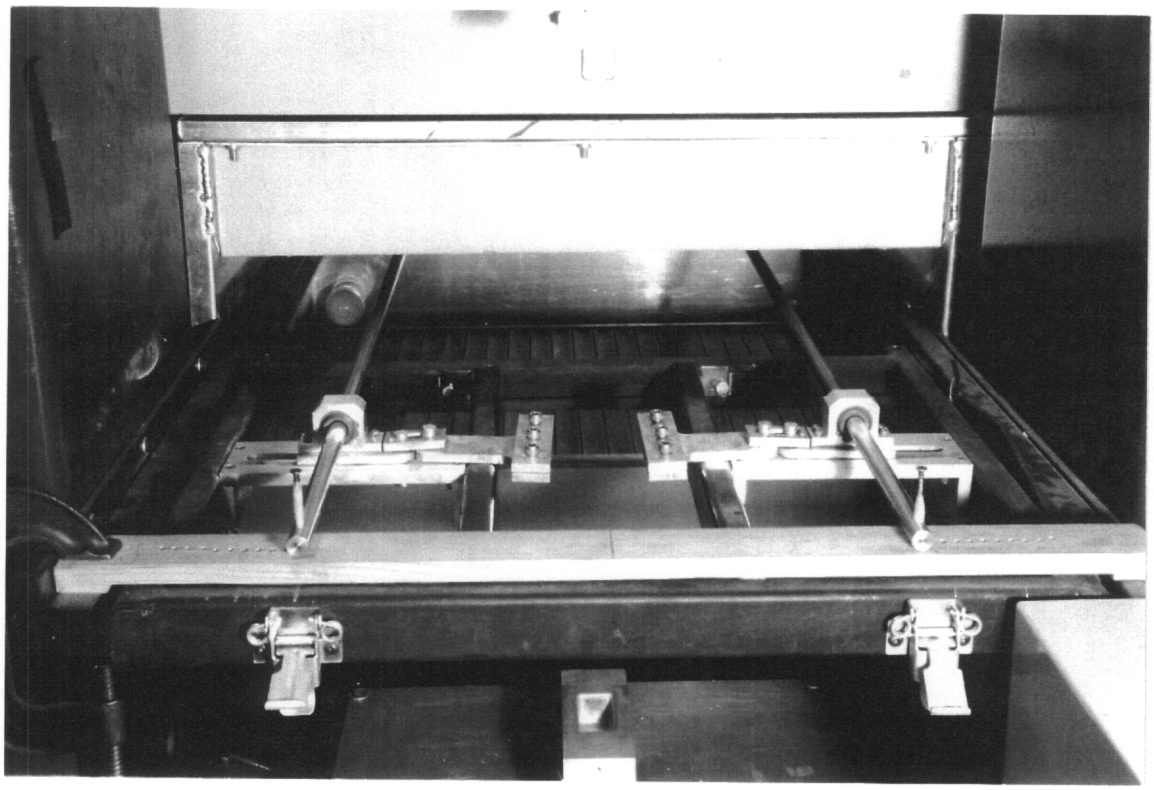

Figure 7.1. Photograph of modified clamping assembly for stretch-thermoforming process.

up by monitoring the variation in the applied load as a function of displacement). The maximum load was then normalized to give the deflection resistance per unit of sample thickness.

7.3 Results and Discussions

The methodology and experimental procedure used to fulfill the objectives of this paper have been discussed in the last section. In this section, the experimental results along with the analysis and discussions will be presented. To make the following discussions as clear as possible, this section has been divided into two main parts. First, in Section 7.3.1 a comparison of the thermoforming performance of glass reinforced PEI and PEI/TLCP blends is presented. Following this, in Section 7.3.2, results from the stretch-thermoforming process are discussed. It should be pointed out, however, that thermoforming experiments were successfully conducted on both PEI/Vectra A and PEI/HX1000 blends with TLCP concentrations of up to 30 weight percent, including both shallow and deep molds. Above this concentration, rupture of the samples, especially at large depths of draw, was observed. The following discussions will concentrate only on a few representative compositions.

7.3.1 Thermoforming Performance of PEI composites

To determine the thermoforming performance of PEI composites, forming studies on molded plaques of both PEI reinforced with 10 wt% glass fibers and an in situ composite based on a PEI/Vectra A 80/20 wt% blend were carried out. The plaques were clamped in such a way that the initial direction of the fibers in the molded sample (oriented in the injection molding flow direction) would remain aligned in parallel to the principal drawing (forming) direction. The results of these experiments are discussed next.

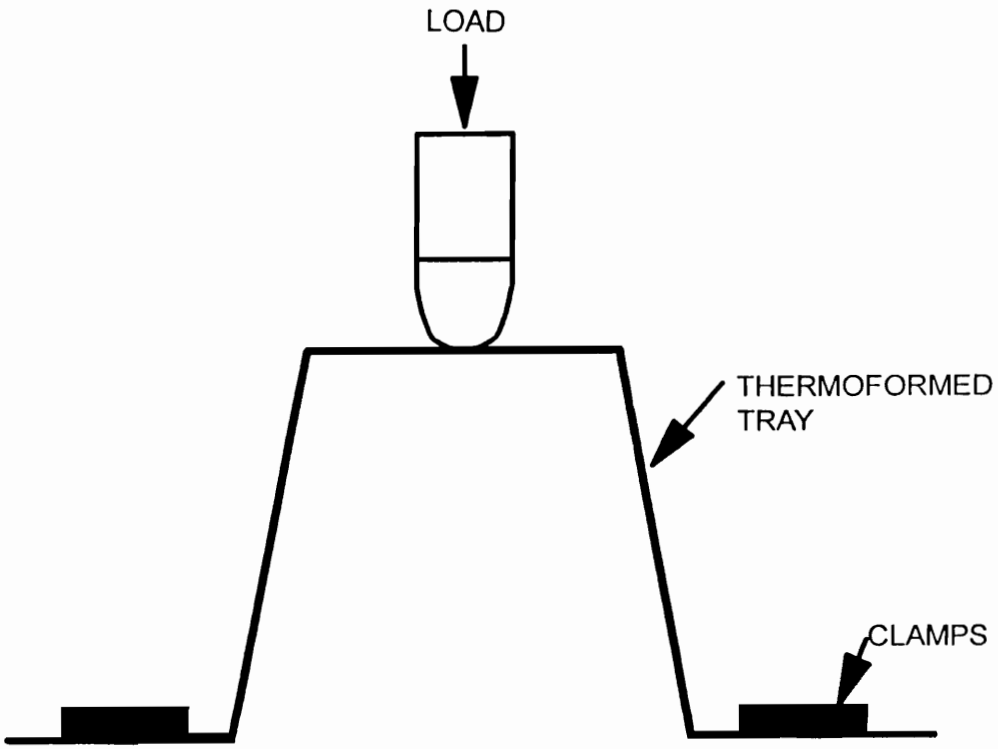

Figure 7.2. Sketch of Deflection Test used to assess the mechanical performance of thermoformed samples.

The effect of thermoforming on the structure of a glass reinforced PEI composite is shown in Figure 7.3, by a scanning electron micrograph obtained from a fracture surface of a formed plaque of PEI reinforced with 10 wt% glass fibers. The fracture surface was parallel to the forming direction and the photograph was taken from an area around the corner of the formed tray (90° bend). As one clearly notices, breakage of the glass fibers upon forming has occurred around the corners of the mold. The breakage of the glass fibers may be associated with the lack of ductility of the glass fibers. As the material has to deform and extend as it is being drawn down to the shape of the mold, the stresses generated during the deformation may exceed the bending stresses limit of the glass fibers and breakage of the glass fibers is observed (especially around the corners of the mold). It is possible that the breakage of the fibers may lead to the appearance of weak points at critical places in the thermoformed part, like for instance around corners and bends. Therefore, in terms of mechanical performance it is possible that reduced impact properties may result because of the breakage of the glass fibers.

On the other hand, a very different scenario has taken place in the thermoforming of a PEI reinforced with 20wt% Vectra A. The structure developed during the thermoforming of PEI/Vectra A 80/20 blend is illustrated in a series of micrographs presented in Figure 7.4. As one notices, as the elongational strains during forming increased the dispersed TLCP phase, which initially was in the form of drops (Fig. 7.4-a), deformed into very long fibrils (easily observed at high values of strain). Furthermore, it seems that the aspect ratio of the TLCP fibrils increased as a function of depth of draw. Therefore, this may suggest that, contrary to glass reinforced PEI in where a weak point, due to the breakage of the glass fibers, may develop upon forming, the mechanical performance of formed articles based on in situ composites may be enhanced upon forming. Another important observation from these experiments is that the elongational strains inherent to the thermoforming process are very effective in deforming the TLCP phase into fibrils, even though the starting morphology of the TLCP phase is that of droplets.

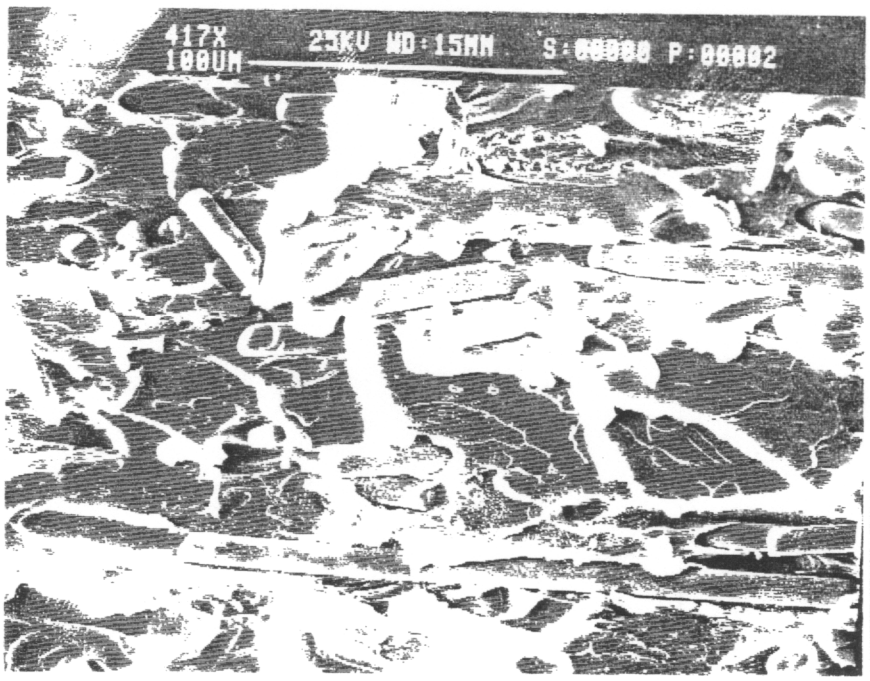

Figure 7.3. Scanning electron micrograph of a fracture surface of a thermoformed plaque of PEI reinforced with 10 wt% glass fibers. The micrograph was taken from a region around the corner of the formed tray (depth of draw = 1/2in).

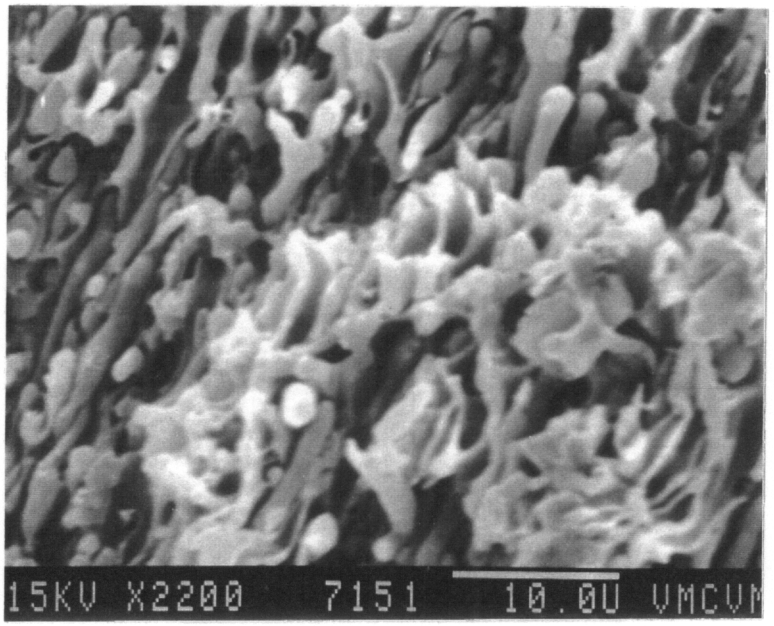

(A)

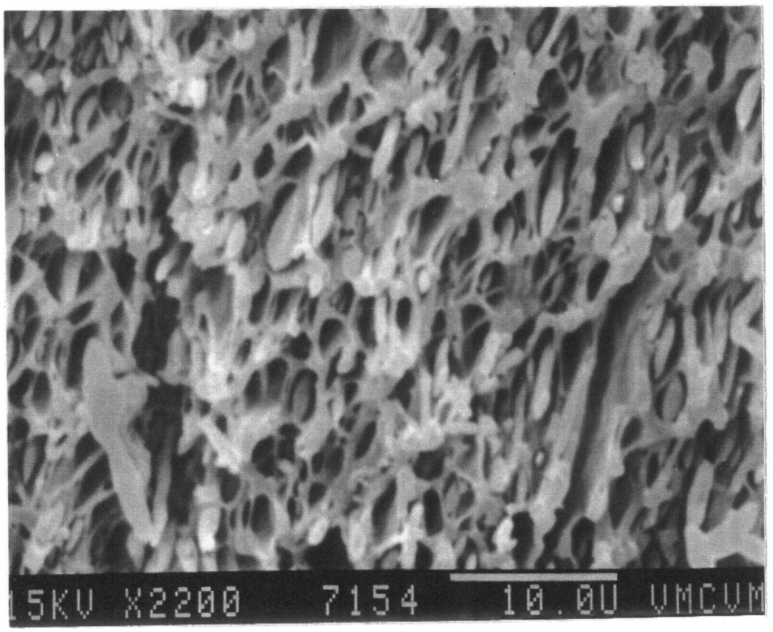

(B)

Figure 7.4. **Scanning electron micrographs of fracture surfaces of thermoformed plaques of PEI/Vectra A900 80/20 composition ratio.** The series of micrographs illustrate the structure developed during the thermoforming of the in situ composite as a function of strain: a) 0.0, b) 0.063, c) 0.31 and d) 0.50.

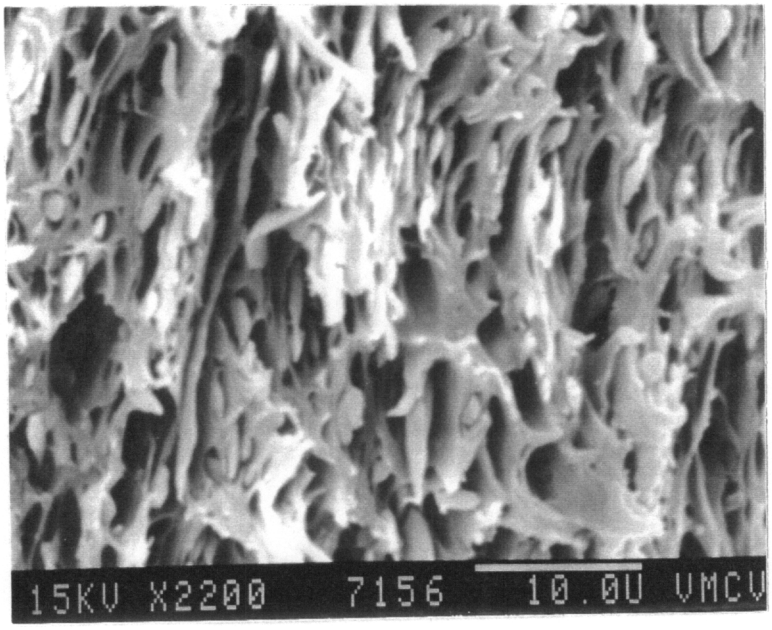

(C)

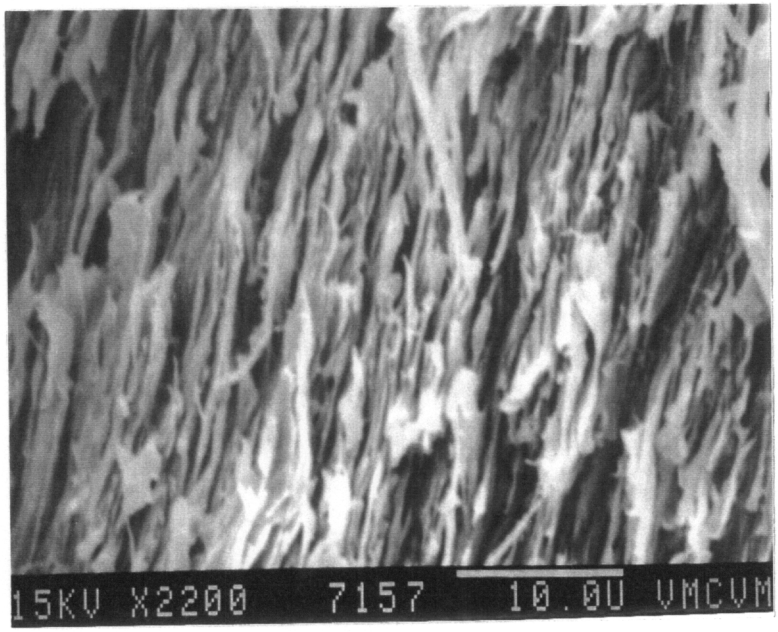

(D)

The effects of thermoforming on the structure of an in situ composite are better illustrated in the following example. In the thermoforming of molded plaques of in situ composites, in which the initial morphology of the TLCP phase is in the form of fiber and drops, the relative direction of the TLCP fibers with respect to the forming direction is an important factor in controlling the final structure of the TLCP phase. For instance, if the initial direction of the TLCP fibers is parallel to the principal drawing direction, the elongational strains generated upon forming will tend to elongate the fibers even more and an increase in the fibers aspect ratio may be expected. This is illustrated in Figure 7.5, in where a PEI/Vectra A 80/20 wt% blend was thermoformed with the initial Vectra A fibers lined up parallel to the drawing direction. However, if the TLCP fibers are lined up transversely to principal drawing direction, the elongational strains generated during forming will tend to deform the TLCP phase into a ribbon like structure, as it is shown in Figure 7.6. Therefore, one clearly notices that depending on the final application of a thermoformed article, it is possible to obtain a morphological structure that best suits application needs. Either elongated fibers can be obtained to improve mechanical properties or even a ribbon-like morphology can be obtained to improve barrier properties in formed articles.

In summary, it is clear from the experiments just discussed that several advantages exit in the thermoforming of in situ thermoplastic composites compared to glass fibers composites. The elongational strains during forming tend to deform the TLCP phase into fibers that, contrary to glass fibers that break upon forming, may lead to the enhancement in the mechanical properties of thermoformed articles. Another important observation is the fact that depending on the relative direction of the TLCP fibers with respect to the forming direction, the TLCP fibers can either increase in aspect ratio or spread into a ribbon-like structure. This is a very important finding because it shows that the process can be easily tailored to fulfil the needs of a particular application.

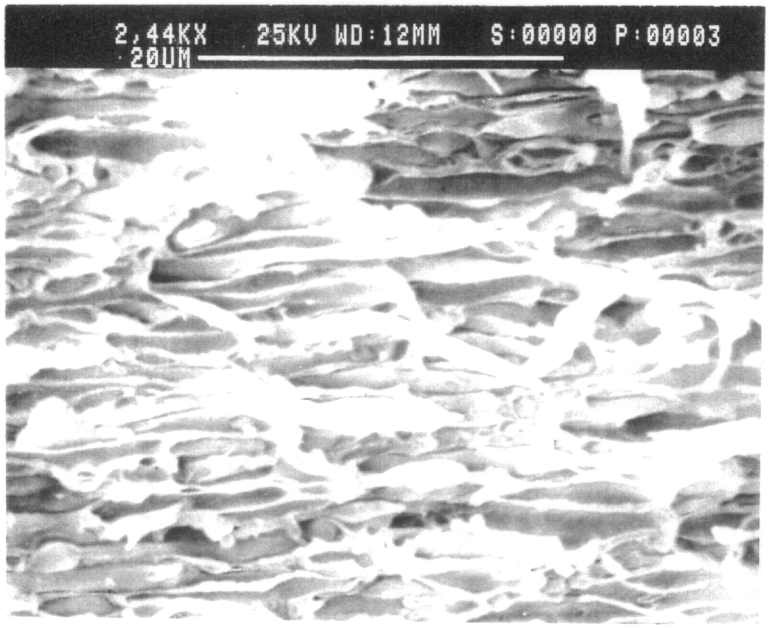

(A)

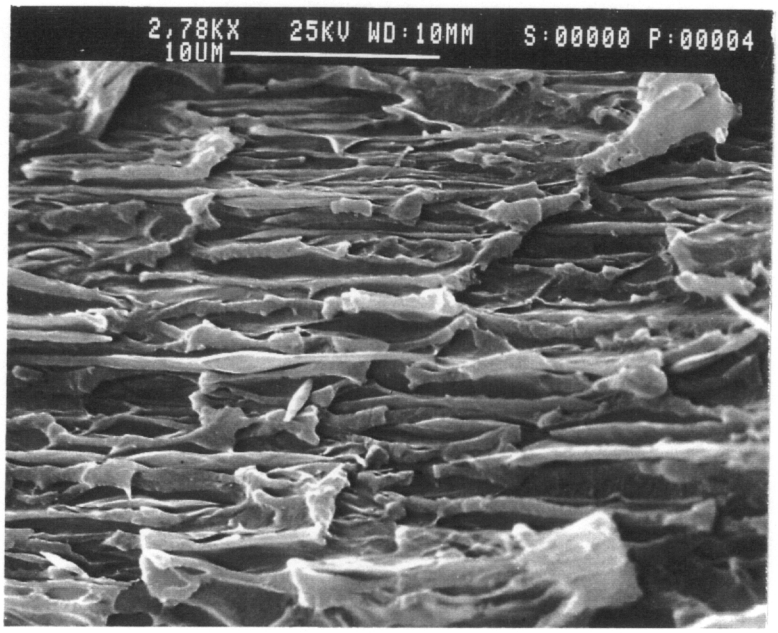

(B)

Figure 7.5. **Scanning electron micrographs of fractured surfaces of thermoformed plaques of PEI/Vectra A900 80/20 wt% blend.** The TLCP fibers were lined up parallel to the drawing direction: a) as molded and b) after forming (depth of draw = 1 in).

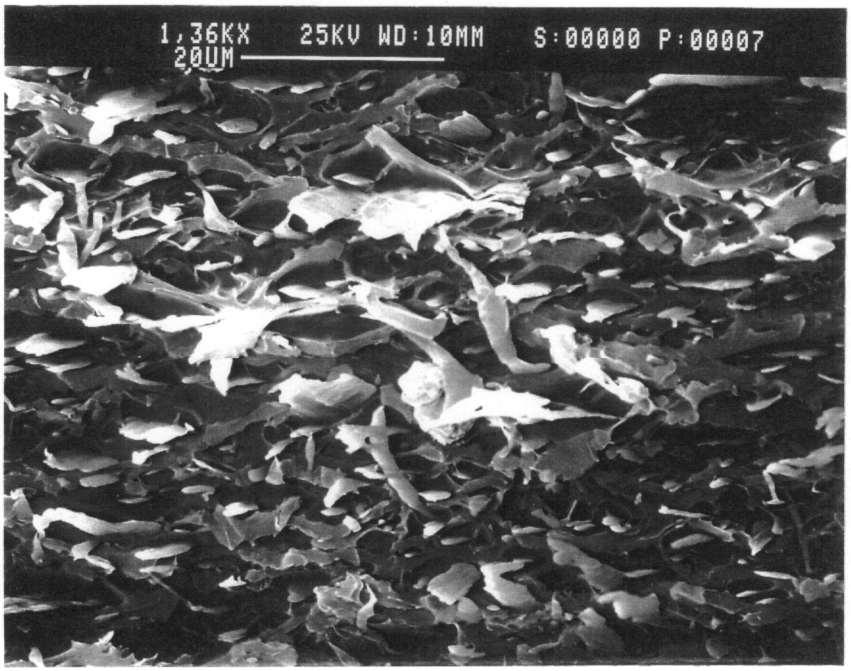

Figure 7.6. Scanning electron micrograph of fracture surface of a thermoformed plaque of PEI/Vectra A900 80/20 wt% blend. The TLCP fibers were initially lined up perpendicular to the drawing direction (depth of draw = 1in).

7.3.2 Stretch-Thermoforming Process

Thermotropic liquid crystalline polymers have the ability to deform into elongated fibrils upon application of an external strain. When in the fiber form, the TLCP acts as a reinforcing agent to the host matrix in a fashion analogous to that of inorganic fibers, such as glass. However, in a process such as injection molding, owing to the flow kinematics, a sheath/core structure is usually found and the full reinforcing potential of TLCPs is not achieved (22). Similarly, in the extrusion process an external drawing is necessary in order to render the TLCP phase into a fibrillar form (38). As shown in Section 7.3.1, in using injection molded plaques of TLCP based in situ composites in the thermoforming process, the deformation of the TLCP phase into fibers comes only from the forming step of the process itself and it is strongly dependent upon the depth of draw. With the stretch-thermoforming process, where an additional stretching is given to the sample prior to thermoforming, the deformation of the TLCP phase into reinforcing fibers becomes a combination of both the pre-stretching strain and the strain inherent to the thermoforming process. The effects of the pre-stretching followed by thermoforming on the structure and mechanical properties of in situ thermoplastic composites are discussed next.

An illustration of the possibilities presented by the stretch-thermoforming process is given in Figures 7.7 and 7.8. In Figure 7.7 is presented scanning electron micrographs of molded plaques of PEI/Vectra A 80/20 wt% blend subjected to conventional thermoforming, that is without pre-stretching. The photographs were taken from the center region of the molded plaques and the fracture surfaces were parallel to the deformation direction. In Figure 7.7-a is shown the initial morphology from the center region of the molded plaque. As expected, undeformed TLCP droplets are found in the core region of the molded plaque. This is attributed to presence of shear flows in the center region of the melt (22). The effects of thermoforming on this initial morphology is presented in Figure 7.7-b. The depth of draw in this case was 1in (1.10 units of strain). It is clear from the micrographs presented in Figure 7.7 that

deformation of the TLCP phase into fibers is apparent. This illustrated the effectiveness of the elongational stresses generated during thermoforming in deforming the TLCP phase into a fibrillar form.

The combine effects of pre-stretching followed by thermoforming on the structure of PEI/Vectra A 80/20 molded plaques are presented in Figure 7.8. In Figure 7.8-a is presented the effects of pre-stretching on the initial morphology of the molded plaque (as illustrated in Figure 7.7-a). A pre-stretching strain of 0.5 units was applied in this case. As one notices, the initial sample morphology has now turned into a fibrillar structure. Submitting this sample to the same thermoforming conditions as before, the resultant morphology is a much more pronounced deformation of the TLCP phase into fibrils. Therefore, by combining the elongational strain from both pre-stretching and thermoforming, the TLCP phase was deformed into much higher aspect ratio fibers when compared to conventional thermoforming. In addition, the increase in the fibrillation of the TLCP phase may lead to improved mechanical properties which may be attractive depending on the application (23). However, the possibilities of the stretch-thermoforming process are not only with respect to the uniaxial stretching of the samples in a direction parallel to the initial direction of the TLCP fibers. The molded plaque could be pre-stretched in a direction transverse to the initial fibers direction, which would rotate the fibers (23), followed by thermoforming. This could generate equal flow and transverse mechanical properties in the initial thermoforming blank and consequently parts showing balanced mechanical properties could be obtained.

The mechanical performance of the thermoformed trays, measured as deflection resistance, as a function of pre-stretching prior to thermoforming is presented in Table 7.1. By applying uniaxial elongation strains (as provided by the initial pre-stretching) prior to thermoforming, the deflection resistance of PEI/Vectra A 80/20 wt% blends was increased from 280 to nearly 430 N/mm of thickness after only 0.5 units of uniaxial stretching. Therefore, one observes that by combining the effects of both pre-stretching and forming strains, the reinforcing potential of the TLCP phase was tremendously increased, as seen by the increase in the deflection resistance of the pre-stretched samples. Therefore, if one considers for ex-

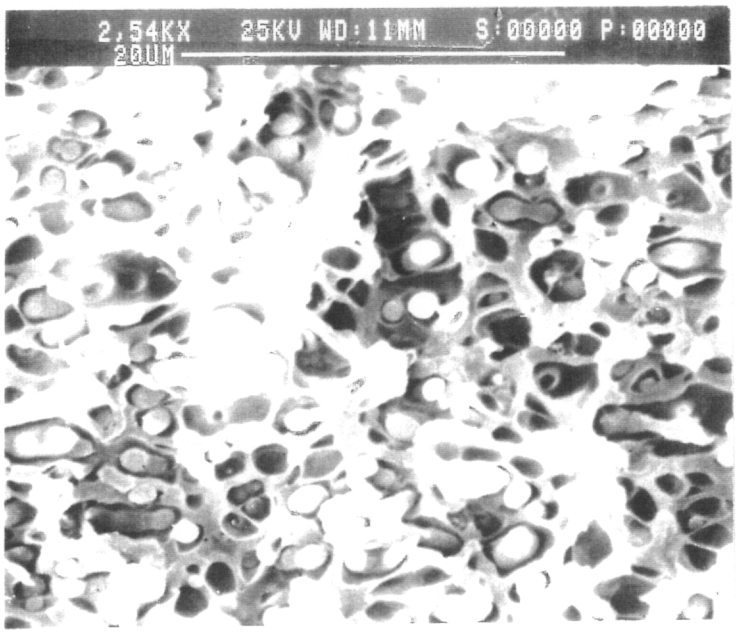

(A)

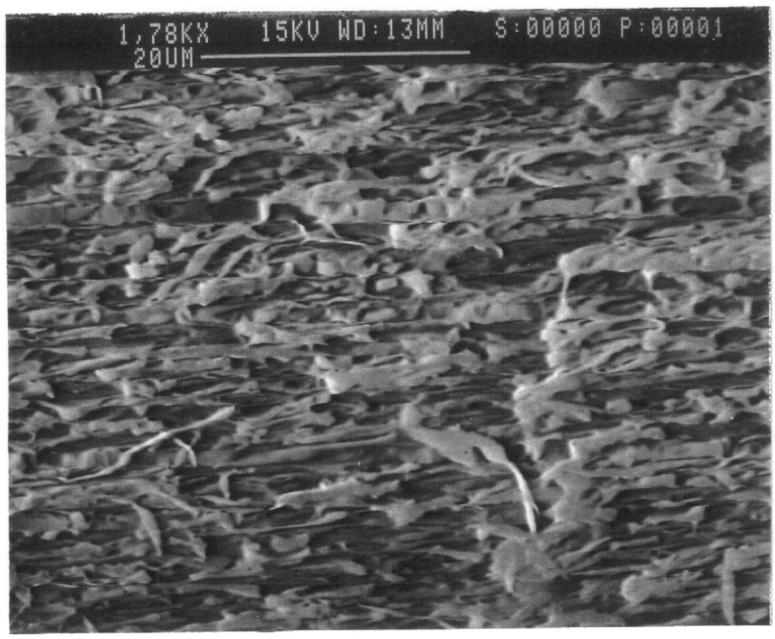

(B)

Figure 7.7. **Scanning electron micrographs of fracture surfaces of a molded plaques of PEI/Vectra A900 80/20 wt% blend** subjected to thermoforming: a) as molded and b) after thermoforming (depth of draw = 1″).

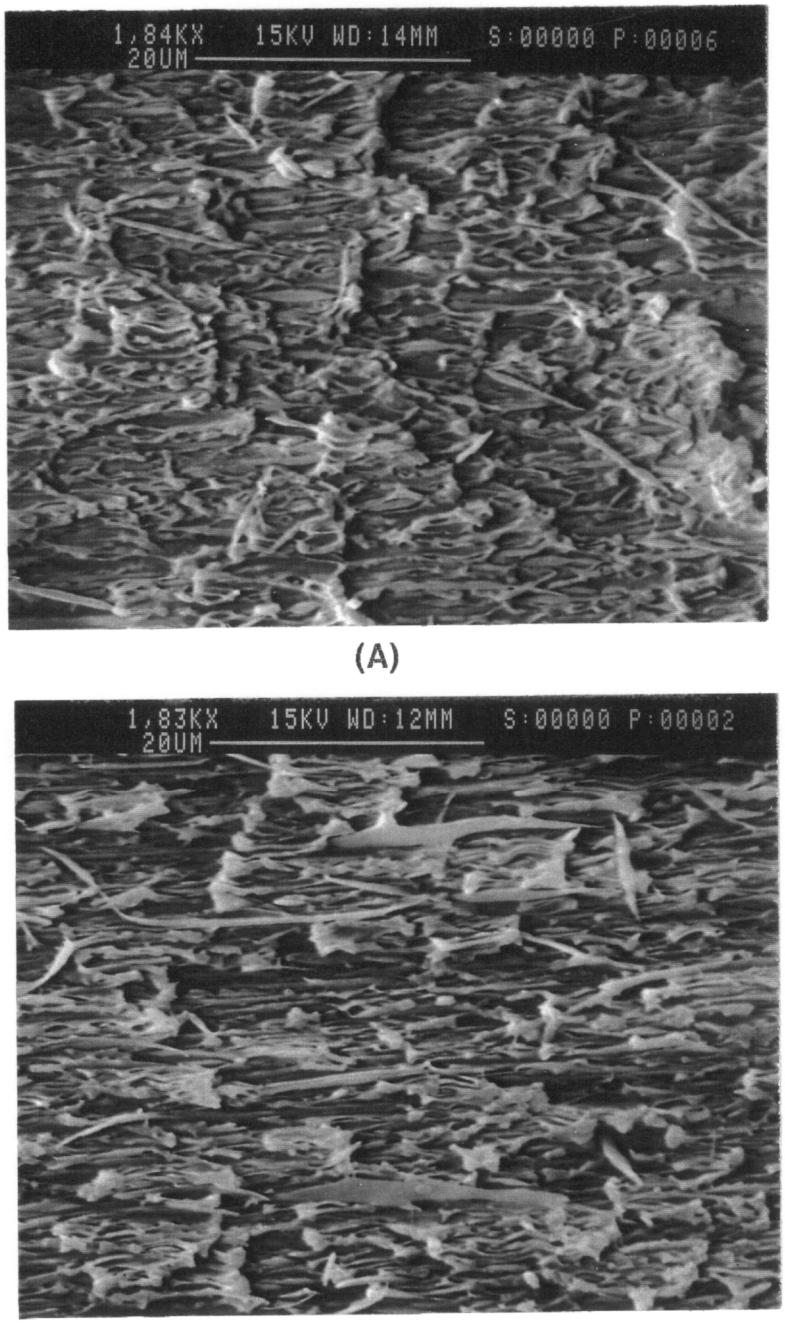

Figure 7.8. **Scanning electron micrographs of fractured surfaces of thermoformed plaques of PEI/Vectra A900 80/20 wt% blend** subjected to pre-stretching prior to thermoforming. Pre-stretch strain applied was 0.5 units: a) pre-stretched and b) after thermoforming (depth of draw = 1″n).

ample thermoforming applications in where small depths of draw are present, the reinforcing potential of a TLCP phase can be enhanced by the pre-stretching of the samples prior to thermoforming.

7.4 Conclusions

The potential application of in situ composites based on blends of thermotropic liquid crystalline polymers with a polyetherimide in the thermoforming process was investigated in this paper. Injection molded and extruded samples, in which the initial morphology of the dispersed TLCP phase was either in the form of fiber or droplets, were subjected to thermoforming conditions. It was found that in the case where the initial morphology of the dispersed TLCP phase was that of droplets, the elongational stresses generated during forming were capable of deforming the droplets into reinforcing fibers. Additionally, the aspect ratio of the fibers was observed to increase with depth of draw. However, when the initial morphology of the the TLCP phase was in the form of fibers, then the relative orientation of the fibers with respect to the forming direction was an important factor in controlling the final structure of the TLCP phase. When the fibers were aligned parallel to the forming direction, the elongational strains generated during forming tended to further increase the aspect ratio of the fibers. In the case where the initial TLCP fibers where aligned transversely to the forming direction, the fibers tended to spread into a ribbon-like structure after forming. This suggests that a specific morphology of the TLCP phase can be obtained to satisfy application needs. For instance, either high aspect ratio fibers or a ribbon-like structure can be obtained to enhance the mechanical properties or the barrier properties of thermoformed articles.

Pre-stretching of the samples prior to thermoforming tended to contribute to an increase in the aspect ratio of the TLCP fibers. As a result, an enhancement of the mechanical

Table 7.1. Deflection Resistance of thermoformed plaques of PEI/Vectra A 80/20 wt% blend as a function of pre-stretching strain.

STRAIN	LOAD/THICKNESS (N/mm)
0.00	280 (70)
0.25	350 (58)
0.50	430 (30)

(*) Standard deviations are given in parenthesis.

properties of the pre-stretched/formed samples, measured as deflection resistance, was observed.

In situ thermoplastic composites seem to be well suited for thermoforming applications. The elongational stresses generated during the process tend to, depending on the alignment of the TLCP fibers with respect to the direction of the deformation, either increase the aspect ratio of the TLCP fibers or deform them into a ribbon-like structure. This is in contrast to glass reinforced composites, in where breakage of the glass fibers, which may affect the mechanical properties, is observed.

7.5 Acknowledgements

Support from the Center for Innovative Technology of Virginia (Grant No. MAT-91-004-02) and the DuPont Company is greatly appreciated.

7.6 References

1. D.G. Baird, in "Liquid Crystalline Order in Polymers", A. Blumstein, ed., Academic Press, New York (1987).
2. D. Demus and L. Richter, "Textures of Liquid Crystalline Polymers", Verlag Chemie, New York (1987).
3. S. Ogoni and T. Asada, "Rheology and Rheo-optics of Polymer Liquid Crystals", 127-147, Rheology, Vol. I, Astarita, Marruci and Nicolais, eds., Plenum Press, New York (1980).
4. K.F. Wissbrum, **Br. Polym. J.** , 12, 163 (1980)
5. F. Cocchini, M.R. Nobile and D. Acierno, **J. Rheol.**, 35, (6), 989 (1990).
6. T.S. Chung, **J. Polym. Sci., Polym. Phys. Ed.**, 26, 1549 (1988).
7. E. Suokas, J. Sarlin, and P. Tormala, **Inst. Phys. Conf. Ser.**, 89 (3), 155 (1988).
8. D. Acierno, F.P. La Mantia, G. Piolizzoti, A. Ciferri, and B. Valenti, **Macro,molecules**, 15, 1455 (1982).
9. K. Itoyama, **J. Polym. Sci., Polym. Let.**, 27, 369 (1989).
10. Q. Lin, J. Jho, and A.F. Yee, **Polym. Eng. Sci.**, 33 (13), 789 (1993).
11. G. Crevecoeur, and G. Groenickx, **Polym. Eng. Sci.**, 33 (15), 937 (1993).
12. A.T. Dibenedetto, L. Nicolais, E. Amendola, C. Carfagna, and M.R. Nobile, **Polym. Eng. Sci.**, 29, 153 (1989).
13. T.S. Chung and P.E. McMahon, **J. Appl. Polym. Sci**, 31, 965 (1986).
14. C.E. McChesney and J.R. Dole, Modern Plastics, 112, Jan (1988).
15. A. Boldizan, **Plast. Rubber Process. Apll.**, 10, 73 (1988).
16. K.G. Blizard and D.G. Baird, **Intern. Polym. Process.**, 3, 1972 (1989).
17. W. Huh, R.A. Weiss and L. Nicolais, SPE Antec, 306 (1986)
18. T. Sun, D.G. Baird, H.H. Huang, D.S. Done, and G.L. Wilkes, **J. Comp. Mat.**, 25, 788 (1991).
19. S.S. Bafna, T. Sun, J.P. de Souza and D.G. Baird, **Polymer**, 34 (4), 708 (1993).

20. D.G. Baird, S.S. Bafna, J.P. de Souza, and T. Sun, **Polym. Comp.**, 14 (3), 214 (1993).

21. A. Metha and A.I. Isayev, **Polym. Eng. Sci.**, 31 (13), 971 (1991).

22. Chapter 3.0 of this dissertation.

23. Chapter 4.0 of this dissertation.

24. Chapter 5.0 of this dissertation.

25. Chapter 6.0 of this dissertation.

26. T. Sun, D.G. Baird, H.H. Huang, D.S. Done, and G.L. Wilkes, **J. Comp. Mat.**, 25, 788 (1991).

27. R.A. Weiss, W. Huh and L. Nicolais, **Polym. Eng. Sci.**, 27 (9), 684 (1987).

28. G. Crevecoeur, and G. Groenickx, **Polym. Eng. Sci.**, 30 (9), 532 (1990).

29. S.H. Jung and S.C. Kim, **Polym. J.**, 20 (1), 73 (1988).

30. A.M. Sukhadia, PhD dissertation, Virginia Tech (1991).

31. J.L. Throne, *Thermoforming*, Hanser Publishers, Munich (1987).

32. G. Gruenwald, *Thermoforming: A Plastics Processing Guide*, Technomic Publishing Company, Lancaster, Pa (1987).

33. J.D. Muzzy, X. Wu, and J.S. Colton, **Polym. Comp.**, 11 (5), 280 (1990).

34. J.E. Manson, T.L. Schneider, and J.C. Seferis, **Polym. Comp.**, 11 (2), 114 (1990).

35. A. Dutta, M. Niemeyer, and M. Cakmak, **Polym. Comp.**, 12 (4), 257 (1991).

36. D.M. Bigg and J.R. Preston, **Polym. Comp.**, 10 (4), 261 (1989).

37. S. Di Pede, and R.T. Woodhams, **Polym. Eng. Sci.**, 30 (19), 1185 (1990).

38. T. Sun, D.G. Baird, H.H. Huang, D.S. Done, and G.L. Wilkes, **J. Comp. Mat.**, 25, 788 (1991).

39. M.Y. Cao, and B. Wunderlich, **J. Polym. Sci., Polym. Phys. ed.**, 23, 521 (1985).

40. S.S. Bafna, T. Sun, J.P. de Souza and D.G. Baird, **Polymer**, 34 (4), 708 (1993).

41. P. Magagnini, in *Thermotropic Liquid Crystal Polymer Blends*, F.P. La Mantia, ed., Chapt. 1, Technomic Publishing Company, Lancaster, Pa (1993).

42. D.G. Baird and D. Collias, *Introduction to Polymer Processing: Principles and Design*, Chapter 10 (1994).

8.0 CONCLUSIONS AND RECOMMENDATIONS

The results and discussions of this work were presented in the previous chapters. In this chapter the conclusions along with the recommendations for future work are presented. In Section 8.1, the main conclusions are presented, followed by the recommendations in Section 8.2.

8.1 Conclusions

8.1.1 Effects of Partial Miscibility

Blends of a polyetherimide with an immiscible (Vectra A) and a partially miscible (HX1000) thermotropic liquid crystalline polymer were investigated under injection molding conditions. In the injection molding process, the deformation of the TLCP phase into reinforcing fibrils was depended upon the position of the TLCP particle in the flow. Closer to the mold walls, where elongational flow from the advancing front and strong shear gradients exist,

the TLCP phase deforms to a higher extent than in the center regions of the molded part, where shear flow dominates. The effects of partial miscibility on the morphology of PEI/TLCP blends under injection molding conditions were as follows. For the partially miscible PEI/HX1000 system, finer, higher aspect ratio HX1000 fibrils were observed, compared to the immiscible PEI/Vectra A system. Tensile and flexural moduli were found to correlate well with the structure developed during molding. For instance, tensile and flexural moduli of PEI/HX1000 blends were greater than those of PEI/Vectra A blends throughout the range of compositions investigated.

For both blends a maximum in the tensile modulus was seen to occur at a TLCP concentration of approximately 90 wt%. This maximum in tensile modulus at 90 wt% TLCP concentration was attributed to a higher molecular orientation of the TLCP phase in the blend than in the neat TLCP, as revealed in the wide-angle x-ray diffraction measurements. Due to a higher blend viscosity at this concentration, stress induced molecular orientation of the TLCP phase may have occurred. The higher molecular orientation of the TLCP phase at 90 wt% TLCP concentration would lead to higher modulus fibers in the blend relative to the pure TLCP.

Ultimate tensile properties, depending on the TLCP concentration, were observed to be affected by either interfacial adhesion or ultimate properties of the TLCP. At low TLCP concentrations, up to 20 wt%, interfacial adhesion was important. In such cases, PEI/HX1000 blends, which show greater interfacial adhesion, exhibited higher tensile strengths than PEI/Vectra A blends. For instance, at 10 wt% TLCP concentration, tensile strengths of about 110 and 140 MPa were observed for PEI/Vectra A and PEI/HX1000, respectively. However, at TLCP concentrations of 70 wt% and above, the tensile strength properties were dominated by the ultimate strength of the TLCP. The TLCPs used, Vectra A and HX1000, show tensile strengths of about 215 and 126 MPa, respectively. Therefore, PEI/Vectra A blends have shown, at these concentrations, considerably higher values of tensile strength than PEI/HX1000. PEI/HX1000 blends have also shown, at low TLCP concentrations, a higher value of transverse

tensile strength than PEI/Vectra A blends. This agrees with the fact that a higher interphase adhesion was observed for the PEI/HX1000 system compared to the PEI/Vectra A system.

Although partial miscibility strongly affected the stiffness of an in situ composite, it was observed that the ultimate properties of a TLCP dominated the ultimate properties of the TLCP/polymer composite. Consequently, the selection of a TLCP to reinforce a polymer matrix does not only depend upon whether partial miscibility between the TLCP and the matrix polymer exists, but also on the overall mechanical properties exhibited by the TLCP.

8.1.2 Effects of Shearfree Deformation

The effects of uniaxial elongation on the morphology and mechanical properties of injection molded plaques and extruded sheets of PEI/Vectra A and PEI/HX1000 blends were investigated. It was found the in the case of injection molded samples, the effect of uniaxial elongation on the morphology and properties was dependent upon the relative direction of the deformation with respect to the initial direction of the fibers. If the direction of the applied uniaxial deformation was parallel to the initial fiber direction, the deformation tended to increase the average aspect ratio of the the TLCP fibers and mechanical properties along the deformation direction were enhanced. On the other hand, if the direction of the applied deformation was transverse to the initial fiber direction, the fibers tended to follow the deformation and a 90° rotation was observed. In terms of mechanical properties, it was observed that a complete inversion occurred after a strain of 0.75 units was applied transversely to the initial flow direction. In addition, equal flow and transverse mechanical properties were found at 0.5 units of uniaxial strain.

The stretching temperature appeared to have a greater effect on the mechanical properties of the PEI/HX1000 blends compared to PEI/Vectra A blends. The magnitude of increase in the mechanical properties was less for PEI/HX1000 at 265°C than at 240°C. Stretching at a temperature of 265°C, which was closer to the melting temperature of TLCP,

the competing effects of deformation and relaxation of the molecular orientation reduced the effectiveness of the deformation in enhancing the mechanical properties of the blend.

The uniaxial stretching of extruded sheets indicated that the initial mechanical properties of the sheets were significantly increased upon stretching. However, the stability of the fibers upon deformation was a function of the compatibility between the TLCP and the PEI phase. Highly stable and elongate TLCP fibrils were found in the PEI/Vectra A blends relative to PEI/HX1000 blends.

The effects of planar deformation on the structure and properties of injection molded plaques and extruded sheets of PEI/Vectra A and PEI/HX1000 were as follows. In the case of injection molded samples, planar deformation led to the spreading of the fibers in the plane of deformation and a ribbon-like morphological structure developed upon planar deformation. However, the extent of fiber spreading was dependent upon the relative direction of the applied planar deformation to the direction of the fibers. At comparative magnitudes of planar strains, transverse planar compression tended to promote a greater spreading of the fibers relative to planar stretching parallel to the initial direction of the fibers.

In the case of extruded sheets, the degree of compatibility between the PEI matrix and the TLCP phase was an important factor in affecting the morphology. For the immiscible PEI/Vectra A system, the initial TLCP drops tended to spread into a more stable ribbon-like structure. For the partially miscible PEI/HX1000 system, stress induced fiber breakup occurred with planar strain.

In addition, planar stretching applied in a direction perpendicular to the initial direction of the TLCP fibers was effective in reducing the mechanical anisotropy of the molded plaques. PEI/Vectra A and PEI/HX1000 80/20 wt% blends showing equal properties, in both flow and transverse directions, were developed when planar strains greater than 0.5 units were applied in a direction perpendicular to the initial direction of the TLCP fibers.

The effects of biaxial elongational on the structure and properties of injection molded plaques and extruded sheets of PEI/Vectra A and PEI/HX1000 were investigated. It was found that in the case of extruded sheets, equal-biaxial deformation tended to deform the TLCP

phase, which initially was in the form of drops, into a two dimensional disc-like structure. However, it appeared that the extent of the deformation was a function of the elongational stress generated during compression. For the PEI/HX1000 system the elongational stresses generated during compression exceeded the critical elongational stress for fiber breakup, and breakup of the dispersed HX1000 phase into much smaller drops occurred. In the case of the PEI/Vectra A system, the elongational stresses during compression were below the critical stresses for breakup, and the Vectra A phase deformed into a flake-like structure.

For unconstrained compression molding, the inhomogeneity of the deformation caused the TLCP phase to deform into a fibrillar structure rather than the flake-like structure observed in the equal-biaxial deformation. In terms of mechanical properties, the magnitude of increase in the properties followed the variations in the elongational strains in the plane of deformation. Nevertheless, for extruded sheets, unconstrained compression molding tended to induce equal machine and transverse mechanical in comparison to molded plaques.

8.1.3 Thermoforming of In situ Composites

The potential application of in situ composites based on blends of thermotropic liquid crystalline polymers with a polyetherimide in the thermoforming process was investigated. Injection molded and extruded samples, in which the initial morphology of the dispersed TLCP phase was either in the form of fibers or droplets, were subjected to thermoforming conditions. It was found that in the case where the initial morphology of the dispersed TLCP phase was that of droplets, the elongational stresses generated during forming were capable of deforming the TLCP droplets into reinforcing fibers. Additionally, the aspect ratio of the fibers was observed to increase with depth of draw. However, when the initial morphology of the the TLCP phase was in the form of fibers, then the relative orientation of the fibers with respect to the forming direction was an important factor in controlling the final structure of the TLCP phase. When the fibers were aligned parallel to the forming direction, the elongational strains

generated during forming tended to further increase the aspect ratio of the fibers. In the case where the initial TLCP fibers were aligned transversely to the forming direction, the fibers tended to spread into a ribbon-like structure after forming. This suggests that a specific morphology of the TLCP phase can be obtained to satisfy application needs. For instance, either high aspect ratio fibers or a ribbon-like structure can be obtained to enhance the mechanical properties or the barrier properties of thermoformed articles.

Pre-stretching of the samples prior to thermoforming tended to contribute to an increase in the aspect ratio of the TLCP fibers. As a result, an enhancement of the mechanical properties of the pre-stretched/formed samples, measured as deflection resistance, was observed.

In situ thermoplastic composites seem to be well suited for thermoforming applications. The elongational stresses generated during the process tended to, depending on the alignment of the TLCP fibers with respect to the direction of the deformation, either increase the aspect ratio of the TLCP fibers or deform them into a ribbon-like structure. This was observed to be in contrast with glass reinforced composites, in where breakage of the glass fibers, which may affect the mechanical properties, is observed.

8.2 Recommendations

It was shown that the addition of a thermotropic liquid crystalline polymer to a thermoplastic matrix may effectively increase its modulus and strength. However, due to the lack of ductility of the TLCP, a dramatic drop in the toughness of the in situ composite is usually observed. Therefore, the development of methods in which the the toughness of the in situ composite may be increased should be considered for future works. One possibility may be through the development of ternary blends in which a third polymer would be used as toughness enhancer.

In order to determine the full potential of TLCP based in situ composites, additional mechanical properties of the blends should be determined. Studies aimed at assessing the impact properties of TLCP based in situ composites are highly recommended.

In order to extend the understanding of the effects of shearfree deformation on the structure and mechanical properties of in situ composites, the use of different thermoplastic matrices and TLCPs should be considered. In addition, experiments should be designed in order to determine the ideal conditions for the deformation of the TLCP phase.

It is clear that the shearfree elongational experiments performed here offer the possibility of morphology and properties control of the TLCP/polymer blend investigated. However, extending the shearfree flow experiments to encompass polymer blends other than in situ composites is recommended. Hence, it would be possible to determine whether the morphology and mechanical properties of the blends can be controlled in a similar manner.

It was shown that planar and biaxial elongation deformation lead to the deformation of the TLCP phase into a flake-like structure. It was suggested that such a morphology would possibility increase the barrier properties of in situ composites. However, due to the limitations of this work, such tests were not performed. Therefore, it is recommended for future studies that barrier properties of composites showing this type of morphology should be determined. This will add a tremendous contribution to future commercialization of TLCP/polymer blends.

It seems that polymer blends containing thermotropic liquid crystalline polymers are ideal candidates for thermoforming applications. The elongational flow prevailing in the process increases the deformation of the TLCP phase into high aspect ratio fibers and an increase in the deflection resistance is also observed. However, studying the application potential of TLCP/polymer blends in other processes in where elongational flow dominates, such as blow molding, stretch blow molding and vacuum forming, is highly recommended. Such studies may eventually correlate more closely the morphological variations and the correspondent mechanical properties of the blends. In addition, such studies would also increase the application potential of in situ composites in process where shearfree flows prevail.

Appendix A. Mechanical Properties of PEI/TLCP Blends

Table A.1. Tensile Properties of PEI/Vectra A blends as a function of Vectra A concentration obtained from molded tensile bars[1]

COMPOSITION	TENSILE MODULUS (GPa)	TENSILE STRENGTH (MPa)	ELONGATION BREAK (%)	TOUGHNESS[2] KJ/m^3
100/0	3.04 (0.18)	100.14 (0.99)	60.0[3]	7750[4]
90/10	3.82 (0.09)	106.77 (7.74)	6.28 (0.59)	5180 (620)
80/20	4.75 (0.40)	125.49 (7.08)	6.27 (0.52)	5710 (520)
70/30	5.83 (0.64)	134.67 (6.42)	4.42 (0.85)	3825 (660)
60/40	6.83 (0.47)	125.29 (9.67)	2.88 (0.22)	2100 (320)
50/50	7.03 (0.46)	129.38 (10.18)	3.15 (0.22)	2450 (415)
40/60	7.84 (0.35)	143.10 (6.09)	3.55 (0.28)	3200 (420)
30/70	9.97 (0.53)	187.05 (10.89)	4.48 (0.48)	5550 (850)
20/80	10.80 (0.32)	193.82 (14.12)	4.42 (0.34)	5900 (700)
10/90	13.47 (0.36)	239.83 (6.08)	4.64 (0.23)	7600 (310)
0/100	10.33 (0.81)	214.53 (3.08)	4.41 (0.11)	5950 (130)

(1) ASTM D 638 TYPE 5.
(2) Calculated as the area under the stress vs. strain curve.
(3) from manufacture's data sheet.
(4) calculated at 10% elongation.
(*) Standard deviations are given in parenthesis.

Table A.2. Tensile Properties of PEI/HX1000 blends as a function of HX1000 concentration obtained from molded tensile bars[1]

COMPOSITION	TENSILE MODULUS (GPa)	TENSILE STRENGTH (MPa)	ELONGATION BREAK (%)	TOUGHNESS[2] KJ/m^3
100/0	3.04 (0.18)	100.14 (0.99)	60.0[3]	7750[4]
90/10	4.89 (0.24)	137.68 (4.83)	5.46 (0.56)	4750 (682)
80/20	6.51 (0.58)	137.68 (5.12)	2.75 (0.24)	2050 (240)
70/30	8.70 (0.59)	129.23 (4.68)	1.94 (0.30)	1675 (150)
60/40	9.63 (0.81)	123.60 (10.62)	1.63 (0.21)	1100 (238)
50/50	11.23 (0.47)	129.85 (7.08)	1.22 (0.11)	830 (172)
40/60	12.60 (0.41)	120.90 (9.00)	1.18 (0.12)	900 (115)
30/70	13.66 (0.55)	126.56 (4.42)	1.14 (0.07)	810 (92)
20/80	15.81 (0.99)	140.04 (15.13)	0.94 (0.17)	770 (124)
10/90	17.33 (0.76)	157.34 (8.77)	1.06 (0.16)	920 (104)
0/100	11.55 (0.57)	126.00 (15.10)	1.77 (0.31)	1350 (330)

(1) ASTM D 638 TYPE 5.
(2) Calculated as the area under the stress vs. strain curve.
(3) from manufacture's data sheet.
(4) calculated at 10% elongation.
(*) Standard deviations are given in parenthesis.

Table A.3. Tensile Properties of PEI/Vectra A blends as a function of Vectra A concentration obtained from molded plaques[1] measured along the injection molding flow direction

COMPOSITION	TENSILE MODULUS (GPa)	TENSILE STRENGTH (MPa)	ELONGATION BREAK (%)
100/0	3.0 (0.2)	100.1 (1.9)	
90/10	3.5 (0.2)	92.4 (2.1)	4.1 (0.3)
80/20	3.8 (0.1)	81.9 (3.8)	3.1 (0.4)
70/30	4.5 (0.4)	92.4 (6.6)	2.9 (0.8)
60/40	4.6 (0.3)	81.3 (8.6)	2.3 (0.2)
50/50	5.3 (0.5)	87.8 (9.3)	2.2 (0.3)
40/60	6.4 (0.6)	94.4 (6.8)	1.9 (0.7)
30/70	7.3 (0.2)	107.7 (5.6)	2.4 (0.2)
20/80	8.8 (0.9)	129.6 (7.4)	2.4 (0.2)
10/90	11.2 (0.7)	160.7 (8.4)	2.3 (0.4)
0/100	8.1 (0.3)	126.5 (1.5)	2.6 (0.1)

(1) 3″x3″x1/8″ film gated rectangular plaque.
(*) Standard deviations are given in parenthesis.

Table A.4. Tensile Properties of PEI/Vectra A blends as a function of Vectra A concentration obtained from molded plaques[1] measured transverse to the injection molding flow direction

COMPOSITION	TENSILE MODULUS (GPa)	TENSILE STRENGTH (MPa)	ELONGATION BREAK (%)
100/0	3.0 (0.2)	100.1 (1.9)	
90/10	2.8 (0.2)	75.0 (10.3)	5.0 (0.9)
80/20	2.8 (0.1)	45.0 (9.1)	2.2 (0.8)
70/30	3.0 (0.1)	37.1 (3.3)	1.5 (0.1)
60/40	2.8 (0.1)	48.1 (3.5)	2.2 (0.3)
50/50	2.8 (0.2)	41.5 (3.9)	1.9 (0.1)
40/60	2.8 (0.2)	37.7 (1.5)	1.9 (0.2)
30/70	2.6 (0.2)	36.5 (4.1)	2.2 (0.4)
20/80	2.6 (0.1)	42.8 (3.5)	3.5 (0.5)
10/90	2.5 (0.2)	43.6 (5.2)	5.3 (1.2)
0/100	2.3 (0.1)	45.7 (1.8)	6.3 (2.2)

(1) 3"x3"x1/8" film gated rectangular plaque.
(*) Standard deviations are given in parenthesis.

Table A.5. Flexural Properties of PEI/Vectra A blends as a function of Vectra A concentration obtained from molded plaques[1]

COMPOSITION	FLEXURAL MODULUS (GPa)	FLEXURAL STRENGTH (MPa)
100/0	3.41 (0.20)	157.49 (3.27)
90/10	4.04 (0.13)	177.24 (3.91)
80/20	5.23 (0.21)	168.02 (6.54)
70/30	5.95 (0.23)	140.0 (9.28)
50/50	7.31 (0.42)	159.20 (9.40)
40/60	8.67 (0.62)	171.18 (10.74)
20/80	12.53 (0.27)	197.32 (4.28)
10/90	14.88 (0.60)	205.79 (5.80)
0/100	13.90 (0.96)	211.13 (4.27)

(1) Rectangular strips cut from 3″x3″x1/8″ film gated rectangular plaques according to ASTM D790.
(*) Standard deviations are given in parenthesis.

Table A.6. Flexural Properties of PEI/HX1000 blends as a function of HX1000 concentration obtained from molded plaques[1]

COMPOSITION	FLEXURAL MODULUS (GPa)	FLEXURAL STRENGTH (MPa)
100/0	3.41 (0.20)	157.49 (3.27)
90/10	5.34 (0.16)	208.16 (5.72)
80/20	7.25 (0.19)	205.50 (16.06)
70/30	8.93 (0.35)	142.34 (8.32)
50/50	11.68 (0.40)	157.50 (10.89)
40/60	13.20 (0.24)	156.60 (6.91)
20/80	15.36 (0.40)	180.71 (7.55)
10/90	16.07 (0.56)	187.57 (8.77)
0/100	14.85 (0.57)	187.70 (15.10)

(1) Rectangular strips cut from 3″x3″x1/8″ film gated rectangular plaques according to ASTM D790.
(*) Standard deviations are given in parenthesis.

Appendix B. Rheological Properties of PEI/TLCP Blends

Table B.1. Frequency sweeps of PEI/Vectra A blends at 360°C and 5% strain (parallel plates).

PEI/Vectra A900 Blends							
	100/0	90/10	70/30	50/50	30/70	10/90	0/100
ω (rad/s)	η^* (Pa.s)	η^* (Pa.s)	η^* (Pa.s)	η^* (Pa.s)	η^* (Pa.s)	η^* (Pa.s)	η^* (Pa.s)
0.100	2254	1109	2171	2769	2621	2348	1101
0.215	2020	1152	1531	1888	1669	1465	634.0
0.464	1885	1038	1201	1494	1236	1039	392.5
1.000	1818	954.8	1031	1268	955.2	796.6	266.9
2.154	1752	902.0	925.8	1096	767.2	633.2	189.6
4.641	1658	858.7	822.3	923.7	599.0	484.5	142.0
10.00	1526	804.2	708.6	750.6	458.7	363.8	108.7
21.54	1350	720.6	580.5	587.1	337.1	259.6	80.84
46.41	1149	621.1	451.9	443.7	240.6	178.8	61.21
100.0	922.2	507.3	332.8	322.7	169.3	121.3	45.51

Table B.2. Frequency sweeps of PEI/HX1000 blends at 360°C and 5% strain (parallel plates).

PEI/HX1000 Blends							
	100/0	90/10	80/20	50/50	20/80	10/90	0/100
ω (rad/s)	η^* (Pa.s)	η^* (Pa.s)	η^* (Pa.s)	η^* (Pa.s)	η^* (Pa.s)	η^* (Pa.s)	η^* (Pa.s)
0.100	2254	832.0	1879	2100	4436	6308	1773
0.215	2020	636.0	1675	1354	3773[1]	4708[1]	1642[1]
0.464	1885	534.9	1441	948.5	1956[2]	2335[2]	1141[2]
1.000	1818	483.6	1324	720.7	1387	1610	937.6
2.154	1752	451.5	1188	572.5	992.3[3]	1113[3]	663.7[3]
4.641	1658	429.8	1043	468.6	532.6[4]	535.3[4]	341.9[4]
10.00	1526	390.7	905.2	385.3	402.8	378.5	240.1
21.54	1350	345.3	762.6	312.5	305.4[5]	271.7[5]	168.5[5]
46.41	1149	291.8	625.4	249.9	176.0[6]	142.6[6]	81.98[6]
100.0	922.2	231.7	490.8	192.0	130.6	102.2	56.24

Measured at frequencies of (1) 0.1778, (2) 0.5632, (3) 1.778, (4) 5.632, (5)17.78 and (6) 56.23 rad/s.

Appendix C. Effects of Shearfree Deformation on the Mechanical Properties of PEI/TLCP Blends

Table C.1. Effects of uniaxial stretching[1,2] applied along the flow direction on the mechanical properties of molded plaques of PEI.

FLOW DIRECTION PROPERTIES			UNIAXIAL STRAIN
Modulus (GPa)	Strength (MPa)	Elongation (%)	
3.04 (0.18)	100.14 (0.99)	7.00 (Y)[1]	0.0
3.36 (0.27)	117.31 (7.42) (Y)[1]	6.75 (0.45) (Y)[1]	0.25
3.54 (0.20)	129.65 (6.87) (Y)[1]	7.05 (0.58) (Y)[1]	0.50
3.31 (0.18)	115.86 (8.39)	4.90 (0.33)	0.75
3.71 (0.10)	112.66 (4.08)	3.55 (0.19)	1.00

(1) Measured at yield
(2) Stretching Temperature: 240°C.
(3) Initial Strain Rate: 0.014 sec^{-1}

Table C.2. Effects of uniaxial stretching[1,2] applied parallel to initial direction of the fibers on the mechanical properties of molded plaques of PEI/Vectra A 90/10 wt%.

FLOW DIRECTION PROPERTIES			TRANSVERSE DIRECTION PROPERTIES			UNIAXIAL STRAIN
Modulus (GPa)	Strength (MPa)	Elongation (%)	Modulus (GPa)	Strength (MPa)	Elongation (%)	
3.50 (0.20)	92.40 (2.10)	4.10 (0.30)	2.80 (0.20)	75.00 (10.30)	5.00 (0.90)	0.0
4.16 (0.46)	122.58 (2.21)	5.93 (0.35)	2.78 (0.33)	80.62 (9.75)	4.09 (0.77)	0.25
4.14 (0.42)	126.12 (9.55)	6.26 (0.21)	2.72 (0.15)	68.92 (9.76)	3.69 (0.10)	0.50
4.32 (0.68)	143.43 (5.13)	4.57 (0.56)	2.46 (0.18)	29.87 (4.09)	1.24 (0.22)	0.75

[1] **Stretching Temperature: 240°C.**
[2] **Initial Strain Rate: 0.014 sec^{-1}**
(★) Standard deviations are given in parenthesis.

Table C.3. Effects of uniaxial stretching[1,2] applied transversely to initial direction of the fibers on the mechanical properties of molded plaques of PEI/Vectra A 90/10 wt%.

FLOW DIRECTION PROPERTIES			TRANSVERSE DIRECTION PROPERTIES			UNIAXIAL STRAIN
Modulus (GPa)	Strength (MPa)	Elongation (%)	Modulus (GPa)	Strength (MPa)	Elongation (%)	
3.50 (0.20)	92.40 (2.10)	4.10 (0.30)	2.80 (0.20)	75.00 (10.30)	5.00 (0.90)	0.0
3.20 (0.30)	79.09 (7.41)	3.49 (0.30)	3.27 (0.32)	104.45 (5.69)	5.32 (0.42)	0.25
2.62 (0.52)	59.71 (3.32)	2.27 (0.22)	3.44 (0.30)	102.44 (8.48)	4.62 (0.23)	0.50
2.54 (0.17)	53.18 (5.13)	2.43 (0.70)	3.59 (0.11)	117.55 (5.98)	4.89 (0.34)	0.75

[1] **Stretching Temperature: 240°C.**
[2] **Initial Strain Rate: 0.014 sec^{-1}**
(★) Standard deviations are given in parenthesis.

Table C.4. Effects of uniaxial stretching[1,2] applied parallel to initial direction of the fibers on the mechanical properties of molded plaques of PEI/HX1000 90/10 wt%.

FLOW DIRECTION PROPERTIES			TRANSVERSE DIRECTION PROPERTIES			UNIAXIAL STRAIN
Modulus (GPa)	Strength (MPa)	Elongation (%)	Modulus (GPa)	Strength (MPa)	Elongation (%)	
4.94 (0.15)	103.46 (6.96)	2.99 (0.33)	2.81 (0.19)	83.87 (3.59)	6.69 (0.25)	0.0
4.80 (0.25)	140.16 (6.25)	5.20 (0.48)	3.00 (0.08)	96.44 (1.19)	5.83 (0.68)	0.25
5.45 (0.16)	151.80 (6.21)	5.05 (0.25)	2.83 (0.17)	63.38 (3.45)	2.72 (0.14)	0.50
6.27 (0.44)	163.75 (10.61)	5.08 (0.65)	2.00 (0.57)	22.54 (4.41)	1.02 (0.16)	0.75

[1] **Stretching Temperature: 240°C.**
[2] **Initial Strain Rate: 0.014 sec^{-1}**
(★) Standard deviations are given in parenthesis.

Table C.5. Effects of uniaxial stretching[1,2] applied transversely to initial direction of the fibers on the mechanical properties of molded plaques of PEI/HX1000 90/10 wt%.

FLOW DIRECTION PROPERTIES			TRANSVERSE DIRECTION PROPERTIES			UNIAXIAL STRAIN
Modulus (GPa)	Strength (MPa)	Elongation (%)	Modulus (GPa)	Strength (MPa)	Elongation (%)	
4.94 (0.15)	103.46 (6.96)	2.99 (0.33)	2.81 (0.19)	83.87 (3.59)	6.69 (0.25)	0.0
3.86 (0.45)	113.21 (2.70)	6.53 (0.25)	3.17 (0.10)	115.30 (1.80)	6.92 (0.21)	0.25
3.27 (0.16)	101.23 (6.44)	6.48 (0.62)	3.69 (0.21)	124.88 (3.01)	6.25 (0.36)	0.50
3.01 (0.26)	75.53 (7.95)	3.44 (0.35)	4.34 (0.26)	141.99 (9.32)	5.21 (0.37)	0.75
			6.25 (0.38)	102.25 (2.09)	2.13 (0.22)	1.00

[1] **Stretching Temperature: 240°C.**
[2] **Initial Strain Rate: 0.014 sec^{-1}**
(★) Standard deviations are given in parenthesis.

Table C.6. Effects of uniaxial stretching[1,2] applied parallel to initial direction of the fibers on the mechanical properties of molded plaques of PEI/Vectra A 70/30 wt%.

FLOW DIRECTION PROPERTIES			TRANSVERSE DIRECTION PROPERTIES			UNIAXIAL STRAIN
Modulus (GPa)	Strength (MPa)	Elongation (%)	Modulus (GPa)	Strength (MPa)	Elongation (%)	
4.50 (0.40)	92.40 (6.60)	2.90 (0.80)	3.00 (0.10)	37.10 (3.30)	1.50 (0.10)	0.0
4.79 (0.19)	73.67 (5.72)	1.69 (0.11)	2.26 (0.06)	33.06 (0.51)	1.69 (0.16)	0.25
5.60 (0.28)	115.75 (5.63)	2.23 (0.31)	2.25 (0.08)	32.25 (2.36)	1.55 (0.10)	0.50
5.63 (0.52)	111.45 (3.85)	2.16 (0.23)	2.34 (0.27)	24.21 (1.61)	1.03 (0.05)	0.75

[1] **Stretching Temperature: 240°C.**
[2] **Initial Strain Rate: 0.014 sec^{-1}**
(★) Standard deviations are given in parenthesis.

Table C.7. Effects of uniaxial stretching[1,2] applied transversely to initial direction of the fibers on the mechanical properties of molded plaques of PEI/Vectra A 70/30 wt%.

FLOW DIRECTION PROPERTIES			TRANSVERSE DIRECTION PROPERTIES			UNIAXIAL STRAIN
Modulus (GPa)	Strength (MPa)	Elongation (%)	Modulus (GPa)	Strength (MPa)	Elongation (%)	
4.50 (0.40)	92.40 (6.60)	2.90 (0.80)	3.00 (0.10)	37.10 (3.30)	1.50 (0.10)	0.0
3.34 (0.06)	68.69 (3.55)	2.52 (0.22)	2.92 (0.19)	56.00 (0.42)	2.25 (0.09)	0.25
3.07 (0.19)	61.43 (7.03)	2.45 (0.19)	3.33 (0.12)	68.75 (4.17)	2.40 (0.23)	0.50
2.70 (0.26)	39.32 (1.94)	1.95 (0.32)	3.56 (0.14)	69.66 (5.06)	1.95 (0.24)	0.75

[1] **Stretching Temperature: 240°C.**
[2] **Initial Strain Rate: 0.014 sec^{-1}**
(★) Standard deviations are given in parenthesis.

Table C.8. Effects of uniaxial stretching[1,2] applied parallel to initial direction of the fibers on the mechanical properties of molded plaques of PEI/HX1000 70/30 wt%.

FLOW DIRECTION PROPERTIES			TRANSVERSE DIRECTION PROPERTIES			UNIAXIAL STRAIN
Modulus (GPa)	Strength (MPa)	Elongation (%)	Modulus (GPa)	Strength (MPa)	Elongation (%)	
7.42 (0.31)	106.43 (9.41)	1.73 (0.14)	2.74 (0.04)	41.61 (2.74)	1.61 (0.04)	0.0
8.81 (0.12)	113.74 (5.01)	1.39 (0.09)	2.83 (0.15)	43.29 (3.01)	1.84 (0.20)	0.25
10.39 (1.36)	137.70 (6.05)	1.32 (0.10)	2.84 (0.29)	37.11 (2.74)	2.95 (0.13)	0.50
(rupture)						0.75

[1] **Stretching Temperature: 240°C.**
[2] **Initial Strain Rate: 0.014 sec^{-1}**
(★) Standard deviations are given in parenthesis.

Table C.9. Effects of uniaxial stretching[1,2] applied transversely to initial direction of the fibers on the mechanical properties of molded plaques of PEI/HX1000 70/30 wt%.

FLOW DIRECTION PROPERTIES			TRANSVERSE DIRECTION PROPERTIES			UNIAXIAL STRAIN
Modulus (GPa)	Strength (MPa)	Elongation (%)	Modulus (GPa)	Strength (MPa)	Elongation (%)	
4.50 (0.40)	92.40 (6.60)	2.90 (0.80)	3.00 (0.10)	37.10 (3.30)	1.50 (0.10)	0.0
6.14 (0.42)	90.92 (6.75)	1.70 (0.10)	3.30 (0.20)	58.91 (0.79)	1.95 (0.18)	0.25
4.26 (0.28)	80.10 (7.96)	2.18 (0.24)	3.87 (0.21)	70.93 (5.86)	1.97 (0.18)	0.50
3.89 (0.36)	68.79 (8.48)	2.01 (0.14)	4.68 (0.54)	68.49 (3.88)	1.58 (0.20)	0.75

[1] **Stretching Temperature: 240°C.**
[2] **Initial Strain Rate: 0.014 sec^{-1}**
(★) Standard deviations are given in parenthesis.

Table C.10. Effects of uniaxial stretching[1,2] applied parallel to the initial direction of the glass fibers on the mechanical properties of molded plaques of PEI reinforced with 15wt% glass fibers.

FLOW DIRECTION PROPERTIES			TRANSVERSE DIRECTION PROPERTIES			UNIAXIAL STRAIN
Modulus (GPa)	Strength (MPa)	Elongation (%)	Modulus (GPa)	Strength (MPa)	Elongation (%)	
4.55	108.72	3.83	3.93	91.98	3.38	0.0
5.10	84.43	2.66 (0.37)	2.99 (0.40)	57.51 (4.63)	3.39 (0.15)	0.40
4.36 (0.10)	121.40 (10.47)	4.05 (0.56)	2.83 (0.10)	59.74 (7.31)	2.92 (0.57)	0.50
4.85 (0.48)	126.78 (8.86)	3.86 (0.32)	2.64 (0.10)	57.10 (0.62)	3.56 (0.25)	0.75

[1] **Stretching Temperature: 240°C.**
[2] **Initial Strain Rate: 0.014 sec^{-1}**
(★) Standard deviations are given in parenthesis.

Table C.11. Effects of uniaxial stretching[1,2] applied transversely to initial direction of the glass fibers on the mechanical properties of molded plaques of PEI reinforced with 15 wt% glass fibers.

FLOW DIRECTION PROPERTIES			TRANSVERSE DIRECTION PROPERTIES			UNIAXIAL STRAIN
Modulus (GPa)	Strength (MPa)	Elongation (%)	Modulus (GPa)	Strength (MPa)	Elongation (%)	
4.50 (0.40)	92.40 (6.60)	2.90 (0.80)	3.00 (0.10)	37.10 (3.30)	1.50 (0.10)	0.0
3.55 (0.28)	63.71 (4.94)	2.40 (0.17)	3.10 (0.14)	73.96 (5.96)	3.60 (0.38)	0.25
3.23 (0.23)	71.93 (6.20)	3.28 (0.12)	3.24 (0.32)	96.28 (2.19)	4.58 (0.37)	0.50
2.98 (0.10)	75.71 (6.59)	3.78 (0.26)	3.73 (0.20)	103.10 (6.17)	4.64 (0.42)	0.75

[1] **Stretching Temperature: 240°C.**
[2] **Initial Strain Rate: 0.014 sec^{-1}**
(★) Standard deviations are given in parenthesis.

Table C.12. Effects of uniaxial stretching[1,2] applied parallel to initial direction of the fibers on the mechanical properties of molded plaques of PEI/HX1000 80/20 wt%.

FLOW DIRECTION PROPERTIES			TRANSVERSE DIRECTION PROPERTIES			UNIAXIAL STRAIN
Modulus (GPa)	Strength (MPa)	Elongation (%)	Modulus (GPa)	Strength (MPa)	Elongation (%)	
5.13 (0.47)	105.36 (4.15)	2.38 (0.15)	2.84 (0.14)	57.10 (3.92)	2.57 (0.23)	0.0
8.18 (0.39)	119.39 (2.68)	1.54 (0.10)				0.25
8.85 (0.39)	164.95 (10.14)	2.42 (0.25)				0.50
(rupture)						0.75

[1] **Stretching Temperature: 240°C.**
[2] **Initial Strain Rate: 0.14 sec^{-1}**
(★) Standard deviations are given in parenthesis.

Table C.13. Effects of uniaxial stretching[1,2] applied transversely to initial direction of the fibers on the mechanical properties of molded plaques of PEI/HX1000 80/20 wt%.

FLOW DIRECTION PROPERTIES			TRANSVERSE DIRECTION PROPERTIES			UNIAXIAL STRAIN
Modulus (GPa)	Strength (MPa)	Elongation (%)	Modulus (GPa)	Strength (MPa)	Elongation (%)	
5.13 (0.47)	105.36 (4.15)	2.38 (0.15)	2.84 (0.14)	57.10 (3.92)	2.57 (0.23)	0.0
4.58 (0.43)	80.09 (9.07)	2.14 (0.32)	3.30 (0.26)	80.40 (9.79)	3.20 (0.79)	0.25
3.80 (0.22)	74.82 (5.88)	2.43 (0.32)	4.40 (0.30)	84.20 (9.83)	2.80 (0.64)	0.50
3.30 (0.09)	55.56 (4.10)	1.88 (0.12)	5.55 (0.18)	85.78 (7.76)	2.12 (0.43)	0.75

[1] **Stretching Temperature: 240°C.**
[2] **Initial Strain Rate: 0.14 sec^{-1}**
(★) Standard deviations are given in parenthesis.

Table C.14. Effects of uniaxial stretching[1,2] applied parallel to initial direction of the fibers on the mechanical properties of molded plaques of PEI/HX1000 80/20 wt%.

FLOW DIRECTION PROPERTIES			TRANSVERSE DIRECTION PROPERTIES			UNIAXIAL STRAIN
Modulus (GPa)	Strength (MPa)	Elongation (%)	Modulus (GPa)	Strength (MPa)	Elongation (%)	
5.13 (0.47)	105.36 (4.15)	2.38 (0.15)	2.84 (0.14)	57.10 (3.92)	2.57 (0.23)	0.0
7.44 (0.56)	93.80 (10.44)	1.35 (0.17)	3.10 (0.49)	39.00 (2.28)	1.54 (0.10)	0.25
7.77 (0.47)	125.48 (7.65)	1.95 (0.33)	2.87 (0.31)	34.47 (2.57)	1.44 (0.12)	0.50
8.30 (0.28)	153.84 (6.60)	2.68 (0.29)	2.56 (0.19)	30.50 (1.44)	1.28 (0.16)	0.75

[1] **Stretching Temperature: 240°C.**
[2] **Initial Strain Rate: 0.0014 sec^{-1}**
(★) Standard deviations are given in parenthesis.

Table C.15. Effects of uniaxial stretching[1,2] applied transversely to initial direction of the fibers on the mechanical properties of molded plaques of PEI/HX1000 80/20 wt%.

FLOW DIRECTION PROPERTIES			TRANSVERSE DIRECTION PROPERTIES			UNIAXIAL STRAIN
Modulus (GPa)	Strength (MPa)	Elongation (%)	Modulus (GPa)	Strength (MPa)	Elongation (%)	
5.13 (0.47)	105.36 (4.15)	2.38 (0.15)	2.84 (0.14)	57.10 (3.92)	2.57 (0.23)	0.0
5.00 (0.34)	87.54 (5.22)	2.20 (0.14)	3.15 (0.12)	64.57 (1.65)	3.17 (0.46)	0.25
4.78 (0.39)	82.95 (8.14)	2.05 (0.20)	3.64 (0.31)	73.80 (8.17)	2.40 (0.20)	0.50
3.79 (0.33)	73.18 (8.89)	1.89 (0.20)	4.60 (0.50)	75.25 (6.57)	1.82 (0.12)	0.75

[1] **Stretching Temperature: 240°C.**
[2] **Initial Strain Rate: 0.0014 sec^{-1}**
(★) Standard deviations are given in parenthesis.

Appendix D. Radiation Heat Transfer Simulations

The results of the numerical calculations used to determine the optimum oven preheating temperature to carry out the thermoforming experiments are presented in this appendix. the simulations were performed utilizing a one-dimensional heat transfer model with a radiation heat flux at the sample surface. The transient heat transfer problem was solved utilizing a finite difference scheme with the resultant algebraic equations being solved with the aid of IMSL®'s DIVPAG subroutine. Time increments of 10 sec were used in the simulations. The objective of the numerical simulations was to determine the lowest infrared oven temperature necessary to heat the sample to a temperature of 240°C at a preheating time of 90 sec (which is the limit for automatic operation of the thermoformer). By selecting such a condition (minimum oven temperature and maximum heating time), the temperature gradient across the thickness of the sample was expected to be minimized. The simulations were performed utilizing the thermal properties of Ultem 1000 which were supplied by the manufacturer:

- Thermal conductivity = 0.220 W/m.°K
- Heat capacity = 1675.75 J/Kg.°K
- Density = 1270.0 Kg/m^3

In Figures D.1 and D.2 are shown the predictions of the numerical simulations taking as initial conditions an oven temperature of 280°C and 320°C, respectively. The initial sample temperature was 25°C and the sample thickness was 2 mm. Therefore, based upon the numerical calculations along with processing constraints, an infrared oven temperature of 280°C was select as the optimum pre-heating temperature.

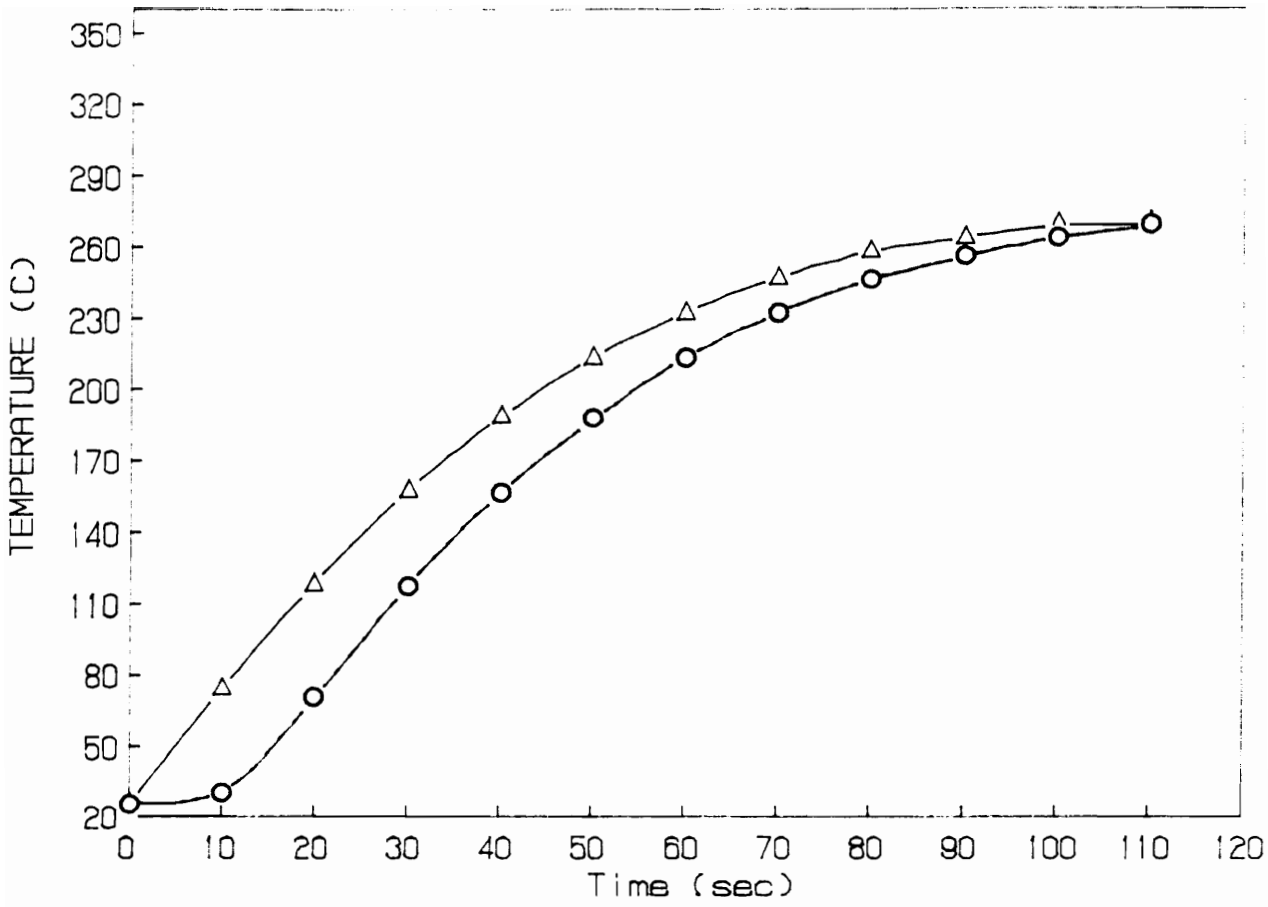

Figure D.1. Predictions of numerical simulations taking as initial conditions an oven temperature of 280°C and a sample temperature of 25°C ((○) center and (△) surface).

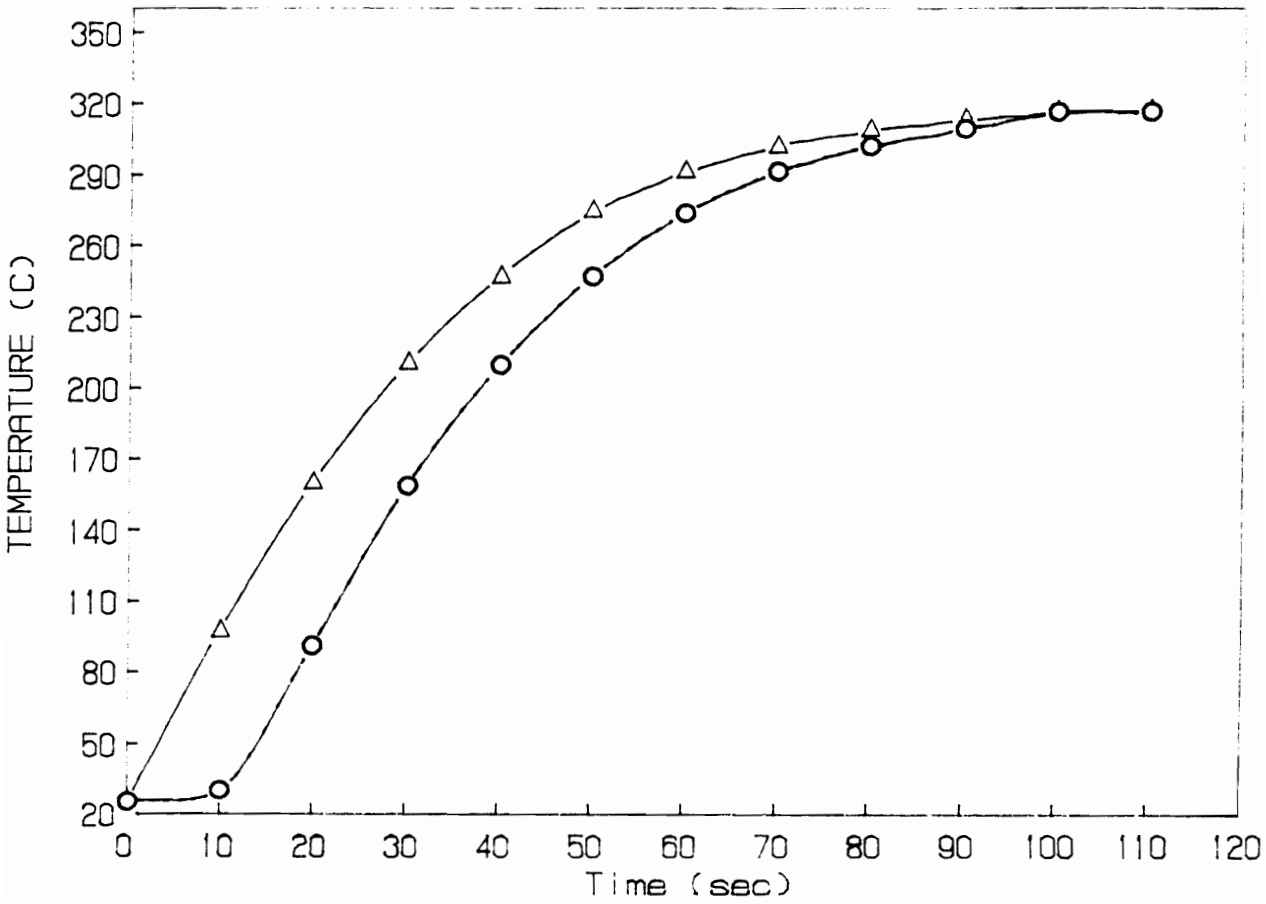

Figure D.2. **Predictions of numerical simulations taking as initial** conditions an oven temperature of 320°C and a sample temperature of 25°C ((○) center and (△) surface).

VITA

J.P. de Souza was born in Santa Catarina, Brazil in the summer of 1958. He was raised in a little piece of paradise called Armacao de Itapocoroy, a small fishing community, like many others along the shores of Santa Catarina, surrounded by beautiful crystal clear beaches and blessed with sunshine year around. In the fall of 1977, he left that tranquil community and enrolled in the chemical engineering program at the Regional University of Blumenau (FURB). He received his engineer degree from FURB in January 1983. During his years at FURB, he met his now wife and mother of his children, Rosecler de Souza. After completion of his degree, he was offered a position as research engineer at Cia. Hansen Industrial. At Hansen, he acquired most of his expertise in the processing and compounding development of thermoplastics. In the spring of 1986, he was offered a supervising position at Polesso Plastics. At Polesso, he worked in the injection molding of structural foamed articles. A few years later, in the fall of 1988, he was granted a scholarship from Atlantic Richfield Foundation, through the Partners of the Americas program, which made possible his attendance at Virginia Tech. He joined the polymer processing and rheology laboratory and under the direction of Professor D.G. Baird, completed graduate studies in the area of liquid crystalline polymer blends.